Mukesh Khare
S.M. Shiva Nagendra

Artificial Neural Networks in Vehicular Pollution Modelling

With 70 Figures and 69 Tables

Springer

Mukesh Khare
Professor in Civil Engineering
Indian Institute of Technology Delhi
New Delhi-110 016, India

At present:
Atlantic LNG Chair
Professor in Environmental Engineering,
University of West Indies
St. Augustine, Trinidad and Tobago
E-mail: mukeshk@civil.iitd.ernet.in & kharemukesh@yahoo.co.in

S.M. Shiva Nagendra
Assistant Professor in Civil Engineering
Indian Institute of Technology Madras
Chennai-600 036, India
E-mail: snagendra@iitm.ac.in & shivanagendra@yahoo.com

Library of Congress Control Number: 2006933174

ISSN print edition: 1860-949X
ISSN electronic edition: 1860-9503
ISBN-10 3-540-37417-5 Springer Berlin Heidelberg New York
ISBN-13 978-3-540-37418-3 Springer Berlin Heidelberg New York

Springer is a part of Springer Science+Business Media
springer.com

Cover design: deblik, Berlin
Typesetting by the authors and SPi.
Printed on acid-free paper SPIN: 11418245 89/SPi 5 4 3 2 1 0

Dedicated
to
our
Parents

WORK IS WORSHIP

Basavanna, 12TH Century

karmany eyvādhikāras te
mā phalesu kadācana
mā karma - phala-hetur bhur
mā te sango 'stv akarmani

You have a right to perform your prescribed duty,
but you are not entitled to the fruits of action.
Never consider yourself the cause of the result of your activities,
and never be attached to not doing your duty.

BHAGAVAD-GITĀ (II-47)

Artificial Neural Networks in Vehicular Pollution Modelling

Mukesh Khare
Professor in Civil Engineering
Indian Institute of Technology Delhi
At present: Atlantic LNG Chair
Professor in Environmental Engineering
University of West Indies
St. Augustine, Trinidad & Tobago

S.M. Shiva Nagendra
Assistant Professor in Civil Engineering
Indian Institute of Technology Madras

PREFACE

Over last five decades, vehicular pollution (VP) models are being used as tool to address the effectiveness of vehicular air pollution control strategies and the economic consequences in implementing the decisions in urban areas. Using meteorological and traffic characteristics as input, VP models provide theoretical estimates of air pollution concentrations as well as temporal and spatial variations for the present and future *what if* scenarios. During last few decades, VP models are advanced steadily in technical sophistication and their ability to deal with complex environmental systems. VP modelling involves deterministic and/or stochastic approaches. However, development of reliable VP models is still a challenge because a number of variables describing the non-linear vehicular pollutant dispersion characteristics including the arbitrary variations in the wind speed, wind direction, and vehicle wake are involved.

Artificial neural networks (ANNs), which are parallel computational models, comprising of interconnected adaptive processing units (neurons) have the capability to predict accurately the dispersive behavior of vehicular pollutants under complex environmental conditions. This book aims at describing step-by-step procedure for formulation and development of ANN based VP models considering meteorological and traffic parameters. The model predictions are compared with existing line source deterministic/statistical based models to establish the efficacy of the ANN technique in explaining frequent dispersion complexities in urban areas.

The book is very useful for hardcore professionals and researchers working in problems associated with urban air pollution management and control.

New Delhi — *M. Khare*
Chennai — *S.M.S. Nagendra*
September, 2006

CONTENTS

1 Introduction

The expansion of industries, growth of cities and concentrated human activities are leading to alarming increase in air pollution levels in almost all metro cities of the world [1]. Vehicular, industrial and domestic sources are major anthropogenic categories causing emission of air pollutants into the environment. In recent years, air pollution from industrial and domestic sources has markedly decreased due to passage of various acts promulgated by different governments in most of the countries. However, a substantial growth of motorized traffic over the years has increased the air pollution levels in urban centers [2]. An investigation by Mage et al. [3] have pointed out that motor traffic is a major source of air pollution in mega-cities with a population of over 10 million[1]. In last five decades, the global vehicle fleet has already grown ten fold and estimated to further double in next 20 to 30 years [5]. Much of the expected growth in vehicle numbers is likely to occur in the developing countries [3] with more people driving more vehicles over greater distances and for longer duration; and exposing larger number of people to elevated concentration of ambient air pollutants for longer period causing adverse health effects [6].

[1] Kretzchmar [4] indicated that in the year 1990, already 12 urban cities had population exceeding 10 million, and estimated to double over the next ten years-seventeen of twenty four mega-cities will be in developing countries. By the year 2030, developing country cities are expected to grow by 160 percent.

M. Khare and S.M. Shiva Nagendra: *Introduction*, Artificial Neural Networks in Vehicular Pollution Modelling (SCI) **41,** 1–6 (2007)
www.springerlink.com

1.1 Air Pollution Definition

Many definitions have been proposed to explain the air pollution. In general, air pollution may be defined as *the presence in the outdoor atmosphere of one or more contaminants or combinations thereof in such quantities and of such duration as may be or may tend to be injurious to human, plant, or animal life, or property or reasonably interfere with the enjoyment of life or the environment [7].*

1.1.1 Composition of Atmosphere

The composition of dry atmospheric air up to a height of 50 km is given in Table 1. In addition, air also consists of 1 to 3 percent (volume/volume) water vapor and tracers of sulfur dioxide (SO_2), formaldehyde (HCHO), iodine (I), sodium chloride (NaCl), ammonia (NH_3), carbon monoxide (CO), dust and pollen.

Table 1 Compositions of dry atmospheric air.

Chemical compound	Concentration (ppm)[a]	Concentration ($\mu g/m^3$)[b]
Nitrogen (N_2)	780,000	8.95×10^8
Oxygen (O_2)	209,400	2.74×10^8
Argon (Ar)	9,300	1.52×10^7
Carbon dioxide (CO_2)	315	5.67×10^5
Neon (Ne)	18	1.49×10^4
Helium (He)	5.2	8.50×10^2
Methane (CH_4)	1.2	7.87×10^2
Krypton (Kr)	1.0	3.43×10^3
Hydrogen (H_2)	0.5	4.13×10^1
Xenon (Xe)	0.08	4.29×10^2
Nitrous oxide (N_2O)	0.5	9.00×10^2
Ozone (O_3)	0.01-0.04	$1.96 \times 10^1 - 7.84 \times 10^1$

[a] parts per million; [b] micrograms per cubic meter

1.2 Air Pollution Problems

Air pollution problem was first experienced in the year 1272 in England. King Edward I, enforced law prohibiting the use of *sea-coal* in furnaces. In 1873, a fog in London reported death of 268 people due to bronchitis problems [7]. Later, during 19th century, a number of air pollution related problems occurred. In December 1930, a heavy industrialized sector of the Muse Valley in Belgium, experienced a severe three day fog resulting into death of 60 persons. In January 1931, 592 people died in Manchester and Salford area of England due to thick fog hovering over the city for nine days. In 1948, in Donora, Pennsylvania, a small town dominated by steel and chemical plants in the USA, about 6000 inhabitants fell sick due to thick fog persisted for four days. A major air pollution disaster hit the London city in December 1952. A thick fog lasted for ten days resulting into death of 4000 people due to asphyxiation. In July 1976, sudden release of the dioxin due to reactor explosion in Seveso, Italy resulted into illness of 187 people. Recently, in December, 1984, release of 30 tones of deadly methyl isocynate gas from storage tanks due to failure of vent scrubber system in Bhopal, India, killed 2500 persons and severely affected the health of more than one lakh people in vicinity of the city [7, 8, 9]. These 'episodes' are mainly caused from 'point/area' sources favored by worse meteorological conditions. However, rapid urbanization of urban regions in last two decades resulted into their exponential growth in almost all over the world. Due to this many urban centers have become 'hot-spots' experiencing frequent 'exceedance' in pollutant concentrations. Motorized traffic is one of the major causes of deteriorating air quality in such urban centers.

Several studies in the past have been carried out investigating the fate of vehicular pollution in such 'hot-spots'. Organisation for Economic Cooperation and Development (OECD) describes the regional and global impacts of vehicular emissions, with more emphasis on impact of vehicular pollution on local urban air quality [10]. A review of road transport emissions and their impact on the environment at all scales from local to global has been reported in Faiz [11]. The Royal Commission on Environmental Pollution has published a

comprehensive report on environmental impact of vehicular pollution [12]. Joumard [13] has described the application of end-of-pipe technology for the abatement of vehicular pollution. Recently, Colvile et al. [14] have reviewed impact of vehicular pollution on human health as well as tropospheric ozone productions.

1.3 Air Pollution Sources

The sources of air pollution are broadly classified into *two* categories, namely, *natural* and *anthropogenic* sources. Volcanic eruptions, forest fires, dust storms are few examples of *natural* sources. *Anthropogenic* sources consist of *stationary* and *non-stationary* (moving) sources. *Stationary* sources are mainly industries and *non-stationary* sources are mainly transport. Further, the *stationary* sources are termed as *point* sources (single industry) and *area* sources (clusture of *point* sources and urban homes). The *non-stationary* sources are mainly vehicles (*line* sources) and other transport means e.g., aeroplanes and railways.

1.3.1 Point Source Emissions

The modelling of point source emission uses Gaussian equation to estimate and predict the spatial and temporal dispersion of air pollutants [8].

1.3.2 Area Source Emissions

An area source is a two-dimensional structure with a limited vertical height. The fundamental approach to developing a diffusion model for area sources is to apply conservation of mass for a particular pollutant with appropriate boundary conditions [15]. The simplest area source model is the BOX model [16]. The pollutant is assumed to be completely mixed within a single box which covers the city and extends upward to the mixing height[2].

[2] The mixing height is the height above which pollutants do not rise due to temperature profile of the atmosphere.

1.3.3 Line Source Emissions

The vehicular pollution dispersion from roadways is modeled as *line source* or *series of point sources*. The *line source* approximation involves solving an integral equation along the specified line, which results in greater computational requirement than the approximation as a series of point sources. However, in both cases, the estimates of emission concentration are based on Gaussian model formulation [17].

1.4 Urban Air Pollution Control Strategies

Urban air pollution control has two major aspects-'strategic' and 'tactical'. The former is the long-term reduction of pollution levels at all scales of the problem from 'local' to 'global'. Long-term strategies are developed by setting goals for air quality improvement for 5, 10 or 15 years ahead and plans are made to achieve the objectives. On the contrary, the 'tactical' approach aims at prevention and control of 'episodes' to prevent an impending disaster. The duration of such 'episodes' usually varies from 36 hours to 3 or 4 days [8].

1.5 Modelling Tools – Conventional and Soft Computational Approach Including ANN

The conventional Gaussian based models are best suitable to predict long-term average concentrations with frequency distribution up to 90 percentiles. These models are deterministic models of 'causal' in nature. However, their predictive performance is considerably reduced when there exist complexities in temporal and spatial relationship between dependent and independent variables. One of the application domains where the Gaussian based models terribly fail in describing the dispersion phenomena is the urban air sheds. Urban air sheds consist of one or more air quality control regions(AQCRs)[3]

[3] It may be defined as fixed boundaries / areas where local authorities are entrusted with the responsibility for assessing and reviewing the local air quality in conformity with the national ambient air quality standards (NAAQS).

wherein pollutant dispersion is affected by complex traffic movements, road geometry, meteorological conditions and roughness elements. Statistical based models comparatively perform better than the deterministic Gaussian based models in such urban air sheds. These models use various statistical theories in estimating/ predicting pollutant concentrations relating time series data on traffic and meteorology. However, the variation in time series data is complex and non-linear and requires prior assumptions concerning their distribution. As a result statistical based models 'underperform' when applied in complex urban air sheds [18]. Artificial neural network based models overcome these shortcomings to some extent because of their special properties like, self-correction, self-learning and parallel processing. As a result these models are able to describe the complex non-linear dispersion phenomena in such urban air sheds and accurately predict the 'exceedances' in pollutant concentrations.

2 Vehicular Pollution

The automobile discovery satisfactorily combines a human desire for rapid transportation with the desire for independence and flexibility. However, rapid proliferation of motor vehicles, in both developed and developing country, poses a serious threat to the urban air quality [3]. This chapter provides an overview of vehicular pollution scenario in metro cities including sources of vehicular pollution, types of vehicular pollutants and their health effects. The chapter also describes the principles of local air quality management, the ambient air quality standards for urban air sheds and overview of vehicular pollution models.

2.1 General

Air pollution from motor vehicles has become a major concern in rapidly urbanizing regions of the world because of increase in number of vehicles in use and the distance traveled by each vehicle each year [19]. Higher incomes, mobility, expansion of cities, and proliferation of employment centers have increased the demand for motorized transport, resulting into a disproportionately high concentration of vehicles in urban centers [20]. In last five decades worldwide, the number of vehicles is growing faster than the global population e.g. about 5 % per year compared to 2 %, for population. Over last 30 years, total global vehicular population has touched 700 millions, which approximately consumes 34 % of total oil produced in the world [21, 22].

M. Khare and S.M. Shiva Nagendra: *Vehicular Pollution*, Artificial Neural Networks in Vehicular Pollution Modelling (SCI) **41,** 7–24 (2007)
www.springerlink.com

2.2 Sources of Vehicular Pollution

Vehicular pollution sources can be classified into four categories: (i) exhaust emissions, (ii) evaporative emissions, (iii) refueling losses and (iv) crankcase losses. Out of the four categories, the exhaust emissions account for about 70 % of the vehicular pollution; whereas, the crankcase emissions account for about 20 % and evaporation from tank and carburetor accounts for remaining part of the pollution percentage [23].

Air pollution from vehicles largely results from combustion of fuel. CO is a product of incomplete combustion. Most hydrocarbons (HCs) are combusted completely, forming carbon dioxide (CO_2) and water; some remain unburned or react to form new HCs. Oxides of nitrogen (NO_x) is produced from oxidation of nitrogen, a reaction that is enhanced at higher temperatures. Diesel, consisting of sulfur impurities, leads to emission of sulphur dioxide (SO_2). Besides, particulate matter (PM) of less than 10 micron diameter (PM_{10}) is one of the major constituents in diesel engines exhausts [24]. Other pollution sources include evaporative emissions of HCs from engines and fuel systems when automobiles are in stationary position. These emissions are classified as 'diurnal' or 'breathing losses', 'transitory trip-end' or 'hot soak losses' and losses from porous fuel tubes. Evaporative emissions from sources other than the tailpipe, are referred as 'running loss emissions' when the engine is in operation. Crankcase emissions of HCs, or 'blow-by losses', originate from disabled or disconnected hoses [25]. The types of pollutants emitted by petrol and diesel engines are similar but vary in proportion due to difference in the mode of operation of engines. Table 2.1 shows that the exhaust emission of diesel engines contains significantly lower concentrations of pollutants than the exhaust emissions from petrol engines.

Motor vehicles are categorized into following three groups, based on working principle of the engine e.g. (i) vehicles with spark ignition engines using petrol, (ii) vehicles with two stroke ignition engines using lubricating oil mixed petrol (two or three wheelers) and (iii) vehicles with compression ignition engines using diesel. In the first type, complete combustion does not take place and so pollutants are produced even at stoichiometric values of air/fuel ratio (A/F)

=14.5. This is due to the fact that spark induced reaction is not fully propagated inside the piston chamber. In the 4-stroke cycle petrol engine, the A/F ratio and operating temperature are low. As a result, substantial quantities of unburnt HCs and CO are emitted with low quantities of NO_x. The second types of engines, i.e. the two and three wheelers (being petrol driven), emit large quantities of unburnt HCs, CO and PM. The third type, i.e. in the diesel engines, due to high A/F ratio and operating temperature, the concentration of NO_x generally remains higher in the exhaust emissions. Since, diesel has low vapor pressure, the emission of fine carbon soot particles is also considerably high. Relative incidences of pollutants in exhaust emissions by vehicle type have been given in Table 2.2.

Table 2.1 Relative composition of exhaust gases (concentrations in ppm[c]/volume).

Engine type	Pollutants	Idling	Acceleration	Deceleration	Cruising
Petrol	Carbon monoxide	69000	29000	39000	27000
	Hydrocarbon	5300	1600	10000	1000
	Nitrogen oxides	30	1020	20	650
	Aldehydes	30	20	290	10
Diesel	Carbon monoxide	Trace	1000	Trace	Trace
	Hydrocarbon	400	200	300	100
	Nitrogen oxides	60	350	30	240
	Aldehydes	10	20	30	10

[c]ppm = parts per million. To convert from units of ppm (volume) to $\mu g/m^3$ under ambient conditions is given by: 1 ppm (volume) pollutant = (40.9 x molecular weight) $\mu g/m^3$
Source: [26].

Table 2.2 Relative incidences of pollutants in exhaust emissions by different vehicle classes (Per 100 % of each pollutant).

Vehicle class	Pollutant		
	CO	NO_x	HC
Two and three wheelers	46	Negligible	70.0
Cars (petrol driven)	25	5.0	8.0
Buses and goods vehicles (diesel driven)	29	94	22.0

Source: [26].

2.3 Types of Vehicular Pollutants

Common vehicular pollutants in urban environment are CO, NO_x, PM_{10}, SO_2, Volatile organic compounds (VOC's) and Lead (Pb). A substantial quantity of CO_2, which is a greenhouse gas, is also released [25]. In the following paragraphs (sections 2.3.1 to 2.3.6), formation of vehicular pollutants and their related statistics have been discussed.

2.3.1 Carbon Monoxide

CO is colorless, odorless and stable gas. It is produced due to incomplete combustion of fuel in motor vehicles. The lifetime of CO is between 2 to 4 months in the atmosphere [27]. Worldwide anthropogenic CO emissions are estimated at 350 million tons, 59 % of which are contributed by the transport sector, 39 % by the residential and commercial sectors, and 2 % by the industrial and power sectors. In developing countries, transport sector accounts for 53 % of CO emissions [24]. These emissions can be reduced by increasing the A/F ratio, but with the risk of increasing the formation of NO_x. Most effective reduction of CO can be achieved by using catalytic converters [25].

2.3.2 Nitrogen Oxides

Nitric oxides (NO and NO_2) are the important pollutants among the six NO_x compounds. NO_x is formed by oxidation of atmospheric nitrogen during combustion. About 90 % of these emissions are in the form of NO. NO is produced in the vehicle engine by combustion of nitrogen at high temperatures. NO_2, formed by oxidation of NO, has a reddish brown color and pungent odor. In the atmosphere, it is involved in a series of reactions (in presence of ultraviolet radiation) that produce photochemical 'smog'. It may also react with moisture in the air to form nitric acid (HNO_3) aerosols i.e. the acid mist. In the lower atmosphere (troposphere), NO_2 forms ozone (O_3) by reacting with HCs. Worldwide anthropogenic NO_x emissions are estimated at 93 million tons, 43 % of which are contributed by transport sector. In developing countries, the transport sector accounts for 49 % of NO_x emissions [10]. NO_x emissions can be reduced by optimization of combustion process or by using catalytic converters [25].

2.3.3 Volatile Organic Compounds

VOC's include variety of HC compounds that are generated due to incomplete combustion of fuels or formed during combustion process. Chemically, HC's are defined as compounds consisting of carbon and hydrogen. In the urban air, most important VOC's are benzene, a series of aldehydes and polyaromatic hydrocarbons (PAH's) [25]. About 55 % of HC emissions from gasoline fueled vehicles with no emission controls, originate in the exhaust system. Out of this 55 %, 13 to 25 % come from the crankcase blow-by, and 20 to 32 % evaporate in the fuel lines, fuel tank and carburetor. Methane consists of 5 to 15 % of HC emission from vehicles not equipped with catalytic converters and up to 40 % of exhaust HC from catalyst equipped vehicles. This is because the catalysts are less effective in oxidizing methane than other HC's [24,28]. Benzene is an aromatic HC present in gasoline. About 85 to 90 % of benzene emissions come from exhaust and the remainder comes directly from gasoline evaporation and through distribution losses [11]. Benzene in exhaust originates both from partial combustion of other aromatic HC compounds in gasoline such as toluene, and xylene. Benzene consists 63 to 85 % of the toxic emissions in the exhaust from gasoline fueled cars equipped with fuel injected engines and 36 to 65 % from older model cars equipped with carburetor engines and catalytic converters [29]. Controlled gasoline fueled cars have higher emissions of formaldehyde than acetaldehyde. Uncontrolled diesel fueled vehicles emit 1-2 grams of aldehyde per liter [30]. PAH's are emitted at a higher rate in the exhaust of diesel fueled vehicles than gasoline fueled. In developed countries, motor vehicles forms about 85 % of total VOC emissions [24].

2.3.4 Sulphur Dioxide

SO_2 is a classical air pollutant associated with fuel consisting of sulphur impurities. SO_2 is a stable, non-flammable, non-explosive, colorless gas that can be detected by taste at concentrations as low as 1,000 $\mu g/m^3$ or by smell at concentrations above 10,000 $\mu g/m^3$ [24]. Diesel vehicles are main sources for SO_2 emissions. SO_2 emissions can successfully be reduced using fuels with low sulphur content. In recent years, the SO_2 concentrations are negligible in vehicle

exhausts as a result of low sulphur diesel fuel used in the transport sector [23].

2.3.5 Particulate Matter

In general, the term 'particulate' refers to all atmospheric substances that are not gases. They can be suspended droplets or solid particles or mixture of the two (aerosol). Particulates can be composed of inert or extremely reactive materials ranging in size from 100 μm down to 0.1 μm and less. Particles, in the range 1-10 μm (PM_{10}) have measurable settling velocities but are readily stirred by air movements; whereas particles of size 0.1-1.0 μm (PM_1) have small settling velocity [8]. Gasoline vehicles have lower PM emission rate than diesel fueled vehicles. PM emissions from gasoline fueled vehicle result from unburnt lubricant oil, and ash forming fuel and oil additives [11]. PM emitted by diesel-fueled vehicles consists of soot, formed during combustion and heavy HC, condensed or adsorbed, on the soot and sulfates. These emissions contain PAH. In older diesel fueled vehicles, combustion of PM emission is between 40 to 80%. However, with the advance of emission control measures in engines, the contribution of soot has been reduced considerably. Heavy HC, referred to as the soluble organic fraction of PM, originates from lubricating oil, unburnt fuel and compounds formed during combustion [31]. Black smoke, associated with soot portion of the PM, emitted by diesel-fueled vehicles is caused by oxygen deficiency during fuel combustion or expansion phase. Blue, gray and white smokes are caused by the condensed HC in the exhaust of diesel-fueled vehicles. Blue or gray smoke results from vaporized lubricating oil and white smoke occurs during engine startup in cold weather. Diesel fuel additives such as barium, calcium, or magnesium reduce smoke emissions, but increase sulfate emissions. These additives may also increase PAH emissions [24].

2.3.6 Lead

Motor vehicles fueled with leaded gasoline are the main sources of Pb in air. Tetraethyl lead is added to gasoline to increase the fuel's octane number, which improves the antiknock characteristics of the

fuel in spark ignition engines. About 70 to 75 % of this Pb is transformed into inorganic Pb upon combustion, and emitted to the atmosphere through the exhaust pipe along with 1 % of the organic Pb that passes through the engine [24]. The rest of Pb remains trapped within the exhaust system. Organic Pb emissions usually occur as vapor, while inorganic Pb is emitted as PM, often less than 1 μm in size. Although Pb in gasoline accounts for less than 10 % of all refined Pb production, about 80 to 90 % of Pb in global ambient air originates from combustion of leaded gasoline [32]. In recent years, Pb has been phased out in most of the countries.

2.4 Health Effects of Vehicular Pollution

Pollutants emitted by motor vehicles have a number of adverse effects on human health. Inhalation is the main route of exposure to pollutants originating from motor vehicle emissions. Other exposure routes are - drinking water contamination, food contamination and absorption through skin. Exposure by inhalation directly affects respiratory, nervous and cardiovascular systems of humans, resulting in impaired pulmonary functions, sickness, and even death [6].

CO absorbed through the lungs reduces the body's capacity to transport available oxygen to the tissues. CO, bonds with hemoglobin (COHb), lowers the oxygen level in the blood. An exposure of 45 $\mu g/m^3$ of CO for more than two hours adversely affects a person's ability to make judgments. Two to four hours of exposure at 200 $\mu g/m^3$ raises the COHb level in the blood to 10 to 30 % and thus increases the possibility of headaches. One-hour exposure to 1,000 $\mu g/m^3$ of CO raises the COHb level in blood to more than 30 % and causes a rapid increase in pulse rate leading to coma and convulsions. One to two hours of exposure at 1, 830 $\mu g/m^3$ results in 40 % COHb in blood, which may cause death [33].

NO_2 is an irritating gas that is absorbed into the mucous membrane of the respiratory tract. The most adverse health effect linked to NO_2 occurs at the junction of the lungs. The upper airways are less affected because NO_2 is not very soluble in aqueous surfaces. Exposure of NO_2 is linked with increased susceptibility to respiratory infection, increased airway resistance in asthmatics and decreased pulmonary

function. Short-term exposure to NO_2 has been associated with illness in children (cough, running nose and sore throat, are among the most common), as well as increased sensitivity to urban dust and pollen. Health effects of occupational exposure of NO_2 range from inflammation of mucous membrane of the tracheobronchial tree to bronchitis, bronchopneumonia and acute pulmonary edema [34]. Lung function is affected by 30-minutes exposure to NO_2 concentration of 560 $\mu g/m^3$ while exercising, 940 $\mu g/m^3$ in asthmatic people and above 1, 300 $\mu g/m^3$ for a 10-15 minute exposure in healthy people [34]. In one of these studies, exposure to a daily mean NO_2 concentration of 244 $\mu g/m^3$ is associated with sore throat among adults [35].

PAH's, absorbed in the lungs and intestines and metabolized in the human body, are mutagenic and carcinogenic. It is estimated that 9 of 100, 000 people exposed to 1 $\mu g/m^3$ of benzo (a) pyrene, over a lifetime, may develop cancer. Aldehydes are absorbed in the respiratory and gastrointestinal tracts and metabolized. Adverse health effects from aldehyde include eye and nose irritation (at a concentration of 0.06 mg/m^3), irritation of mucous membrane and alteration in respiration (at concentration of 0.12 mg/m^3), coughing, nausea and shortness of breathe. Occupational exposure of formaldehyde is associated with the risk of cancer [34].

SO_2, is associated with reduced lung function and increased risk of mortality and morbidity. Adverse health effects of SO_2 include coughing, phlegm, chest discomfort, and bronchitis [25]. WHO [36] has determined that the effects of 24-hour human exposure to SO_2 include mortality at ambient concentrations above 500 $\mu g/m^3$ and increased acute respiratory morbidity at ambient concentrations above 250 $\mu g/m^3$. Annual exposure to SO_2 causes increased respiratory symptoms or illness at ambient concentrations above 100 $\mu g/m^3$.

PM, greater than 10 μm in diameter is deposited in the extra thoracic part of the respiratory tract through nasal breathing, while the 2.5 μm to 10 μm fraction (PM_{10}) is deposited near the fine airways. $PM_{2.5}$ (particles in range 2.5-1.0 μm) is a larger health concern because it can evade the lung tissue, where it can remain imbedded for years, or in the case of soluble particles, be absorbed into bloodstream

[8,37]. Based on 24-hour exposure, smoke at 250 $\mu g/m^3$ is associated with increased acute respiratory morbidity among adults, and total suspended particulate (TSP) at 180 $\mu g/m^3$ levels and PM_{10} at 110 $\mu g/m^3$ with decrements in lung functions among children. Increased respiratory symptoms or illness would be expected at an annul mean exposure to 100 $\mu g/m^3$ of smoke and decrements in lung function would be expected at an annual mean exposure to 180 $\mu g/m^3$ of TSP [36]. However, more recent studies suggest that health may be affected even at lower concentrations [34].

Pb in ambient air is in the form of tiny particles with an aerodynamic diameter of less than 10 microns (PM_{10}). Ambient air also contains organic lead compounds as gases. The proportion of lead absorbed from gastrointestinal tract is about 10 to 15 % for adults and up to 50 % for children. Pb adsorption increases in diets with low levels of calcium, vitamin D, iron and zinc. Pb, absorbed in the human body, is distributed among bones, teeth, blood and soft tissues. Organic Pb is mainly absorbed by the lungs through the respiratory tract and also through skin [34]. Based on a review of epidemiological studies, an increase of 1 $\mu g/m^3$ in Pb concentrations in ambient air has been associated with an increase in blood Pb levels of 0.3 $\mu g/dl$ to 0.5 $\mu g/dl$ [38]. Adverse effects of Pb exposure have been observed in small children, women of reproductive age, and male adults. Newborns and young children are most vulnerable to Pb exposure.

Figure 2.1 shows the pathway from vehicular pollution generation to health effect. Table 2.3 describes, in brief, major health effects from vehicular pollutants.

2.5 Meteorological and Topographical Factors Affecting Vehicular Pollution Dispersion in Urban Air Sheds

The dispersion and transportation of vehicular pollution in an urban air shed are mainly controlled by its meteorological and topographical characteristics. The primary meteorological parameters affecting the vehicular pollution dispersion are wind speed, wind direction, mixing height and atmospheric stability. Wind speed is directly influenced by topography of the urban area. It increases with height.

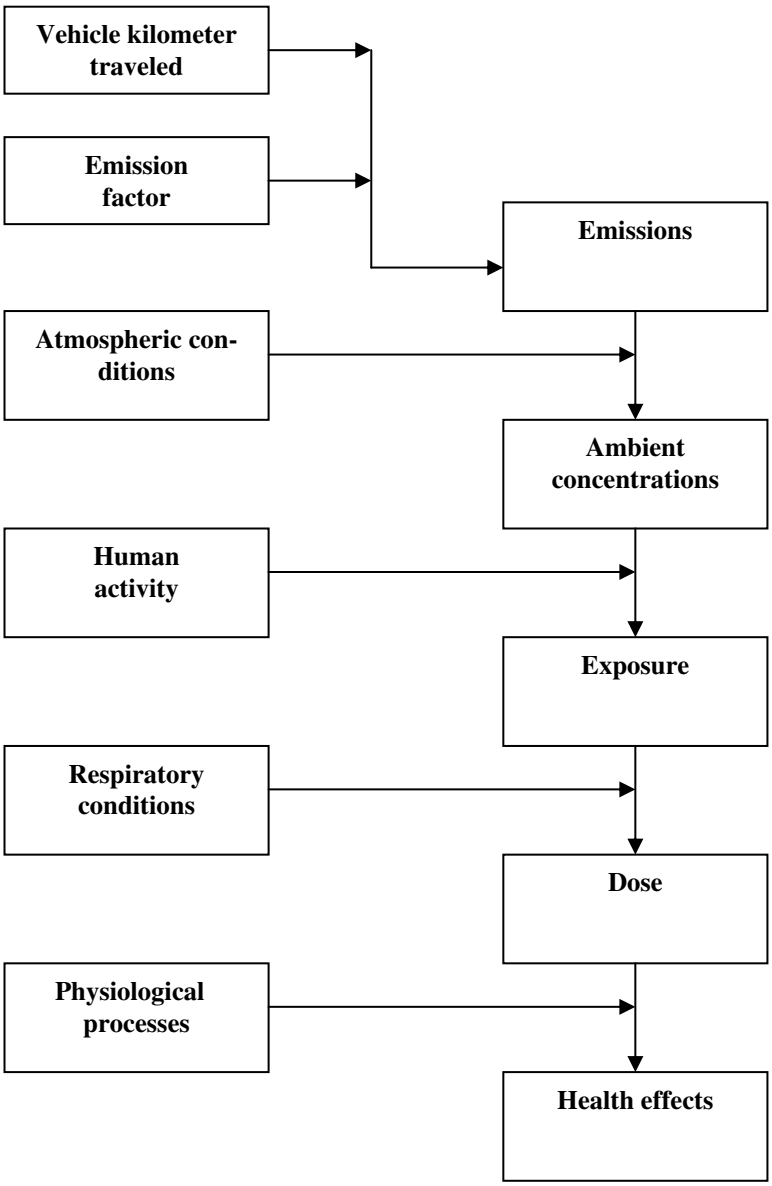

Fig. 2.1. Pathway from transport emission to health effect.

Table 2.3 Health effects of vehicular pollutants.

Pollutants	Health effects
CO	Reduces delivery of oxygen to the body, which is particularly serious for those with cardiovascular disease, causes impairment of function in healthy people.
NO_2	In high concentrations, irritates lungs and lowers resistance to respiratory infection; an important precursor to ozone and acid precipitation which can damage sensitive ecosystems
VOC	Results in ozone, which can damage lung tissue, reduces lung function, and causes irritation (these effects occur even at low levels in healthy people who engage in moderate exercise); also causes ecosystem degradation, mainly through damaging foliage.
PM_{10}	In high concentrations aggravates existing respiratory and cardiovascular disease, alters the immune system, can be carcinogenic, and causes lung damage.
SO_2	Major contributor to acid rain; degrades lung function and lower lung defenses while aggravating existing respiratory disease
Lead	Accumulates in the body and affects kidney, liver and nervous system; causes neurological impairments.

Source: [25].

A number of formulations describe the variation of wind speed in the surface boundary layer. However, Power law profile is frequently used. The initial direction of movement of vehicular pollution in urban roadways is determined by the wind direction. It is sensitive parameter. A shift in wind direction of as little as 5 degree causes 10 % decrease in vehicular pollution concentrations at the receptor under stable conditions, about 50 % under neutral conditions and 90 % under stable conditions. Wind rose diagram provides details regarding prevailing wind speed and direction. Mixing height is another important parameter that controls vertical dispersion of the vehicular pollution. Mixing height is the height above the earth's surface to which released pollutants extends, primarily due the atmospheric turbulence. The most important mixing process in the atmosphere, which causes the dilution of air pollutants, is called *eddy diffusion*. The atmospheric eddies mixes the parcels of polluted air with

relatively unpolluted air. Eddy diffusion is most efficient when the size of eddy is similar to that of the pollutant puff. Small size eddies are effective in diluting the edges of the pollutant mass. However, larger eddies are mainly responsible for the transport (advection) of polluted air mass as a whole. The size of eddies and its effect on the vertical expansion of rising air parcels depend on vertical temperature structure. There are two mechanisms by which eddies are formed in the atmosphere, *one*, heating from earth surfaces (solar radiation) and *other*, the wind shear. The turbulence structure and wind speed in the atmosphere are used in defining its dispersive ability (stability). The amount of turbulence in the atmosphere is used to categorize the stability classes. The most widely used category is the Pasquill-Gifford (PG) stability classes i.e. A, B, C, D, E and F. Class A denotes the most unstable or turbulent condition and class F denotes the most stable or least turbulent conditions. The atmospheric turbulence is affected by many factors, such as wind flows over rough terrain, trees or buildings (*roughness*).

2.6 Ambient Air Quality Monitoring

Ambient air quality monitoring involves the measurement of pollutants in the atmosphere. Ambient air quality monitoring in urban areas may have number of objectives. Foremost, is to generate information on the spatial and temporal distribution of air pollution [8]. Monitored data are then compared against national ambient air quality standards (NAAQS) to identify potential risks to human health or to the environment. WHO studies [5] have shown high pollutant concentration at 'hot spots' (*central business district*) in metro cities during certain periods of the day (i.e. peak traffic flow during morning and evening hours). These data assist policy makers to implement and evaluate the effectiveness of the control measures like formulation of the *hazard warning system* which initiates necessary preventive measures against health related risks when pollutant concentrations are above the NAAQS [39].

2.7 Local Air Quality Management

'Episodes' of poor air quality in cities indicate a need of local air quality management system (LAQMS) in order to protect humans and materials from adverse effects of air pollution [39]. There are several distinct strategies to control the air quality, which can be used in isolation or as a package to provide a response to national or regional requirements and philosophies [40]. Theoretically, air quality may be viewed as a function of *four* variables: meteorology and climatology, geography and topography, urban form and emission source density and intensity. Of these variables, the one, most directly amenable to human managerial intervention, is that of emissions. The density of emission sources and the intensity of releases from individual sources are affected by variety of direct and indirect actions. Therefore, any air quality management plan has to address the density and intensity of emission sources, if the desired outcomes are to be achieved. Such a response requires the management of urban environment and the processes affecting its development. Four key principles of air quality management are *emissions*, *impacts, cost-benefit analysis* and *controls* [41].

The general concept of air quality management may be defined as "the application of a systematic approach to the control of air quality issues" [42]. A fuller definition would need to incorporate aspects of integration, cooperation and communication as a system designed to consider air quality in a holistic way. Griffin [43] expresses air quality management as comprising of five continuous steps: *definition, planning, control, implementation* and *evaluation*. These are translated into air quality management terms as shown in Figure 2.2.

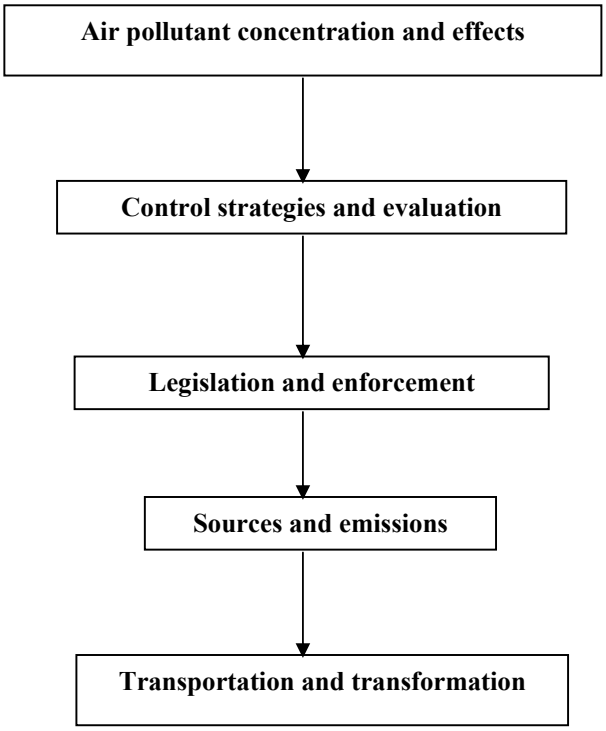

Fig. 2.2. Concepts of air quality management given by Griffin [43].
Source: [39]

An air quality management plan provides a basis for necessary liaison between different actors and agencies involved, both directly and indirectly in determining the local air quality. It may be defined as "the application of a systematic approach to the control of air quality problems and this represents one mechanism where by integration could be achieved". A schematic representation of the functions and processes involved in a theoretical air quality management plan is shown in Figure 2.3. The framework in Figure 2.3 incorporates all necessary functionality of an air quality management plan as described below [41].

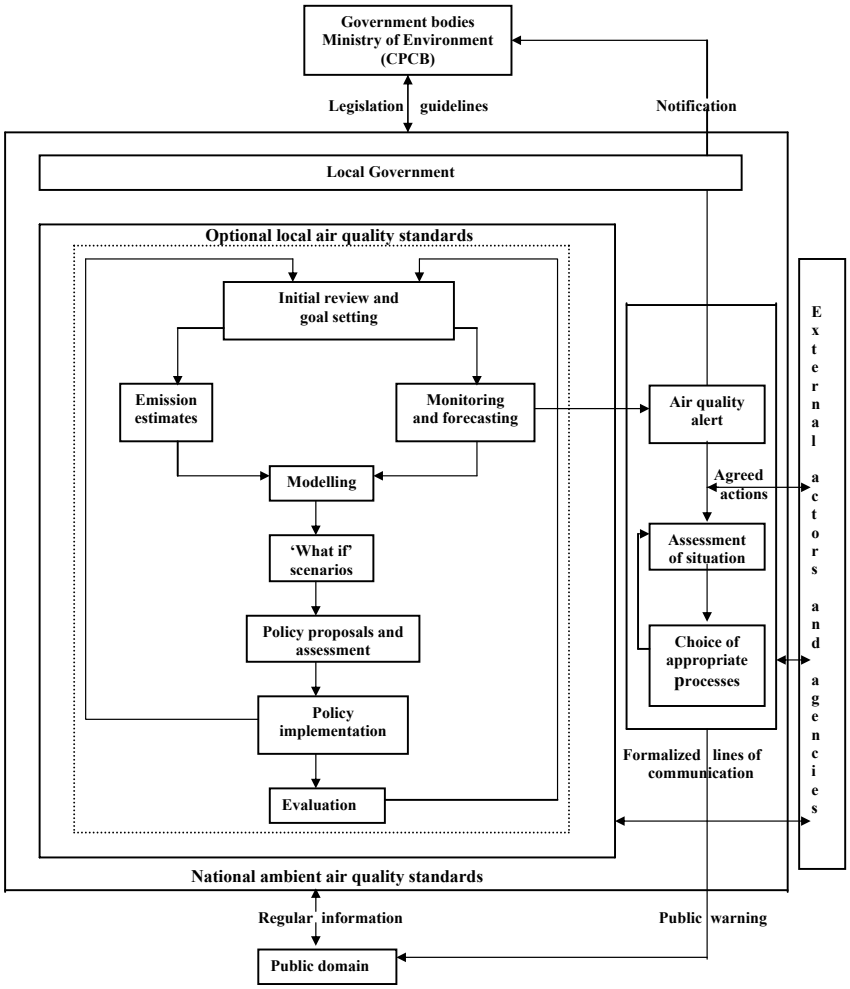

Fig. 2.3. A hypothetical frame work far an air quality management plan.
Source: [39]

(i) The plan needs to be flexible to allow modifications for new knowledge about emissions or concentrations and yet for a suitable framework within which all groups coexist.

(ii) An air quality management plan at the local scale would then ideally be a tier of a regional plan, which in turn, may be a part of a national plan.

(iii) An air quality management plan provides opportunity for setting local air quality standards or guidelines, new possibilities for public information and education and new mechanisms for the integration of a wide range of local authority and national policies.

(iv) An air quality management plan is a set of procedures for dealing with the occasional occurrence of very poor air quality.

The air quality management plan is, therefore, assessed in relation to a number of NAAQS within which air quality must be maintained. An area where it is likely to exceed the NAAQS, an AQCR is created wherein, an action plan is developed by which air quality is brought within the NAAQS.

2.8 Options for Control of Vehicular Pollution

Rao [9] has discussed the following options to control the vehicular pollution:

(i) Reduction in amount of pollutants formed during combustion by suitable modifications in the internal combustion engine.
(ii) Development of exhaust system reactors that will complete the combustion process and change potential pollutants into more acceptable materials.
(iii) Development of alternative fuels that may produce low concentration of pollutants upon combustion.
(iv) Replacement of internal combustion engine with low pollution engines.
(v) Introduction of an effective inspection and maintenance (I & M) programme.
(vi) Phasing out of old vehicles.

2.9 Ambient Air Quality Standards

The ambient air quality is a dynamic and complex environmental phenomenon exhibiting relations with time and space. Ambient air quality standards are set to protect society and the environment from the harmful effects of air pollutants. They are designed to achieve a given desirable level of air quality, and frequently serve as a reference base for other standards such as emission standards and fuel quality standards [44]. Ambient air quality standards are of two types e.g. primary and secondary. Primary ambient air quality standards are directed towards the protection of the most vulnerable groups of population, mainly the young, the old and people in poor health. Short-term standards and guidelines are established to control *acute* effects that result when high levels of pollution persist for short periods. Typical short-term standards are for 1-, 8- and 24-hour average of pollutant concentrations. Long-term standards and guidelines are designed to protect human health from regular exposure to high levels of pollution over a long period of time e.g. one year or more [5].

Secondary ambient air quality standards are established for non-health impacts such as those involving soil crops, vegetations, man made materials, animals, wildlife, atmospheric visibility, property damage, transportation hazards and effects on the economy and personal comfort [45]. Its evaluation is the fundamental requirement towards assessment of the nature and extent of air quality variations.

2.10 Overview of Vehicular Pollution Modelling

There are two general approaches used in vehicular pollution modelling-deterministic and statistical [46]. Deterministic models calculate the pollutant concentration from an emission inventory and meteorological variables according to the solutions of differential equations, which represent the relevant physical processes. The models are developed with set of assumptions while deriving solution to differential equation. Deterministic models are most suitable for long term planning decisions [46, 47]. For vehicular pollution related episodes, characterized by fast dynamics, these models perform unsatisfactorily

[48, 49]. In contrast to deterministic models, statistical models are empirical models. They estimate the pollutant concentration by statistical equation, describing the relationship between *predictors* (meteorological and traffic parameters) and *predictant* (pollutant concentrations). In recent past, time series analysis technique, popularly known as Box-Jenkins' models [50, 51, 52] have widely been used to describe the dispersion of air pollutants on the local scale [17, 53, 54]. Previous studies [55, 56, 57, 58, 59] have indicated that the data of ambient air quality are stochastic time series, thereby making it possible to make a short term forecast on the basis of historical data. However, when applying the conventional time series model to the ambient air pollution forecast, the pollutant level variations are generally not simple autoregressive or moving average models [60]. In that case, the analyst has to employ statistical graphs of the autocorrelation function (ACF) and partial autocorrelation function (PACF) to identify an appropriate time series model. In the model identification stage, the resulting model quality frequently relies on individual's experience and knowledge of the time series statistics [61].

To overcome these shortcomings, the air quality modelers have used alternative techniques called "Artificial Neural Network (ANN)". The ANN approach is a promising alternative substitute to conventional time series models for forecasting vehicular pollution because of their special properties like, self-correction, self-learning and parallel processing [17, 61, 62].

3 Artificial Neutral Networks

3.1 General

Building intelligent systems that can model human behavior has captured the attention of the world in recent past. So, it is not surprising that a technology such as neural networks has generated great interest in pattern recognition. This chapter begins with a view of what neural networks are and why they are so appealing. A typical biological neuron is explained to understand the concept used in artificial neuron model. With this basic concept, a simple neuron model has been described including the fundamental elements of neural network, such as *input*, *hidden* and *output* layers and connection between the layers, types of neural network, transfer function and learning algorithm.

3.2 What Artificial Neural Networks are?

ANNs are parallel computational models comprising of densely interconnected adaptive processing units. These networks are fine-grained parallel implementation of nonlinear static or dynamic systems [63, 64]. Neural networks are intended for modelling the organizational principles of the central nervous system, expecting that the biologically inspired computing capabilities of the ANN will allow the cognitive and sensory tasks to be performed more easily and more satisfactorily then the conventional serial processor [65]. The important feature of these networks is their adaptive nature, where 'learning by example replaces programming' in solving problems [66]. This feature makes such computational models very appealing in application domains where one has little or incomplete

M. Khare and S.M. Shiva Nagendra: *Artificial Neutral Networks*, Artificial Neural Networks in Vehicular Pollution Modelling (SCI) **41,** 25–39 (2007)
www.springerlink.com

understanding of the problem to be solved and training data is readily available [67]. In general, neural networks can be thought of as a '*black box*' device that accepts *inputs* and produce *outputs*. Their applications are almost limitless but fall into a few simple categories namely data classification, modelling/forecasting and system control [68].

3.3 Basic Concepts of Neural Network

A neural network is a large-scale parallel network system consisting of a basic block called 'neuron'. These neurons are inter-connected in single or multi layers [66, 69]. These are biologically inspired i.e. they are composed of elements that perform in a manner that is analogous to the most elementary functions of the biological neurons. These elements are then organized in a way that may (or may not) be related to the anatomy of the brain. Despite this superficial resemblance, ANNs exhibit a number of brain characteristics [69].

A classical comparison of the information processing capabilities of the human and the computer is highlighted by an attempt to mechanize human information processing. The computer can multiply large numbers at high speed yet it cannot recognize unconstrained, speaker-independent speech [70]. Human abilities complement those of computer by easily recognizing speech, even when it is slurred and the environment is noisy. A conventional computer uses algorithm based program that operates serially and is controlled by a central processing unit, and stores information at addressed locations in memory. On the other hand, brain operates with highly distributed transformations that operate in parallel, have distributed control through thousands of interconnected neurons, and appear to store information as distributed correlation amongst the neurons [71, 72].

3.3.1 Human Biological Neuron

The human brain is made up of a vast network of computing elements called 'neurons', coupled with sensory receptors. The average human brain, roughly three pounds in weight and 90 cubic inches in

volume, is estimated to contain about 100 billion cells of various types. There are about 10 billion neurons in the human brain and remaining 90 billion cells are called 'glial' or 'glue cells', and these serve as support cells for the neuron [65]. The neuron is a fundamental unit of the biological nervous system. It is a simple processing unit, which receives and processes the signal from other neuron through its paths called 'dendrites' (Figure 3.1). An activity of a neuron is an 'all-or-none' process. If the combined signal is strong enough, it generates the output signal to its output path

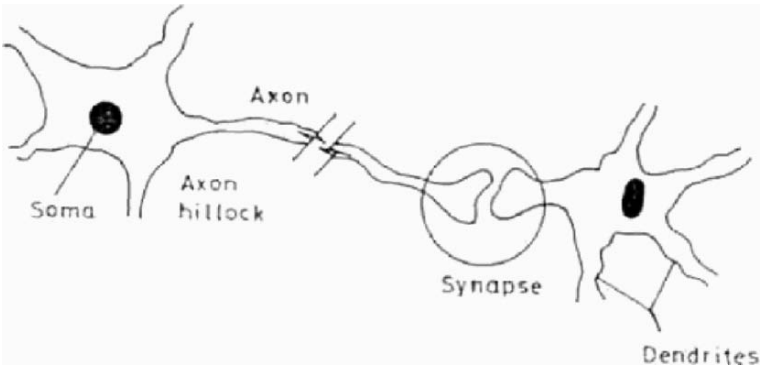

Fig. 3.1. Basic neurobiology of man.

(called axon) which splits up and connects the other neurons input paths through a junction referred to as a 'synapse'. The amount of signals transferred, depends upon the synaptic strength of the junction which is chemical in nature. This synaptic strength is found to be modified during the learning process of the brain; therefore, it can be considered as a memory unit of each interconnection [66]. Following are the basic characteristics of a neural network:

(i) It consists of simple processing units called 'neurons', which perform local computation on their input to produce an output.
(ii) Memory and processing elements of neural network are collocated.
(iii) Neural networks are trained by adjusting the connection weights.
(iv) Knowledge stored in the neural network is adaptable.

(v) Neural networks are self-organized (arrangement of hidden layer neurons) during learning process.

3.3.2 Simple Neuron Model

McCulloch and Pitts [73] developed the first artificial neuron to mimic the characteristics of biological neuron. In essence, a set of inputs is applied, each representing the output of another neuron. Each input is multiplied by a corresponding weight, analogous to a synaptic strength, and all of the weighted inputs are then summed to determine activation level of the neuron. Figure 3.2 shows a simple neuron model designed by McCulloch and Pitts. A set of inputs

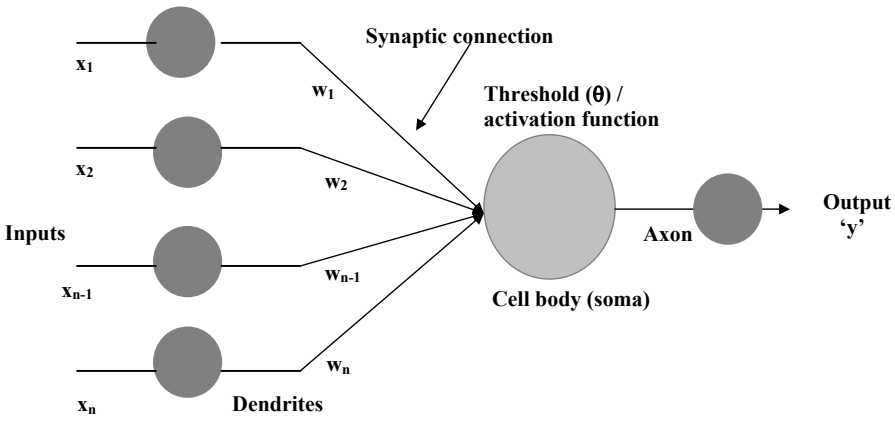

Fig. 3.2. Simple neuron model first designed by McCulloch and Pitts [73].

labeled X_1, X_2, X_3…. X_n is applied to the artificial neuron. These inputs collectively referred to as the vector 'X', corresponding to the signals into the synapse of a biological neuron. Each signal is multiplied by an associated weight W_1, W_2, W_3,…. W_n before it is applied to the threshold unit (Y = threshold constant). Each weight corresponds to the "strength" of a single biological synaptic connection, collectively refereed to as vector 'W'. The threshold unit, corresponding roughly to the biological cell body, adds all of the

weighted inputs algebraically and processed by an activation function to produce the neurons output signal ‘y’ [65]. The threshold logic unit (TLU) computes a neuron output value ‘y’, according to the equation 3.1:

$$y = \begin{cases} 1 & if \sum_{i=1}^{n} w_i \, x_i \geq 0 \\ 0 & otherwise \end{cases} \tag{3.1}$$

3.4 History of Artificial Neural Network

Pattern recognition is one of the reasonable methodologies for evaluation of a process and a sound basis for decision making. Patterns are either derived from a series of several accompanying experiments or they are estimate of ‘state’ variables. There are three main pattern recognition methods- statistical pattern recognition, subspace pattern recognition and fuzzy pattern recognition [74].

The recent progress in artificial intelligence and neural computation has been attracting much attention in the field of pattern recognition. From last five decades, scientists are trying to emulate the real neural structure of human brain and to develop an algorithm equivalent to the learning process. According to Mammone [75], ANN was first used in the 1940’s, when McCulloch and Pitts [73] proposed a computational model based on a simple neuron-like logical element. Donald Hebb [76] have described a learning rule for adapting the connection strength of these artificial neurons, which is also called as famous ‘Hebbian learning rule’ or ‘Delta rule’ [66]. In the 1950’s and 1960’s a group of researcher have combined these biological and psychological insights to produce the first ANNs [69]. Later, Rosenblatt [77] has constructed a perceptron- an arrangement of processing elements representing the nerve cells into a network (single layer of artificial neurons). These networks are applied to diverse problems such as weather prediction, electrocardiogram analysis, and artificial vision. Minsky and Papert [78] have

derived that the single layer networks when in use, are theoretically incapable of solving many simple problems. Nevertheless, a few dedicated scientists such as Jeuvo Kohonen, Stephan Grossberg and James Anderson continued their efforts in this field.

In the past few years, ANN theory has been translated into application. With four major conventions in 1987 in the field of ANNs, and several hundred technical papers published, the growth rate has been phenomenal. Werbos [79], Parker [80] and Rumelthart, Hinton and Williams [81] have developed independently back-propagation algorithm, which provided a systematic means for training multilayer networks.

3.5 Artificial Neural Network Architecture

ANN architecture includes defining the number of layers, the number of neurons in each layer, and the interconnection scheme between the neurons. Figure 3.3 shows neural network architecture for three-layer network with fully connected neurons of different layers. Selection of number of layers is controlled by training algorithm. Some training algorithms may require only one layer while other may require a minimum of three layers. For instance, back-propagation algorithm requires an input layer, an output layer and a hidden layer. The number of hidden layers is selected based upon the problem complexity. The number of 'neurons' in input and output layer is problem specific. The interconnections between 'neurons' are controlled by the training algorithm and the nature of the problem.

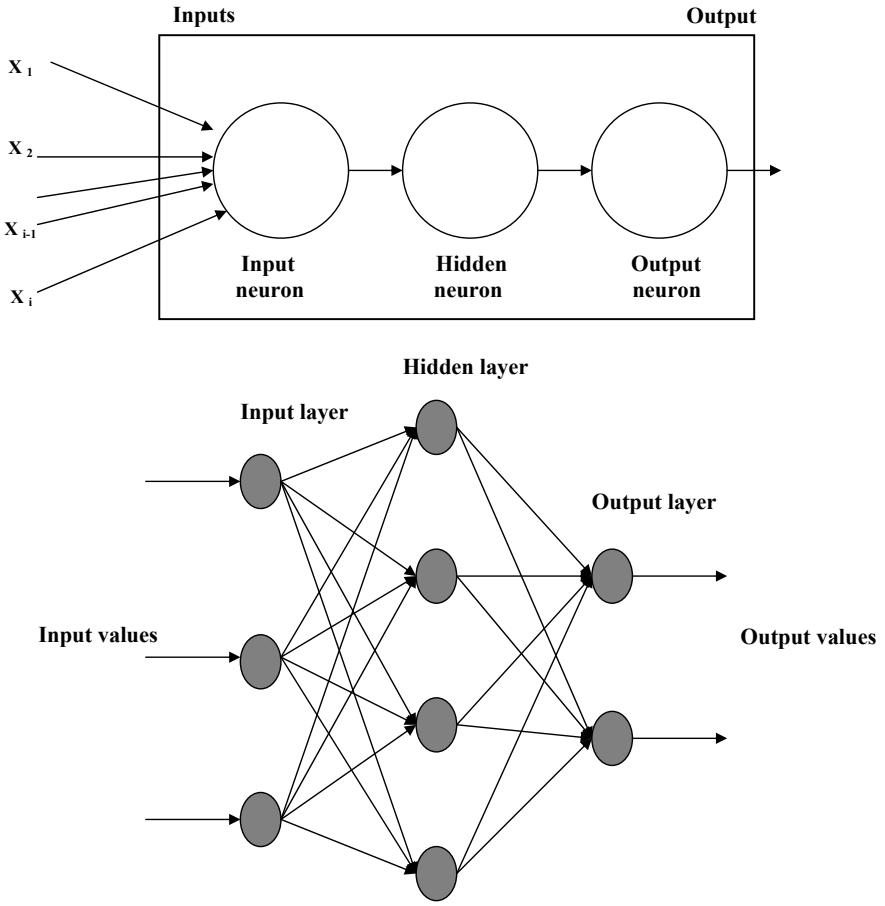

Fig. 3.3. Configuration of multilayer artificial neural network.

3.6 Types of Neural Networks

ANN's are broadly classified into 'non –recurrent' (feed-forward) and 'recurrent' (involving feed back) neural networks. Figure 3.4 illustrates the taxonomy of the neural networks.

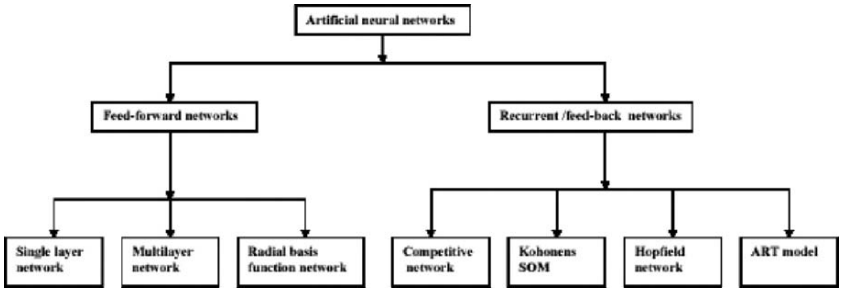

Fig. 3.4. A taxonomy of neural network architecture.

3.6.1 Feed-Forward Networks

A feed-forward network (FFN) has input, output and hidden layers (Figure 3.5a). It also has subgroups of processing elements. A layer of processing elements makes independent computations on data that it receives and passes the results to another layer. The next layer may in turn make its independent computations and passes on the result to yet another layer. Finally, a subgroup of one or more processing elements determines the output from the network. Each processing element makes its computation based upon a weighted sum of its inputs. A threshold function is some times used to quantify the output of a neuron in the output layer.

3.6.2 Recurrent Neural Networks

A recurrent neural network (RNN) has feedback paths, which makes it a 'sequential' rather than a 'combinatorial' network, permitting it to exhibit temporal behavior. All possible connections between neurons are allowed. Once cyclic connections are included, a neural network becomes a non-linear dynamic system. Such a system has very rich temporal and spatial behavior. These behaviors can be utilized to model certain cognitive functions, such as associative memory, unsupervised learning, self organizing maps, and temporal reasoning. Figure 3.5b illustrate recurrent networks with the hidden

neurons. The feedback connections shown in the figure originate from the hidden neurons as well as from the output neurons. RNNs with cyclic connections are much harder to analyze and describe than FFN, reflecting the difficulties of limited mathematical tools for non-linear dynamic systems. Multilayer FFN's have proved to be extremely successful in pattern recognition problems, while RNN's have been used in associative memories as well as for the solution of optimization problems [74].

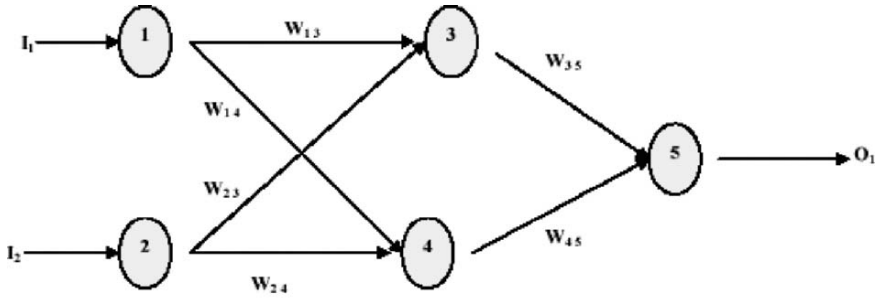

a) Feed forward network

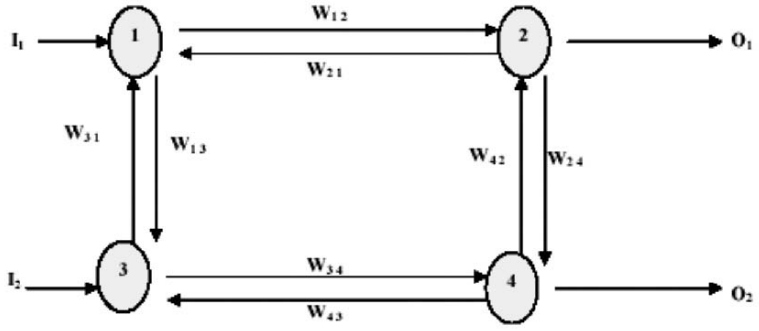

b) Recurrent neural network

Fig. 3.5. Types of neural networks.

3.7 Transfer Functions and Learning Algorithms

The transfer function and learning algorithm are two important components of information processing in neural networks.

3.7.1 Transfer Functions

The transfer function is the mechanism of translating input signals to output signals for each processing element. There are three types of transfer functions, as listed below:

(i) Hard limit transfer function (Step function)
(ii) Linear transfer function (Ramp function)
(iii) Log –Sigmoid transfer function (Sigmoid function)

Log-Sigmoid transfer function (Sigmoid function) is the most commonly used function in air quality modelling [18, 67, 82, 83]. Figure 3.6 describes the Sigmoid transfer function, which has a graph similar to a stretched letter 'S'. It consists of two functions- logistic and tangential. The values of tangent function vary from –1 to +1 and for logistic function, between 0 and 1.

3.7.2 Learning Methods

A 'learning' process, or 'training', forms the interconnections (correlations) between neurons. It is accomplished by providing known input and output data in an ordered manner to the neural network. The learning corresponds to parameter (weight) changes. A network can be subjected to 'supervised' or 'unsupervised' learning. In former case, external prototypes are used as 'target' outputs for specific inputs, and the network is given a learning algorithm to follow and calculate new connection 'weights' that bring the output closer to the 'target' output. Unsupervised learning is the sort of learning that takes place without a 'teacher'. In learning without supervision, the desired response is not known, thus explicit error information cannot be used to improve network behavior.

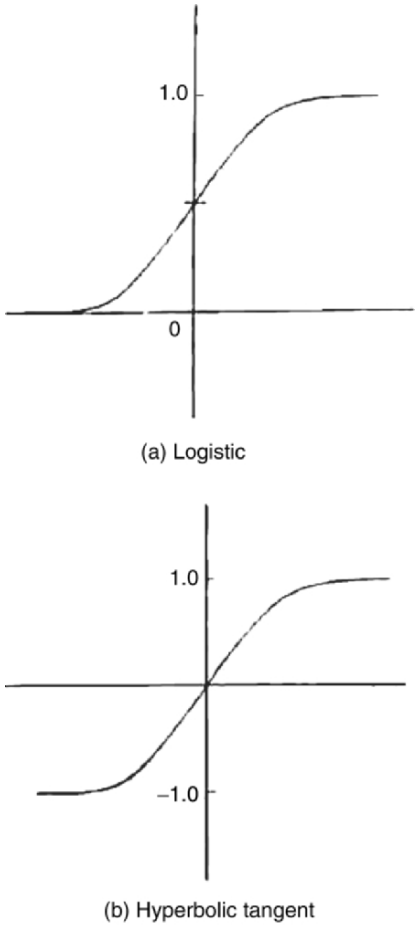

Fig. 3.6. Sigmoid transfer function.

Most of the neural networks are trained using a 'supervised' learning algorithm. There are several supervised learning algorithms, but one of the most widely used is back-propagation algorithm.

3.8 Back-Propagation Learning Algorithm

According to Rao and Rao [63], Paul Werbos has developed the back-propagation training algorithm for FFN and later Parker, and

Rumelhart and McClelland [84] have improved it. The back-propagation training algorithm uses gradient descent procedure to locate the absolute (or global) minimum of the error surface. In back-propagation, there are two phases in its learning cycle- *one*, to propagate the input pattern through the network and the *other*, to adopt the output by changing the weights in the network. It is the error signals that are back-propagated in the network operation to the hidden layer(s). The error in the output layers is used as a basis for adjustment of connection weights between the input and hidden layers. The adjustment of connection weights between the input and the hidden layers and subsequent recalculation of the output values become an iterative process which is carried out until the error falls below a tolerance level. A momentum parameter can be used in scaling the adjustment from a previous iteration and adding to the adjustments in the current iteration.

Before starting the training process, the weights in the network are initially set to small random values. This is synonymous with selecting a random point on the error surface. The back-propagation algorithm then calculates the local gradient of the error surface and changes the weights in the direction of steepest local gradient.

The back-propagation training process starts by inputting training data set to the network. The training data set consists of input and output vectors. When these vectors sequentially presented to the neural network, the following calculations are performed.

$$Z_j = \Sigma\, W_{ij}\, (X_i + b_j), \quad i = 1,2,\ldots.n\ ;\ j = 1,2,\ldots..H \tag{3.2}$$

Where Z_j = input to the j^{th} hidden layer neuron.
X_i = numerical value of the i^{th} input vector.
W_{ij} = weight of the i^{th} input layer neuron to the j^{th} hidden layer neuron.
N = number of input layer neurons.
H = number of hidden layer neurons.
B = bias value for the j^{th} hidden layer neuron.

The output of hidden layer using sigmoid function, is calculated as follows.

$$h_j = f(Z_j) = \frac{1}{(1 + e^{-Z_j})} \qquad j = 1,2,.....H \tag{3.3}$$

where h_j = output of the hidden layer neuron, j.
f = transfer function for the hidden layer.

In the training process, the network output, in general, may not be equal to the desired output. Consequently, the output error is calculated as the difference between the network output and the desired output. If the output error does not achieve the tolerance level, the network modifies the connection weights according to the value of the output error; then, training data are inputted again to the network and the network output is calculated. The training cycle is continued until the network achieves the desired tolerance level. If the error value is within the tolerance limit, the network becomes a 'trained' network. Thus, the back-propagation algorithm is summarized into seven steps:

(i) initialize the network weights,
(ii) present the first input vector, from the training data, to the network,
(iii) propagate the input vector through the network to obtain an output,
(iv) calculate an error signal by computing actual output to the desired (target) output,
(v) propagate error signal back through the network,
(vi) adjust weights to minimize the overall error,
(vii) repeat steps (ii) to (vii) with next input vector, until overall error is satisfactorily small.

The above implementation of the back-propagation algorithm is known as on line training, whereby, the network weights are adopted after each pattern has been presented. The alternative is known as batch training, where the summed error for all patterns is used to update the weights. The benefits of each approach are discussed in Battii [85]. In practice, many hundreds of training iterations are required

before the network error reaches a satisfactory level. The training should be stopped when the performance of the neural network on independent test data reaches a maximum [18,86]. The error surface contains more than one minima, global or local (Figure 3.7). It is desirable that the training algorithm does not become trapped in local minimum.

The back-propagation algorithm contains two adjustable parameters, a learning rate (η) and a moment term (μ), which can assist the training process in avoiding local minima. The 'η' determines the step taken along the iterative gradient descent learning process. If this is

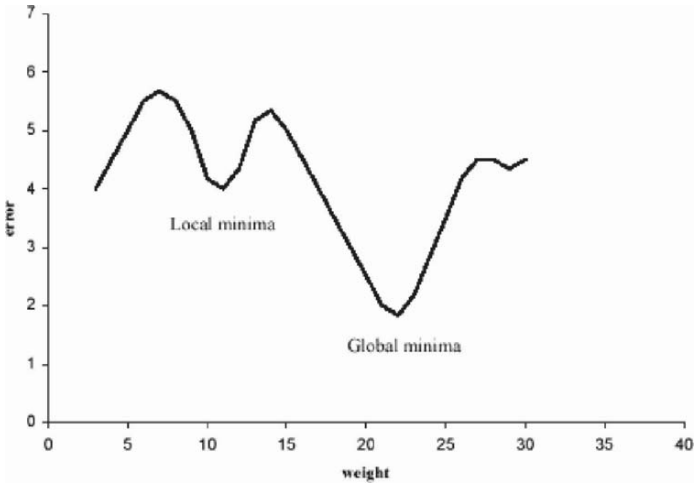

Fig. 3.7. Neural network error surface in two dimensional space.

too large then the network error will change erratically due to large weight changes, with the possibility of jumping over global minima. Conversely, if the 'η' is too small then training will take a long time. The 'μ' is used to assist the gradient descent process if it becomes stuck in a local minimum. By adding a proportion of the previous weight change to the current weight change (which will be very small in a local minimum), it is possible that the weight can escape the local minimum. By selecting a suitable set of connecting weight and transfer functions, it has been proved that a neural networks can approximate any smooth function, measurable function between the input and output vectors [87]. A schematic, illustrating the iterative

training procedure using the back-propagation algorithm is shown in Figure 3.8.

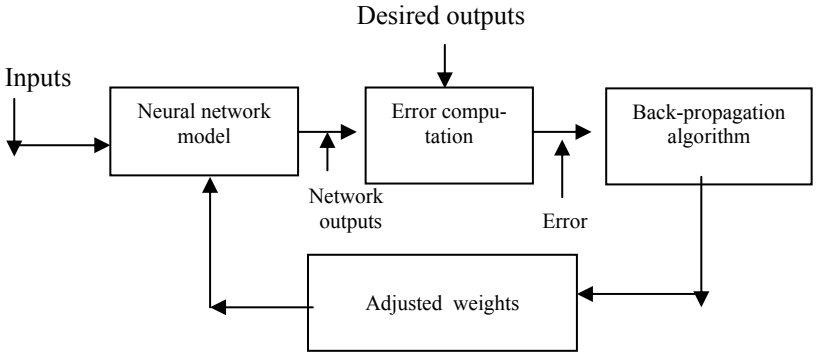

Fig. 3.8. Schematic of neural network training by back-propagation algorithm.

3.9 Summary

ANN's are biologically inspired parallel computational models. They are useful tools for prediction/forecasting, function approximation and classification. In general, FFN's are applied for air pollution forecasting problems. The transfer function and the learning algorithm are two important components of ANN based modelling. The sigmoid function is the most commonly used function in air quality modelling. Back-propagation is one of the most widely used supervised training algorithms, because of its mathematical simplicity. Neural networks can be used for problems that cannot be solved with known formula and for problems with incomplete or noisy data. Neural networks seem to have the capability to recognize patterns in the data presented to it, and are thus useful in many types of pattern recognition problems.

4 Vehicular Pollution Modelling – Conventional Approach

In last five decades, a number of vehicular pollution models based on deterministic and/or stochastic techniques have been developed describing temporal and spatial distribution of exhaust emissions on roadways. However, during the recent past, ANN technique has become one of the upcoming techniques in modelling the exhaust emission dispersion phenomena. In the following sections, existing literature on deterministic, numerical, statistical and ANN based exhaust emission dispersion models have been reviewed. The limitations associated with deterministic and statistical approach have also been discussed.

4.1 General

Vehicular pollution models, also known as line source models, are widely used to study the dispersion characteristics of exhaust emissions near the roadways [88]. These models provide theoretical estimates of air pollution concentrations, as well as temporal and spatial variations for the present and future conditions. They are used in almost all aspects of urban air quality planning. The models are used to assess the current and potential future air quality due to vehicular emissions for framing policy decisions. The current vehicular emissions and meteorological data are used as 'input' to the line source dispersion models to forecast future changes based on 'what if' scenarios [89]. The modelling approaches includes deterministic, statistical, hybrid of deterministic and statistical distribution and artificial neural network [17].

M. Khare and S.M. Shiva Nagendra: *Vehicular Pollution Modelling – Conventional Approach*, Artificial Neural Networks in Vehicular Pollution Modelling (SCI) **41,** 41–66 (2007)
www.springerlink.com

4.2 Theoretical Approaches of Vehicular Pollution Modelling

The deterministic mathematical models estimate the pollutant concentrations from emission inventory and meteorological variables, according to solution of various equations that represent the relevant physical processes. In other words, differential equation is developed by relating the rate of change of pollutant concentration in terms of average wind and turbulent diffusion, which, in turn, is derived from the mass conservation principle. The common Gaussian line source model is based on the superposition principle, namely concentration at a receptor, which is the sum of concentrations from all the infinitesimal point sources making up a line source. This mechanism of diffusion from each point source is assumed to be independent of the presence of other point sources. The other assumption considered in deterministic model, is the emission from a point source spreading in the atmosphere in the form of a plume, whose concentration profile is generally Gaussian in both horizontal and vertical directions. Considering the above assumptions, the basic approach to develop deterministic line source model is the coordinate transformation between wind coordinate system (X_1, Y_1, Z_1) and line source coordinate system (X, Y, Z). Figure 4.1 shows the details of line source and wind coordinate systems. Let the length of the roadway be 'L', which makes an angle 'θ' with the wind vector. The middle point of the line source can be assumed as 'origin' for both coordinate systems, having same Z-axis. The line source is along 'Y-axis' and the wind vector is in the X_1 direction. In the line source coordinate system all parameters viz., X, Y, Z and L are known from the road geometry. A hypothetical line source is assumed to exist along Y_1 that makes the wind direction perpendicular to it. Eq. 4.1 gives the concentration at the receptor [90].

$$C = \frac{Q_L}{2\pi\sigma'_Y \sigma'_Z \bar{u}} \left[\exp\left\{ -\frac{1}{2}\left(\frac{Z-H}{\sigma'_Z} \right)^2 \right\} + \exp\left\{ -\frac{1}{2}\left(\frac{Z+H}{\sigma'_Z} \right)^2 \right\} \right] x \int_{-L/2}^{L/2} \exp\left[-\frac{1}{2}\left(\frac{Y_1' - Y_1}{\sigma'_Y} \right)^2 \right] dY_1' \tag{4.1}$$

where, Q_L = line source strength (unit/ m^3); $\sigma 9_Y$, $\sigma 9_Z$ = horizontal and vertical dispersion coefficients respectively, and are functions of distance X and stability class; X_1 = receptor distance from the line

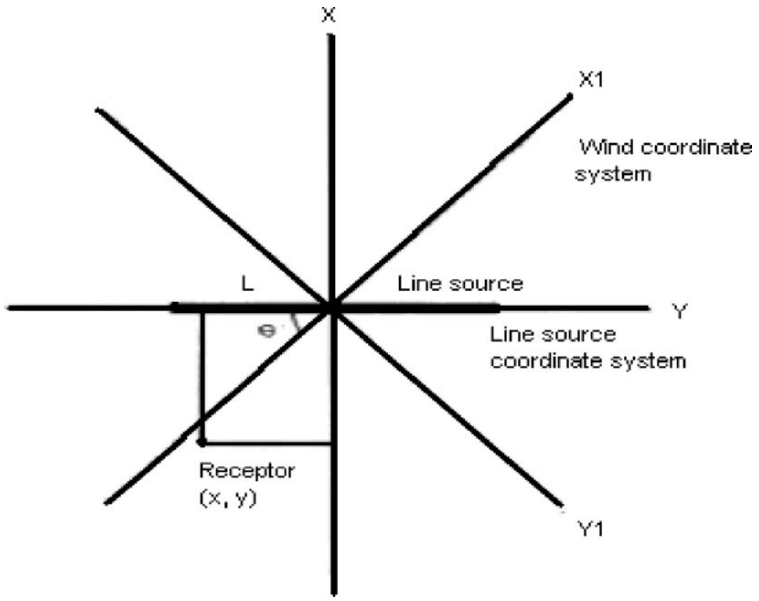

Fig. 4.1. Orientation of line source and wind direction coordinate system.

source; Z = receptor height above ground level (m); H = height of line source (m); u = the mean ambient wind speed at source height (m/s); L= length of the roadway (m).

Using the above relationship between wind and line source coordinate system, Luhar and Patil [91] have developed a general finite line source model (GFLSM) as given below:

$$C = \frac{Q_L}{2\sqrt{2\pi}\sigma_Z \bar{u}_e}\left[\exp\left\{-\frac{1}{2}\left(\frac{Z-h_o}{\sigma_Z}\right)^2\right\} + \exp\left\{-\frac{1}{2}\left(\frac{Z+h_o}{\sigma_Z}\right)^2\right\}\right] x \left[erf\left\{-\frac{\sin\theta\left(\frac{L}{2}-Y\right) - X\cos\theta}{\sqrt{2}\sigma_Y}\right\} + erf\left\{-\frac{\sin\theta\left(\frac{L}{2}+Y\right) + X\cos\theta}{\sqrt{2}\sigma_Y}\right\}\right] \tag{4.2}$$

where, θ makes angle between roadway and wind direction, $u_e = u \sin\theta + u_o$, u_o is wind speed correction due to traffic wake[92], $h_o = H + H_p$, H_p = plume rise. The detailed formulation of the equation (4.2) has been discussed in Appendix-A. Numerical line source modelling is based on numerical approximation of partial differential equations representing atmospheric dispersion phenomena. First order closure models, also called K- models, have their common

roots in the atmospheric diffusion equation derived by using K-theory approximation for the closure of the turbulent diffusion equation. These models are time dependent and applied through computer codes; Eulerian grid, Lagrangian trajectory, The Eulerian-Lagrangian and Random Walk Particle Trajectory approaches are some very commonly used techniques. Juda, [46] has given detailed methodology for developing the numerical line source models. In contrast to deterministic modelling, the statistical models calculate concentrations by statistical methods from meteorological and traffic parameters after an appropriate statistical relationship has been obtained empirically from measured concentrations. Regression, multiple regression and time series technique are some of the commonly used methods. The time series analysis techniques (Box–Jenkins models) are widely used to describe the dispersion of exhaust emissions at trafficked intersection and at busy arterial roads. Autoregressive integrated moving averages (ARIMA), ARIMA with exogenous inputs (ARMAX) and transfer function noise (TFN) algorithm have been adopted in line source modelling studies [59]. The Box–Jenkins [51, 52] models are empirical models and it is important that the iterative model building process proposed by Box and Jenkins is always followed. Further, ARIMA models do not specifically distinguish the physical causes of dispersion phenomena (e.g. meteorological variables, emission rates of the sources, etc.) in their input. Such models represent 'black box' approach. All possible uncertainties of the model are taken into account by the 'noise' variable with assigned statistical properties [46]. The TFN model is a dynamic model describing the dependent variable as a response to the 'impulses' of the independent variables, with the latter playing the role of time dependent forcing functions in an ordinary linear differential equation. The characteristics of the response are described by the impulse response functions. The technique is quite general and useful in handling multivariate time series. It specifically builds into the model dynamics of impulse and response that is capable of describing a wide range of physical phenomena (in linear regime). One important feature of TFN modelling is its inherent capability of avoiding spurious correlations and true causality in time series [53]. The formulation of univariate B-J model for forecasting CO concentrations on urban roadways has been presented in

Appendix-B. The hybrid approach as described by Jakeman et al. [93], combine the useful components of both deterministic and statistical models. The hybrid approach facilitates strengthening of the deterministic model's prediction accuracies i.e. to use it for predicting concentrations that occur relatively frequently (mean pollutant concentrations). The statistical component is used to analyze the parametric distributional form of air pollutant data to estimate percentiles including *extreme values*. This approach is based largely on the ability of deterministic models to make *causal* links between emissions, meteorology and mean ground level concentrations and the ability of statistical models to predict the distribution of all events about mean, once the appropriate distributional form is identified for the historical air pollution data [93]. The hybrid approach first uses the pollutant concentration data generated by the deterministic model within its range of greatest reliability. Then the parameters of suitable statistical model are estimated from this *truncated* sample. Once parameterized by a suitable estimation method, the statistical component then provides a description of air quality data for the entire range of percentiles.

ANN is a kind of statistical modelling technique offering several advantages over traditional phenomenological or semi-empirical models, since they require known input data set without any assumptions [17, 62]. For line source modelling, the multilayer neural network seems to be the most suitable for predicting exhaust emissions [94]. The multilayer neural network consists of a system of layered interconnected 'neurons' or 'nodes' as illustrated in Figure 4.2. The neural network model (Figure 4.2) represents a non-linear mapping between an input vector and output vector [18]. The 'nodes' are arranged to form an input layer, one or more 'hidden' layers, and an output layer with nodes in each layer connected to all nodes in neighboring layers [82]. The input layer 'neurons' serve as a buffer that distribute input signals to the next layer, which is a hidden layer. Each 'neuron' in the hidden layer sums its input signal, processes it with simple non-linear *transfer* or *activation* function (e.g., logistic and hyperbolic tangent), and distributes the result to the output layer. The 'neurons' in the output layer compute their output signal in the similar manner. The output signals from each neuron in multilayer neural network

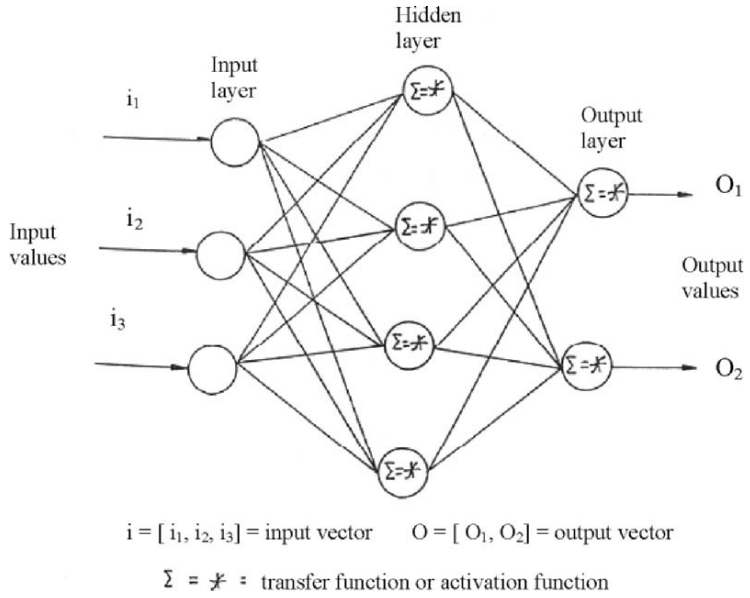

Fig. 4.2. A multilayer neural network with hidden layer.

propagate in forward direction; therefore multilayer neural network is also called as 'FFN' neural network [86]. A multilayer neural network can approximate any smooth, measurable function between input and output vectors by selecting a suitable set of connecting weights and transfer functions [87]. Multilayer neural network has the ability to learn through training. A supervised back-propagation algorithm is commonly employed in training of multilayer neural network [86]. Training requires a set of data, which consists of a series of input and associated output vectors. During training, the multilayer neural network is repeatedly presented with training data, and the weights in the network are adjusted until the desired input - output mapping occurs. During training, the output from the multilayer neural network is compared with desired output. If the network output is not matched with desired output, an error signal is propagated back through the network. Training uses the magnitude of these error signals to adjust the weights and the process continues till the network output matches the desired output.

4.3 Vehicular Pollution Deterministic Models

Historically, the work of Sutton [95] may be regarded as first of its kind in air quality modelling. One of the early studies on deterministic vehicular pollution modelling has been reported in Waller et al. [96]. The analytical method for estimating the pollution levels from motor vehicles in the vicinity of highways of common geometric configuration has been developed by Chen and March [97]. The preliminary computational examples indicate that this method is capable of representing, in a realistic manner, of all the physical variations accounted in the derivation. Dilley and Yen [98] have derived an analytical solution to a two-dimensional transport and diffusion equation that describes the downwind pollutant concentration from an infinite crosswind line source. Both large scale and mesoscale winds are included in their model. Further, the analysis shows that mesoscale winds are not significant in reducing pollutant concentration. Peters and Klinzing [99] describe two separate equations for ground level as well as elevated line source, and analyze the effects of diffusion coefficient in line source dispersion. Using diffusion equation, Lamb and Neiburger [100] have come out with a model for computing pollutant concentrations resulting from both point and line sources. Later, this model has been tested with respect to its diffusion characteristics by computing the hourly CO concentrations on a particular day, at 760 locations in the Los Angeles basin. The model results show reasonably good agreement with observed values. Csanady [90] has developed a hypothetical model for a finite line source and it is applicable only when the wind is perpendicular to the roadway. Calder [101] has studied the effect of oblique wind on line source pollution dispersion near roadways. He describes that the concentration at roadside receptor increases marginally, as wind direction becomes parallel to highway. Dabberdt et al. [102] have presented a practical multipurpose urban diffusion model (APRAC-1A) for predicting inert vehicular pollutant concentration. The model requires routinely available meteorological and traffic parameters for prediction of concentration isopleths, sequential hourly values and frequency distributions. A model for the diffusion of pollutants from a line source in an urban atmosphere has also been developed by

Sharma and Myrup [103]. This study reveals that wind shear (variation of wind with height) is responsible for turbulent diffusion in lower atmosphere. Based on the finite length approximation, Stukel et al. [104] have formulated a line source dispersion model for estimating particulate/gaseous pollutant concentration in urban roadways. In another study, Nicholson [105] have presented a scalar budget box diffusion model for prediction of CO concentration in street canyons. Fay and King [106] have formulated a Gaussian model, considering vehicle-induced effects on the dispersion of pollutants. This model assumes that vehicle wake induced turbulence dominates over the natural turbulence near the road. Therefore, dispersion of pollutants is assumed to be independent of atmospheric parameters except wind speed, and dependent upon the drag characteristics of passing vehicles.

The General Motor (GM) corporation experiments as reported by Cadle et al. [107] are the earliest field experiments used for understanding traffic influences on adjacent roadways. These data have been measured over a simulated test track of four lanes free way of 5 km long at the GM proving grounds in Milford, Michigan, U.S.A. Chock [108] has conducted a number of experiments to evaluate the influence of traffic on the dispersion of pollutants near urban roadways. He has observed the variations in upwind dispersion due to crossroad wind, which has occurred within a few meters of the road. The U.S. EPA has developed a number of air pollution models for highways, which include CALINE [88], EGAMA [109], and HIWAY [110]. The HIWAY model is based on the Gaussian equation with the assumption of a series of finite line sources. CALINE model is also Gaussian based line source model, but it has got separate equations for calculating pollutant concentration under cross-wind and parallel wind conditions. Chock [111] and Noll et al. [112] have evaluated these models and found that the EPA-HIWAY model overestimates pollutant concentrations adjacent to the highway. This model avoids the cumbersome integration necessary for conventional Gaussian model that makes point source assumption; instead, it uses an infinite line source approach and specifies one dispersion parameter as a function of wind road orientation from the source. Later, a series of improved versions of CALINE model viz. CALINE-2, CALINE-3 and CALINE-4 have been developed by

Ward et al. [113] and Benson [114,115]. Middleton et al. [116] have developed a dispersion model for estimating the concentration of inert gaseous pollutants from the curved circular and straight sections of a complex road interchange. For small wind angles, pollutant concentration predicted from finite road length matches well with the concentration estimates obtained from infinite line source model. For complex roadway geometry, Colwill et al. [117] have conducted experiments to observe change in pollutant concentration over a short distance at a site downwind of an isolated motorway and within a road complex. DeTar [118] has come out with a model which estimates the concentration of pollutants from line sources. This model is applicable at various receptor heights, distances, wind speed and direction. In another study, Green et al. [119] have found that the actual ground level concentrations may decrease with decreasing wind speed particularly when it drops below some critical value. Data from an ongoing model validation program for dispersion of pollutants from roadways in Texas has shown that pollutant concentrations do not increase with decreasing wind speed as predicted by most models that are based on Gaussian formulation. Rao et al. [120] have studied the impact of traffic-induced turbulence on the near roadway dispersion of air pollutants. The study concludes that, there is a noticeable augmentation of turbulent kinetic energy due to wake generated by moving traffic. Later, Rao et al. [121] have evaluated four Gaussian models, namely, GM [92], HIWAY [110], AIRPOL-4 [122], CALINE-2 [113] and three numerical models – DANARD [123], MROAD-2 [124] and ROADS [125]. Their comparative results have shown that GM model simulations are more precise than any other models. Peterson [126] has presented an updated version of HIWAY model i.e. HIWAY –2, released by EPA in May 1980. The latter model gives more realistic concentration estimates as it uses an updated dispersion algorithm. Rao and Keenan [127] have modified the Pasquill-Grfford dispersion curves of the EPA - HIWAY model, and have found that modified HIWAY model (HIWAY-3) better simulates the near roadway dispersion when compared to original HIWAY model. Further, an empirical aerodynamic drag factor has also been developed to handle pollutant dispersion under low wind conditions. Later, the HIWAY-4 (an improved version of HIWAY-3) has been developed in which the

modified dispersion curves and aerodynamic drag factor are incorporated. Chang et al. [128] have evaluated the EPA rollback (EPARM) and the generalized rollback (GRM) models. Both models show similar predictions when identical inputs were used for estimation. Sedefian et al. [129] have utilized data from GM dispersion experiments to assess the characteristics of traffic-generated turbulence and its effects on the dispersion process near roadways. It is observed that the dispersion next to highway is greatly influenced by the traffic and its influence decreasing considerably at further downwind distances vis - a - vis at higher elevations. However, at low wind speeds the traffic contribution to the total diffusivity is about 50% at a downwind distance of 30 m. Munshi and Patil [130] have first used analytical models for estimating the vehicular pollution dispersion on Indian urban roadways under heterogeneous traffic conditions [*heterogeneity in traffic refers to categories of vehicles having different axel weight, size, and shape moving in the same lane and constituting mixed traffic conditions*]. Hickman and Colwill [131] have described a simple and effective method of estimating pollutant concentrations around highways using the empirically modified Gaussian dispersion theory. It accurately represents the roadside situation. This model later has been calibrated and validated with the measured CO concentration at three different locations in UK. Using Texas and GM data, Rodden et al. [132] have evaluated 5-line source dispersion models namely, CALINE-3, CALINE-2, AIRPOL-4, HIWAY and TRAPS-IIM [133]. All four models show poor performance when compared with observed data. Eskridge and Rao [134] have discussed the time resolution and vertical spacing necessary to resolve vehicle wake turbulence and the role of pseudo turbulence in modelling pollutant diffusion near roadways. The study reveals that velocity variances in GM experiment data are dominated by 'wake passing effect' (time variation in the wind velocity as the vehicles wake passes the observation point), and are inadequate to resolve the wake turbulence effect. Nelli et al. [135] has developed the Texas Instrumentation model (TEXIN) for predicating air quality near roadway intersections. Later, the TEXIN model predictions have been compared with predictions of three intersection models - inter section midblock model, program MICRO and indirect source guidelines. The results show that TEXIN model

predictions are better than other three models. Using the Gaussian equation, Segal [136] has presented a graphical input microcomputer model (GIMM) for predicting CO concentration from different types of line sources. Hickman and Waterfield [137] have developed a computer code for predicting air pollutant concentrations from roadway traffic. The code has provided a wide range of information required for air quality assessment, such as, concentration of pollutants corresponding to traffic flows, weather conditions and exposure periods. Cohn and Gaddipati [138] have developed an interactive graphics method for highway air pollution analysis. This approach has resolved problems associated with use of coordinates in CALINE-3 and HIWAY-2 models. Padmanabhamurthy and Gupta [139] have described meteorological aspects of air pollution dispersion. Later, Beiruti and Al-Omishy [140] have developed a digital computer simulation of the traffic flow and used this simulation model to predict NO_2 and HC concentrations at three busy traffic roads in Baghdad, Iraq. Cooper [141] has reviewed various models used for estimating the impact of indirect sources on air quality. A methodology for predicting 8-hour concentration by using 1-hour CO concentrations has also been discussed. Hlavinka et al. [142] have developed an improved version of TEXIN model i.e. TEXIN-2. This model uses critical movement analysis (CMA) - for estimating traffic flow parameters; MOBILE-3 - to determine free flowing traffic cruise emissions; and CALINE-3 - to model the pollutant distribution downwind of an intersection. Kunler et al. [143] have discussed the applicability of various air quality models in describing the dispersion of car exhaust emissions and its effect on forest cover. Hoydysh et al. [144] have used four distinct approaches i.e. solution of the Navier-stokes equations, two dimensional semi-empirical models, zero-dimensional semi-empirical models and empirical adaptation of Gaussian line source dispersion to model air flow and mass dispersion in street canyons. The results indicate that none of the approaches give accurate distribution of pollutant concentrations in street canyons. In another study, Khalil and Rasmussen [145] have applied a chemical mass balance (CMB) model for CO apportionment among residential wood burning sources and automobile sources in Olympia, Washington. Gronskei [146] has studied the influence of car speed on dispersion of exhaust emissions. He has

observed that vertical diffusion of exhaust gas increases with increase in the speed. His experimental results, when compared with HIWAY-2 predictions, show that HIWAY-2 under-predicts the pollutant concentrations. Sculley [147] has reviewed four representative approaches namely, IIM, MICRO2, TEXIN2 and CALINE4. The study suggests an alternative emission analysis procedure, which can be used in standard line source models to estimate the dispersion at the intersections. Using historical meteorological and vehicular data, Cooper [148] has derived 'meteorological persistence factor' (MPF) and 'vehicular persistence factor' (VPF) for the Florida City. Further, a worst case 'total persistence factor (TPF)' has also been derived. The TPF equals to the product of the mean annual second highest MPF and the mean VPF. Luhar and Patil [91] have developed a simple general finite line source model (GFLSM) based on Gaussian diffusion equation, pertaining to Bombay traffic conditions. The GFLSM predictions are compared with GM, CALINE-3 and HIWAY-2 model predictions. The results show satisfactory performance of the GFLSM for Indian traffic conditions. Singh et al. [149] have developed an analytical dispersion model (IITCO) for computing CO concentrations for Delhi road conditions. The performance of IITCO model has been compared with Pollution Episode Model (PEM) and Intersection Midblock Model (IMM). The results show better performance of IITCO model when compared to PEM and IMM. Kono and Ito [150] have developed a microscale dispersion model i.e. the OMG volume source model. Later, the OMG volume source and EPA HIWAY-2 model results have been compared with measured SF_6 concentrations. It has been observed that OMG volume source model predictions are better than the other models [151]. In another study, Singh et al. [149] has applied IITCO model to Kuwait traffic conditions. The results have been compared with U. S. operational model, namely, Intersection Midblock Model [152]. Among the simulations obtained from both the models, the performance of IMM has been better than IITCO. Miles et al. [153] have developed a hybrid approach for assessing air quality implications of urban planning. This approach is a combination of deterministic and statistical approaches. It is a function of vehicular traffic and basic meteorology. Nieuwstadt [154] has studied large eddy simulation using theory of the dispersion characteristics of a passive

line source pollutant in the convective atmospheric boundary layer. Further, the author has also studied the dynamics of line source in two parts i.e. part-I, governed by the internal buoyancy, and part-II, governed by the ambient turbulence. For the latter part, he has developed a simple integral plume rise model [155]. Benson [156] has studied recent versions of CALINE models, namely, CALINE-3 and CALINE-4. He has evaluated the predictive capability of CALINE-4 and found its performance better than CALINE-3. In another study, Alexopolos et al. [157] have come out with a model for spatial and temporal evaluation of traffic emissions in metropolitan areas. The model is useful when raw traffic data, network and number of trip data are difficult to generate. Qin and Kot [158] have carried out dispersion studies in low wind conditions for three streets in Guangzhou city. Using the observed data, a simple operational model has been proposed to simulate the dispersion of vehicular emissions in street canyons. Burden et al. [159] have used CALINE–4 and DMRB models for predicting NO_2 concentration at roadway intersections, in Bristol, U.K. The two models satisfactorily predict the NO_2 concentrations under flexible traffic volume. Akeredoiu et al. [160] have used the CALINE-4 model for forecasting CO at a roadway intersection. Chan et al. [161] have tested the applicability of four simple dispersion models, namely, APRAC, GZE, CALINE-4 and PWILG. These models are evaluated by comparing the predicted CO and NO_x concentrations with measured values at street canyons in Guangzhou city. The models perform accurately in predicting the maximum ground level concentrations. Derwent et al. [162] have used one-year air quality data collected at one of the urban roadside locations in central London to evaluate Gaussian and Box models. The predicted results have been used for a comprehensive validation of the published emission inventory estimates of the London city. Esplin [163] has given approximate explicit solutions to the general line source problems at different wind angles. Clifford et al. [164] have studied the mechanisms involved in the dispersion of pollutants around slow moving vehicles. The spatial distribution of tracer gas along and across the vehicles shows that a significant level of pollution is received by a commuter in a slow moving vehicle from the automobile immediately in front. Dabberdt et al. [165] have evaluated two Gaussian based models namely, HIWAY2 and

CALINE 4 and a numerical model for air quality prediction near urban intersection. The model results indicate that numerical model predictions are more accurate than two Gaussian based models. Using traffic counts and fleet composition, Yu et al. [166] have developed a mathematical model for predicting trends in CO emissions. Chock and Winkler [167] have compared the impact on air quality predictions using the fixed - and varying - layer depth structures in an urban airshed model (UAM). The analysis shows that the fixed layer-depth approach yields substantially higher concentrations of CO, NO and VOC in lower layers of atmosphere in isolated areas at early morning than the varying layer depth approach. Gualteri and Tartaglia [168] have presented a geographical information system (GIS) based line source model for predicting air quality near roadsides. Karim and Matsui [169] and Karim et al. [170] have developed a computer model consisting of wind distributions, emission dispersion and modified Gaussian equation to identify street canyon and vehicle wake effects on transport of air pollution from the urban road microenvironments. The model simulates and analyzes the wind flow and their components in the street canyon considering a two-dimensional street canyon flow pattern. Later, Karim [171] has developed a traffic pollution inventory and modeled dispersion of vehicular pollutants in an urban environment. Khare and Sharma [172] have developed the Delhi finite line source model (DFLSM), (a deterministic based model), for Delhi traffic conditions. This model shows better prediction accuracy for CO when compared to the GFLSM [91]. The formulation of DFLSM has been discussed in Appendix-A. In an another study, Sivacoumar and Thanasekaran, [173] have applied GFLSM to predict CO concentrations at four sections of major highway in Madras. The model results are comparable to measured CO concentrations. Goyal and Ramakrishna [174] have developed the Gaussian based finite line source model for describing downwind dispersion of CO in urban roads. The model results, when compared with CALINE 3, show that both the models perform satisfactorily. Buckland and Middleton [175] have given nomograms for screening of vehicular pollution in congested street canyons. Hao et al. [176] have described a method for estimating the spatial and temporal distribution of exhaust emissions in Beijing, based on limited database including vehicle type, density and vehicle distance

travelled. Later, the estimated emission data are validated using a mathematical dispersion model i.e. the industrial sources complex short-term version 3 (ISCST 3) by simulating the pollutant concentration distribution in an urban area. Kousa et al. [177] have developed computer simulation code for predicting the traffic volume and emission at an urban centre. The simulation code predictions, when compared with 1996-1997 monitored data at Helsinki metropolitan in Finland, has been found to be satisfactory. Sivacoumar and Thanasekaran [178] have evaluated four Gaussian based dispersion models, namely, GM, CALINE-3, PAL-2 and ISCST-2 for Indian traffic conditions. The study reveals that GM model perform best, followed by CALINE-3, ISCST-2, and PAL-2. Kiihlwein et al. [179] have developed a Gaussian based multi-source model for estimating pollutant concentration at selected locations in Augsburg (South Germany). Jorquera [180] has applied box model for assessing the air pollution standards in Santiago, Chile after a shift was made from unleaded gasoline to compressed natural gas. Nagendra and Khare [17] have given a comprehensive review of literature on line source deterministic based models. As mentioned earlier, line source approximation as series of point sources significantly increases the amount of time required to run an atmospheric dispersion model. Also these models aim to resolve the underlying physical and chemical equations controlling exhaust emissions dispersion, and therefore require detailed meteorological and traffic characteristic data. As a result, the researchers start looking for other alternative modelling techniques, e.g., numerical and statistical.

4.4 Vehicular Pollution Numerical Models

A number of numerical models have been used for simulation of highway dispersion. Danard [123] has developed a two- dimensional eularian model i.e. DANARD. It solves the mass conservation equation based on numerical methods outlined by Dufort and Frankel [181]. Using the boundary conditions imposed in DANARD, Ragland and Pierce [182] have derived the continuity equation for parallel and non-parallel diffusivity classes by an efficient matrix inversion technique. The model predicts concentration for oblique and

perpendicular cases by ignoring lateral diffusion. For parallel cases, the model solves the equation in three dimensions including lateral diffusion. Kirsch and Mason [124] have developed the MROAD-2 model, a Eulerian two-dimensional grid model. It numerically solves the mass conservation equation. The user can specify the size of the grid and model allows the existence of several line sources (all assumed to be perpendicular to the plane of the road), including elevated roadways. Pitter [125] has described ROADS model, a two-dimensional conservation model. The model determines the steady state concentrations of pollutants by numerically solving the equations using the Lax-Wendroff finite difference scheme. Eskridge et al. [183] have presented a finite difference highway model. The model uses surface layer similarity theory and vehicle wake theory of Eskridge and Hunt [184] to determine the atmospheric structure along the roadway. Chock [185] has formulated a numerical model to solve advection diffusion equation for a line source. In this model traffic effects are considered as additive components of the eddy diffusivity tensor (K_{ij}) over that of atmospheric effects in the following form:

$$K_{ij} = K^{a}{}_{ij} + K^{t}{}_{ij} \tag{4.3}$$

where K^{a}_{ij} is the ambient /atmospheric eddy diffusivity tensor and K^{t}_{ij} is traffic induced component of eddy diffusivity tensor. Later, this model is validated for GM experiment data and is reported to be valid within ± 10 % accuracy limits. Eskridge and Thomsion [186] have developed the ROADWAY model, which predicts pollutant concentration near a roadway. It assumes a surface layer described by surface layer similarity theory with the superposition of the effects of vehicle wakes. The ROADCHEM model [186] is a version of ROADWAY, which incorporates the chemical reactions involving NO, NO_2 and O_3 as well as advection and dispersion phenomena. In this version, surface layer similarity theory is used to produce vertical angle turbulence profiles. Maddukuri [187] has described a numerical model for the estimation of CO dispersion. The model is based upon the semi empirical equation of turbulent diffusion equation. Eskridge and Rao [188] have modified the ROADWAY model by using experimentally determined eddy diffusion coefficients. The

revised version of ROADWAY is completely independent of the GM sulfate experiment data, whereas the initial version has used the GM data to determine the diffusion coefficients needed in the wake theory. Later versions of ROADWAY model predictions are closer to GM data than the initial version. Thompson and Eskridge [189] have experimentally studied the influence of vortex pair in turbulent diffusion behind vehicles. These experimental results are incorporated into ROAWAY model for improving its predicting efficiency. The model physics is based primarily on the vehicle speed, turbulence and diffusion of the tracer. The CAR model (Calculation of Air Pollution from Road Traffic), developed by the Dutch national institute of environmental health [190] and Dutch institute of applied scientific research [191], has been evaluated for a Dutch city by Eerens et al. [192]. The calibration of the model is done by using data from the Dutch national air quality-monitoring network [193] and wind tunnel experiments [191]. The CAR model satisfactorily estimates the air pollutant concentrations in urban streets. CAR-FMI [194,195,196] is a road network dispersion model, developed by the Finnish Meteorological Institute. The Norwegian Institute of Air Research (NILU) has also developed the ROADAIR and CONTILENK models for open roads and NERI OSRM for street canyons, respectively [197]. A recent study by Karppinen et al. [198.199] have described the application of CAR-FMI model in estimating the contribution from mobile sources in predicting the emission, dispersion and chemical transformation of NO_x in an urban area. Maurizi and Tampieri [200] have shown that large variation of skewness and kurtosis and atmospheric turbulent flow has to be taken into account when a probability density function is proposed for modelling pollutant dispersion using Lagrangian stochastic models. In another study Koeltzsch [201] has developed a theoretical relationship between Lagrangian and Eulerian time scales. Recently, Huang et al. [202] have developed a two-dimensional air quality numerical model using atmospheric convection diffusion equations and a K-$\in$ turbulent model. Later, the model is applied to predict the air quality impact by exhaust emissions near urban streets. In another study, Karppinen et al. [203] have formulated a numerical model for evaluating the traffic characteristics and dispersion of pollutants in Helsinki, Finland. Later, this model is validated with urban and

suburban air quality data [204]. Chang et al. [205] have developed a two-dimensional numerical model based on joint-scalar probability density function approach, coupled with a turbulence model. Recently Rao et al. [206] have developed the ROADWAY 2 model by incorporating vehicle wake parameters in earlier version of ROADWAY model. Further, using a towed array of 3-D sonic anemometers, first field measurements of velocities and turbulence in the vehicle wake have also been made. The results indicate that pollutant concentration decreases with increasing distance from the road more rapidly for horizontal wind case than for the perpendicular wind. In addition, Nagendra and Khare [17] have also made a comprehensive review of literature on line source numerical models.

Numerical line source model seems to be the most desirable solution to exhaust emission dispersion, provided adequate data and computing resources are available [18]. However, in general, due to complex interaction between meteorology and traffic characteristics with exhaust emission dispersion leads to lack of theoretical understanding and therefore statistical models are required.

4.5 Vehicular Pollution Stochastic Models

McGuire and Noll [207] have studied the relationship between maximum concentration and average time for CO, NO_x and NO_2 pollutants collected at 17 monitoring stations in California city. From the past studies on air pollution modelling, there exists substantial evidence that the series of pollution concentration and meteorological data are highly auto-correlated irrespective of the time [55]. McCollister and Wilson [60] have used the B-J (Box-Jenkins) type models for short-term forecast of oxidant and CO in Los Angeles basin. The model is one dimensional and shows poor prediction for extreme events. Tiao et al. [208] have studied the effects of intervention caused by a new highway on the oxidant time series in the Los Angeles basin. A univariate analysis of the weekly averages of the daily maxima of oxidant, CO, NO_2, and total HC has been done by Chock et al. [56] for Riverside, California. The relationships between the weekly averages of the daily maxima of the oxidant and the weekly averages of meteorological parameters are also investigated.

Based on least square technique, Aron and Aron [209] have developed the stochastic model for forecasting daily maximum CO concentrations at Los Angles basin. The results show that preceding days CO concentration, pressure differences between nearby stations, surface temperature, day of the week, length of daylight, solar radiation and inversion height are the most significant variables in model development. Hirtzel and Quon [210] have used auto-correlation function to model hourly and average 8 hourly CO concentrations measured at the continuous air monitoring program station in Chicago. In another study, Ledolter and Tiao [211] have described a statistical model that predicted CO concentration on both sides of the freeway in Los Angles. Regression analysis technique has been used by Chang et al. [212] to determine the relative impact of mobile and stationary sources on high NO_2 concentrations. The analysis shows that hourly NO_2 concentrations observed in Los Angles basin arise largely from vehicle emissions and support the assumptions used in generalized rollback model [128]. Lincoln and Rubin [213] have applied multiple regression analysis to correlate CO with daily average haze coefficient and total suspended particulate (TSP) in downtown urban area of Los Angeles. Zamurs and Piracci [214] have developed a multiple linear regression model to predict CO concentration at selected intersections. Using a statistical theory, a simple formula for calculating dispersion from continuous finite line source has been presented by Mikkelsen et al. [215]. Jakeman et al. [216] have used a hybrid (deterministic + stochastic) model to predict seasonal extremes of one-hour average CO concentration. Bardeschi et al. [217] have noted the importance of time series of concentration emission and meteorological conditions during the hours prior to the high CO concentrations. In recent past, a number of studies have been carried out using multivariate time series analysis in which various B-J modelling techniques have been applied for homogeneous traffic conditions [53, 54, 218, 219, 220, 221]. Liu et al. [222] have used Monte Carlo simulation method to predict personal exposure levels to CO in Taipei. The skewness and kurtosis methods have been used by Zhang et al. [223] to investigate the statistical distribution of CO and HC emissions on a road in Denver, U. S. A. Glen et al. [224] have developed an empirical model predicting monthly CO concentrations for long-term trend assessment. In

another study, Cernuschi et al. [225] have described the empirical models establishing relationships between annual average pollutant concentration and air quality related parameters. Comrie and Diem [226] have examined the relationships between meteorology, traffic patterns and CO concentration at seasonal, weekly and diurnal time scales in Phoenix, Arizona. Maffeis [227] has formulated FOREPOLL model to forecast the probability of a CO concentration violation at traffic intersection in Lombardy region. Sharma et al. [228] have applied extreme value theory to know the expected number of violations of the NAAQS to hourly and eight-hourly average CO concentrations for an AQCR comprising of an urban road intersection, followed by the development of an intervention analysis model (IAM) for the same AQCR [229]. Further, Sharma and Khare [230,231] have used Box- Jenkins modelling techniques to provide short-term and real-time forecast of the ambient air pollution levels due to vehicular sources at an urban intersection. A linear regression model has been developed by Olcese et al. [232] to predict the CO and NO_x concentration near traffic roads. Stedman et al. [233] have presented maps (based on empirical linear relationships) for estimation of annual average NO_2 concentrations near roadside locations in major cities in the UK. A detailed review on analytical modelling techniques, including deterministic and statistical modelling approaches for exhaust emission can be found in Sharma and Khare [2]. Further, model performance evaluation and comparative assessment have also been discussed in this review. In addition, Nagendra and Khare [17] have presented a comprehensive review of literature on line source stochastic models.

In current research scenario, the primary concern before the researcher is how to develop a general vehicular pollution prediction model that may work with reasonable accuracy under varied environmental conditions. In such situations, numerical modelling is perhaps the most desirable approach. However, with increase in complexity of the problem, the theoretical understanding decreases due to 'ill-defined' interactions between environmental systems. In such cases, statistical approaches become most suitable. However, the main drawback in statistical techniques lies in prior assumptions concerning data distribution, as well as their site-specific nature [53,54]. Recent studies by Hornik et al. [87] and Schalkoff [234]

have shown that neural networks can be considered as an effective alternative tool to statistical modelling techniques. The ANN can model highly non-linear functions, which can be trained to accurately generalize when presented with entirely new set of unseen data. Recent advances in neural networks precisely show the benefits that the ANN offer in form of prediction accuracy when compared to more traditional statistical modelling techniques [83]. In the following section, a review on application of ANN pertaining to vehicular pollution modelling has been presented.

4.6 ANN based Vehicular Pollution Models

The ANN approach offers several advantages over traditional phenomenological or semi-empirical models. In that, it exhibits rapid information processing, and its ability to develop a mapping of the input and output variables [235]. ANN based models have significant advantage over analytical and statistical models, since they require known input data set without any assumptions. Using those inputs, the neural network model automatically develops its own internal model and subsequently predicts the output.

Literature on application of ANN in line source modelling is scanty [17, 62, 236]. Moseholm, et al. [94] have studied the usefulness of neural network in understanding the relationships between traffic parameters and CO concentrations measured near an intersection, which is sheltered from wind by multi-storied buildings. In another work, Dorzdowicz et al. [237] have developed a line source neural network model for estimating hourly mean concentrations of CO in the urban area of Rosario city. Eleven inputs e.g. vehicular flux-vehicles/hr (cars, taxis, median vehicles, trucks and buses), wind speed and direction, solar radiation, humidity, pressure, rain intensity and temperature have been used for development of the three ANN based models. The first model with eleven input variable set; the second, with seven variable set (excluding humidity, pressure, rain intensity and temperature); and the third, with six input variables (eliminating solar radiation in addition to variables excluded in second model). These models are later validated for each type of network (i.e., considering different number of input variable sets),

and using approximately a set of 100 patterns. The results show that eliminating variables from the input set does not show any major influence on the predicted CO concentrations. Gardner and Dorling [83] have developed multilayer perceptron (MLP) neural network models using hourly NOx and NO_2 and meteorological data of the Central London. The predicted results show better performance when compared with previously developed regression models [238] for the same location. Perez and Trier [239] have developed a multilayer neural network based model to predict NO and NO_2 concentrations at a traffic junction in Santiago, Chile. Later, model results, when compared with persistence and regression models, show that neural network based model performs much better than the persistence and regression models. Viotti et al. [240] have presented ANN based short and long-term air quality models for forecasting vehicular air pollutant concentrations in the city of Perugia, Italy. The ANN based models show reasonable accuracy in predicting short and long-term air pollutant concentration. Kukkonen et al. [241] have evaluated five neural network, a linear statistical and deterministic based models in predicting the NO_2 and particulate matter concentrations in the central Helsinki, Finland. Recently, Nagendra and Khare [242] have developed ANN based line source models for predicting CO concentrations on an urban roadway. Ten meteorological and six traffic characteristic variables have been used for developing these models. The results show that the neural network models are able to capture traffic 'wake' effects on the CO dispersion in the near field regions of the roadway. Further, Nagendra and Khare [17, 62] have presented a comprehensive review on ANN based vehicular pollution models.

Most of the ANN studies have addressed the problem associated with pattern recognition, forecasting and comparison of the neural network with other traditional approaches in atmospheric sciences. However, the step-by-step procedure involved in development of ANN based models are not discussed. In the following chapters, the methodology consisting of step-by-step approach in developing the ANN based vehicular pollution models at urban roadways for heterogeneous traffic conditions and tropical meteorology has been described. Besides, the application of ANN based vehicular pollution

models in predicting the CO and NO_2 concentrations at two AQCRs have also been included.

4.7 Limitations of Vehicular Pollution Models

Deterministic vehicular pollution modelling approach is the most logical and traditional approach for the prediction of air pollution concentrations, yet it is not free from limitations. These models most often arrive by deducing arguments at mathematical formulae which, it is opted, reflect more or less accurately the physics of the process. To be useful, these formulae need first an adequate amount of meteorological input about the state of the atmosphere (wind speed and direction, stability, turbulence, etc.) and similarly detailed data on emissions [243]. The limitations of the deterministic vehicular pollution models are three fold - *first*, the understanding of the physics, *second*, the explicit or implicit simplifying assumptions, and *third*, the accuracy of the various input parameters. For instance, when unit time interval is short (i.e., ≤ 1 day) and 'steady state' assumptions required for the application of Gaussian type models are not met, the deterministic based models do not give satisfactory results [244]. Besides, the Gaussian dispersion equation has a singularity at zero wind speeds. Therefore, all Gaussian based models perform poorly when wind speeds are less than 1m/s [91].

In general, Gaussian based model predictions are reasonably accurate for long-term average concentrations and for the frequency distribution up to 90 percentile [245]. However, the predictions become inaccurate when the frequency distribution is 98 percentile [246]. Further, deterministic models are not suitable for extreme value predictions [247]. However, they are most suitable for long term planning decisions [89, 248, 249]. Table 4.1 summarizes the limitations of selected vehicular pollution models.

Numerical models have common limitations arising from employing the K-theory for the closure of diffusion equation. The K-theory diffusion equation is valid only if the size of the 'plume' or 'puff' of pollutants is greater than the size of the dominant turbulent eddies. The K-model assumption is also not valid for the convective boundary layer under strong instability. The other limitations of

Table 4.1 Applicability and limitations of selected vehicular pollution models.

Sl. No	Model	Applicability		Limitations
		Pollutant type	Receptor location and traffic type	
1.	California line source model [88]	CO, NO_x, SPM	Roadside Homogeneous	Tendency to predict high pollutant concentration for parallel wind case. No treatment of plume rise due to hot exhaust of vehicles.
2.	HIWAY-1 [110]	CO	Roadside Homogeneous	Predicts poorly for low winds. Overestimates pollutant concentration for stable atmospheric condition and parallel wind case. No treatment of plume rise due to hot exhaust of vehicles.
3.	CALINE-2 [113]	CO, NO_x, SPM	Roadside Homogeneous	Predicts poorly for unstable and neutral stability conditions. Over predicts the pollutant concentration for parallel wind cases and under predicts for oblique wind conditions.
4.	GM model [92]	CO	Roadside Homogeneous	Tendency to over predict the concentration under parallel wind conditions. Predicts poorly for low winds.
5.	CALINE-3 [114]	CO, NO_x, SPM	Roadside Homogeneous	Tendency to predict high for parallel wind condition. No proper treatment for mechanical and thermal turbulence created by vehicle exhaust.
6.	HIWAY-2 [126]	CO	Roadside Homogeneous	Inadequate dispersion parameters. No treatment of plume rise due to hot exhaust of vehicles.
7.	HIWAY-3 [121]	CO	Roadside Homogeneous	Predicts poorly for low winds. Tendency to predict high for parallel wind condition. No treatment of plume rise due to hot exhaust of vehicles.
8.	HIWAY-4 [121]	CO	Roadside Homogeneous	Tendency to predict high for parallel wind condition. No treatment of plume rise due to hot exhaust of vehicles.
9.	CALINE-4 [115]	CO, NO_x, Aerosol	Roadside Homogeneous	Tendency to predict high for parallel wind condition.
9.	ISCST-2 [250]	CO, NO_x, SPM	Roadside Homogeneous	Tendency to predict high for parallel wind condition. No treatment for turbulence caused by heated exhaust.
10.	GFLSM [91]	CO, SPM	Roadside Heterogeneous	Predicts poorly for low winds.
11.	DFLSM [172]	CO	Roadside Heterogeneous	Predicts poorly for low winds.

numerical models are large computational costs in terms of time and storage of data. It also requires large amounts of input data. The solutions obtained from numerical model are approximate one. Past studies have revealed that the performance of numerical models namely, DANARD [123], MROAD-2 [124], ROADS [125], ROADWAY [183] are not better than the Gaussian based deterministic line source models [121, 251, 252].

The statistical model inference is descriptive. It is a summarization of the data already on record completed by the assumption that the record either is stable or contains trends or cycles, which may somehow be extrapolated. Most of the statistical models are based on a group of observations; therefore statistical models are empirical in nature. Limitations of statistical models include the requirements of long historical data sets and lack of physical interpretation. Statistical models are generally devised to determine the underlying relationship between a set of input data (predictors) and targets (predictants). Regression modelling is an example of statistical approach; often under perform when used to model non-linear systems [18]. Another limitation of statistical model is that they cannot provide information about how pollutant levels would respond to emission controls, though statistical distribution modelling has been reported to be used in developing simple roll-back formulae for determining a desirable level of source emission control to meet with the objectives of air quality management [253].

Generally, the Box-Jenkins algorithm is considered to be the most sophisticated method for time series analysis. Kapoor and Terry [254] have indicated that a time series model requires considerable knowledge in time series statistics. Since, the vehicular pollution variations are generally not simple autoregressive (AR) or moving average (MA) models [60], analysts must employ statistical graphs of the autocorrelation function (ACF) and partial auto correlation function (PACF) to identify an appropriate time series model. In model identification stage, the resulting model quality frequently relies on individual experiences and knowledge of time series statistics. In addition different analyst might render contradictory interpretations, given the same data [61]. The statistical models are, therefore site specific.

In developing the ANN based vehicular pollution models for line sources, no procedure has yet been formulated for selecting proper network architecture [67]. Technically only one hidden layer is required to approximate any smooth measurable function between inputs and outputs [87]. The optimum number of nodes required in hidden layer is problem dependent, being related to the complexity of the input and output mapping, the amount of noise in the data and the amount of training data available. Multilayer neural network performs well when used for interpolation, but poorly, if used for extrapolation. Apart from these, no thumb rules exist in selection of data set for training, testing and validation of neural network based model.

4.8 Summary

The vehicular pollution modelling is an useful tool for predicting the urban air quality. Analytical modelling approaches including deterministic and statistical techniques are commonly used for vehicular pollution modelling. Choosing the most suitable approach depends on the complexity of the problem being addressed to and the degree to which the problem is understood. Deterministic approach seems to be the most logical and traditional approach for modelling air pollution concentrations. The prediction capability of deterministic models depends on the conditions fulfilling the simplifying assumptions, which are made in the model formulation. The Gaussian model is generally accepted for prediction of long-term average concentrations. Numerical models are most desirable solution, if adequate data, computational resources and other theoretical understanding of dispersion phenomena are available. Statistical models are site specific and do under perform when modeled with highly non-linear data. The ANN approach, particularly multilayer neural networks are most suitable where a full theoretical (deterministic and statistical) models cannot be constructed; and especially when dealing with complex conditions.

5 Vehicular Pollution Modelling - ANN Approach

The chapter describes the formulation and development of ANN based vehicular pollution models. Section 5.1 briefly describes the history of ANN modelling approach, followed by theoretical aspects of development of ANN based vehicular pollution model (section 5.2). The step-by-step ANN model building and training procedures are presented in section 5.3 and 5.4 respectively. The statistics for model testing and evaluation are given in section 5.5. The development of ANN based vehicular pollution models for different time resolutions, following NAAQS, are presented in Section 5.6 (*case studies*).

5.1 General

Modelling of vehicular pollution dispersion is actively researched for many decades. However, because of the vast number of the variables and the arbitrary variations in the wind speed and direction, and vehicle wake, the development of reliable vehicular pollution model is still a challenge [17]. As mentioned in chapter 4, existing vehicular pollution dispersion model can be classified as either 'phenomenological/deterministic' or 'statistical'. On one hand, phenomenological approaches are based on underlying phenomena described by advection and diffusion processes of the atmosphere. On the other hand, statistical approaches are based on semi empirically developed relationships between the downwind concentrations with emission rates and meteorological variables.

In late 1950's, the perceptron was introduced as a learning model and thereafter understanding of biological nervous systems entered a new era. This modelling technique becomes a vital tool in modelling of nonlinear dynamic processes. The neural network approach offers several advantages over traditional phenomenological or semi

M. Khare and S.M. Shiva Nagendra: *Vehicular Pollution Modelling – ANN Approach*, Artificial Neural Networks in Vehicular Pollution Modelling (SCI) **41,** 67–119 (2007)
www.springerlink.com

empirical models. It exhibits rapid information processing, and it is able to develop a mapping of the input and output variables. Such a mapping can subsequently be used to predict desired output variables as a function of suitable input variables [234]. Presently, ANN, and in particular, the multi layer neural network are found wide application in solving complex air pollution problems [17; 18, 62, 236]. In recent past, number of multilayer neural network modelling studies have been carried out on forecasting of O_3, SO_2, NO_2 and PM concentrations and found their importance in modelling complex air pollution problems [67, 82, 83, 255, 256, 257]; whereas, to date, multilayer neural networks are limited application in modelling of vehicular pollution dispersion [17, 62]. This chapter describes the step-by-step procedure to model the vehicular pollution dispersion phenomena near urban roadways using the ANN technique.

5.2 ANN Approach to Vehicular Pollution Modelling

Multilayer neural networks are capable of modelling highly non-linear relationship and can be trained to accurately generalize, when presented with new unseen data [87]. The neural network learns to model a relationship during a supervised training procedure, when they are repeatedly presented with series of input and associated output data [83].

During ANN based vehicular pollution model training, it is important to avoid over training of the neural networks [67]. Over training occurs when the model learns the lousy details present in the training data which, results in poor model generalization when, it is tested with new unseen data [83]. In order to avoid over training, ANN based vehicular pollution model is usually trained on a subset of inputs and outputs to determine weights, and subsequently validated on the remaining (quasi-independent) data to asses the accuracy of the neural network model predictions [82]. It is advisable to divide the data into three partitions namely, the ‘training data set’, ‘test data set’ and ‘evaluation data set’. The ‘training data set’ forms the bulk of the data used for training purpose; the ‘test data set’ is used during training in order to check the generalization performance of the neural network model. Training can be stopped when the

model performance on the 'test data set' reaches maximum. Finally, the 'evaluation data set' is used to evaluate the final neural network model. This suggests that the 'training data set' is adequately extensive and representative. Neural networks perform well, when used for interpolation, but poorly in cases of extrapolation [18]. The 'training data set' must fully represent all the cases about which the ANN based vehicular pollution model is required to generalize. Since, the ANN based vehicular pollution model is trained on data of a selected site/air quality control region (AQCR), it can therefore, only be used, with confidence at the AQCR i.e. site dependent [82]. Further, the local traffic characteristics and building arrangements that determine the processes controlling the pollutant behavior, is important in determining the extent to which the model predictions can be extrapolated. In the present ANN based vehicular pollution modelling, the input data for neural network model consists of meteorological and traffic characteristic variables and the associated output is CO or NO_2 concentrations. Back-propagation with momentum term algorithm, which is implemented in the Stuttgart Neural Network Simulator (SNNS) is used to train the ANN based vehicular pollution models. The software runs under the UNIX operating system, freely available via the internet (ftp://ftp.informatik.uni-stuttgart.de). In the recent past, SNNS is widely applied in solving large number of air pollution problems [83, 255, 256]. The details of SNNS are briefly described in Appendix-B.

5.3 Algorithm for ANN based Vehicular Pollution Model

The ANN based vehicular pollution model-building process consists of six sequential steps:

(i) selection of the optimal ANN based vehicular pollution model architecture,
(ii) selection of the best activation function,
(iii) selection of the optimum learning parameters, 'n' (learning rate) and 'μ' (momentum rate),
(iv) initialization of the network weights and bias,
(v) training and generalization of the model,
(vi) evaluation of the model.

5.3.1 Selection of the Optimal ANN based Vehicular Pollution Model Architecture

The architecture of ANN based vehicular pollution model consists of number of neurons in the input, hidden and output layers and their interconnections. The number of neurons in the input layer equals the number of input variables (i.e. for vehicular pollution modeling, meteorological and traffic characteristic variables). The output layer consists of one neuron i.e. the pollutant concentration. The number of neurons in the hidden layer depends upon the number of training patterns, the number of input/output neurons, the amount of *noise* in the data, the network architecture, the type of activation function used in the hidden layer and the training algorithm [258, 259]. One hidden layer is sufficient to approximate any non-linear function in addition to input and output layers. Training several networks and estimating the corresponding errors on the test data set obtain the number of neurons in the hidden layer. A few neurons in the hidden layer produce high training and testing errors due to under-fitting and statistical bias. On the contrary, too many hidden layer neurons lead to low training error, but high testing error, due to over fitting and high variance [259]. In the past, researchers have used 'rule of thumb' to find the number of neurons (H) in the hidden layer, as described below:

(i) H = (number of input neurons + number of output neurons)

(ii) The maximum number of neurons in the hidden layer (H_{max}) is given by Swingler [260] and Berry and Linoff [261]: H_{max} = 2 times the number of input layer neurons

(iii) H = the number of the training patterns divided by 5 times of the number of input and output neurons.

The 'rule of thumb' has failed to provide 'optimal' number of hidden layer neurons that subsequently affected the model prediction accuracy. In the present ANN based vehicular pollution modelling work has demonstrated that the iterative approach is more efficient and accurate in determining the optimal number of hidden layer neurons, yielding minimum model prediction error on the 'test data set'.

5.3.2 Selection of the Best Activation Functions

The non-linear relationship between input and output parameters in any network requires a function, which can appropriately connect and/or relate the corresponding parameters. Neurons in the neural networks transform their net input by using a "scalar to scalar" function called the "activation function", yielding a value called the neurons "activation". The activation function is sometimes called a "transfer function", and activation functions with a bound range, are often called as "squashing function", or sigmoid functions (hyperbolic tangent and logistic functions). If a neuron does not transform its net input, then it is called an 'identity' or 'linear' activation function [69].

Activation functions for the hidden neurons are needed to introduce non-linearity into the network. Without the non-linearity, the hidden neuron would not make neural networks more powerful. For the hidden neurons, sigmoid activation functions are generally used in the ANN based air pollution modelling [82, 235, 255]. This is due to a very small change in the weights that usually produce a change in the outputs, which make it possible to tell whether that change in the weight is converging or not. Further, this function is monotonic, continuously differentiable and bounded.

For the output neuron, the activation function depends on the distribution of the target values. For continuous value targets with a bound range, the *logistic* and the *hyperbolic* tangent functions are useful. But, if the target values have no known bound range, it is better to use an unbound activation function, most often the "identity function". For ANN based vehicular pollution modelling, the hyperbolic tangent function is used in the hidden layer neurons, and the unbound identity function is used for the input and the output layer neurons.

5.3.3 Selection of the Optimum Learning Parameters

Multilayer neural network has the ability to learn through training. Training requires a set of data consisting of a series of input and associated output vectors. A supervised back-propagation algorithm is most commonly employed in training the multilayer neural network. In the back-propagation training, η and μ are used to 'speed up' or

'slow down' the convergence of error [81]. The back-propagation training algorithm gives an "approximation" to the trajectory in weight space, computed by the gradient descent method [85]. The decrease in value of 'η' results in smaller changes in the synaptic weight from one iteration to the next and reduces the training speed. But, the increase in value of 'η' helps in faster training of the network due to the large changes in the synaptic weight and thus making the network as unstable (i.e. oscillatory). The term 'μ' is used to avoid the network oscillation in back propagation training algorithm. The values of 'η' and 'μ' are set between 0 to 1 [71, 235]. The following guidelines exist in evaluating the optimal value of 'η' and 'μ' [86].

(i) The 'η' and 'μ' converge to a local minimum in the error surface of the network with the least number of epochs.

(ii) The 'η' and 'μ' converge to a least global minimum in the error surface with the least number of epochs.

(iii) The 'η' and 'μ' converge to the network configuration that is best generalized with the least number of epochs.

In the vehicular pollution modelling work, the optimal values of learning parameters are evaluated using guideline (iii).

5.3.4 Initialization of the Network Weights and Bias

Before starting neural network training, initialization of neural network weights and bias (free parameters) are required. A good choice for the initial values of the synaptic weights and bias of the network can be of help in fast convergence of training processes. In cases, where prior information is available, it may be preferable to use the prior information to guess the initial values of the free parameters. If no prior information is available, the customary practice is to set all the free parameters of the network to the random numbers that are uniformly distributed inside a small range of values [69]. The reason for making the range small is to reduce the likelihood of the neurons in the network saturating and producing small error gradients.

However, the range should not be made too small, as it can cause the very small error gradients, and therefore may increase training time. For sigmoid (hyperbolic tangent) functions, a possible choice for initialization is to pick the random values for the weights that are uniformly distributed inside the range $[(-2.4/F_i), (+2.4/F_i)]$, *where,* F_i is, total number of inputs [86]. In many cases, it is desirable to provide each neuron with a trainable bias. This offsets the origin of the sigmoid function, producing an effect that is similar to adjusting the threshold of the perceptron neuron, thereby permitting more rapid convergence of the training process.

The wrong choice of initial weights may lead to premature saturation [262]. This phenomenon refers to a situation where the instantaneous sum squared errors remains constant for some period of time during the training process. Such phenomena cannot be considered as a local minimum, because the sum-squared error continues to decrease after this period is finished. In other terms, the premature saturation phenomenon corresponds to a "saddle point" in the error surface. The premature saturation can be avoided by choosing the initial values of the synaptic weights and bias values of the network, uniformly distributed inside a small range of values. Further, premature saturation is less likely to occur when the number of hidden neurons is less [69].

5.3.5 Training Procedure

The object of training the ANN based vehicular pollution model is to adjust the weights so that application of a set of inputs (meteorological plus traffic characteristic variables) produces the desired set of outputs. Training involves finding the set of neural network weights, which enables the ANN based vehicular pollution model to represent the underlying patterns in the training data. This is achieved by minimizing the ANN based vehicular pollution model error, for all the input patterns, with respect to the associated network output patterns. Unfortunately the error surface is often complex and contains many local minima. For instance, if the training algorithm becomes trapped in local minimum, then final ANN based vehicular pollution model will be suboptimal. Typically, when the global minimum is

not reached, the local minima can be considered as an acceptable solution. Therefore, training a number of ANN based vehicular pollution models and selecting the model having minimum error on 'test data set', may reduce the likelihood of local minima.

The patterns of the input-output sets can be referred to as vectors. Training assumes that each input vector is paired with a target vector representing the desired output; together these are called a training pair. Usually, a network is trained over a number of training pairs. During training, the ANN based vehicular pollution model is repeatedly presented with training data and the weights in the network are adjusted until the desired input-output mapping occurs. Training an ANN based vehicular pollution model with back-propagation algorithm consists of initializing the weights to small random values (Section 5.3.4). The input-output vectors are then sequentially presented to the network. When an input-output vector is presented, the following calculations are performed.

(i) Multiply all the input by an initial random weight and sum the result as

$$P_j = \sum_{j=1}^{H} w_{ij}\ x_i + b_j \qquad \begin{matrix} i=1,2,....n \\ j=1,2,.....H \end{matrix} \tag{5.1}$$

Where P_j = input to the 'j' hidden layer neuron.
x_i = numerical value of the i^{th} input layer neuron.
w_{ij} = weight of the i^{th} input layer neuron to j^{th} hidden layer neuron.
n = number of the input layer neurons.
H = number of the hidden layer neurons.
b_j = bias value for the j^{th} hidden layer neuron.

(ii) Transform the hidden layer output by a sigmoid transfer function f (P_j).

$$Q_j = \frac{1}{1+e^{-P_j}} \qquad j = 1, 2, \quad ....H \tag{5.2}$$

Where Q_j = output of the hidden layer neuron 'j'.

(iii) Multiply the hidden layer outputs by the hidden-output layer weight and sum as:

$$R_k = \sum_{j=1}^{H} Q_j \, w_{jk} + b_k \qquad k = 1, 2, \ldots m \tag{5.3}$$

Where R_k = input to the k^{th} output layer neuron.
W_{jk} = weight of the j^{th} hidden layer neuron to the k^{th} output layer neuron.
M = number of the output layer neuron.
b_k = bias value for the k^{th} output layer neuron.

(iv) Transform the output, R_k by the transfer function to obtain the network outputs Y_k. The network outputs are compared with actual values, and an error at the k^{th} output neuron is computed:

$$E_k = T_k - Y_k \tag{5.4}$$

where, T_k = teaching (actual) value

The general principle used in the back-propagation learning method is the 'delta rule' (Appendix-B), which is based on the minimization of the sum of squares of the error obtained in equation (5.4). The reduction in the sum of squares of the error is performed by iteratively modifying the numerical values of the weights in the direction of the steepest descent with respect to the error. Hence, this procedure is called the 'steepest descent method' [85]. The weights in the hidden-output layer are adjusted first, and then the weights in the input-hidden layer are adjusted. The weights in the successive iterations are modified according to the following equation for layer 1 and t^{th} iteration:

$$w_{jk}(t+1) = w_{jk}(t) + \eta \, \delta_j(t) \, Q_{jk}(t) + \mu \, [w_{jk}(t) - w_{jk}(t-1)] \tag{5.5}$$
$$j = 1, 2, \ldots H; \qquad k = 1, 2, \ldots m$$

where δ_j = local gradient of the network

local gradient for the hidden-output layer δ_k is computed as follows

$$\delta_k (t) = E_k (t)\, Y_k (t)\, [1- Y_k (t)] \quad k = 1, 2, \ldots..m \tag{5.6}$$

local gradient for the input-hidden layer

$$\delta_j (t) = Q_j (t)\, [1-Q_j (t)]\, \Sigma\, \delta_k (t)\, w_{jk} \tag{5.7}$$

Stopping criteria

The stopping criteria for the back-propagation algorithm are listed below.

(i) The back-propagation algorithm is considered to have converged when the absolute rate of change in the mean squared error (MSE) per epoch is very small.

(ii) After an each training iteration, the network is tested for its generalization performance. The training process stops when the generalization performance reaches the maximum on the test data set.

The *first* criterion of minimizing the MSE over a training data set does not necessarily imply good generalization. The *second* criteria trains the network iteratively based on number of training epochs. Each training epoch decides the value of synaptic weight and bias of the network. Thereafter, the trained network is tested on the 'test data' set, which gives the prediction error. If the prediction error exceeds the statistical standards (i.e. the degree of agreement, 'd'), the network is again trained with increased number of epochs and so the process is repeated. The *second* stopping criterion is adopted due to its superior learning efficiency. Table 5.1 summarizes the criteria used in developing the ANN based vehicular pollution models.

Table 5.1 Criterion used in the ANN based vehicular pollution modelling.

Sl. No.	Item	Criterion used in the present study	Similar criterion used in the previous studies
1.	Criteria for selection of neural network architecture	Input neurons= number of input variables Output neurons= number of output variable Hidden neurons= smallest number of neurons that yields a minimum prediction error on the test data set [86].	[18], [82], [83], [239] and [240]
2.	Criteria for selection of neuron activation functions	Input neurons= identity function Output neurons= identity function Hidden neurons = hyperbolic tangent function [69]	[82], [83], and [240]
3.	Criteria for selection of learning parameters	The learning parameters converge to the network configuration and give best performance on the test data with least number of epochs/iterations [86].	[240]
4.	Criteria for initialization of network weights	Network weights are uniformly distributed inside in the range of [$(-2.4/F_i)$, $(+2.4/F_i)$], where F_i = total number of inputs [86].	[18]
5.	Training algorithm	Back-propagation [71], [84]	[82], [83], [235], [239] and [240]
6.	Stopping criteria for neural network training	Stopping criteria: after each training iterations/epochs the network is tested for its performance on test data set. The training process is stopped when the performance reach the maximum on test data set [86], [259].	[18],[83],[235] and [240]
7.	Statistics for model testing	RMSE and 'd' [263]	[18], [82], [83] and [240]
8.	ANN modelling data set	***Training data set*****:** for training neural network. ***Test data set*****:** for testing of neural network during training. ***Evaluation data set*****:** for performance evaluation of trained neural network model.	[82], [83], and [240]

5.4 Statistics for Testing ANN based Vehicular Pollution Models

The statistical indicators for testing and evaluating the ANN based vehicular pollution model are systematic and unsystematic root mean square error ($RMSE_S$ and $RMSE_U$), mean bias error (MBE), mean square error (MSE), coefficient of determination (r^2), linear best fit constant (a) and gradient (b), mean of the observed and

predicted concentration ($\overline{O}$ and $\overline{P}$, respectively) and their standard deviations (σ_o and σ_p, respectively) and 'd' values [263]. It is not uncommon to find models that are evaluated by the correlation coefficient 'r^2'. However, the 'r^2' statistic may not be appropriate in assessing the accuracy of air quality model predictions. The model evaluation based on 'r^2' statistics mostly fails due to the presence of 'lag' between source emission quantity and the ambient pollutant concentration. The 'lag' is due to adverse meteorological conditions (inversion) which implies the accumulation of pollutants in the ambient environment during 'odd' hours of the day when there are no source emissions [172]. The 'd' is a descriptive statistics. It reflects the degree to which the observed variate is accurately estimated by the simulated variate. The 'd' is not a measure of correlation or association in the formal sense, but rather a measure of the degree (based on ensemble average) to which the model predictions are error free. At the same time, 'd' is a standardized measure in order that it may be easily interpreted and cross-comparisons of its magnitudes for a variety of models, regardless of units, can readily be made. It varies between 0 and 1. A computed value of 1 indicates perfect agreement between the observed and predicted observations, while 0 connotes complete disagreement [263]. The value of 'd' is expressed as:

$$d = 1 - \frac{\sum_{i=1}^{N}(P_i - O_i)^2}{\sum_{i=1}^{N}\left[\left|P_i - \bar{O}\right| + \left|O_i - \bar{O}\right|\right]^2} \tag{5.8}$$

$\bar{o}$ = average of the observed data
p = predicted data

5.5 Development of ANN based Vehicular Pollution Models

Near the traffic intersections and busy roads, the vehicular pollution dispersion is influenced by two factors; *one*, the natural turbulence

and *second*, the traffic generated turbulence (traffic wake). The natural turbulence is represented by meteorological variables and the 'traffic wake' relates to the traffic characteristic variables [83, 184]. Therefore, ANN based vehicular pollution models are developed considering both the meteorological and the traffic characteristic variables. The models are formulated using three choices of input data sets. *Firstly*, considering both meteorological and traffic characteristics input data; the *second*, considering only meteorological input data; and the *third*, considering only traffic input data. The output corresponding to these inputs is the vehicular pollution concentration. The choice of inputs to model are directly connected to the quantity of information given to the neural network and is generally constituted from the meteorological and traffic characteristic data.

A back-propagation technique with momentum term algorithm, implemented in the SNNS, is used to train the models. The criteria summarized in Table 5.1 are adopted for training the ANN based vehicular pollution models. The trained models are saved at frequent intervals of training epochs that are used for prediction. Several hundreds of experiments are performed to determine the best combination of model parameters – learning rate (η), momentum constant (μ), number of the hidden layers, number of hidden neurons (H), learning algorithm and activation function. The root mean square error (RMSE) and degree of agreement (d values) are estimated to check the applicability of the trained ANN based models.

5.6 Case Study

This section discusses the development of ANN based vehicular pollution models for predicting 1-hr, 8- hr average CO and 24-hr average NO_2 concentrations at two air quality control regions (AQCRs), one representing a traffic intersection (AQCR1) and other, an arterial road (AQCR2), in the Delhi city, India.

Figure 5.1 shows the study area along with air quality sampling stations being monitored by Central Pollution Control Board (CPCB), New Delhi. AQCR1 is located adjacent to kerb side of highly trafficked road- Bhadur Shah Zafar marg, which is one of the roads

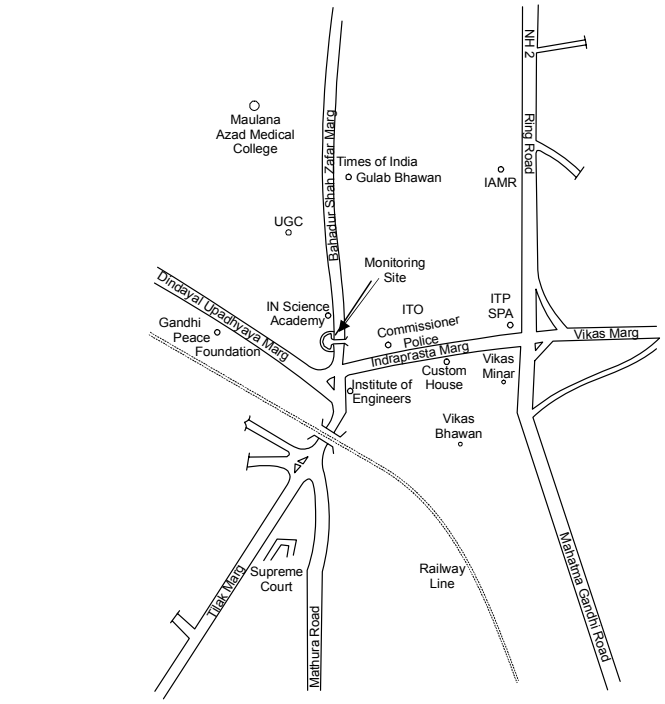

(a) AQCR1

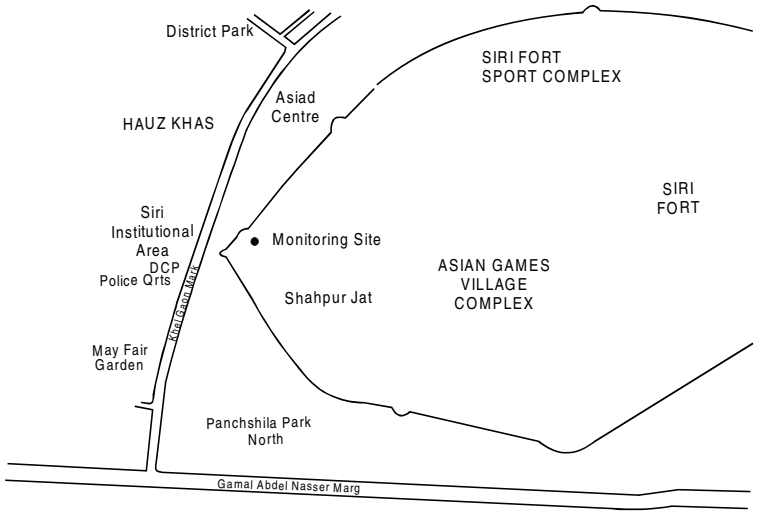

(b) AQCR2

Fig. 5.1. Details of AQCRs in Delhi city.

crossing income tax office (ITO) intersection. This region comes under the central business district housing a number of government office buildings along with reputed educational institutes. The region is considered to be an area of most intense human activity and also tagged for the 'worst air quality' in the city. The AQCR2 - Sirifort monitoring station, is located in the south of central Delhi. The surrounding area is comprised of dense residential localities, commercial establishments, institutional areas and famous sport complex. This station is situated near moderately busy traffic road, Khelgaon marg.

5.6.1 Pollutant Data

The 1-hr average CO concentrations are collected from the CPCB between January 1997 and December 1999 for two AQCRs. Similarly for the same duration, the daily average NO_2 data (working days-Monday to Friday) are collected at AQCR1 and AQCR2. A standardized (DIN specification) sample collection system is installed at both the AQCRs to collect the representative roadside samples [264]. The sampling point is about three meters from the ground level. At both the AQCRs, CO is measured by non-dispersive infrared (NDIR) absorption gas analyzer. The NO_2 samples at AQCR1 are collected by the high volume sampler and analysed by Jacob and Hochhesier modified (Na-Arsenite) method; where as at AQCR2, NO_2 concentrations are recorded by Chemiluminescent detector [23].

The analysis of pollutant data shows highest ground level concentrations of CO and NO_2 during winters (November to March); while lowest during tropical monsoon period (July to September). Table 5.2 shows the average monthly CO at both the AQCRs. The monthly average CO concentrations at AQCR1 ranged between 8.8 ppm (November, 1998) - 1.84 ppm (June, 1999) and at AQCR2, it ranged between 5.97 ppm (November, 1997) - 1.29 ppm (April, 1997). Table 5.2 shows the maximum, minimum 1-hr average CO concentrations at both AQCRs. The 1-hr maximum CO concentration of 39.6 ppm and 37.5 ppm are recorded during winter period at AQCR1 and

AQCR2, respectively, while the lowest is 0.1 ppm at both the AQCRs.

Table 5.2 Hourly maximum, minimum and daily mean CO concentrations for each month of the period January 1997 to December 1999.

(a) AQCR1

Month	CO concentration, ppm								
	1997			1998			1999		
	Maxi-mum	Mini-mum	Aver-age	Maxi mum	Mini-mum	Aver-age	Maxi mum	Mini-mum	Aver-age
January	39.6	1.4	6.84	21.6	0.2	3.96	14.1	1.3	4.04
February	19.5	0.7	4.11	21.8	0.5	3.78	16.9	2.7	4.93
March	20.6	0.9	4.38	12.9	1.4	3.56	10.2	1.6	3.15
April	21.8	1.1	4.3	14.9	0.9	3.44	16.8	0.9	3.79
May	20.5	0.4	4.38	16.8	0.3	3.3	14.2	0.7	3.28
June	15.3	0.4	3.91	11.6	0.5	2.98	9.4	0.2	1.84
July	9.2	1	3.37	10	1.1	3.56	6.6	0.1	2.35
August	11.4	0.7	2.68	17.7	1.5	5.78	7.2	0.4	2.17
September	13.7	0.4	3.29	26.4	1.1	4.26	9.3	1	3.25
October	14.9	1.1	3.69	18.7	1.5	5.57	17.2	1.5	5.33
November	32.3	1.3	5.45	33.8	2.5	8.8	21.1	1.2	4.86
December	0.1	0.2	4.04	37.1	1.1	7.15	29.6	0.3	5.14

(b) AQCR2

Month	CO concentration, ppm								
	1997			1998			1999		
	Maxi-mum	Mini mum	Av-erage	Maxi-mum	Mini-mum	Aver-age	Maxi-mum	Mini-mum	Aver-age
January	31.4	0.1	4.39	18.7	0.9	3.42	13.3	0.5	2.34
February	16.6	0.6	2.47	11.7	0.8	2.41	17.7	0.1	2.83
March	14.8	0.4	1.78	10.6	1	2.27	17.2	0.1	1.97
April	14.5	0.1	1.29	10.5	1.1	3.18	18	0.1	2.34
May	11.1	0.1	1.49	17.5	0.2	2.33	6.9	0.7	2.36
June	7.3	1.2	2.11	8.1	0.3	1.66	4.3	0.8	2.3
July	8.1	0.5	2.0	6.9	0.7	2.76	NR	NR	NR
August	7.7	0.8	2.04	4.2	0.7	1.59	NR	NR	NR
September	8	1.2	3.09	10.5	0.6	2.4	NR	NR	NR
October	26.2	1.3	3.78	17.6	0.6	3.47	20.6	0.9	5.83
November	30	1.4	5.97	17	1	4.61	37.5	0.3	5.14
December	27.2	1.1	4.58	31.2	1	4.63	9.75	2.2	4.59

Note: NR = Due to instrument malfunction CO readings are not recorded.

Table 5.3 provides the pattern of monthly NO_2 concentration data at AQCR1 and AQCR2. The levels of NO_2 in winter months

(November-March) are higher in comparison to summer (April-June) and monsoon month values (July-September).

Table 5.3 Daily maximum, minimum and mean NO_2 concentrations for each month of the period January 1997 to December 1999.

(a) AQCR1

Month	NO_2 concentration, ppb								
	1997			1998			1999		
	Maxi-mum	Mini mum	Aver-age	Maxi mum	Mini-mum	Av-erage	Maxi mum	Mini-mum	Aver-age
January	63.3	9	26.4	76.3	16.3	43.9	35.8	13.5	24.0
February	29.6	10.5	19.9	71.5	15.6	37.8	45.1	13.8	29.2
March	43.9	20.9	28.8	55.2	19	34.6	43	17.4	29.0
April	42	21.8	32.5	44.5	22.6	31.4	37.4	20.5	28.3
May	53.1	27.1	38.5	53.1	13.4	30.3	36.3	18	26.1
June	46.2	19.2	32.0	39.5	9.3	24.1	32	20.5	26.0
July	37.2	18.2	28.2	29.4	14.5	21.4	35.8	19	27.4
August	41.3	19.5	27.1	55.1	21.6	35.1	37.2	24.6	29.9
September	50.3	18.3	32.4	47.8	19.7	30.7	45.1	27.2	34.5
October	92.3	34	54.8	47.8	22.4	36.5	52.3	32.6	43.8
November	105.4	32.5	55.6	53.9	12.9	33.6	58.1	26.2	43.7
December	89.7	21.1	43.1	89.2	27.6	43.6	65.3	21.2	40.4

(b) AQCR2

Month	NO_2 concentration, ppb								
	1997			1998			1999		
	Maxi-mum	Minim um	Aver age	Maxi mum	Minim um	Aver age	Maxim um	Mini-mum	Aver-age
January	51.1	30.3	41.0	NR	NR	NR	70.9	21.13	41.6
February	63.0	27.3	45.4	NR	NR	NR	12.3.3	19.5	52.5
March	40.3	14.0	19.2	NR	NR	NR	43.3	22.3	32.1
April	42.5	15.1	25.0	NR	NR	NR	85.4	14.8	46.0
May	17.1	11.6	13.8	NR	NR	NR	85.4	22.8	52.4
June	40.8	12.4	18.2	30.6	16.3	24.4	NR	NR	NR
July	41.3	26.2	28.9	30.2	16.3	23.8	NR	NR	NR
August	NR	NR	NR	26.8	15.7	19.5	33.4	14.3	18.4
September	NR	NR	NR	56.2	10.5	22.2	70.8	16.2	41.4
October	NR	NR	NR	90.6	26.3	53.9	NR	NR	NR
November	NR	NR	NR	NR	NR	NR	NR	NR	NR
December	NR	NR	NR	NR	NR	NR	NR	NR	NR

Note: NR = Due to instrument malfunction NO_2 readings are not recorded.

5.6.2 Traffic Data

Hourly traffic volume data are collected from the Central Road Research Institute (CRRI), New Delhi for both AQCRs for the three year study period (January 1997 to December 1999). The vehicles are classified into four groups (Table 5.4), for which emission factors are developed by the Indian Institute of Petroleum (IIP), Deharadun [265]. The daily average traffic volume at AQCR1 (ITO crossing) is three fold than that of the traffic volume at AQCR2 (KGM road). The estimated average daily traffic flow at AQCR1 and AQCR2 ranges between 1 76,000 to 1 13,000 and 62,000 to 40, 000 respectively. The analysis of traffic data showed that the traffic pattern on Monday and Friday, being the first and the last day of the working week respectively, is comparable. Similarly, the traffic pattern for the mid weekdays do not show significant difference. However, traffic pattern on weekends i.e. on Saturday and Sunday, show lean traffic flow than working weekdays traffic flow. The maximum daily average traffic flow is higher during Monday and Friday followed by Tuesday, Wednesday, Thursday, Saturday and Sunday. The composition of the traffic on all the weekdays is almost same on both the AQCRs. The total traffic composition at AQCR1 is dominated by two wheelers, followed by four wheeler gasoline-powered, three wheelers and four wheeler diesel-powered vehicles. Where as, at AQCR2, four wheeler gasoline-powered vehicles dominated the traffic, followed by two wheelers, three wheelers and four wheeler diesel-powered vehicles. The proportion of the morning peak flow at the AQCRs for weekdays varied between 8 to 12 % of the average daily traffic and morning peak hours occurred between 9 AM to 11 AM; while the proportion of evening varied from 7 to 9 % and evening peak occurs from 5 PM to 9 PM. The proportion of the morning and evening peak flows, as average of all weekdays (Monday to Sunday), is in more or less same range as in the working days (Monday to Friday).

The average weekday traffic flows are marginally low as compared to the average working day flows primarily due to low traffic volumes on Sunday.

Table 5.4 Vehicle classification and their emission factors.

Sl. No.	Classification	Vehicles classified	Emission factors				
			Pollutant	Up to 1991	1991-1995	1996-2000	2000-2005
1	Light duty gasoline powered vehicles	Cars, Jeeps, Vans, Taxis, etc.	CO	25	19.8	6.45	3.16
			NO_2	2.0	2.0	1.14	0.56
2	Light duty diesel powered vehicles	Buses, Mini-buses, Jeeps, Vans, etc.	CO	12.7	12.7	9.96	5.35
			NO_2	21	21	16.8	9.34
3	Two wheelers gasoline powered	Motor vehicles, Scooters, Mopeds	CO	8.3	6.49	5.0	2.4
			NO_2	0.1	0.1	0.1	0.1
4	Three wheelers gasoline powered	Autorickshaws	CO	12	12	8.1	4.8
			NO_2	0.26	0.26	0.26	0.26

5.6.3 Meteorological Data

The meteorological data is taken from Indian Meteorological Department (IMD), New Delhi. The hourly observations of cloud cover, pressure, mixing height, sun shine hours, visibility, temperature, humidity, rainfall, wind speed and direction are collected for the same period, for which air quality observations are made. Pasquill-Gifford stability scheme (Classes A to F) is used to determine hourly stability categories [266]. The average annual rainfall, humidity, pressure, cloud cover, temperature, visibility, wind speed, mixing height and sunshine hours in Delhi are 657 mm, 64.2 %, 483.4 mba, 2.8 okta, 24.7^{o}C, 94.6, 1.3 m/s, 322.2 m, and 6 hr/day, respectively. Table 5.5 lists the seasonal daily mean meteorological variables.

Table 5.5 Seasonal daily mean values of meteorological parameters recorded during the period January 1997 to December 1999.

Sl No.	Parameter	Winter	Summer	Monsoon	Post Monsoon
1	Cloud cover, okta	2.2	2.2	4.9	2.7
2	Humidity, %	68.6	45.6	75.8	72.7
3	Pasquill stability category (A-F: 1-6)	3.9	3.7	3.5	3.8
4	Pressure, mba	490	478.7	475.9	484.7
5	Rainfall, mm/day	0.48	1.44	4.08	2.64
6	Sunshine hours, hour/day	5.2	8.0	4.8	6.2
7	Temperature, ^{0}C	17.0	31.5	30.6	26.6
8	Visibility[d]	94.1	95.3	95.1	94.7
9	Wind direction, degree	133.9	165.7	130.6	102.9
10	Wind speed, ms^{-1}	1.1	1.9	1.5	0.9
11	Mixing height, m	298.8	387.2	311.9	305.8

[d] IMD synoptic codes for representing visibility

Code	Visibility	Code	Visibility
90	< 50 m	95	2000 m
91	50 m	96	4000 m
92	200 m	97	10 kms
93	500 m	98	20 kms
94	1000 m	99	≥ 50 kms

5.6.4 Models Development

The data at each AQCR has been classified into 'training', 'test' and 'evaluation' data sets. Two year data from 1st January 1997 to 31st December 1998 is used for model training. Data for the months January, February, 1st to 15th March, April, 1st to 15th May, July, 1st to 8th August, 16th to 30th September and 1st to 10th October 1999 are used for model test purposes. Further the data for the months of 16th to 31st March, 16th to 31st May, June, 9th to 31st August, 1st to 15th September, 11th to 31st October, November and December 1999 are used for the evaluation of the ANN based vehicular pollution models. The random selections of the data for training, generalization

and for the evaluation purposes are based on seasonal variations in meteorological and pollutant concentration in the AQCRs.

I 1-hr average ANN based CO models

(i) 1-hr average CO model with meteorological and traffic characteristic variables as input to the multilayer neural network ($ANNCO_{1hrA1}$ and $ANNCO_{1hrA2}$ models for AQCR1 and AQCR2, respectively).

(ii) 1-hr average CO model with meteorological variables as input to the multilayer neural network ($ANNCO_{1hrB1}$ and $ANNCO_{1hrB2}$ models for AQCR1 and AQCR2, respectively).

(iii) 1-hr average CO model with traffic characteristic variables as input to the multilayer neural network ($ANNCO_{1hrC1}$ and $ANNCO_{1hrC2}$ models for AQCR1 and AQCR2, respectively).

II 8-hr average ANN based CO models

(i) 8-hr average CO model with meteorological and traffic characteristic variables as input to the multilayer neural network ($ANNCO_{8hrA1}$ and $ANNCO_{8hrA2}$ models for AQCR1 and AQCR2, respectively).

(ii) 8-hr average CO model with meteorological variables as input to the multilayer neural network ($ANNCO_{8hrB1}$ and $ANNCO_{8hrB2}$ models for AQCR1 and AQCR2, respectively).

(iii) 8-hr average CO model with traffic characteristic variables as input to the multilayer neural network ($ANNCO_{8hrC1}$ and $ANNCO_{8hrC2}$ models for AQCR1 and AQCR2, respectively).

III 24-hr average ANN based NO_2 models

(i) 24-hr average NO_2 model with meteorological and traffic characteristic variables as input to the multilayer neural network ($ANNNO2_{24hrA1}$ and $ANNNO2_{24hrA2}$ models for AQCR1 and AQCR2, respectively).

(ii) 24-hr average NO_2 model with meteorological variables as input to the multilayer neural network ($ANNNO2_{24hrB1}$ and $ANNNO2_{24hrB2}$ models for AQCR1 and AQCR2, respectively).

(iii) 24-hr average NO_2 model with traffic characteristic variables as input to the multilayer neural network ($ANNNO2_{24hrC1}$ and $ANNNO2_{24hrC2}$ models for AQCR1 and AQCR2, respectively).

Table 5.6 describes the number of patterns used in each model type for training, testing and evaluation. The list of input parameters used for each model type is given in Table 5.7. It is important to mention that wind direction[e] data is dichotomised using the sine and cosine functions. This enabled the neural network algorithm to work properly despite discontinuities in the original cyclic signals [267].

Table 5.6 Training, test and evaluation data sets for each ANN based vehicular exhaust emission model type and for each site.

Site	Model ID	Number of patterns		
		Training	Test	Evaluation
AQCR1	$ANNCO_{1hrA1}$ $ANNCO_{1hrB1}$ $ANNCO_{1hrC1}$	16708	4218	4194
	$ANNCO_{8hrA1}$ $ANNCO_{8hrB1}$ $ANNCO_{8hrC1}$	2113	534	532
	$ANNNO2_{24hrA1}$ $ANNNO2_{24hrB1}$ $ANNNO2_{24hrC1}$	522	128	133
AQCR2	$ANNCO_{1hrA2}$ $ANNCO_{1hrB2}$ $ANNCO_{1hrC2}$	14363	2049	2527
	$ANNCO_{8hrA2}$ $ANNCO_{8hrB2}$ $ANNCO_{8hrC2}$	1834	266	326
	$ANNNO2_{24hrA2}$ $ANNNO2_{24hrB2}$ $ANNNO2_{24hrC2}$	262	74	47

[e] The non-cyclic wind direction variable has been converted into cyclic variable using the expression sin (wind direction) and cos (wind direction), where wind direction is expressed in degrees.

Table 5.7 Model input variables for the ANN based vehicular exhaust emission models.

Model ID	Input variables
$ANNCO_{1hrA1}$ $ANNCO_{1hrA2}$ $ANNCO_{8hrA1}$ $ANNCO_{8hrA2}$ $ANNNO2_{24hrA1}$ $ANNNO2_{24hrA2}$	Cloud cover, humidity, mixing height, pressure, Pasquill stability, sunshine hour, temperature, visibility, sin(wind direction), cos(wind direction), wind speed, two wheeler, three wheeler, four wheeler(gasoline), four wheeler (diesel), source strength (CO) and source strength (NO_2)
$ANNCO_{1hrB1}$ $ANNCO_{1hrB2}$ $ANNCO_{8hrB1}$ $ANNCO_{8hrB2}$ $ANNNO2_{24hrB1}$ $ANNNO2_{24hrB2}$	Cloud cover, humidity, mixing height, pressure, sunshine hour, temperature, visibility, sin(wind direction), cos(wind direction) and wind speed
$ANNCO_{1hrC1}$ $ANNCO_{1hrC2}$ $ANNCO_{8hrC1}$ $ANNCO_{8hrC2}$ $ANNNO2_{24hrC1}$ $ANNNO2_{24hrC2}$	Two wheeler, three wheeler, four wheeler(gasoline), four wheeler (diesel) and source strength (CO) / (NO_2)

Data normalization

In order to use with the multilayer neural networks, all the data are normalized between the range, –1.0 to +1.0. This is carried out by determining the maximum (X_{max}) and minimum (X_{min}) values of each variables (X_i) over the entire period and calculating normalized variable using following formulation:

$$x_{i-norm} = 2\left[\frac{(x_i - x_{min})}{(x_{max} - x_{min})}\right] - 1.0 \qquad (5.9)$$

Scaling is provided because, during training initial neural network, weights are chosen randomly. If one input has large range and another has a small range, but both exhibit a similar amount of variance, then the network may ignore the small input due to the large contribution from the other input.

The data is later returned to original units using the following formulation [83]:

$$x_i = \left[\frac{(x_{i-norm} + 1.0)(x_{max} - x_{min})}{2}\right] + x_{min} \tag{5.10}$$

Using the processed data, 1-hr, 8-hr average ANN based CO models and 24-hr average ANN based NO_2 models are developed. The details are discussed below:

Development of 1-hr Average ANN based CO Models

(i) $ANNCO_{1hrA1}$ model (1-hr average meteorological and traffic characteristic variables as model input)

1-hr average ANN based CO models are developed using hourly meteorological and traffic characteristic variables as model input. The input in the ANN based vehicular pollution model consists of the 17 independent variables. The original total data set of 1-hr CO values for the three-year period at AQCR1, included 26280 values. The total of 1160 missing values represented 4 % of the whole data set. About 64 % of the total data set is used for model training, 16 % for test and 16 % for evaluation of the model. The 'training data set' should contain as many significant meteorological and traffic situations as possible. When a representative 'training data set' of patterns is not available, accurate prediction cannot be obtained from the neural network model [67]. For the present work, 'training data set' consists of all the seasonal patterns of hourly CO concentrations. Figure 5.2 shows the hourly CO values used for training the ANN based vehicular pollution model. Several hundreds of experiments

are performed to determine best combination of the 'η', μ, number of the hidden layers, H, learning algorithm and activation function.

Table 5.8 shows the statistics of 1-hr average ANN based CO models with the number of neurons in the hidden layer. As a result of several experiments, a fully connected feed-forward neural network, with seventeen neurons in the input layer, three neurons in the single hidden layer and one neuron in the output layer, shows satisfactory prediction on 'test data set'. Figure 5.3 shows the CO patterns used for the ANN based CO model testing. A number of computational runs are conducted using SNNS to find the optimum number of neurons in the hidden layer.

The inputs to these runs are the meteorological and traffic variables in the input layer, the output is in terms of pollutant concentration i.e. CO and the number of neurons in the hidden layer are varied from 2 to 34. The descriptive statistics tests i.e. 'd' value and RMSE are applied to arrive at the optimum number of neurons in the hidden layer. Table 5.8 describes the above statistical test values, which are used to find out number of neurons in the hidden layer. The architecture of the 1-hr average ANN based CO model with the meteorological and the traffic characteristic variables as inputs, is shown in Figure 5.4. Each neuron, out of seventeen input neurons, represents each of the meteorological and the traffic characteristic variables. The one output neuron represents the hourly estimates of the CO concentration. The guidelines, explained in the section-5.3, are considered for choosing the optimum 'η', 'μ', the number of hidden layers, H, the learning algorithm and the activation function. Trained ANN based CO model network is saved at frequent intervals of training epochs. The RMSE and 'd' values are estimated to check the applicability of the trained ANN based CO model. This procedure is followed till the trained ANN based vehicular pollution model gives the best prediction performance on 'test data set' (Table 5.9). After several experimentation, the best RMSE and 'd' values are found for the model parameters 'η' = 0.001 and 'μ' = 0.7. The final neuron definitions and synaptic weights of the $ANNCO_{1hrA1}$ model are presented in Table D.1a and D.1b respectively in Appendix-D.

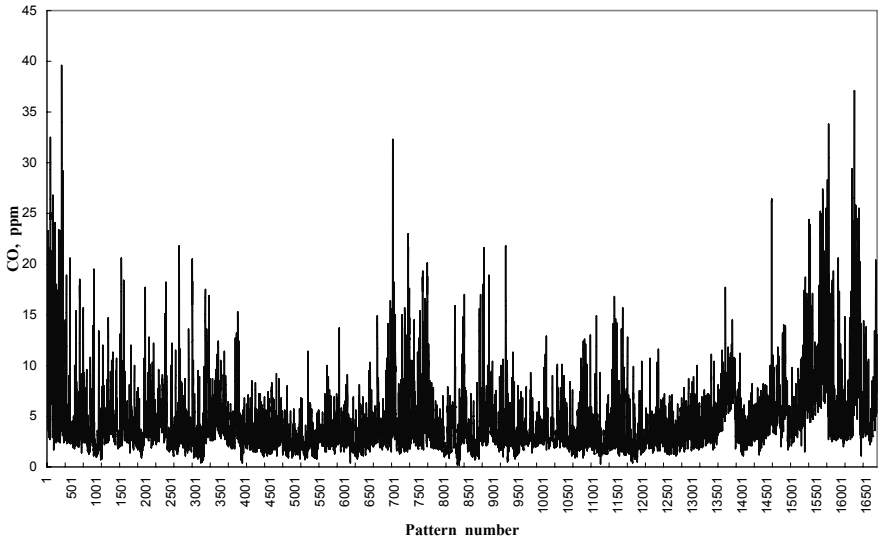

Fig. 5.2. CO training pattern used for development of 1-hr average ANNCO models at AQCR1.

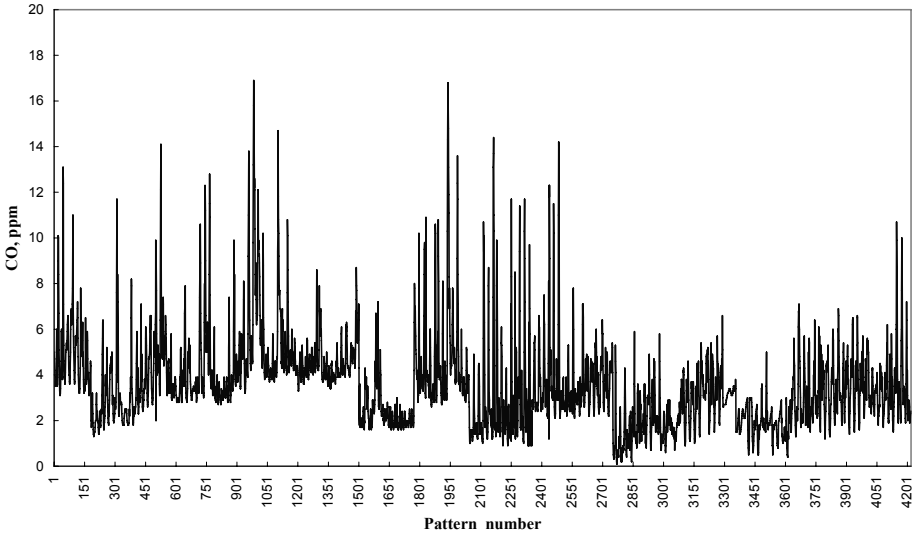

Fig. 5.3. CO test pattern used for generalization of 1-hr average ANNCO models at AQCR1.

Table 5.8 Experimental simulation results for optimization of the hidden layer neurons for the 1-hr average ANN based CO model.

Number of hidden neurons	Mean square error after network stabilization	Statistical parameter	
		d	RMSE
2	0.01564	0.5959	2.22
3	0.01569	0.6250	2.18
4	0.01560	0.6132	2.24
5	0.01567	0.6124	2.26
6	0.01573	0.6058	2.29
7	0.01574	0.6048	2.30
8	0.01559	0.6163	2.23
9	0.01577	0.6028	2.33
10	0.01567	0.6025	2.34
11	0.01577	0.5999	2.37
12	0.01570	0.6016	2.35
13	0.01571	0.5985	2.37
14	0.01575	0.5949	2.40
15	0.01576	0.5976	2.37
16	0.01577	0.5959	2.38
17	0.01577	0.5949	2.41
18	0.01573	0.5948	2.39
19	0.01580	0.5954	2.41
20	0.01577	0.5924	2.44
21	0.01577	0.6061	2.34
22	0.01578	0.5971	2.40
23	0.01577	0.5932	2.43
24	0.01575	0.5939	2.41
25	0.01579	0.5949	2.42
26	0.01573	0.5971	2.38
27	0.01574	0.5927	2.43
28	0.01578	0.6011	2.35
29	0.01575	0.5915	2.45
30	0.01576	0.5954	2.38
31	0.01570	0.5935	2.41
32	0.01572	0.5920	2.45
33	0.01574	0.5945	2.42
34	0.01571	0.5948	2.40

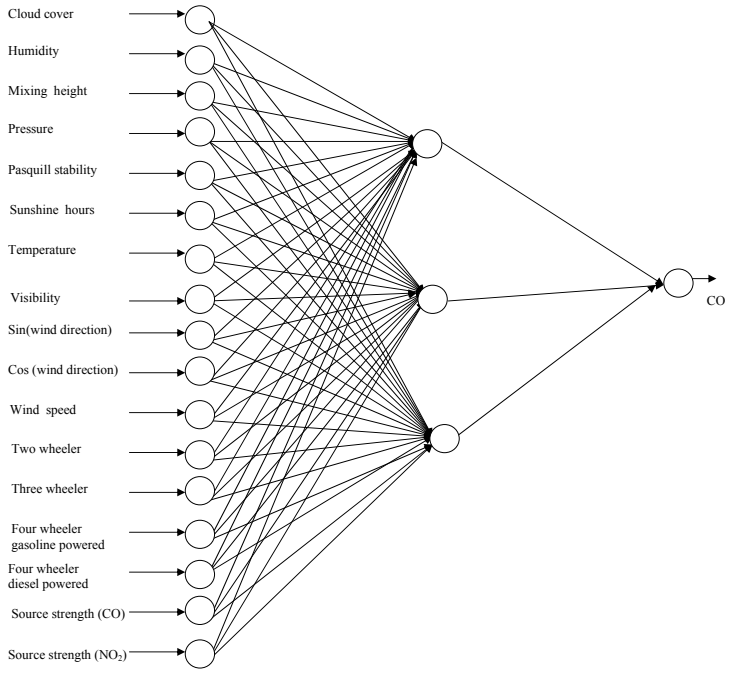

Fig. 5.4. Structure of 17:3:1 ANN based CO model.

Table 5.9 Estimates of the statistics during generalization of the $ANNCO_{1hrA1}$ model.

Epoch	d	RMSE
100	0.626	2.1823
200	0.6435	2.1200
300	0.6526	2.1000
400	0.6568	2.1000
500	0.6587	2.0999
600	0.6598	2.0988
700	0.6607	2.0976
800	0.6611	2.0970
900	0.6621	2.0960
1000	0.6623	2.0930
1100	0.6624	2.0906
1200	0.6624	2.0905
1300	0.6626	2.0899
1400	0.6630	2.0893
1500	0.6620	2.0904
1600	0.6610	2.0910
1700	0.6600	2.0920
1800	0.6600	2.0930
1900	0.6600	2.0940
2000	0.6600	2.0950

(ii) ANNCO$_{1hrB1}$ model (1-hr average meteorological variables as model input)

The objective of this model is two fold. *First*, is to develop ANN based vehicular pollution model to forecast 1-hr average CO concentration using routinely monitored meteorological variables. *Second*, to study the sensitivity of the traffic characteristic variables in 1-hr average ANN based CO model.

The number of training patterns and test patterns remain same as that of ANNCO$_{1hrA1}$ model. In order to meet the second criteria, the number of neurons is also been kept constant (i.e. 3) in the hidden layer. The final architecture of the ANN based CO model (ANNCO$_{1hrB1}$) with the meteorological predictor as input variable, is expressed as 10:3:1 (Figure 5.5). By following the step-by-step training procedures, with $\eta = 0.001$ and $\mu = 0.3$, the best model prediction on 'test data set' is achieved at 2000 epoch. The estimates of the statistics during generalization of the ANNCO$_{1hrB1}$ model on 'test data set' are presented in Table 5.10. The final neuron definitions and synaptic weights of the ANNCO$_{1hrB1}$ model are presented in Table D.2a and D.2b respectively in Appendix-D.

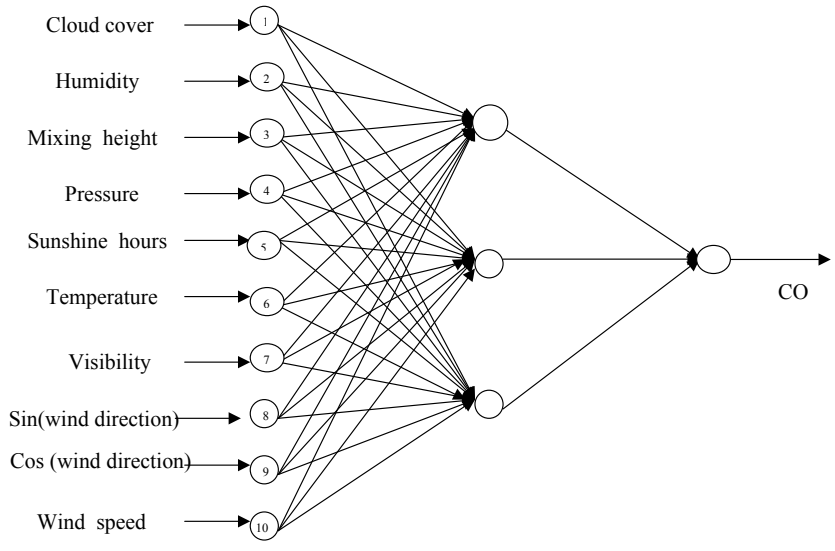

Fig. 5.5. Structure of 10:3:1 ANN based CO model.

Table 5.10 Estimates of the statistics during generalization of the $ANNCO_{1hrB1}$ model.

Epoch	d	RMSE
200	0.49	3.03
400	0.51	2.89
600	0.52	2.81
800	0.53	2.75
1000	0.54	2.7
1200	0.545	2.65
1400	0.547	2.6
1600	0.55	2.58
1800	0.552	2.58
2000	0.552	2.57
2200	0.55	2.58
2400	0.55	2.59
2600	0.55	2.59
2800	0.55	2.60
3000	0.55	2.61

(*iii) $ANNCO_{1hrC1}$ (1-hr traffic characteristic variables as model input)*

This model is developed with five traffic characteristic variables as input to the ANN based CO model ($ANNCO_{1hrC1}$), i.e. two-wheeler, three-wheeler, four wheeler-gasoline-powered, four-heeler diesel-powered and source strength of CO. The objective of this model is to study the sensitivity of meteorological variables in the 1-hr average ANN based CO model. Figure 5.6 show the structure of the ANN based CO model having traffic characteristic variable as input to the model. Table 5.11 lists the statistics of $ANNCO_{1hrC1}$ model during generalization. The final neuron definitions and synaptic weights of the $ANNCO_{1hrC1}$ model are provided in Table D.3a and D.3b respectively in Appendix-D.

(iv) $ANNCO_{1hrA2}$ (1-hr average meteorological and traffic characteristic variables as model input at AQCR2)

At AQCR2, out of three-year data set of 1-hr CO values (26280), a total of 7341missing values represented 28 % of the whole data set. About 55 % the of total data is used for the ANN based CO model

Table 5.11 Estimates of the statistics during generalization of the $ANNCO_{1hrC1}$ model.

Epoch	d	RMSE
5	0.4	3.73
10	0.41	3.72
15	0.41	3.73
20	0.41	3.74
25	0.41	3.75
30	0.41	3.76
35	0.41	3.77
40	0.41	3.77
45	0.41	3.78
50	0.41	3.78
55	0.41	3.79
60	0.41	3.79
65	0.41	3.79
70	0.41	3.79
75	0.41	3.80

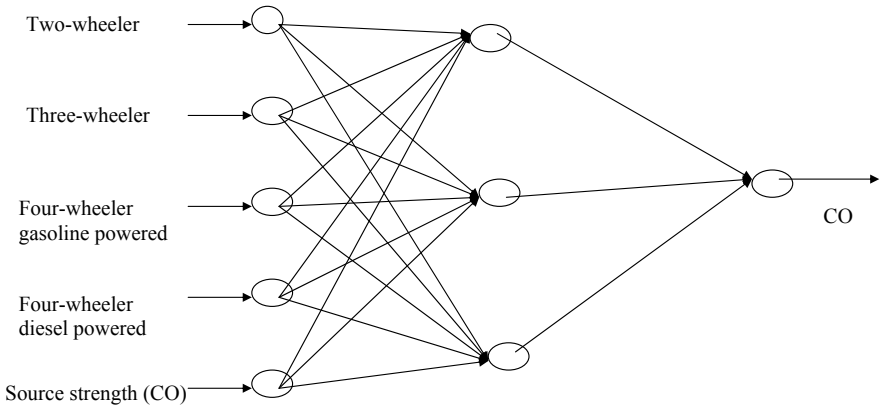

Fig. 5.6. Structure of 5:3:1 ANN based CO model.

training, 7.5 % for the model testing and 9.5 % for the final ANN based CO model evaluation. Network architecture of 17:3:1 is used for the development of $ANNCO_{1hrA2}$ model. This model is similar to $ANNCO_{1hrA1}$ model of AQCR1, consisting of seventeen input variables. Figure 5.7 and 5.8 show the 1-hr average CO patterns used for the training and testing of $ANNCO_{1hrA2}$ model, respectively. After repeated experiments, the best prediction is obtained at 200 epoch with 'η' = 0.001 and 'μ' = 0.3. Table 5.12 shows the statistics estimated during generalization of the $ANNCO_{1hrA2}$ model on 'test data set'. The final neuron definitions and synaptic weights of the $ANNCO_{1hrA2}$ model are described in Table D.4a and D.4b respectively in Appendix-D.

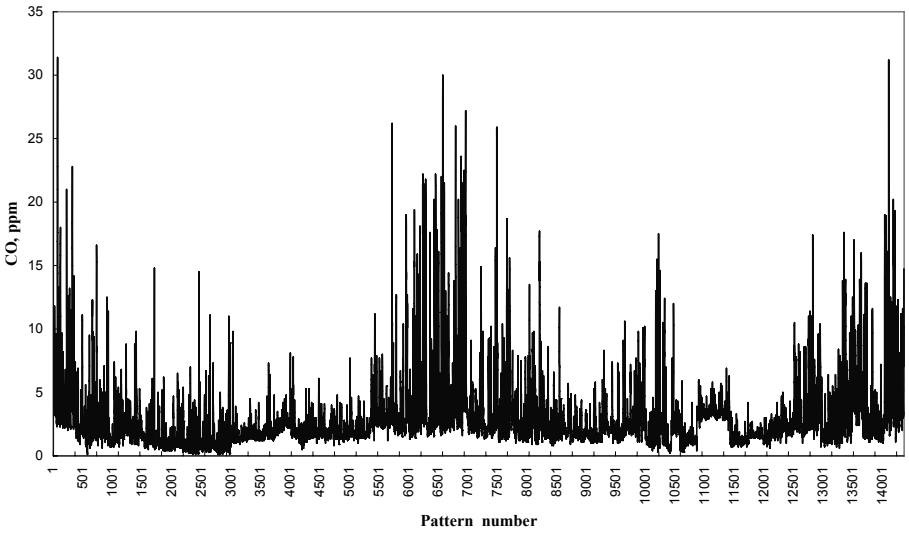

Fig. 5.7. CO training pattern used for development of 1-hr average ANNCO models at AQCR2.

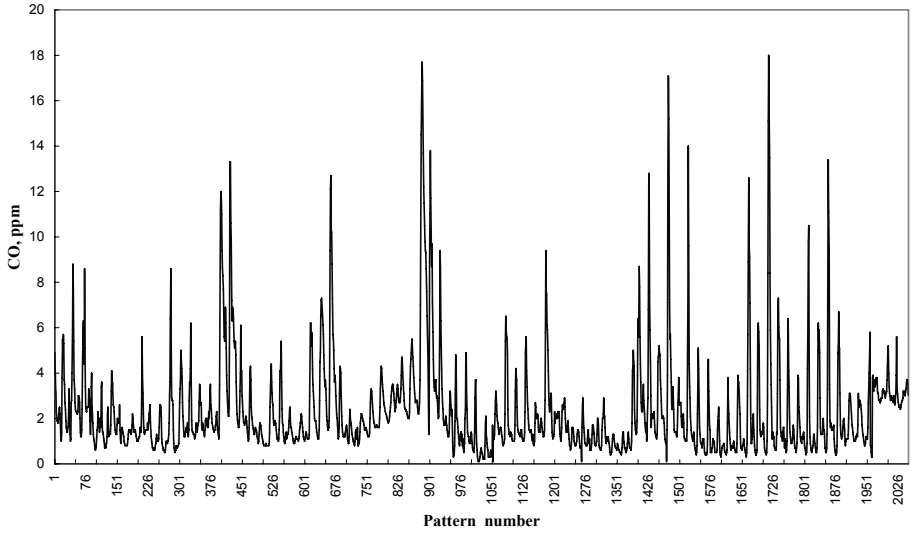

Fig. 5.8. CO test pattern used for generalization of 1-hr average ANNCO model at AQCR2.

Table 5.12 Estimates of the statistics during generalization of the $ANNCO_{1hrA2}$ model.

Epoch	d	RMSE
50	0.648	2.238
100	0.647	2.21
150	0.645	2.207
200	0.655	2.105
250	0.647	2.208
300	0.647	2.209
350	0.648	2.213
400	0.648	2.217
450	0.648	2.219
500	0.648	2.220

(v) $ANNCO_{1hrB2}$ (*1-hr average meteorological variables as model input at AQCR2)*

Neural network architecture of 10:3:1 is used in the development of the $ANNCO_{1hrB2}$ model. Table 5.13 presents the generalization statistics of the $ANNCO_{1hrB2}$ model on 'test data set'. The best model prediction is obtained at 'η' = 0.001 and 'μ' = 0.3 with 600 epoch. The final neuron definitions and synaptic weights of the $ANNCO_{1hrB2}$ model are summarized in Table D.5a and D.5b respectively in Appendix-D.

Table 5.13 Estimates of the statistics during generalization of the $ANNCO_{1hrB2}$ model.

Epoch	d	RMSE
50	0.644	2.26
100	0.649	2.186
150	0.65	2.15
200	0.65	2.146
250	0.65	2.144
300	0.649	2.14
350	0.649	2.14
400	0.65	2.14
450	0.65	2.139
500	0.65	2.137
600	0.65	2.136
700	0.64	2.139
800	0.64	2.147
900	0.636	2.158
1000	0.632	2.167
1100	0.629	2.169
1200	0.629	2.18
1300	0.629	2.18
1400	0.629	2.18
1500	0.629	2.19

(vi) $\mathbf{ANNCO_{1hrC2}}$ *(1-hr traffic characteristic variables as model input at AQCR2)*

Five traffic variables are used in the development of the $ANNCO_{1hrC2}$ model. The structure of this model is 5:3:1. With 'η'= 0.001 and 'μ' = 0.1, the $ANNCO_{1hrC2}$ model gives satisfactory performance on 'test data set' at 20 epoch (Table 5.14). The final neuron definitions and synaptic weights of the $ANNCO_{1hrC2}$ model are given in Table D.6a and D.6b respectively in Appendix-D.

Table 5.14 Estimates of the statistics during generalization of the $ANNCO_{1hrC2}$ model.

Epoch	D	RMSE
10	0.43	3.05
20	0.44	3.04
30	0.44	3.04
40	0.44	3.04
50	0.44	3.04
60	0.44	3.04
70	0.44	3.04
80	0.44	3.04
90	0.44	3.04
100	0.44	3.04

Development of 8-hr Average ANN based CO Models

(i) $ANNCO_{8hrA1}$ *(8-hr average meteorological and traffic characteristic variables as model input at AQCR1)*

The total data set of 8-hr average CO value at AQCR1 includes 3285 values. The total of 106 missing values represented 3 % of the whole data set. About 65% of the total data is used for model training, 16 % for testing, and 16 % for final evaluation of the 8-hr average ANN based CO model. To develop the $ANNCO_{8hrA1}$ model, hourly meteorological, traffic characteristic and CO data are processed to obtain 8-hr average values. A maximum of two hourly missing values are considered acceptable in order to remove uncontrolled bias due to equipment malfunction or equipment calibration [162]. A 17:3:1

structure is used for the development of $ANNCO_{8hrA1}$ model. Figure 5.9 and 5.10 show CO patterns, used in the training and testing of the $ANNCO_{8hrA1}$ model respectively. Table 5.15 describes performance of the $ANNCO_{8hrA1}$ model during generalization on the 'test data set'. The final neuron definitions and synaptic weights of the $ANNCO_{8hrA1}$ model are presented in Table D.7a and D.7b respectively in Appendix-D.

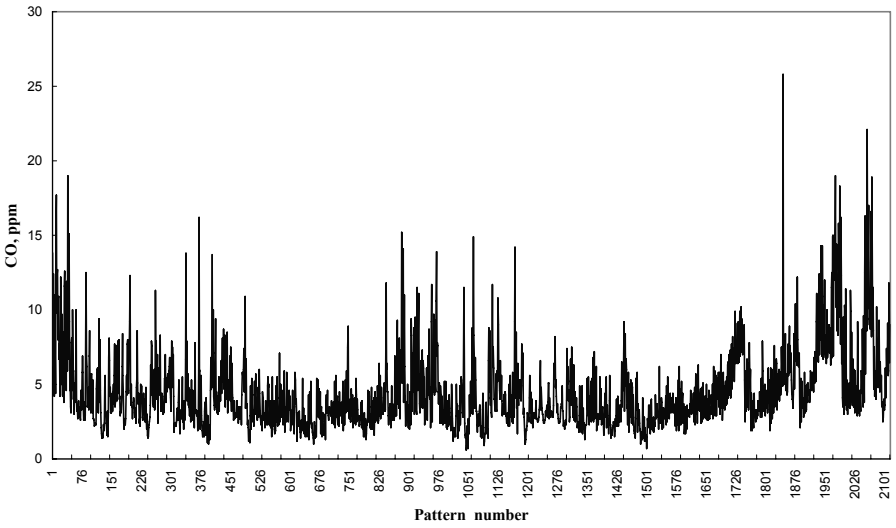

Fig. 5.9. CO training patterns used for development of 8-hr average ANNCO models at AQCR1.

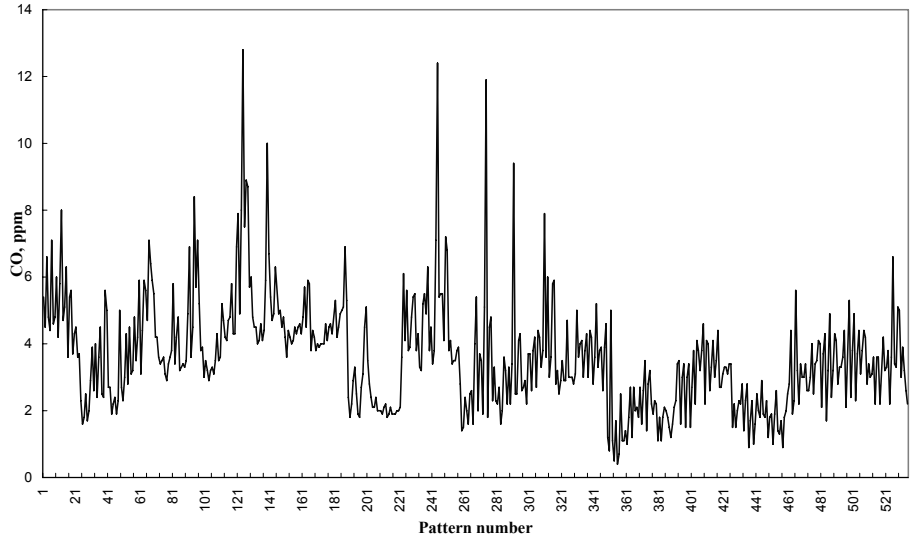

Fig. 5.10. CO test patterns used for generalization of 8-hr average ANNCO models at AQCR1.

Table 5.15 Estimates of the statistics during generalization of the $ANNCO_{8hrA1}$ model.

Epoch	d	RMSE
100	0.627	2.12
200	0.635	2.07
300	0.639	2.04
400	0.64	2.04
500	0.639	2.05
600	0.636	2.07
700	0.635	2.09
800	0.633	2.10
900	0.631	2.12
1000	0.63	2.13
1100	0.629	2.14
1200	0.628	2.16
1300	0.626	2.17
1400	0.624	2.18
1500	0.622	2.19
1600	0.618	2.22
1700	0.614	2.24
1800	0.609	2.27
1900	0.605	2.29
2000	0.602	2.31

(ii) ANNCO$_{8hrB1}$ (8-hr average meteorological variables as model input at AQCR1)

Neural network architecture of 10:3:1 is used for the development of the ANNCO$_{8hrB1}$ model. Table 5.16 summarizes performance of the ANNCO$_{8hrB1}$ model during generalization on the 'test data set'. The final neuron definitions and synaptic weights of the ANNCO$_{8hrB1}$ model are listed in Table D.8a and D.8b respectively in Appendix-D.

Table 5.16 Estimates of the statistics during generalization of the ANNCO$_{8hrB1}$ model.

Epoch	d	RMSE
100	0.62	2.03
200	0.638	1.92
300	0.644	1.92
400	0.648	1.90
500	0.65	1.88
600	0.653	1.87
700	0.654	1.87
800	0.654	1.87
900	0.655	1.86
1000	0.656	1.86
1100	0.656	1.86
1200	0.656	1.86
1300	0.655	1.87
1400	0.655	1.87
1500	0.655	1.87
1600	0.655	1.87
1700	0.655	1.88
1800	0.655	1.88
1900	0.655	1.88
2000	0.655	1.88

(iii) ANNCO$_{8hrC1}$ (8-hr average traffic characteristic variables as model input)

Neural network architecture of 5:3:1 is used for the development of the ANNCO$_{8hrC1}$ model. The performance of the ANNCO$_{8hrC1}$ model during generalization on 'test data set' is given in Table 5.17. The

final neuron definitions and synaptic weights of the $ANNCO_{8hrC1}$ model are given in Table D.9a and D.9b respectively in Appendix-D.

Table 5.17 Estimates of the statistics during generalization of the $ANNCO_{8hrC1}$ model.

Epoch	d	RMSE
5	0.438	2.18
10	0.438	2.13
15	0.439	2.13
20	0.44	2.12
25	0.44	2.12
30	0.44	2.13
35	0.44	2.14
40	0.44	2.14
45	0.44	2.14
50	0.44	2.15
55	0.44	2.15
60	0.44	2.16
65	0.44	2.16
70	0.44	2.16
75	0.44	2.16

(iv) $ANNCO_{8hrA2}$ (8-hr average meteorological and traffic characteristic variables as model input at AQCR2)

At AQCR2, a total of 859 missing values represented 26 % of the whole data (3285). Out of the total data, 56 % is used for training purpose, 8 % for testing and another 10 % for final 8-hr average ANN based CO model evaluation. A 17:3:1 structure is used for the development of the $ANNCO_{8hrA2}$ model. Figure 5.11 and 5.12 show CO patterns used for training and testing of the $ANNCO_{8hrA2}$ model respectively. The performance of the $ANNCO_{8hrA2}$ model during generalization on 'test data set' is shown in Table 5.18. The final neuron definitions and synaptic weights of the $ANNCO_{8hrA2}$ model are listed in Table D.10a and D.10b respectively in Appendix-D.

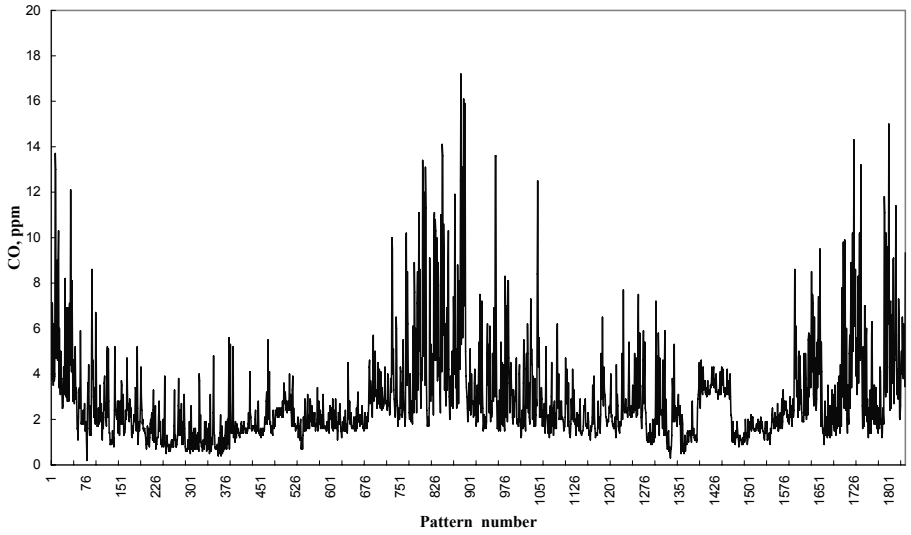

Fig. 5.11. CO training pattern used for development of 8-hr average ANNCO models at AQCR2.

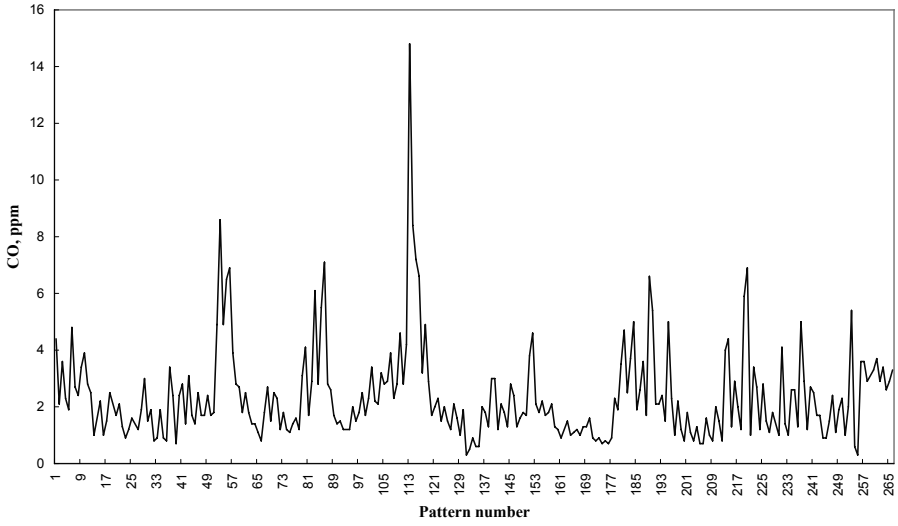

Fig. 5.12. CO test pattern used for generalization of 8-hr average ANNCO models at AQCR2.

Table 5.18 Estimates of the statistics during generalization of the $ANNCO_{8hrA2}$ model.

Epoch	d	RMSE
200	0.665	1.665
400	0.682	1.626
600	0.688	1.605
800	0.689	1.594
1000	0.689	1.587
1200	0.688	1.585
1400	0.689	1.580
1600	0.687	1.580
1800	0.687	1.580
2000	0.687	1.580
2200	0.686	1.580
2400	0.686	1.580
2600	0.686	1.580
2800	0.686	1.580
3000	0.686	1.580

(ii) $ANNCO_{8hrB2}$ (8-hr average meteorological variables as model input at AQCR2)

A 10:3:1 structure is used for the development of the $ANNCO_{8hrB2}$ model. The performance of the $ANNCO_{8hrB2}$ model during generalization on 'test data set' is shown in Table 5.19. The final neuron definitions and synaptic weights of the $ANNCO_{8hrB2}$ model are described in Table D.11a and D.11b respectively in Appendix-D.

Table 5.19 Estimates of the statistics during generalization of the $ANNCO_{8hrB2}$ model.

Epoch	d	RMSE
1000	0.69	1.567
2000	0.69	1.565
3000	0.7	1.530
4000	0.71	1.530
5000	0.7	1.550
6000	0.698	1.560
7000	0.69	1.570
8000	0.687	1.580
9000	0.684	1.580
10000	0.679	1.580

(iii) ANNCO$_{8hrC2}$ (8-hr average traffic characteristic variables as model input at AQCR2)

Neural network architecture of 5:3:1 is used for the development of the ANNCO$_{8hrC2}$ model. Table 5.20 shows the performance of the ANNCO$_{8hrC2}$ model during generalization on 'test data set'. The final neuron definitions and synaptic weights of the ANNCO$_{8hrC2}$ model are presented in Table D.12a and D.12b respectively in Appendix-D.

Table 5.20 Estimates of the statistics during generalization of the ANNCO$_{8hrC2}$ model.

Epoch	d	RMSE
10	0.42	1.99
20	0.43	1.98
30	0.44	1.97
40	0.43	1.98
50	0.43	1.99
60	0.43	1.99

Development of 24-hr Average ANN based NO_2 Models

(i) ANNNO2$_{24hrA1}$ (24-hr average meteorological and traffic characteristic variables as model input at AQCR1)

The 24-hr average ANN based NO_2 models are developed using daily average meteorological and traffic characteristics variables (seventeen) as model input. The total data set included 783 values. About 67 % of the total data is used for the model training, 16% the model testing and 17 % for the final evaluation of ANN based NO_2 models. Figure 5.13 and 5.14 show NO_2 patterns used for training and testing of the ANN based NO_2 models respectively.

Several hundred experiments are performed to determine the best combination of 'η','μ', the number of hidden layers, H, the learning algorithm and the transfer function. As a result, a fully connected feed-forward neural network with seventeen neurons in the input layer, a single hidden layer with five hidden neurons and a

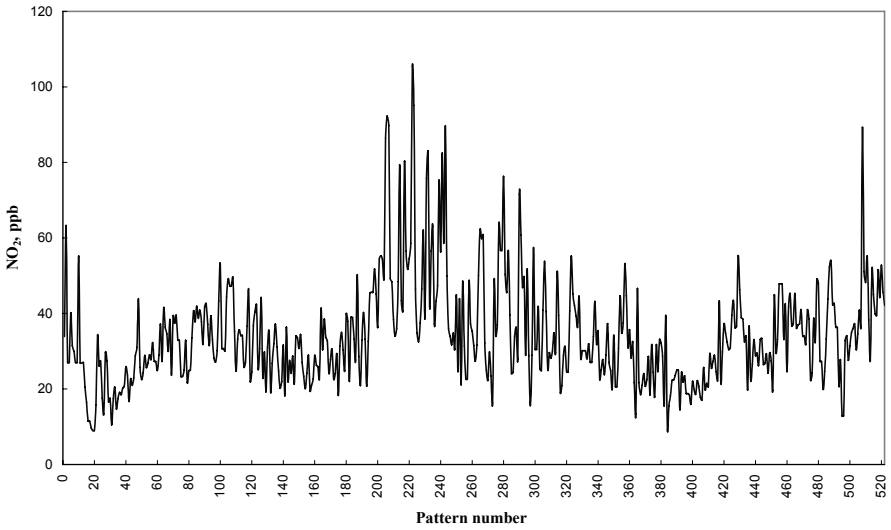

Fig. 5.13. Training patterns used for development of 24-hr average ANNNO2 models at AQCR1.

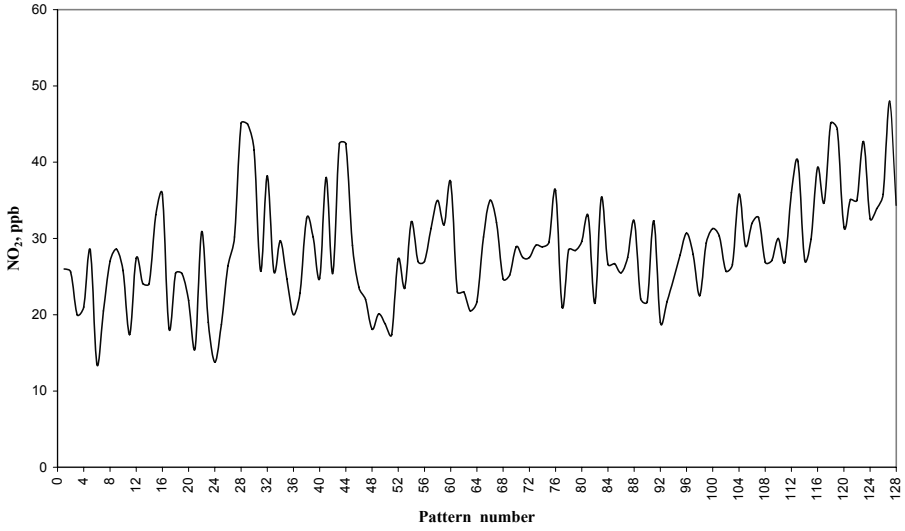

Fig. 5.14. Test pattern used for generalization of 24-hr average $ANNNO_2$ model at AQCR1.

single neuron in the output layer, shows satisfactory prediction on 'test data set'. Similar to 1-hr and 8-hr average model, the inputs used in the computational runs, are 17 (meteorological and traffic characteristics variables), while the output is NO_2 concentration (i.e.1) and the number of neurons in the hidden layer are varied from 2 to 34. Table 5.21 describes the RMSE and 'd' values, which are used to find out number of neurons in the hidden layer. Figure 5.15 shows the architecture (17:5:1) of the ANN based NO_2 model with seventeen input variables. Table 5.22 lists the performance of the $ANNNO2_{24hrA1}$ model during generalization on 'test data set'. The final neuron definitions and synaptic weights of the $ANNNO2_{24hrA1}$ model are described in Table D.13a and D.13b respectively in Appendix-D.

Table 5.21 Experimental simulation results for optimization of the hidden layer neurons for the 24- hr average ANN based NO_2 model.

Number of hidden neurons	Mean square error after network stabilization	Statistical parameter	
		d	RMSE
2	0.04657	0.58	7.96
3	0.04046	0.44	10.29
4	0.03803	0.47	10.45
5	0.03777	0.63	7.18
6	0.03774	0.44	10.69
7	0.03802	0.48	10.18
8	0.03657	0.45	9.89
9	0.03647	0.44	11.13
10	0.03758	0.45	11.11
11	0.03703	0.40	11.98
12	0.03984	0.40	11.13
13	0.03994	0.42	10.49
14	0.04030	0.44	10.18
15	0.03982	0.42	10.52
16	0.03731	0.39	12.35
17	0.04014	0.40	11.08
18	0.03815	0.39	11.93
19	0.03798	0.39	11.99
20	0.04151	0.40	10.80
21	0.03896	0.39	12.00
22	0.04000	0.47	9.81
23	0.03888	0.40	11.83
24	0.04538	0.56	7.91
25	0.03896	0.40	11.87
26	0.03843	0.44	11.13
27	0.04216	0.56	9.07
28	0.04604	0.58	7.70
29	0.04464	0.52	8.34
30	0.04576	0.57	7.80
31	0.04606	0.58	7.67
32	0.03871	0.40	11.95
33	0.04299	0.43	9.74
34	0.04614	0.58	7.69

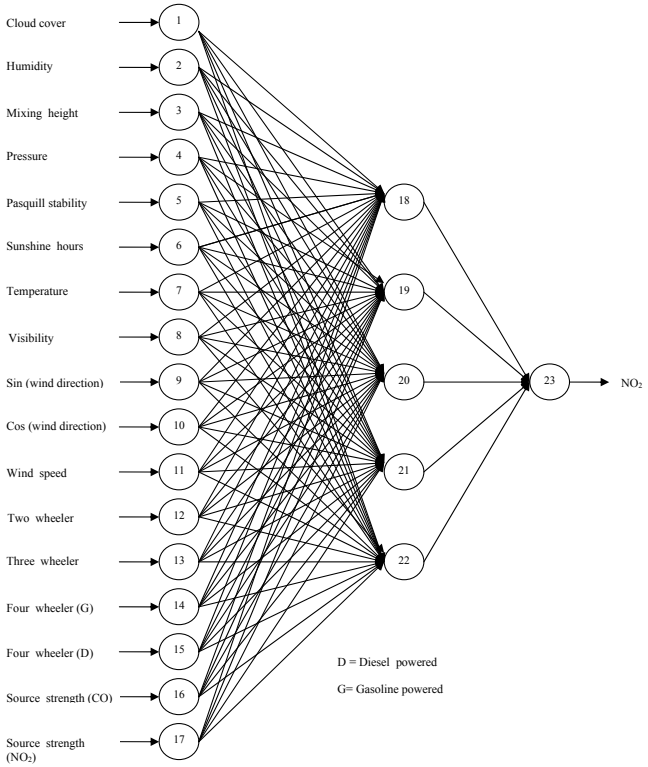

Fig. 5.15. Structure of 17:5:1 ANN based NO_2 model.

Table 5.22 Estimates of the statistics during generalization of the $ANNNO2_{24hrA1}$ model.

Epoch	d	RMSE
50	0.597	7.58
100	0.625	7.20
150	0.627	7.18
200	0.625	7.29
250	0.622	7.32
300	0.467	9.0
350	0.47	9.95
400	0.44	10.69
450	0.44	10.48
500	0.44	10.78

(ii) ANNNO2$_{24hrB1}$ (24-hr average meteorological variables as model input at AQCR1)

The ANNNO2$_{24hrB1}$ model is developed, with ten meteorological variables, as inputs. Figure 5.16 shows the architecture of the ANNNO2$_{24hrB1}$ model. Table 5.23 shows the performance of the ANNNO2$_{24hrB1}$ model during generalization on 'test data set'. The final neuron definitions and synaptic weights of the ANNNO2$_{24hrB1}$ model are provided in Table D.14a and D.14b respectively in Appendix-D.

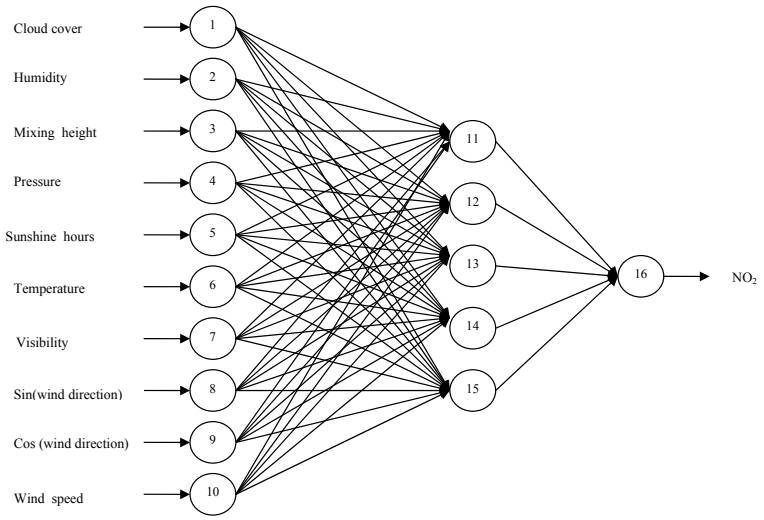

Fig. 5.16. Structure of 10:5:1 ANN based NO_2 model.

Table 5.23 Estimates of the statistics during generalization of the ANNNO2$_{24hrB1}$ model.

Epoch	d	RMSE
100	0.58	8.23
200	0.59	8.06
300	0.59	7.93
400	0.598	7.86
500	0.598	7.82
600	0.595	7.82
700	0.594	7.85
800	0.594	7.87
900	0.593	7.89
1000	0.592	7.90

(iii) ANNNO2$_{24hrC1}$ (24-hr average traffic characteristic variables as model input at AQCR1)

Neural network architecture of 5:5:1 is used for the development of the ANNNO2$_{24hrC1}$ model (Figure 5.17). This model consists of five traffic variables as input. Table 5.24 shows the performance of the ANNNO2$_{24hrC1}$ model during generalization on 'test data set'. The final neuron definitions and synaptic weights of the ANNNO2$_{24hrC1}$ model are presented in Table D.15a and D.15b respectively in Appendix-D.

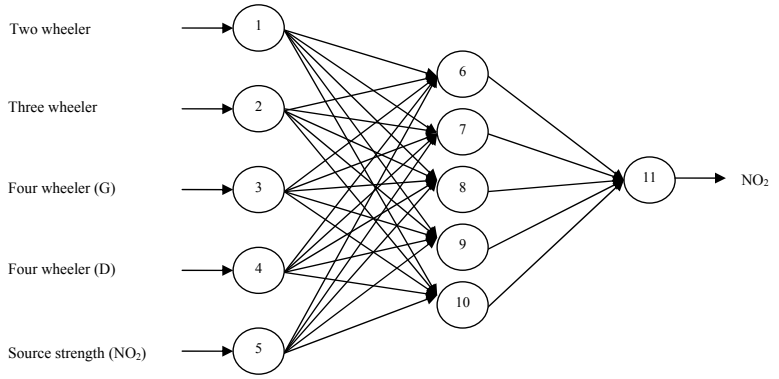

Fig. 5.17. Structure of 5:5:1 ANN based NO_2 model.

(iv) ANNNO2$_{24hrA2}$ (24-hr average meteorological and traffic characteristic variables as model input at AQCR2)

For AQCR2, about 51 % of the total data values are found to be missing, therefore training, test and 'evaluation' data set are selected randomly for the development of the ANN based NO_2 model. Out of 49 % of available data, 33 % data are used for training, 10 % used for testing and 6 % for the final model evaluation. Figure 5.18 and 5.19 represent NO_2 patterns used for the training and test of the ANN based NO_2 model at AQCR2. Network architecture of 17:5:1 is used to develop the ANNNO2$_{24hrA2}$ model. Table 5.25 shows the performance of the ANNNO2$_{24hrA2}$ model during generalization on 'test data set'. The final neuron definitions and synaptic weights of the ANNNO2$_{24hrA2}$ model are listed in Table D.16a and D.16b respectively in Appendix-D.

Table 5.24 Estimates of the statistics during generalization of the $ANNNO2_{24hrC1}$ model.

Epoch	d	RMSE
5	0.265	29.21
10	0.34	23.07
15	0.43	12.59
20	0.44	9.76
25	0.44	9.03
30	0.44	8.84
35	0.44	8.77
40	0.44	8.75
45	0.43	8.75
50	0.40	8.75
55	0.40	8.75
60	0.40	8.75
65	0.40	8.75
70	0.40	8.75
75	0.40	8.75
80	0.40	8.75
85	0.40	8.75
90	0.40	8.75
95	0.40	8.75
100	0.40	8.75

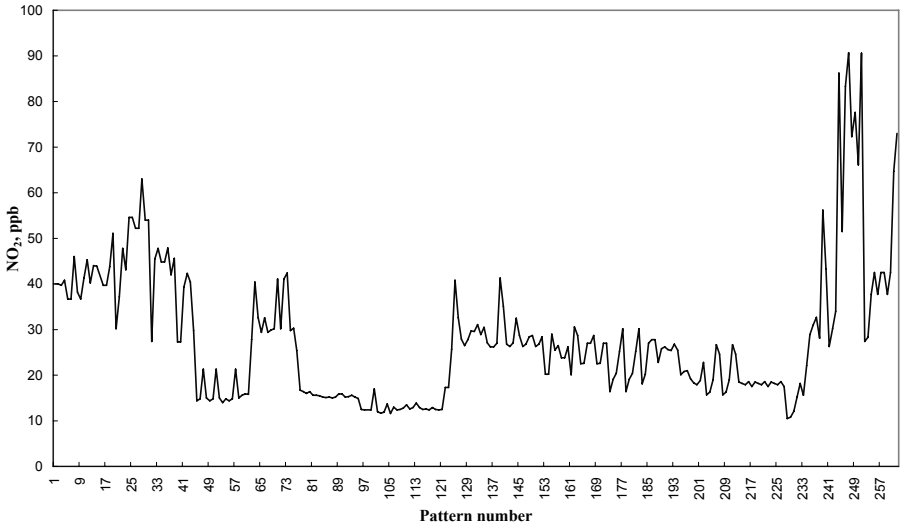

Fig. 5.18. Training patterns used for development of 24-hr average $ANNNO_2$ models at AQCR1.

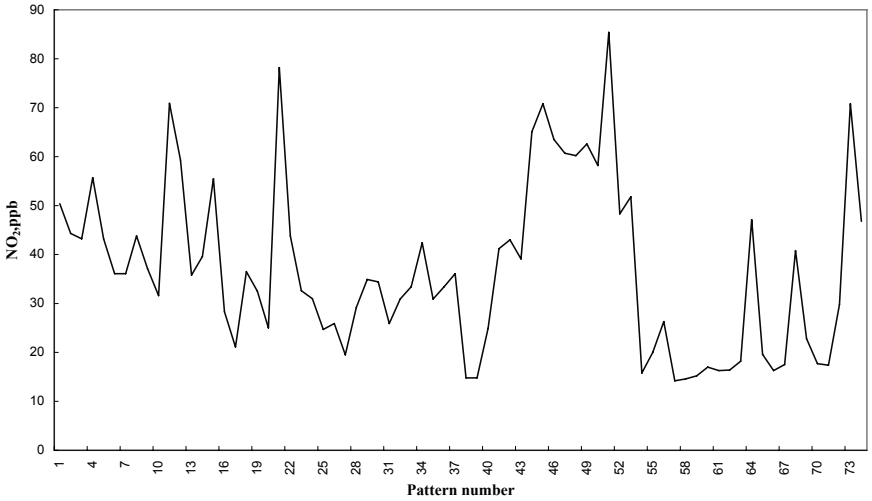

Fig. 5.19. Test patterns used for generalization of 24-hr average ANNNO^2 model at AQCR1.

Table 5.25 Estimates of the statistics during generalization of the ANNNO2$_{24hrA2}$ model.

Epoch	d	RMSE
50	0.51	20.2
100	0.54	19.3
150	0.539	18.85
200	0.545	18.66
250	0.546	18.65
300	0.543	18.79
350	0.535	19.06
400	0.529	19.38
450	0.523	19.67

(v) ANNNO2$_{24hrB2}$ (24-hr average meteorological variables as model input at AQCR2)

Network architecture of 10:5:1 is used to develop the ANNNO2$_{24hrB2}$ model. The performance of the ANNNO2$_{24hrB2}$ model during generalization on 'test data set' is provided in Table 5.26. The neuron definitions and synaptic weights of the ANNNO2$_{24hrB2}$ model are presented in Table D.17a and D.17b respectively in Appendix-D.

Table 5.26 Estimates of the statistics during generalization of the $ANNNO2_{24hrB2}$ model.

Epoch	d	RMSE
50	0.524	19.4
100	0.528	19.16
150	0.528	19.16
200	0.528	19.15
250	0.529	19.13
300	0.529	19.11
350	0.53	19.11
400	0.53	19.10
450	0.539	19.11
500	0.539	19.11
550	0.533	19.12
600	0.533	19.13
650	0.529	19.16
700	0.529	19.18
750	0.528	19.23

(vi) $ANNNO2_{24hrC2}$ (24-hr average traffic characteristic variables as model input at AQCR2)

Neural network architecture of 5:5:1 is used for the development of the $ANNNO2_{24hrC2}$ model. The performance of the $ANNNO2_{24hrC2}$ model during generalization on 'test data set' is given in Table 5.27. The final neuron definition and synaptic weights of the $ANNNO2_{24hrC2}$ model are provided in Table D.18a and D.18b respectively in Appendix-D.

The summary of the 1-hr and 8-hr average ANN based CO and 24-hr average ANN based NO_2 models parameter and their performance statistics on test data set at both the AQCRs are presented in Table 5.28.

Table 5.27 Estimates of the statistics during generalization of the $ANNNO2_{24hrC2}$ model.

Epoch	d	RMSE
20	0.41	19.55
40	0.41	19.55
60	0.41	19.55
80	0.41	19.54
100	0.41	19.52
120	0.41	19.52
140	0.41	19.51
160	0.41	19.48
180	0.41	19.50
200	0.41	19.52

Table 5.28 Summary of the 1-hr, 8-hr and 24-hr ANN based vehicular pollution model parameters and the model performance statistics on test data set.

Site	Time resolu-tion	Model	Number of epoch	η	μ	RMSE	d
AQCR1	1-hr average	$ANNCO_{1hrA1}$	1400	0.001	0.7	2.0893	0.663
		$ANNCO_{1hrB1}$	2000	0.001	0.3	2.57	0.552
		$ANNCO_{1hrC1}$	10	0.001	0.7	3.72	0.41
	8-hr average	$ANNCO_{8hrA1}$	400	0.001	0.3	2.04	0.64
		$ANNCO_{8hrB1}$	1000	0.001	0.1	1.86	0.656
		$ANNCO_{8hrC1}$	20	0.001	0.1	2.12	0.44
	24-hr average	$ANNNO2_{24hrA1}$	150	0.01	0.7	7.18	0.627
		$ANNNO2_{24hrB1}$	500	0.001	0.9	7.82	0.598
		$ANNNO2_{24hrC1}$	40	0.001	0.3	8.75	0.44
AQCR2	1-hr average	$ANNCO_{1hrA2}$	200	0.001	0.3	2.105	0.655
		$ANNCO_{1hrB2}$	600	0.001	0.3	2.136	0.65
		$ANNCO_{1hrC2}$	20	0.001	0.1	3.04	0.44
	8-hr average	$ANNCO_{8hrA2}$	1400	0.001	0.5	1.58	0.689
		$ANNCO_{8hrB2}$	4000	0.001	0.7	1.53	0.71
		$ANNCO_{8hrC2}$	30	0.001	0.7	1.97	0.44
	24-hr average	$ANNNO2_{24hrA2}$	250	0.001	0.3	18.65	0.546
		$ANNNO2_{24hrB2}$	400	0.001	0.5	19.1	0.53
		$ANNNO2_{24hrC2}$	160	0.001	0.5	19.48	0.41

5.7 Summary

A step-by-step procedure for building ANN based vehicular pollution models has been described in this chapter. The development of ANN based vehicular pollution models for different time resolutions have been explained with the help of case study. The regularly monitored meteorological and traffic characteristic variables are used for the development of the ANN based vehicular pollution models for different time resolution (1-hr and 8-hr average CO models and 24-hr average NO_2 models) following NAAQS. A 17:3:1 and 17:5:1 architectures are used for the development of the ANN based CO and NO_2 models respectively for both meteorological and traffic characteristic variables as input to the model. While, 10:3:1 and 10:5:1 architectures are used for the development of the ANN based CO and NO_2 models respectively for regular meteorological variables as input to the model. Network architecture of 5:3:1 and 5:5:1 are used for the ANN based CO and NO_2 models respectively for traffic characteristic variables as input to the model.

6 Application of ANN based Vehicular Pollution Models

This chapter presents *case studies* analyzing the performance of the ANN based vehicular pollution models applied at the urban intersection and straight corridor in the city of Delhi, India. Statistical indicators, used in evaluating the model performance, are also been explained. Further, predictions of the ANN based vehicular pollution models have also been compared with conventional models e.g. deterministic and stochastic.

6.1 General

The performance of the ANN based vehicular pollution models have been evaluated using relevant statistical parameters e.g. index of agreement (d), the mean and the deviations of the observed and predicted concentrations, mean bias error, mean square error, systematic and unsystematic root mean square error, coefficient of determination and linear best fit constant and gradient [263]. The degree of agreement (d) between a set of predicted and observed concentration is normally accepted as one of the major statistical criterion for the assessment of the air quality model performance [263, 268]. In general, there are three steps that need to be considered while evaluating the performance of an air quality model. *First*, the assessment of model inputs; *second*, the comparison between predictions and observations and *third*, the sensitivity analysis of the model predictions [269]. In vehicular pollution modelling studies, the assessment of model inputs refers to the essential correction of the model, in terms of its representation of the basic processes involved in the dispersion of exhaust emissions. The dispersion, near the traffic intersections and busy roads, is influenced mainly by two factors; *first*, the natural turbulence and *second*, the traffic generated turbulence (traffic

M. Khare and S.M. Shiva Nagendra: *Application of ANN based Vehicular Pollution Models*, Artificial Neural Networks in Vehicular Pollution Modelling (SCI) **41,** 121–156 (2007)
www.springerlink.com

wake). The natural turbulence is represented by meteorological variables, while 'traffic wake' is related to the traffic characteristic variables [183,184]. The ANN based vehicular pollution models consider both the characteristic variables i.e. the meteorological and the traffic.

Comparison between the predictions and observations is a crucial component of the model evaluation and is emphasized in many air quality-modelling studies [121, 172, 269]. It is difficult to analyze whether discrepancies between predictions and observations are due to errors in the input data, or in the representation of the dispersion processes. One-way of understanding the case of discrepancies between predictions and observations is to carry out the parameter sensitivity i.e. to analyze the input variables to which the model is most sensitive. It allows one to evaluate how the model responds when its parameters are separately perturbed and aids the assessment of the physical response of the model components [270]. The sensitivity analysis for the present ANN based vehicular pollution models has been carried out in two stages. *Firstly*, by eliminating the traffic characteristic variables and keeping the meteorological variables as the only model input. *Secondly*, eliminating the meteorological variables and keeping the traffic characteristic variables as the only model input.

6.2 Model Performance Indicators

Fox [271] and Willmott [263] have described about the presence of inconsistencies in testing and evaluating the air quality models. It is not uncommon to find models that are evaluated by the correlation coefficient 'r^2'. Such statistics may not be useful in assessing the accuracy of the model predictions and thus may seriously hinder model interpretations [82]. Therefore, the selected statistical indicators as suggested by Willmott [263,268] and Willmott et al. [272] have been used to describe the goodness of the model predictions.

6.2.1 Root Mean Square Error

Two commonly reported measures of residual error include the mean absolute error and the root mean square error (RMSE). These

two errors summarize the difference between the observed and the predicted concentrations [263]. The power term in the RMSE calculations makes it more sensitive to extreme values than mean absolute error. The RMSE explains the actual size of the error produced by the model. The RMSE may further be divided into two components - *systematic* ($RMSE_S$) and *unsystematic* ($RMSE_U$). The $RMSE_S$ (also known as the model oriented error) is based on the difference between expected predictions and actual observations; $RMSE_U$ (also called data oriented error) is based on the difference between actual and expected predictions [268]. The $RMSE_S$ and $RMSE_U$ are derived by first fitting a line by least square regression and then decomposing the RMSE, using the following formulations:

$$RMSE_S = \left[\frac{1}{N} \sum_{i=1}^{N} (\hat{P}_i - O_i)^2 \right]^{1/2} \tag{6.1}$$

$$RMSE_U = \left[\frac{1}{N} \sum_{i=1}^{N} (\hat{P}_i - P_i)^2 \right]^{1/2} \tag{6.2}$$

Where $\hat{P}_i$ = least square estimate
N = number of values
O_i = observed values
P_i = predicted values

6.2.2 Coefficient of Determination

The coefficient of determination (r^2) is an intuitively attractive statistic. It indicates how much of the variations in the observed data are being reproduced by the model.

$$r^2 = \frac{\sum_{i=1}^{N} (P_i - \overline{O})^2}{\sum_{i=1}^{N} (O_i - \overline{O})^2} \tag{6.3}$$

where $\overline{O}$ = average of observed values

6.2.3 Mean Bias Error

The mean bias error (MBE) is defined as the difference between the mean of the predicted and observed concentrations. It indicates the degree to which the observed concentrations are 'over' or 'under' predicted by the model. The MBE is estimated by following equation:

$$MBE = \left[\frac{1}{N} \sum_{i=1}^{N} (P_i - O_i) \right] \tag{6.4}$$

6.2.4 Standard Deviations

The standard deviation (σ) of the predictions quantifies the amount of the variance that the model is capturing when compared to the variations in the observed data.

$$\sigma_O = \left[\frac{1}{N} \sum_{i=1}^{N} (O_i - \overline{O})^2 \right]^{1/2} \tag{6.5}$$

$$\sigma_P = \left[\frac{1}{N} \sum_{i=1}^{N} (P_i - \overline{P})^2 \right]^{1/2} \tag{6.6}$$

Where $\overline{P}$ = average of predicted values

σ_O = standard deviation of the observations
σ_P = standard deviation of the predictions

$$\overline{O} = \sum_{i=1}^{N} O_i \tag{6.7}$$

$$\overline{P} = \sum_{i=1}^{N} P_i \tag{6.8}$$

6.2.5 Slope and Intercept of the Least Square Regression Equation

A model that exactly reproduces the actual observations has slope, 'b' as 1.0 and, intercept 'a' as 0.0. The parameters 'a' and 'b' are estimated following least square procedure as given below.

$$\hat{P} = \text{b} + \text{a O} \tag{6.9}$$

6.2.6 Degree of Agreement

Willmott [263] and Willmott et al. [272] advocated that the degree of agreement (d) is a useful measure of model performance. The value of'd' is a descriptive statistics that reflects the degree to which the observed variate is accurately estimated by the simulated variate. It is the most commonly used statistical indicator in air quality model performance studies [59, 172, 83, 255, 82, 91].

6.3 Application of ANN Based Vehicular Pollution Models at Urban Intersection and Straight Road Corridor

6.3.1 1-hr Average CO Models

Table 6.1 lists the performance statistics of the $ANNCO_{1hrA1}$ and the $ANNCO_{1hrA2}$ model predictions on the test data set at AQCR1 and AQCR2 respectively. At AQCR1, the mean of the predicted CO

Table 6.1 Performance statistics of the $ANNCO_{1hrA1}$ and $ANNCO_{1hrA2}$ models (with the meteorological and the traffic characteristic inputs).

Site	Model ID	Statistic											
		$\overline{O}$	$\overline{P}$	σ_O	σ_P	MBE	MSE	RMSE		r^2	d	a	b
		ppm	ppm	ppm	ppm	ppm	ppm	$RMSE_S$ ppm	$RMSE_U$ ppm			ppm	
AQCR1	$ANNCO_{1hrA1}$	3.79	4.54	3.33	2.31	0.75	6.4	1.91	1.69	0.47	0.78	2.75	0.47
AQCR2	$ANNCO_{1hrA2}$	3.98	3.65	4.19	2.02	-0.32	6.7	2.94	1.58	0.39	0.67	2.46	0.3

concentration ($\overline{P}$ = 4.54 ppm) is higher than that of the observed mean (3.79 ppm); while at AQCR2, it is lower ($\overline{P}$ = 3.65 ppm) than the observed mean value (3.98 ppm). The MBE value at AQCR1 is positive-indicating a tendency of the model to over predict; while at AQCR2, it is negative - indicating a tendency of the model to under predict. The standard deviation (σ_P) of the $ANNCO_{1hrA1}$ model prediction is matching with the standard deviation of the observed data at AQCR1. At AQCR2, the difference between the standard deviation of the observed and the predicted data is quite high. This explains that the $ANNCO_{1hrA1}$ is reproducing the variations in the test data set at AQCR1; where as, at AQCR2, the $ANNCO_{1hrA2}$ model is unable to reproduce the variations in the test data set. The $RMSE_S$ and $RMSE_U$ errors for the $ANNCO_{1hrA1}$ model are 1.91 and 1.69 ppm respectively; where as, for the $ANNCO_{1hrA2}$ model, these are 2.94 and 1.58 ppm. A low $RMSE_S$ value at AQCR1 indicates that the $ANNCO_{1hrA1}$ model predictions are closely matching with the actual observations when compared with the $ANNCO_{1hrA2}$ model predictions at AQCR2. Further, the 'd' values for $ANNCO_{1hrA1}$ and $ANNCO_{1hrA2}$ models are 0.78 and 0.67 respectively. It implies that at AQCR1, 78 % of the model predictions are error free while at AQCR2, only 67 % are error free. It shows that $ANNCO_{1hrA1}$ model is more reliable and accurate than $ANNCO_{1hrA2}$ model. Figure 6.1 and 6.2 show observed versus predicted CO concentrations at AQCR1 and AQCR2 respectively, indicating that both models under predict the CO concentrations when observed values are towards higher side.

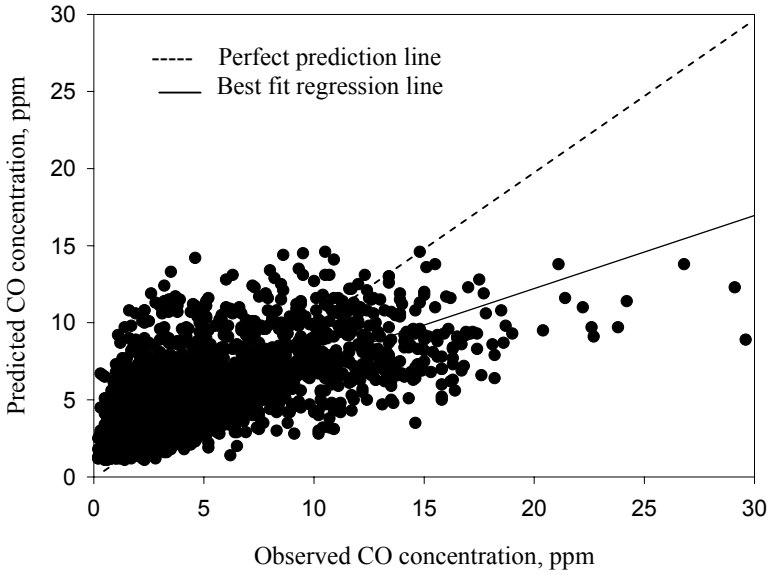

Fig. 6.1. Scatter plots of 1-hr average CO observations vs the $ANNCO_{1hrA1}$ model predictions for the evaluation data set at AQCR1.

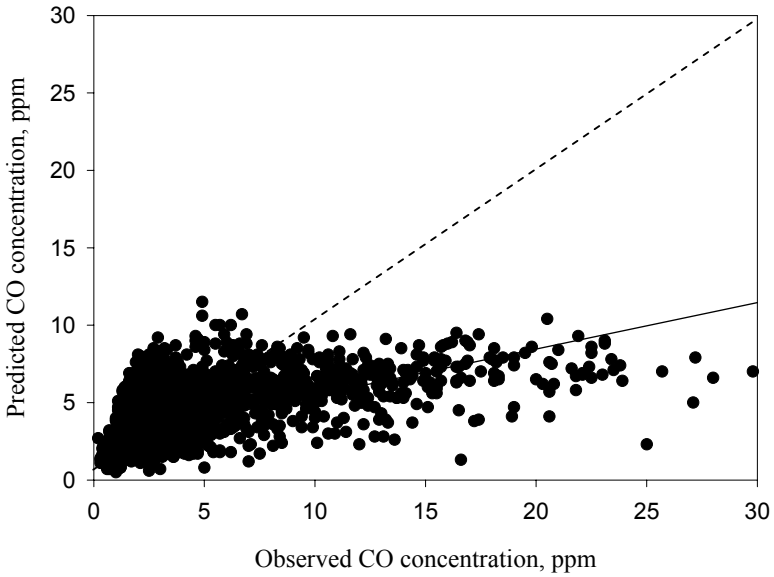

Fig. 6.2. Scatter plots of 1-hr average CO observations vs the $ANNCO_{1hrA2}$ model predictions for the evaluation data set at AQCR2.

Table 6.2 Performance statistics of the $ANNCO_{1hrB1}$ and $ANNCO_{1hrB2}$ models (with the meteorological inputs).

Site	Model ID	Statistic											
		$\overline{O}$ ppm	$\overline{P}$ ppm	σ_O ppm	σ_P ppm	MBE ppm	MSE ppm	RMSE		r^2	D	a ppm	b
								$RMSE_S$ ppm	$RMSE_U$ ppm				
AQCR1	$ANNCO_{1hrB1}$	3.79	5.43	3.33	1.71	1.63	9.8	2.82	1.36	0.36	0.65	4.26	0.31
AQCR2	$ANNCO_{1hrB2}$	3.98	3.75	4.19	1.87	-0.22	7.0	3.11	1.51	0.35	0.63	2.70	0.26

Table 6.2 provides the performance statistics of the $ANNCO_{1hrB1}$ and $ANNCO_{1hrB2}$ model predictions on the test data set at AQCR1 and AQCR2 respectively. The mean of predicted CO concentration at AQCR1 is higher than the observed mean; while at AQCR2, it is matching with the observed mean. At AQCR1, the MBE value is positive (1.63 ppm), indicating a tendency of the model to over predict; while, at AQCR2, it is negative (-0.22 ppm), indicating a tendency of the model to under predict. The standard deviations (σ_P) of the $ANNCO_{1hrB1}$ and $ANNCO_{1hrB2}$ model predict-tions are lower than the standard deviations (σ_O) of the observed data set. This explains that both models seem to be inadequate to reproduce the variations in the test data set. $RMSE_S$ values for the $ANNCO_{1hrB1}$ and $ANNCO_{1hrB2}$ models are closely matching with each other. High $RMSE_S$ values indicate that both the models perform satisfactorily on the test data set. The'd' values also explain that at AQCR1, 65 % of the model predictions are error free; while at AQCR2, 63 % predictions are error free. It shows that both the models predict with reasonably good accuracy. Figure 6.3 and 6.4 show observed versus predicted CO concentrations at AQCR1 and AQCR2 respectively indicating that both the models under predict CO concentrations when observed values are towards higher side.

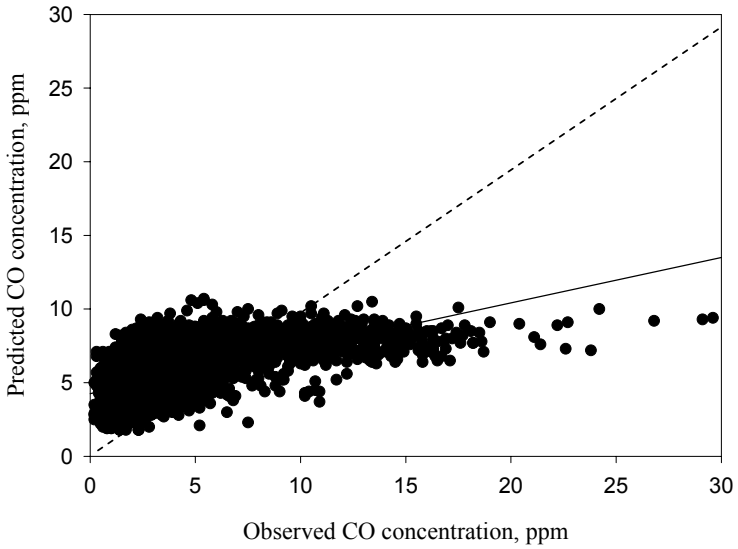

Fig. 6.3. Scatter plots of 1-hr average CO observations vs the $ANNCO_{1hrB1}$ model predictions for the evaluation data set at AQCR1.

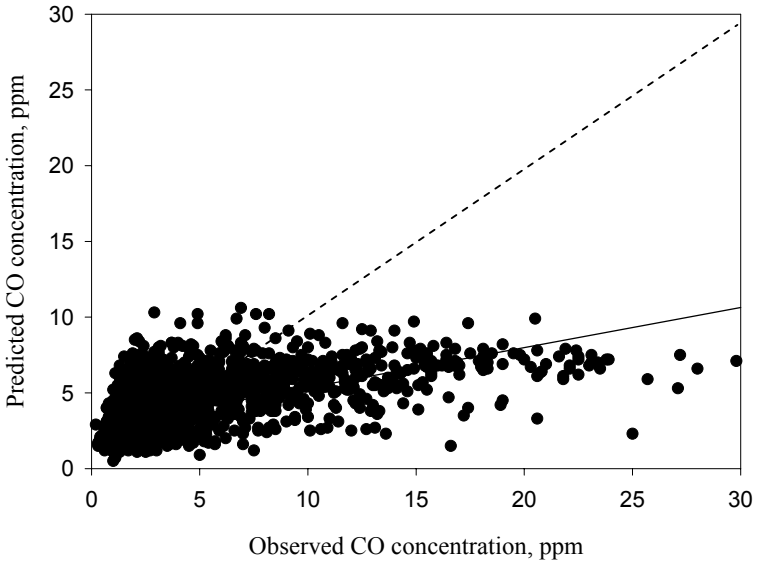

Fig. 6.4. Scatter plots of 1-hr average CO observations vs the $ANNCO_{1hrB2}$ model predictions for the evaluation data set at AQCR2.

Comparative performance of $ANNCO_{1hrB1}$ vs $ANNCO_{1hrA1}$ and $ANNCO_{1hrB2}$ vs $ANNCO_{1hrA2}$

For short-term average data (1-hr), the relationship between exhaust emissions, and meteorological and traffic characteristic variables is highly complex and non-linear. Gardner and Dorling [83,255] demonstrated that ANN can accurately model such non-linear relationships and so concluded that increase in the number of input variables further improves the prediction performance of an ANN model. The present study also supports the above findings. However, the location of the monitoring station with respect to the line source is important factor that affects the prediction performance of the ANN model. A line source monitoring station can be considered as 'near-field' (≤ 3 m) and/or far field (> 30 m) [120, 127, 129, 183, 184]. In the 'near field' region, the 'traffic wake' generated by moving vehicles, dominantly disperses the pollutants. In the 'far-field' region, 'traffic wake' effects gradually reduce and meteorological variables dominate the dispersion and dilution of the pollutants [120, 129]. In the present study, AQCR1 lies in 'near-field' (≈ 3 m); while AQCR2 lies in 'far-field' region (≈ 100 m).

The results show that $ANNCO_{1hrB1}$ model (developed for AQCR1 which is in the 'near-field' region and in which traffic characteristic variables are not included), poorly performs on the test data, in terms of 'd' value, which is decreased by 13 %, when compared with $ANNCO_{1hrA1}$ model (developed for AQCR1 which is in 'near-field' region and in which traffic characteristic variables are included). However, this reduction in 'd' value is marginal (only 4 %), when the $ANNCO_{1hrB2}$ model (developed for AQCR2 which is in 'far-field' region and in which traffic characteristic variables are not included) prediction results are compared with $ANNCO_{1hrA2}$ model predictions (developed for AQCR2 which is in the 'far-field' region and in which traffic characteristic variables are included). It clearly shows that in 'far-field' regions, the exclusion of traffic characteristic variables from the ANN model input marginally affect its prediction performance because at such distances, the effect of traffic generated turbulence (traffic wake) on pollutant dispersion gradually diminishes.

Table 6.3 Performance statistics of the $ANNCO_{1hrC1}$ and $ANNCO_{1hrC2}$ models (with the traffic characteristic inputs).

Site	Model ID	Statistic											
		$\overline{O}$ ppm	$\overline{P}$ ppm	σ_O ppm	σ_P ppm	MBE ppm	MSE ppm	RMSE $RMSE_S$ ppm	RMSE $RMSE_t$ ppm	r^2	d	a ppm	b
AQCR1	$ANNCO_{1hrC1}$	3.79	6.75	3.33	0.75	2.95	19.18	4.33	0.73	0.05	0.44	6.56	0.05
AQCR2	$ANNCO_{1hrC2}$	3.98	4.38	4.19	0.96	0.4	9.72	3.96	0.93	0.06	0.31	4.15	0.06

Table 6.3 summaries the performance statistics of the $ANNCO_{1hrC1}$ and the $ANNCO_{1hrC2}$ models prediction on test data set at AQCR1 and AQCR2 respectively. The means of the predicted CO concentrations at both the AQCRs are higher than the observed means. The MBE values at both AQCRs are positive, indicating the tendency of the models to over predict. The standard deviations (σ_P) of the $ANNCO_{1hrC1}$ and $ANNCO_{1hrC2}$ model predictions are low when compared to the observed standard deviations (σ_O). It explains that both the models are inadequate to reproduce the variations in the test data set. Further, the high $RMSE_S$ values indicate that both models perform poorly on the test data set. The 'd' values for the $ANNCO_{1hrC1}$ and $ANNCO_{1hrC2}$ models explain that at AQCR1, 44 % of the model predictions are error free; while at AQCR2, 31 % of the model predictions are error free. Figure 6.5 and 6.6 show observe versus predicted CO concentrations at AQCR1 and AQCR2 respectively indicating that both the models under predict CO concentrations when observed values are towards higher side and over predicts when observed values are towards lower side.

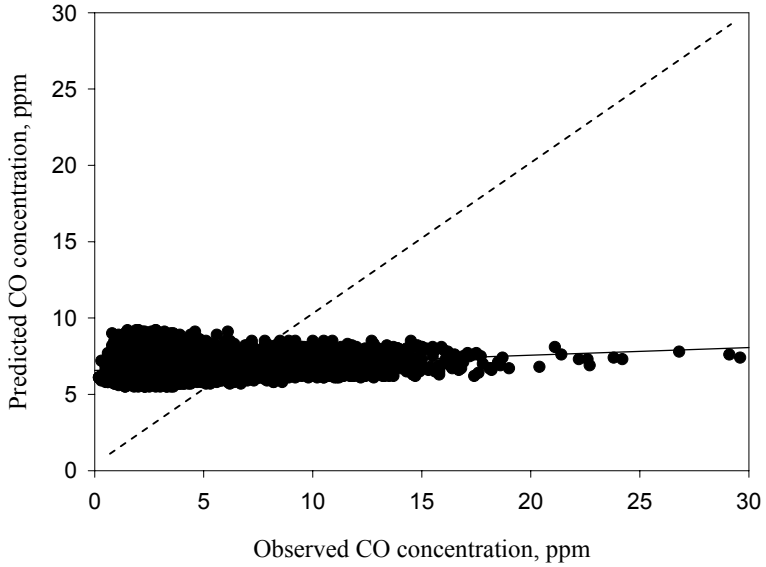

Fig. 6.5. Scatter plots of 1-hr average CO observations vs the $ANNCO_{1hrC1}$ model predictions for the evaluation data set at AQCR1.

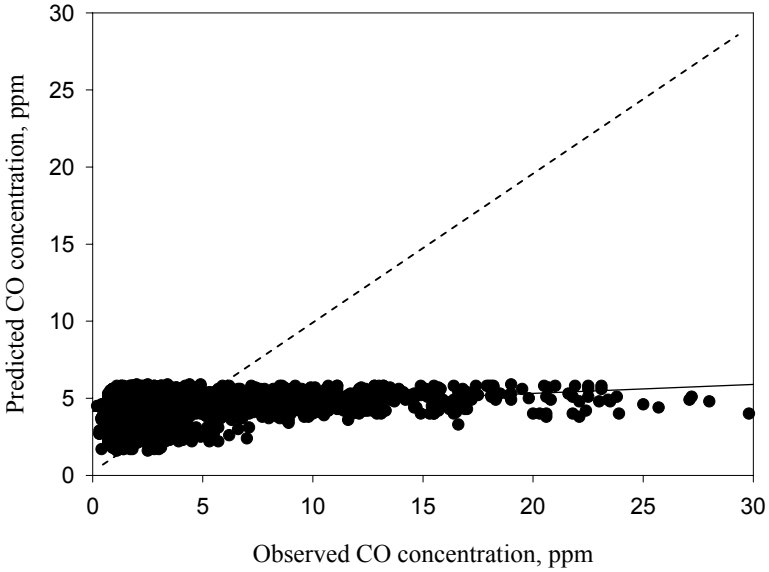

Fig. 6.6. Scatter plots of 1-hr average CO observations vs the $ANNCO_{1hrC2}$ model predictions for the evaluation data set at AQCR2.

Comparative performance of $ANNCO_{1hrC1}$ vs $ANNCO_{1hrB1}$ and $ANNCO_{1hrA1}$ and $ANNCO_{1hrC2}$ vs $ANNCO_{1hrB2}$ and $ANNCO_{1hrA2}$

The $RMSE_S$ value for the $ANNCO_{1hrC1}$ model increases by 2.42 and 1.51 ppm when compared with $ANNCO_{1hrA1}$ and $ANNCO_{1hrB1}$ models respectively. However, for $ANNCO_{1hrC2}$ model, the $RMSE_S$ values increases by 1.02 and 0.85 ppm when compared with $ANNCO_{1hrA2}$ and $ANNCO_{1hrB2}$ models respectively. Further, the 'd' values for AQCR1 indicates that $ANNCO_{1hrC1}$ model (d=0.44) performs poorly, when compared with $ANNCO_{1hrA1}$ (d=0.78) and $ANNCO_{1hrB1}$ (d=0.65) models. At AQCR2, the $ANNCO_{1hrC2}$ model (d=0.31) also shows poor performance when compared with the $ANNCO_{1hrA2}$ (d=0.67) and $ANNCO_{1hrB2}$ (d=0.63) models. The poor performance of $ANNCO_{1hrC1}$ and $ANNCO_{1hrC2}$ models can be explained by the following facts. *Firstly*, these models are developed considering only traffic characteristic variables as their inputs. As a result of which the models explain the CO dispersion due to 'traffic wake' effect only. *Secondly*, due to the absence of meteorological input variables, these models fail to take into account the 'lag effect'- *it is a phenomena that results into the accumulation of CO in the atmosphere during inversion conditions resulting into high concentration while the traffic is trickle* [172]. This phenomenon frequently occurs during critical winter periods (November to March), when inversion conditions prevail during nighttime, particularly 4 to 6 hrs after 6 PM (10 PM to 6 AM). The $ANNCO_{1hrC1}$ and $ANNCO_{1hrC2}$ models fail to recognize and learn these phenomena. It verifies the fact that, as described by Gardner and Dorling [83,255] that decrease in number of variables affects the prediction accuracy of ANN based vehicular pollution models.

6.3.2 8-hr Average CO Models

Table 6.4 gives the performance statistics of $ANNCO_{8hrA1}$ and $ANNCO_{8hrA2}$ model predictions on test data set at AQCR1 and AQCR2 respectively. The mean of predicted CO concentration at AQCR1 (P= 5.56 ppm) is much higher than that of the observed mean (3.78 ppm); while at AQCR2, it is lower (P = 3.39 ppm) than

Table 6.4 Performance statistics of the $ANNCO_{8hrA1}$ and $ANNCO_{8hrA2}$ models (with the meteorological and the traffic characteristic inputs).

Site	Model ID	Statistic											
		$\overline{O}$ ppm	$\overline{P}$ ppm	σ_O ppm	σ_P ppm	MBE ppm	MSE ppm	RMSE		r^2	d	a ppm	b
								$RMSE_S$ ppm	$RMSE_t$ ppm				
AQCR1	$ANNCO_{8hrA1}$	3.78	5.56	2.45	2.35	1.78	5.71	1.87	1.48	0.61	0.78	2.72	0.75
AQCR2	$ANNCO_{8hrA2}$	4.18	3.39	3.35	2.10	-0.79	11.83	2.27	1.71	0.33	0.69	1.89	0.36

the observed mean value (4.18 ppm). At AQCR1, the MBE value is positive (1.78 ppm), indicating the tendency of the model to over predict; while, at AQCR2, it is negative (-0.79 ppm), indicating the tendency of the model to under predict. The standard deviations (σ_P) of the $ANNCO_{8hrA1}$ and $ANNCO_{8hrA2}$ model predictions are 2.35 and 2.1 ppm respectively. At AQCR1, σ_P is matching with the standard deviation of the observed data. At AQCR2, the difference between the standard deviations of observed and predicted data is marginal (1.25 ppm). This explains that $ANNCO_{8hrA1}$ model is reproducing the variations in the test data set with reasonable accuracy; where as, the $ANNCO_{8hrA2}$ model is showing moderate variations in the test data set. A low $RMSE_S$ value at AQCR1 indicates that the $ANNCO_{8hrA1}$ model predictions are closely matching with the actual observations when compared to the $ANNCO_{8hrA2}$ model predictions at AQCR2. Further, the 'd' values for the $ANNCO_{8hrA1}$ and $ANNCO_{8hrA2}$ models are 0.78 and 0.69 respectively. This explains that at AQCR1, 78 % of the model predictions are error free; while at AQCR2, only 69 % of model predictions are error free. It shows that $ANNCO_{8hrA1}$ model predictions are more accurate than the $ANNCO_{8hrA2}$ model. Figure 6.7 and 6.8 show observed versus predicted CO concentrations at AQCR1 and AQCR2 respectively, indicating that both models under predict CO concentrations, when observed concentrations are towards higher side.

Table 6.5 lists the performance statistics of the $ANNCO_{8hrB1}$ and $ANNCO_{8hrB2}$ model predictions on test data set at AQCR1 and AQCR2 respectively. The mean of the predicted CO concentration at AQCR1 is higher than the observed mean; while at AQCR2, the mean of the predictions is slightly lower than that of the observed mean. The MBE value at AQCR1 is positive (1.95 ppm), indicating the tendency of the model to over predict; while at AQCR2, it is

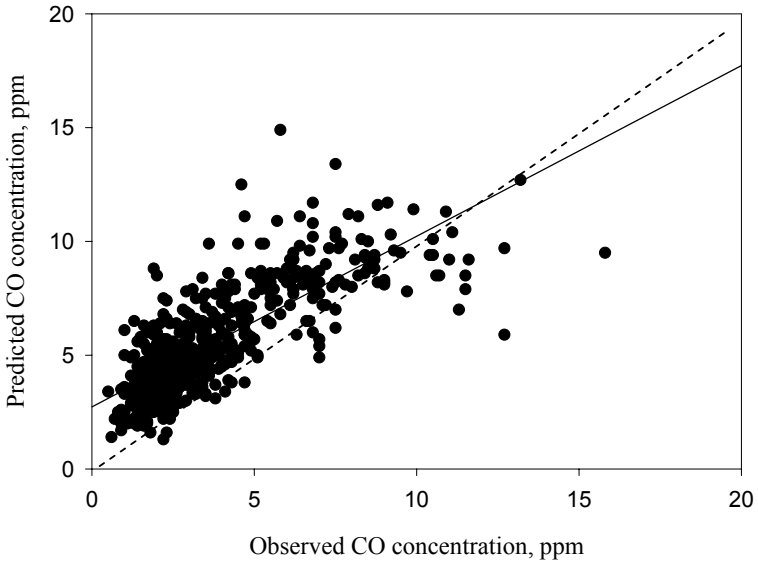

Fig. 6.7. Scatter plots of 8-hr average CO observations vs the $ANNCO_{8hrA1}$ model predictions for the evaluation data set at AQCR1.

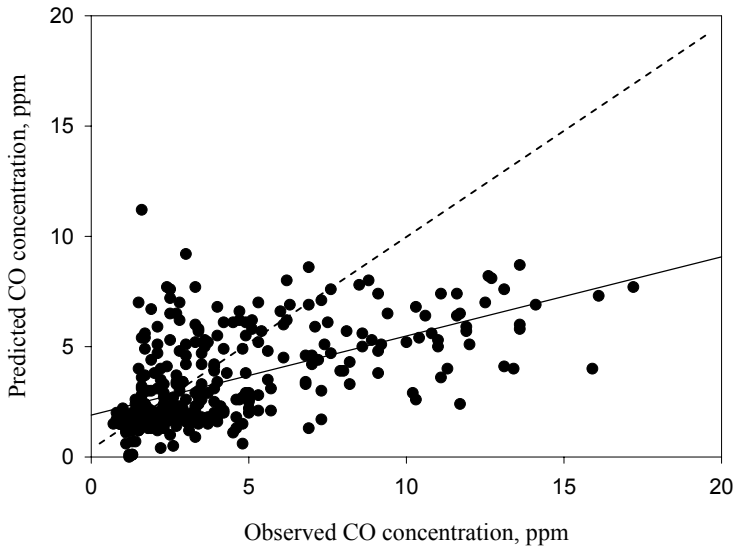

Fig. 6.8. Scatter plots of 8-hr average CO observations vs the $ANNCO_{8hrA2}$ model predictions for the evaluation data set at AQCR2.

Table 6.5 Performance statistics of the $ANNCO_{8hrB1}$ and $ANNCO_{8hrB2}$ models (with the meteorological inputs).

Site	Model ID	Statistic											
		$\overline{O}$ ppm	$\overline{P}$ ppm	σ_O ppm	σ_P ppm	MBE ppm	MSE ppm	RMSE		r^2	d	a ppm	b
								$RMSE_S$ ppm	$RMSE_U$ ppm				
AQCR1	$ANNCO_{8hrB1}$	3.78	5.24	2.45	2.09	1.95	4.88	1.97	1.40	0.58	0.77	2.84	0.63
AQCR2	$ANNCO_{8hrB2}$	4.18	3.45	3.35	1.96	-0.71	8.35	2.38	1.64	0.3	0.67	2.13	0.32

negative (-0.71 ppm), indicating its tendency to under predict. The standard deviation of the $ANNCO_{8hrB1}$ model predictions is matching with the standard deviation of the observed data set at AQCR1. At AQCR2, the difference between the standard deviation of observed and predicted data is quite high. It explains that $ANNCO_{8hrB1}$ model is able to reproduce the variations in the test data set at AQCR1; where as, at AQCR2, $ANNCO_{8hrB2}$ model fails to reproduce the variations in the test data set. A low $RMSE_S$ value at AQCR1 indicates that $ANNCO_{8hrB1}$ model predictions are closely matching with the actual observations when compared with the $ANNCO_{8hrB2}$ model predictions at AQCR2. Further, the 'd' values for the $ANNCO_{8hrB1}$ and $ANNCO_{8hrB2}$ models explains that at AQCR1, 77 % of the model predictions are error free, while at AQCR2, 67 % are error free. It shows that $ANNCO_{8hrB1}$ model is more accurate in its prediction performance than the $ANNCO_{8hrB2}$ model. Figure 6.9 and 6.10 show observed versus predicted CO concentrations at AQCR1 and AQCR2 respectively, indicating that both models under predict CO concentrations when observed concentrations are towards higher side.

Comparative performance of $ANNCO_{8hrB1}$ vs $ANNCO_{8hrA1}$ and $ANNCO_{8hrB2}$ vs $ANNCO_{8hrA2}$

The $RMSE_S$ values for $ANNCO_{8hrB1}$ and $ANNCO_{8hrB2}$ models increase marginally when compared to $ANNCO_{8hrA1}$ and $ANNCO_{8hrA2}$ respectively. Further, 'd' values for $ANNCO_{8hrB1}$ model (d=0.77) and $ANNCO_{8hrB2}$ (d=0.67) also show a marginal decrease when compared with 'd' values of $ANNCO_{8hrA1}$ (d=0.78) and

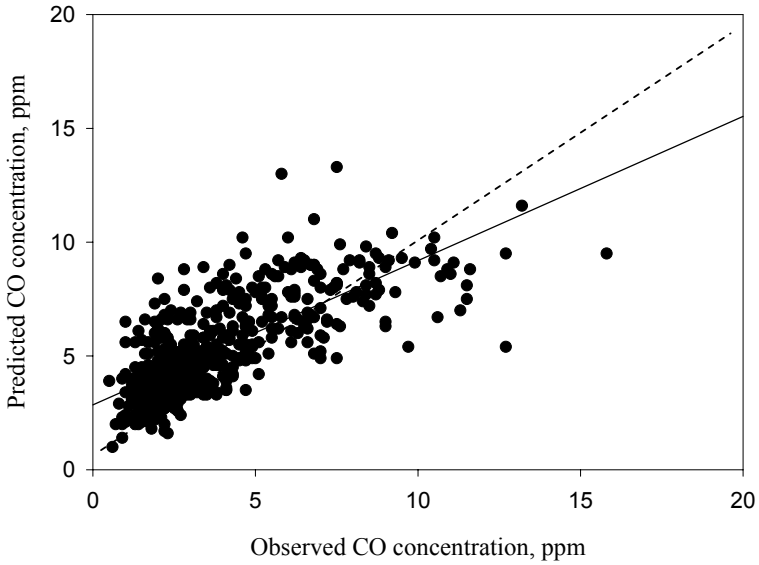

Fig. 6.9. Scatter plots of 8-hr average CO observations vs the $ANNCO_{8hrB1}$ model predictions for the evaluation data set at AQCR1.

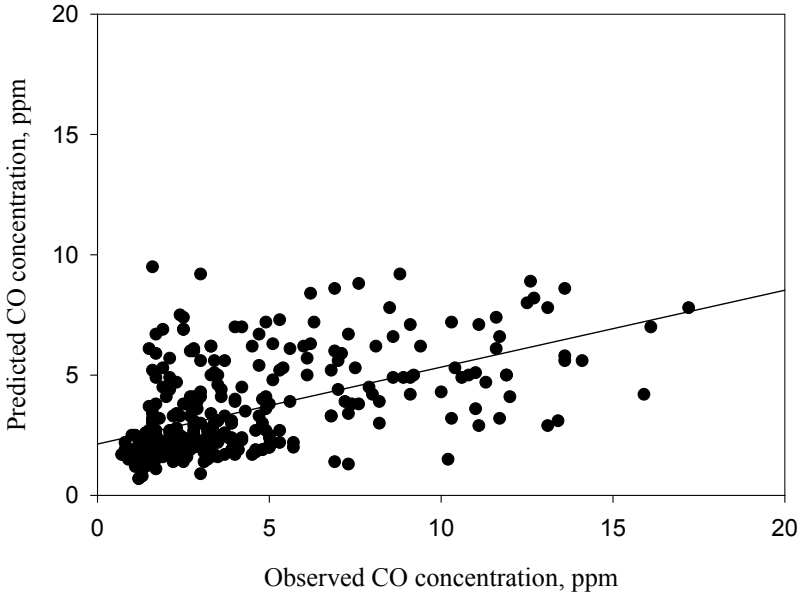

Fig. 6.10. Scatter plots of 8-hr average CO observations vs the $ANNCO_{8hrB2}$ model predictions for the evaluation data set at AQCR2.

$ANNCO_{8hrA2}$ models (d=0.69) respectively. It may be due to the increase in time averaging interval (1-hr to 8-hr) which smoothens out the temporal variations of CO concentration with meteorological and traffic characteristic variables which, in turn, implies that the real non-linear CO-meteorology and CO-traffic relationships gradually approach to linear form. As a result, the elimination of traffic characteristic variables from the model input finds no dramatic improvements in its performance. Comrie [82] and Gardner and Dorling [18, 255] have observed the out-performance of neural network model at sub daily time scale when the non-linearity of the system has been more apparent, while only small to marginal gains in model performance at the daily time scale.

Table 6.6 explains the performance statistics of the $ANNCO_{8hrC1}$ and $ANNCO_{8hrC2}$ models prediction on test data set at AQCR1 and AQCR2 respectively. At AQCR1, the mean of the predicted CO concentration (5.03 ppm) is higher than the observed mean (3.78 ppm); while at AQCR2, it is lower (3.49 ppm) than the observed mean value (4.18 ppm). The MBE values at AQCR1 is positive, indicating the tendency of the model to over predict; while at AQCR2, it is negative, indicating its tendency to under predict. The standard deviations (σ_P) of the $ANNCO_{8hrC1}$ and the $ANNCO_{8hrC2}$ model predictions are lower than the observed standard deviations (σ_O). It explains that both models are inadequate to reproduce the variations in the test data set. The high $RMSE_S$ values indicate that both models perform poorly on the test data set. The 'd' values for the $ANNCO_{1hrC1}$ and $ANNCO_{1hrC2}$ models are 0.4 and 0.26 respectively. This explains that at AQCR1, 40 % of the model predictions are error free; while at AQCR2, 26 % are error free. Figure 6.11 and 6.12 show observed versus predicted CO concentrations at AQCR1 and

Table 6.6 Performance statistics of the $ANNCO_{8hrC1}$ and $ANNCO_{8hrC2}$ models (with the traffic characteristic inputs).

Site	Model ID	Statistic											
		$\overline{O}$ ppm	$\overline{P}$ ppm	σ_O ppm	σ_P ppm	MBE ppm	MSE ppm	RMSE		r^2	d	a ppm	b
								$RMSE_S$ ppm	$RMSE_U$ ppm				
AQCR1	$ANNCO_{8hrC1}$	3.78	5.03	2.45	0.37	1.24	7.4	2.70	0.36	0.03	0.4	4.93	0.02
AQCR2	$ANNCO_{8hrC2}$	4.18	3.49	3.35	0.52	-0.69	11.02	3.28	0.50	0.07	0.26	3.33	0.04

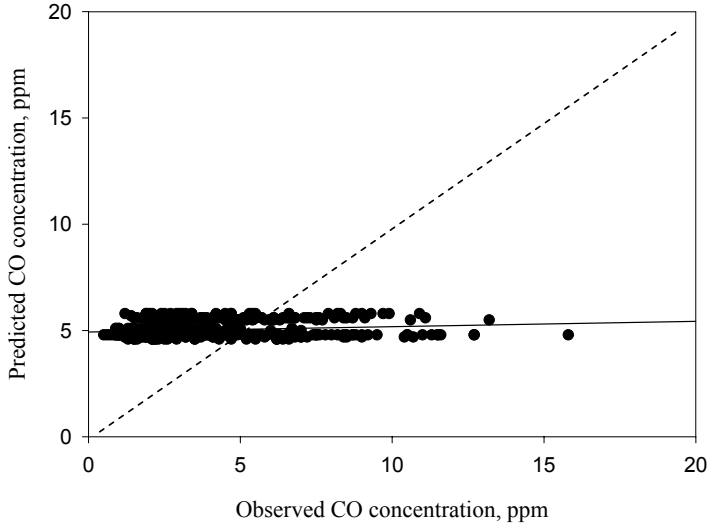

Fig. 6.11. Scatter plots of 8-hr average CO observations vs the $ANNCO_{8hrC1}$ model predictions for the evaluation data set at AQCR1.

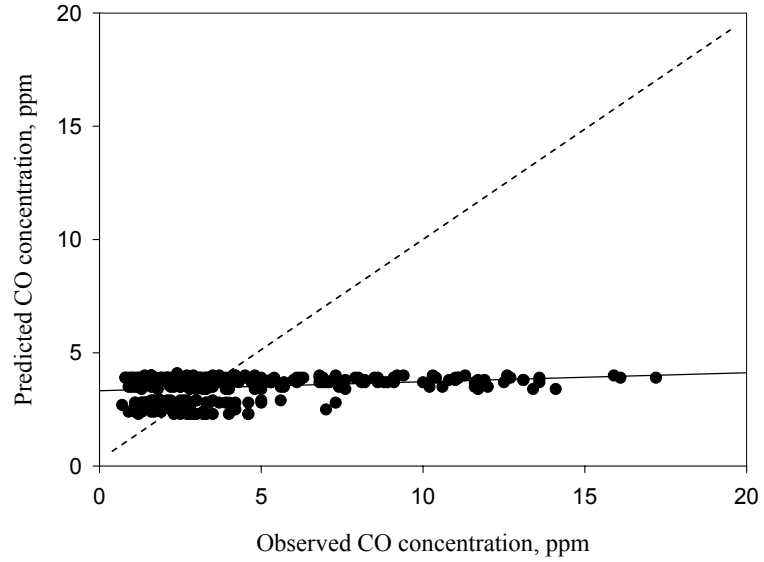

Fig. 6.12 Scatter plots of 8-hr average CO observations vs the $ANNCO_{8hrC2}$ model predictions for the evaluation data set at AQCR2.

AQCR2 respectively, indicating that both models under predict CO concentrations when observed concentrations are towards higher side and over predicts when observed concentrations are towards lower side.

Comparative performance of $ANNCO_{8hrC1}$ vs $ANNCO_{8hrB1}$ and $ANNCO_{8hrA1}$ and $ANNCO_{8hrC2}$ vs $ANNCO_{8hrB2}$ and $ANNCO_{8hrA2}$

The $RMSE_S$ value for $ANNCO_{8hrC1}$ model increases by 0.83 and 0.73 ppm when compared with $ANNCO_{8hrA1}$ and $ANNCO_{8hrB1}$ models respectively. However, for $ANNCO_{8hrC2}$ model, this value increases by 1.01 and 0.9 ppm when compared with $ANNCO_{8hrA2}$ and $ANNCO_{8hrB2}$ models respectively. Further, 'd' values indicate that $ANNCO_{8hrC1}$ model (d=0.4) performs poorly at AQCR1, when compared with $ANNCO_{8hrA1}$ (d=0.78) and $ANNCO_{1hrB1}$ models (d=0.77). At AQCR2, the $ANNCO_{8hrC2}$ model (d=0.26) also shows poor performance when compared with the $ANNCO_{8hrA2}$ (d=0.69) and $ANNCO_{8hrB2}$ models (d=0.67). The reason for the poor performance of $ANNCO_{8hrC1}$ and $ANNCO_{8hrC2}$ models seems due to their inability to take into account the 'lag effect' in absence of meteorological data as input to these models. It again verifies the fact that, as described by Gardner and Dorling [83,255] that decrease in number of variables, affects the prediction accuracy of ANN based vehicular pollution models.

6.3.3 24-hr Average NO_2 Models

Table 6.7 provides the performance statistics of the $ANNNO2_{24hrA1}$ and $ANNNO2_{24hrA2}$ model predictions on the test data set at AQCR1 and AQCR2 respectively. The mean values of $ANNNO2_{24hrA1}$ and $ANNNO2_{24hrA2}$ model predictions are slightly lower than the observed mean values. The MBE values at AQCR1 and AQCR2 are negative, indicating the tendency of the models to under predict. The standard deviations (σ_P) of the $ANNNO2_{24hrA1}$ and $ANNNO2_{24hrA2}$ models prediction are 6.9 and 4.87 ppb respectively. At AQCR1, standard deviation of the predictions (σ_P) is close to the standard deviation of the observed data. At AQCR2, the difference between the

Table 6.7 Performance statistics of the $ANNNO2_{24hrA1}$ and $ANNNO2_{24hrA2}$models (with the meteorological and the traffic characteristic inputs).

Site	Model ID	Statistic											
		$\overline{O}$ ppb	$\overline{P}$ ppb	σ_O ppb	σ_P ppb	MBE ppb	MSE ppb	RMSE		r^2	d	a ppb	b
								$RMSE_S$ ppb	$RMSE_U$ ppb				
AQCR1	$ANNNO2_{24hrA1}$	35.1	31.7	10.4	6.9	-3.4	69.06	6.5	5.05	0.47	0.76	15.7	0.46
AQCR2	$ANNNO2_{24hrA2}$	30.2	27.8	9.4	4.87	-2.34	77.44	8.01	4.41	0.18	0.59	21.2	0.2

standard deviations of the observed and predicted data is quite high. This explains that the $ANNNO2_{24hrA1}$ model is reproducing the variations in the test data set at AQCR1 with improved accuracy than $ANNNO2_{24hrA2}$ model. A low $RMSE_S$ value at AQCR1 indicates that the $ANNNO2_{24hrA1}$ model predictions are closely matching with actual observations, when compared with $ANNNO2_{24hrA2}$ model predictions at AQCR2. Further, the 'd' values for the $ANNNO2_{24hrA1}$ and the $ANNNO2_{24hrA2}$ models are 0.76 and 0.59 respectively. This explains that at AQCR1, 76 % of the model predictions are error free; while at AQCR2, only 59 % of model predictions are error free. It shows that $ANNNO2_{24hrA1}$ model is more reliable and accurate than $ANNNO2_{24hrA2}$. Figure 6.13 and 6.14 show observed versus predicted NO_2 concentrations at AQCR1 and AQCR2 respectively, indicating that both models under predict NO_2 concentrations when observed concentrations are towards higher side.

Table 6.8 summaries the performance statistics of the $ANNNO2_{24hrB1}$ and $ANNNO2_{24hrB2}$ model predictions on the test data set at AQCR1 and AQCR2 respectively. The mean values of the predicted NO_2 concentration at both the AQCRs are lower than observed mean values. The MBE values at AQCR1 and AQCR2 are negative (-4.29 and -3.5 ppm respectively), indicating the tendency of the models to under predict. The difference between the standard deviation of observed and predicted data at AQCR2 is higher than at AQCR1. It explains that $ANNNO2_{24hrB1}$ model predictions are closer to observed values when compared with the $ANNNO2_{24hrB2}$ model. Further, a low $RMSE_S$ value at AQCR1 also indicates that $ANNNO2_{24hrB1}$ model predictions are closely matching with actual observations when compared to $ANNNO2_{24hrB2}$ model predictions.

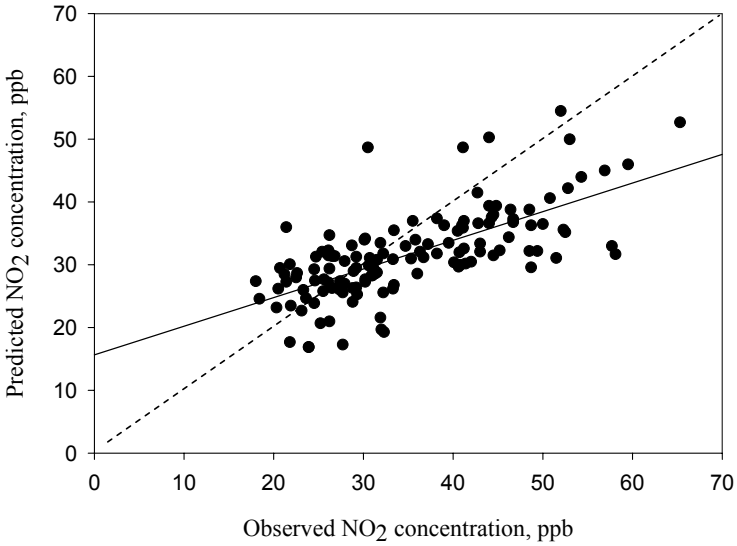

Fig. 6.13. Scatter plots of 24-hr average NO_2 observations vs the $ANNNO2_{24hrA1}$ model predictions for the evaluation data set at AQCR1.

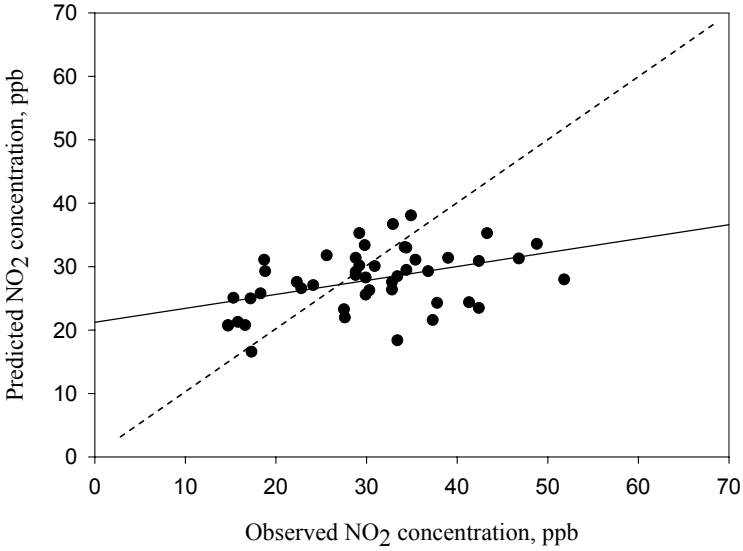

Fig. 6.14. Scatter plots of 24-hr average NO_2 observations vs the $ANNNO2_{24hrA2}$ model predictions for the evaluation data set at AQCR2.

Table 6.8 Performance statistics of the $ANNNO2_{24hrB1}$ and $ANNNO2_{24hrB2}$ models (with the meteorological inputs).

Site	Model ID	Statistic											
		$\overline{O}$ ppb	$\overline{P}$ ppb	σ_O ppb	σ_P ppb	MBE ppb	MSE ppb	RMSE		r^2	d	a ppb	b
								$RMSE_A$ ppb	$RMSE_I$ ppb				
AQCR1	$ANNNO2_{24hrB1}$	35.1	30.8	10.4	6.56	-4.29	78.32	7.41	4.86	0.45	0.73	16.04	0.42
AQCR2	$ANNNO2_{24hrB2}$	30.2	26.7	9.4	4.68	-3.5	90.25	8.53	4.35	0.12	0.55	21.46	0.17

The 'd' values for the $ANNNO2_{24hrB1}$ and $ANNNO2_{24hrB2}$ models explains that at AQCR1, 73 % of the model predictions are error free; while at AQCR2, 55 % are error free. It shows that $ANNNO2_{24hrB1}$ model at AQCR1 is more accurate than $ANNNO2_{24hrB2}$ at AQCR2. Figure 6.15 and 6.16 show observed versus predicted NO_2 concentrations at AQCR1 and AQCR2 respectively indicating that both models under predict NO_2 concentrations when observed concentrations are towards higher side.

Comparative performance of $ANNNO2_{24hrB1}$ vs $ANNNO2_{24hrA1}$ and $ANNNO2_{24hrB2}$ vs $ANNNO2_{24hrA2}$

The $RMSE_S$ values increase by 0.91 ppb for $ANNNO2_{24hrB1}$ model when compared to $ANNNO2_{24hrA1}$. However, the $RMSE_S$ value for $ANNNO2_{24hrB2}$ model is showing 0.52 ppb increase when compared to $ANNNO2_{24hrA2}$. Further, 'd' values for AQCR1 indicates that $ANNNO2_{24hrB1}$ (d=0.73) model performance decreases marginally when compared to the $ANNNO2_{24hrA1}$ (d=0.76). Similarly, at AQCR2, the $ANNNO2_{24hrB2}$ model (d=0.55) performance also shows marginal decrease when compared to the $ANNNO2_{24hrA2}$ (d=0.59). The reasons for this appear to be the same as explained in section 6.3.2.

Table 6.9 provides the performance statistics of the $ANNNO2_{24hrC1}$ and $ANNNO2_{24hrC2}$ model predictions on test data set at AQCR1 and AQCR2 respectively. The mean value of the predicted NO_2 concentrations at AQCR1 is closely matching with the observed mean. At AQCR2, the mean of predicted NO_2 concentrations is lower than the observed mean value. The MBE values at AQCR1 and AQCR2 are negative, indicating the tendency of the models to under predict. The standard deviations (σ_P) of the $ANNNO2_{24hrC1}$ and the $ANNNO2_{24hrC2}$ model predictions are very

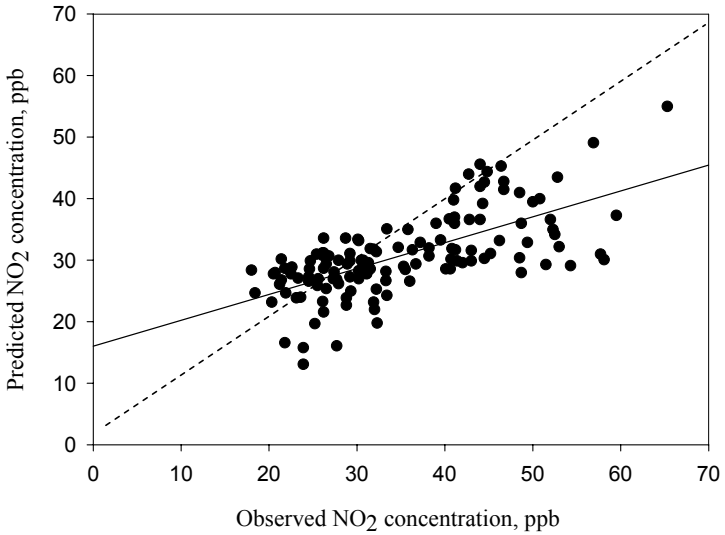

Fig. 6.15. Scatter plots of 24-hr average NO_2 observations vs the $ANNNO2_{24hrB1}$ model predictions for the evaluation data set at AQCR1.

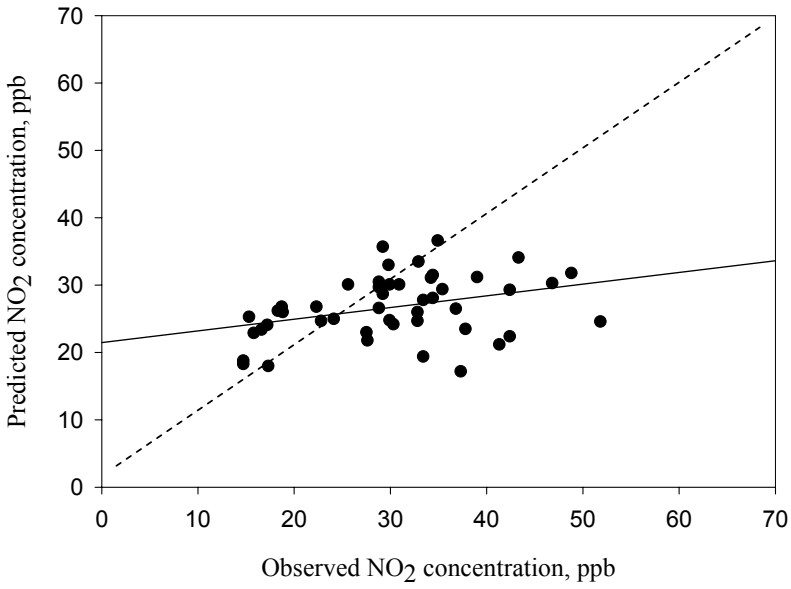

Fig. 6.16. Scatter plots of 24-hr average NO_2 observations vs the $ANNNO2_{24hrB2}$ model predictions for the evaluation data set at AQCR2.

Table 6.9 Performance statistics of the $ANNNO2_{24hrC1}$ and $ANNNO2_{24hrC2}$ models (with traffic characteristic inputs).

Site	Model ID	Statistic											
		$\overline{O}$ ppm	$\overline{P}$ ppm	σ_O ppb	σ_P ppb	MBE ppb	MSE Ppb	RMSE		r^2	d	a ppb	b
								$RMSE_S$ ppb	$RMSE_U$ ppb				
AQCR1	$ANNNO2_{24hrC1}$	35.1	33.1	10.4	0.74	-1.94	110.9	10.49	0.75	0.1	0.25	32.89	0.007
AQCR2	$ANNNO2_{24hrC2}$	30.2	27.3	9.4	0.44	-2.85	96.43	9.86	0.44	0.03	0.3	27.57	-0.01

low when compared with observed standard deviations (σ_O). It explains that both models are inadequate to reproduce the variations in the test data set. Further, the high $RMSE_S$ and low 'd' values also indicate that both the models perform poorly on the test data set. Figure 6.17 and 6.18 show observed versus predicted NO_2 concentrations at AQCR1 and AQCR2 respectively, indicating that both models under predict CO concentrations when observed concentrations are towards higher side.

Comparative performance of $ANNNO2_{24hrC1}$ vs $ANNNO2_{24hrB1}$ and $ANNNO2_{24hrA1}$ and $ANNNO2_{24hrC2}$ vs $ANNNO2_{24hrB2}$ and $ANNNO2_{24hrA2}$

The 'd' value indicates that $ANNNO2_{24hrC1}$ model (d=0.25) performs poorly at AQCR1 when compared with $ANNNO2_{24hrA1}$ (d=0.76) and $ANNNO2_{24hrB1}$ (d=0.73) models. At AQCR2, the $ANNNO2_{24hrC2}$ model (d=0.3) also shows poor performance when compared with $ANNNO2_{24hrB2}$ (d=0.55) and $ANNNO2_{24hrA2}$ models (d=0.59). The reason for this seems to be the absence of meteorological variables as input to the $ANNNO2_{24hrC1}$ and $ANNNO2_{24hrC2}$ models. With the result, the models fail to explain the seasonal variations present in the NO_2 dispersion characteristics. Similar to 1- and 8-hr average ANN based CO models, it again shows that decrease in number of input variables affects the prediction accuracy of ANN based vehicular pollution models [83,255].

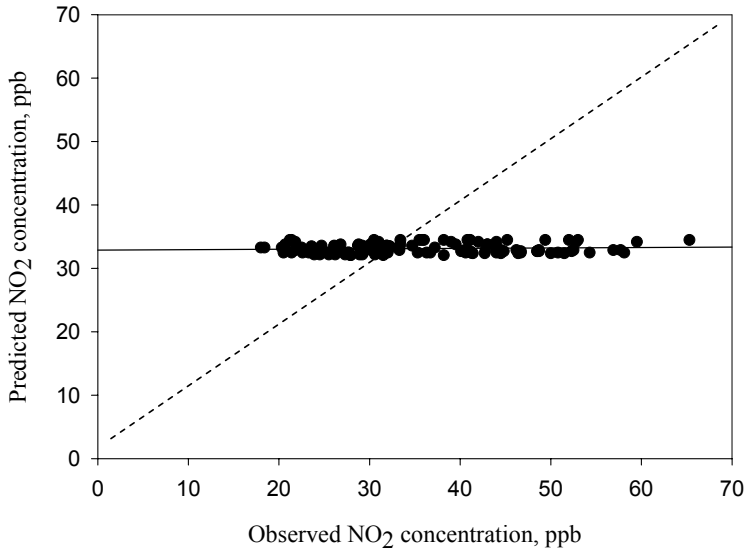

Fig. 6.17. Scatter plots of 24-hr average NO_2 observations vs the $ANNNO2_{24hrC1}$ model predictions for the evaluation data set at AQCR1.

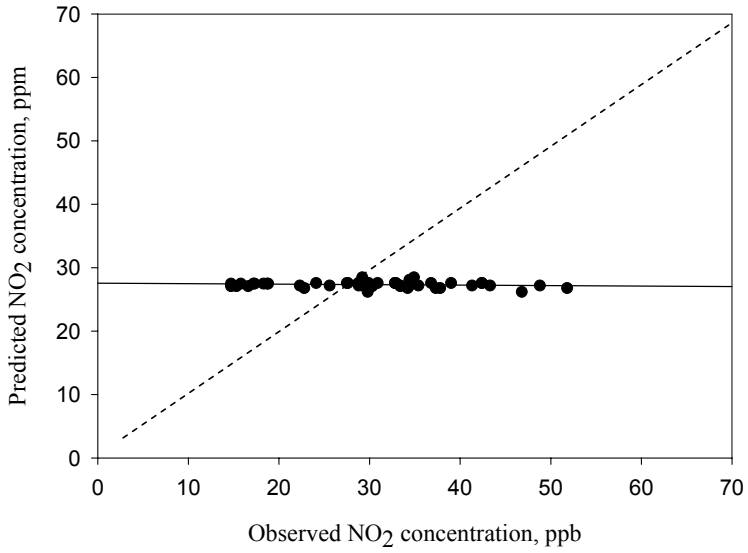

Fig. 6.18. Scatter plots of 24-hr average NO_2 observations vs the $ANNNO2_{24hrC2}$ model predictions for the evaluation data set at AQCR2.

6.4 Performance Evaluation and Comparison of ANN based Vehicular Pollution Models with Conventional Models

Prediction performances of the 1-hr average ANN based CO models are compared with, univariate stochastic model (Appendix C) and one of the existing deterministic model (Appendix A) for the *critical period* test data set (21^{st} - 31^{st} December, 1999).

6.4.1 Performance of ANN based CO Models for the Critical Period Test Data

The $ANNCO_{1hrA1}$ and $ANNCO_{1hrA2}$ models are used for prediction of CO concentration for the critical period at AQCR1 and AQCR2 respectively. Table 6.10 gives the performance statistics of the $ANNCO_{1hrA1}$ and $ANNCO_{1hrA2}$ model predictions on the critical period test data set. At both the AQCRs, the means of predicted CO concentration are higher than that of the observed mean values. The MBE values are positive at both the AQCRs, indicating the tendency of the models to over predict. The standard deviation (σ_P) of the $ANNCO_{1hrA1}$ model prediction is lower than the standard deviation of the observed data at AQCR1. At AQCR2, the difference between the standard deviation of the observed and predicted data is quite low. This explains that the $ANNCO_{1hrA2}$ model is reproducing the variations in the critical period test data set; where as, $ANNCO_{1hrA2}$ model is unable to reproduce the variations. Further, a low $RMSE_S$ value and a high 'd' value (0.69) at AQCR2 indicate that the $ANNCO_{1hrA2}$ model predictions are closely matching with the actual observations when compared with the $ANNCO_{1hrA1}$ model predictions at AQCR1. Figure 6.19 and 6.20 show observed versus predicted CO concentrations at AQCR1 and AQCR2 respectively, indiindicating that both models under predict CO concentrations when observed concentrations are towards higher side.

Table 6.10 Performance statistics of the 1-hr average ANN based CO models.

Site	Model ID	Statistic											
		$\overline{O}$ ppm	$\overline{P}$ ppm	σ_O ppm	σ_P ppm	MBE ppm	MSE ppm	RMSE		r^2	d	a ppm	b
								$RMSE_S$ ppm	$RMSE_U$ ppm				
AQCR1	$ANNCO_{1hrA1}$	5.24	6.6	4.24	2.37	1.0	13.1	3.06	1.94	0.33	0.67	4.82	0.32
AQCR2	$ANNCO_{1hrA2}$	4.07	5.06	3.08	2.27	0.89	8.12	2.09	1.93	0.27	0.69	3.45	0.39

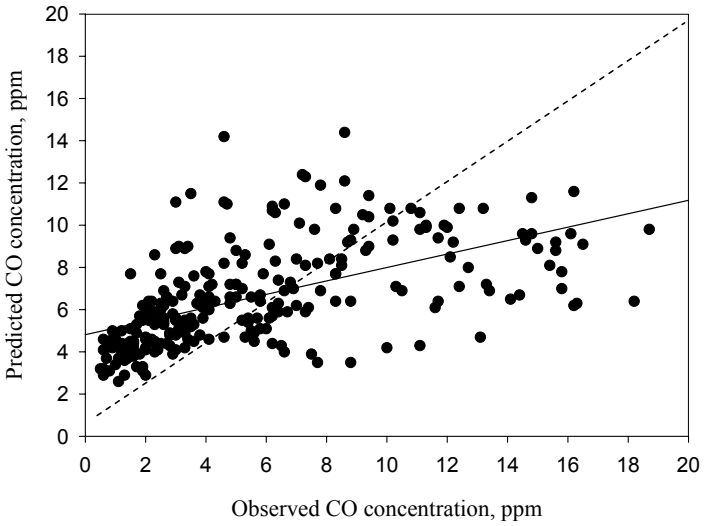

Fig. 6.19. Scatter plots of 1-hr average CO observations vs the ANN based CO model ($ANNCO_{1hrA1}$) predictions for the critical period data set at AQCR1.

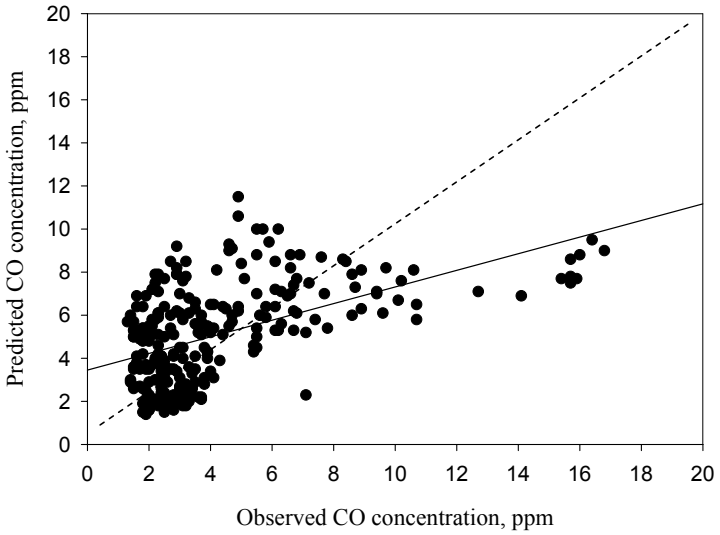

Fig. 6.20. Scatter plots of 1-hr average CO observations vs the ANN based CO model ($ANNCO_{1hrA2}$) predictions for the critical period data set at AQCR2.

6.4.2 Performance of Univariate Stochastic Models for the Critical Period Test Data

Table 6.11 provides the performance statistics of the ARIMA $(1,1,1)x(0,1,1)_{24}$ and ARIMA$(1,1,0)x(0,1,1)_{24}$ model predictions on the critical period test data set at AQCR1 and AQCR2 respectively. The mean values of predicted CO concentrations are lower than the observed mean values at both the AQCRs. The MBE values are negative at both the AQCRs, indicating the tendency of the models to under predict. The standard deviations (σ_P) of the ARIMA $(1,1,1)x(0,1,1)_{24}$ and ARIMA$(1,1,0)x(0,1,1)_{24}$ model predictions are low when compared to the observed standard deviations (σ_O). This explains that univariate stochastic models are unable to reproduce the variations in the critical period test data set at respective AQCRs. The $RMSE_S$ and $RMSE_U$ errors for the ARIMA (1,1,1) x $(0,1,1)_{24}$ model are 5.0 and 0.51 ppm respectively; where as, for the ARIMA (1,1,0) x $(0,1,1)_{24}$ model, these are 5.65 and 0.36 ppm. A lower $RMSE_S$ value at AQCR1 indicates that the ARIMA (1,1,1) x $(0,1,1)_{24}$ model predictions are moderately matching with observed values when compared to the ARIMA $(1,1,0)x(0,1,1)_{24}$ model predictions at AQCR2. Further, the 'd' values for the ARIMA$(1,1,1)x(0,1,1)_{24}$ and the ARIMA$(1,1,0)x(0,1,1)_{24}$ models are 0.49 and 0.43 respectively. This explains that at AQCR1, 49 % of the model predictions are error free; while at AQCR2, only 43 % predictions are error free. Figure 6.21 and 6.22 show observed versus predicted CO concentrations at AQCR1 and AQCR2 respectively indicating that both models under predict CO concentrations when observed concentrations are towards higher side.

Table 6.11 Performance statistics of the univariate stochastic models.

Site	Model ID	Statistic											
		$\overline{O}$ ppm	$\overline{P}$ ppm	σ_O ppm	σ_P ppm	MBE ppm	MSE ppm	RMSE		r^2	d	a ppm	B
								$RMSE_S$ ppm	$RMSE_U$ ppm				
AQCR1	ARIMA $(1,1,1)(0,1,1)_{24}$	5.24	0.99	4.24	0.75	-4.61	35.05	5.0	0.51	0.21	0.49	0.27	0.13
AQCR2	ARIMA $(1,1,0)(0,1,1)_{24}$	4.07	0.57	3.08	0.38	-3.59	21.62	5.65	0.36	0.11	0.43	0.4	0.04

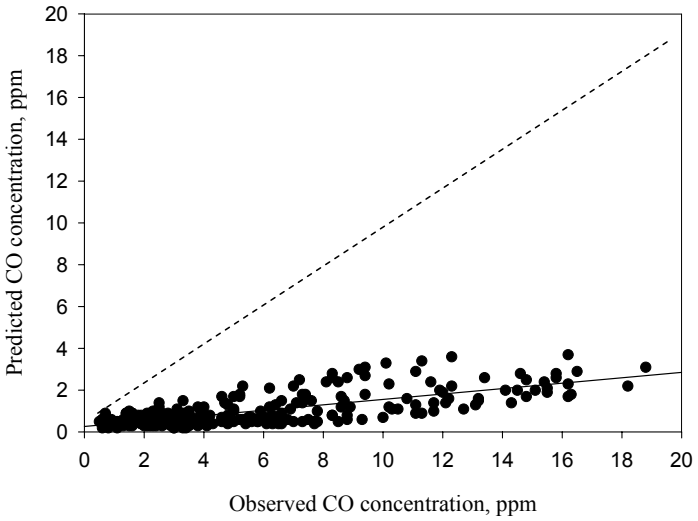

Fig. 6.21. Scatter plots of 1-hr average CO observations vs the univariate stochastic model predictions for the critical period data set at AQCR1.

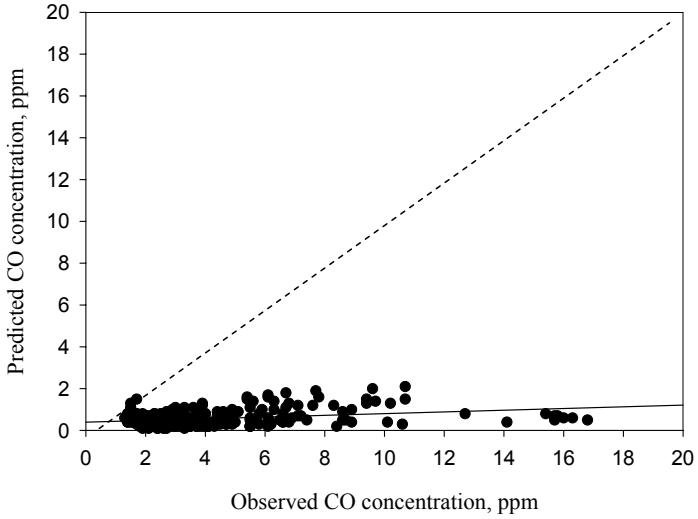

Fig. 6.22. Scatter plots of 1-hr average CO observations vs the univariate stochastic model predictions for the critical period data set at AQCR2.

6.4.3 Performance of Deterministic Model for the Critical Period Test Data

Table 6.12 summarizes the performance statistics of the DFLS model [172] predictions on the critical period test data set at AQCR1 and AQCR2 respectively. The mathematical formulation and inputs for DFLS model are given in Appendix-A. The mean values of predicted CO concentrations are lower than that of the observed mean values at both the AQCRs. The MBE values are negative at both the AQCRs, indicating the tendency of the model to under predict. At both the AQCRs, the standard deviations (σ_P) of the DFLS model predictions are lower than the observed standard deviations of the critical period data. This explains that the DFLS model is inadequate to reproduce the variations in the critical period test data set at both the AQCRs. Further, a lower $RMSE_S$ value at AQCR1 indicate that the DFLS model predictions are moderately matching with observed values when compared to the DFLS model predictions at AQCR2. The 'd' values for the DFLS model at AQCR1 and AQCR2 are 0.43 and 0.41 respectively. This explains that at AQCR1, 43 % of the model predictions are error free; while at AQCR2, 41 % predictions are error free. It shows that the DFLS model performance at both the AQCRs is more or less similar. Figure 6.23 and 6.24 show observed versus predicted CO concentrations at AQCR1 and AQCR2 respectively, indicating that both models under predict CO concentrations when observed concentrations are towards higher side.

Table 6.12 Performance statistics of the deterministic model (DFLSM).

Site	Model ID	Statistic											
		$\overline{O}$ ppm	$\overline{P}$ ppm	σ_O ppm	σ_P ppm	MBE ppm	MSE ppm	RMSE		r^2	d	a ppm	b
								$RMSE_S$ ppm	$RMSE_U$ ppm				
AQCR1	DFLSM	5.24	1.81	4.24	1.38	-3.43	31.58	5.45	1.38	0.1	0.43	1.81	0.0001
AQCR2	DFLSM	4.07	0.23	3.0	0.16	-3.83	23.62	5.87	0.16	0.1	0.41	0.21	0.005

Comparative performance of ANN based vehicular pollution *model vs univariate stochastic and deterministic models*

Table 6.13 summarizes the comparative performance statistics of ANN based, univariate stochastic and deterministic models on the critical period test data set. At AQCR1, the $RMSE_S$ value for the

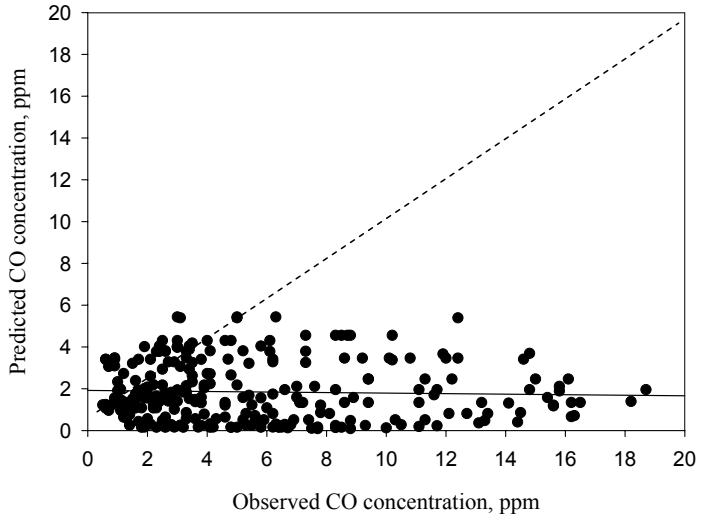

Fig. 6.23. Scatter plots of 1-hr average CO observations vs the deterministic (DFLS) model predictions for the critical period data set at AQCR1.

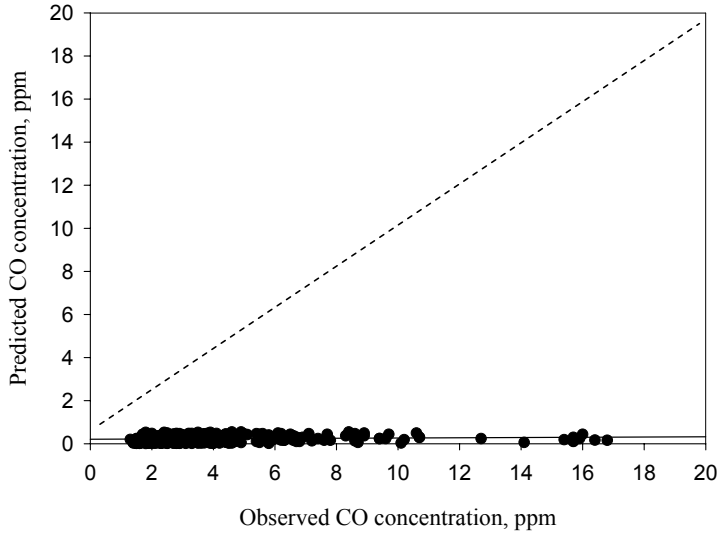

Fig. 6.24. Scatter plots of 1-hr average CO observations vs the deterministic (DFLS) model predictions for the critical period data set at AQCR2.

Table 6.13 Summary of ANN based CO model vs univariate stochastic and deterministic model comparison.

Site	AQCR1			AQCR2		
Model ID	**$ANNCO_{1hrA1}$**	**Univariate**	**DFLS**	**$ANNCO_{1hrA2}$**	**Univariate**	**DFLSM**
$RMSE_S$	3.06	5.0	5.45	2.09	5.65	5.87
d	0.67	0.49	0.43	0.69	0.43	0.41

DFLS model increases by 2.39 and 0.45 ppm when compared with the $ANNCO_{1hrA1}$ and univariate stochastic model. However, at AQCR2, it increases by 3.78 and 0.22 ppm when compared with the $ANNCO_{1hrA2}$ and univariate stochastic model. Further, the 'd' values at both the AQCRs indicate poor performance of DFLS and univariate stochastic models. The sequence of the predicted and observed values of the CO concentration for ANN based CO model, univariate stochastic model and DFLS model is shown in Figures 6.25 and 6.26 respectively. These figures show that at both the AQCRs, DFLS model predictions are comparable to the observed values during 'working hours' (8 AM – 6 PM). This may be due to the presence of sufficient traffic flow (emission rate) along with the meteorology, which are the vital input parameters of this Gaussian based deterministic model. However, during after hours (i.e., after 10 PM), the DFLS model fails to predict CO concentration adequately due to the presence of "lag effect" during which the accumulation of CO takes place without any dispersion while the traffic flow is trickle [172]. This indicates that Gaussian based deterministic models are not able to explain non-linear relationship between the vehicular pollution, meteorological and traffic characteristic variables.

The stochastic model takes into account all possible uncertainty in form of 'noise' variable with assigned statistical properties. The time series of CO concentration at both the AQCRs contain no forward information on "lag effect". Therefore, the persistence of inversion conditions has not been explained by the noise term in the univariate model. Further, the statistical analysis of CO concentration variation in critical period is generally not following the theoretical ACF and PACF graphical form [273]. With the result, univariate stochastic model fails to reproduce the CO time series for critical periods at both the AQCRs.

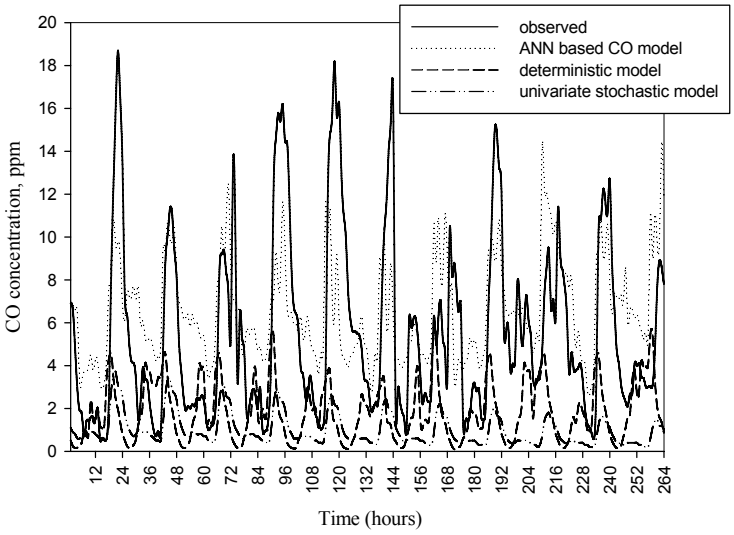

Fig. 6.25. Comparison of 1-hr average CO concentrations predicted by ANN based CO, univariate stochastic and deterministic models for the critical period data set at AQCR1.

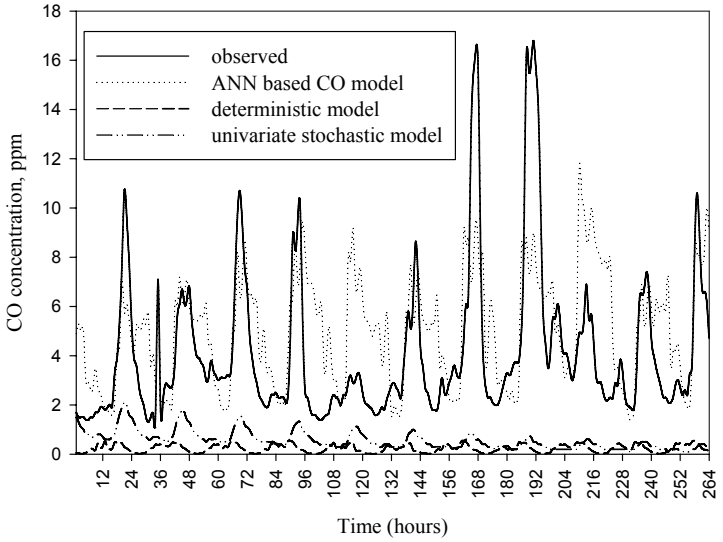

Fig. 6.26. Comparison of 1-hr average CO concentrations predicted by ANN based CO, univariate stochastic and deterministic models for the critical period data set at AQCR2.

In contrast with univariate stochastic and deterministic models, ANN based vehicular pollution models show best performance on the critical period test data set at both the AQCRs (Table 6.13). It is due to the inclusion of all those relevant meteorological and traffic parameters that affect CO concentrations during the critical periods. Further, the neural network model also takes into account the 'lag effect' that prevails during the critical periods. Further, they are also able to capture non-linear relationship between CO dispersion and meteorological and traffic characteristics due to its self-learning capabilities.

6.5 Summary

The application of ANN based vehicular pollution models to the urban context in India have been presented. A range of statistical indicators as suggested by Fox [271] and Willmott [263] are used for model performance evaluation. The performance of 1-, 8- and 24-hr average ANN based vehicular pollution models are evaluated on the test data set at two AQCRs. For 'near-field' region (AQCR1), the forecast performances of 1-hr average ANN based CO models with meteorological and traffic characteristic inputs are satisfactory, while there is a significant decrease in model performance when only meteorological inputs are used. For 'far-field' region (AQCR2), the forecast performance of 1-hr average ANN based CO models with meteorological and traffic characteristic input as well as with only meteorological input are satisfactory. The study also reveals the effect of the location of the monitoring station on pollutant dispersion. The forecast performance of 8-hr average ANN based CO models with meteorological and traffic inputs, and only with meteorological inputs, respectively, is equally satisfactory. Similar observations have also been observed for 24-hr average ANN based NO_2 models. The performance of 1-, 8- and 24-hr average ANN based vehicular pollution models with only traffic characteristic variables input is unsatisfactory. The performance of the ANN based vehicular pollution models have been compared with one of the

deterministic and the univariate stochastic models. It is observed that ANN based vehicular pollution model predictions are more reliable than that of deterministic and univariate statistical models for the critical period data set.

7 Epilogue

The development of effective air quality management strategies at local urban scale requires analysis of complex interaction between exhaust emission with meteorological and traffic characteristics. A well-structured air quality management system must be based on efficient tools that integrate a diverse set of information's–vehicular emissions, traffic characteristics, meteorological variables and local air quality data. Therefore, extensive meteorological and traffic characteristics, emissions and air quality data are required for the development of efficient air quality management models.

In last 50 years, several line source models are developed to describe temporal and spatial distribution of exhaust emission on urban roadways. Most of these models are developed either by deterministic and/or stochastic approaches. During the recent past, ANN technique is becomes one of the upcoming techniques in modelling the exhaust emission dispersion phenomena. In this book, the development of ANN based vehicular pollution models of different time resolutions are described. ANN based vehicular pollution modelling approach does not require in depth knowledge of physical phenomena. Instead, the neural network develops suitable mapping of the vehicular pollution dispersion, based on the data with which is trained. The training is mostly done by back-propagation method. The models are formulated following three choices of input data sets. *Firstly*, with both meteorological and traffic input data. *Secondly*, with only meteorological input data and *lastly* with only traffic input data.

A step-by-step procedure has been formulated for the development of ANN based vehicular pollution models. The procedure provides vital statistics and clues on some parameters e.g. when to stop the training process and determination of learning parameters in back-propagation learning algorithm. ANN based vehicular pollution models are developed for different time resolutions as per

M. Khare and S.M. Shiva Nagendra: *Epilogue*, Artificial Neural Networks in Vehicular Pollution Modelling (SCI) **41,** 157–161 (2007)
www.springerlink.com

NAAQS, to assess the future air quality, particularly during inversion conditions. Based on future changes in the traffic characteristics and meteorology, these models may be used as efficient tools to assess the future urban air quality.

The 1-hr average ANN based CO models (developed with both meteorological and traffic characteristics as inputs) show best performance on the test data set at both the AQCRs. It demonstrates that ANN can accurately model the short-term non-linear CO dispersion phenomena. However, the location of the AQCR with respect to the line source plays a vital role in evaluating the prediction performance of the neural network based model. The 1-hr average ANN based vehicular pollution model (developed with only meteorological inputs, excluding traffic characteristic variables) shows poor performance on the test data set at AQCR1 which is situated at 'near-field' region (< 3 m from the line source), when compared to ANN based vehicular pollution model with both meteorological and traffic characteristics, as inputs. It supports the findings of Rao et al. [120], which explain the dominance of 'wake effects' on pollutant dispersion in 'near-field' region of roadways. The 1-hr average ANN based vehicular pollution model, developed with only meteorological inputs (excluding traffic characteristic variables), shows marginal difference in its performance on the test data set at AQCR2 which is situated at 'far-field' region (> 30 m from the line source), when compared to ANN based vehicular pollution model developed with both meteorological and traffic characteristics as inputs. It indicates that in 'far-field' region, meteorological variables dominate the pollutant dispersion [120, 129]. The 8-hr average ANN based CO and 24-hr average ANN based NO_2 models, developed with both meteorological and traffic characteristics as inputs, show satisfactory performance on the test data set at both the AQCRs. The results also show that increase in the number of input variables further improves the performance of ANN based models.

The increase in time average interval (1-hr to 8-hr and 24-hr) smoothens out the temporal variations in pollutant concentrations. As a result, the 8-hr average ANN based CO and 24-hr average ANN based NO_2 models (developed with only meteorological inputs, excluding traffic characteristic variables), show no improvements in model performance on the test data set at both the AQCRs.

The 1- and 8-hr average ANN based CO models (developed with only traffic characteristics as inputs) show poor performance on the test data set at both the AQCRs. It reflects the models' inability to take into account the 'lag effect' [172], in absence of meteorological data as inputs. The 24-hr average ANN based NO_2 models (developed with only traffic characteristics as inputs) show poor performance on the test data set at both the AQCRs. It demonstrates that these models are not able to explain the seasonal variations, present in the NO_2 dispersion characteristics in absence of meteorological data.

The comparison of ANN based vehicular pollution models with a univariate stochastic and a deterministic (DFLS) models shows that ANN based models have an edge over them in terms of their prediction accuracy as well as applicability. The DFLSM failed to predict CO concentration during after hours (i.e. after 10 PM) due to its inability to take into account the 'lag effect' [172]. The univariate stochastic model also failed to explain the 'lag effect', there by, showing poor performance. The ANN based models performed satisfactorily in predicting the pollutant concentration during all the hours of the day for the critical period data set. It clearly demonstrates the self learning capabilities of ANN based models which resulted into capturing CO dispersion phenomena through meteorological and traffic characteristic variables.

The current deterministic and stochastic line source models are widely used by local air quality authorities to make short-term pollution forecasts for public advisories and for input into decision regarding air quality management. However, in the presence of 'lag effect' these models fail to provide reliable short-term pollution forecasts during critical periods. In this book shows that neural networks can accurately develop mapping of the 'lag effect' phenomena based on the data with which it has been trained. Further, it also demonstrates that neural network methods are viable when compared to deterministic and stochastic approaches.

This book explains the capabilities of neural network approach in studying the 'near-field' and 'far-field' short-term exhaust emission dispersion characteristics. With the available meteorological and traffic characteristics data, the trained neural network has been

found to be able to identify the traffic 'wake effects' on pollutant dispersion on urban roadways.

From last five decades a considerable amount of research work are carried on the development of exhaust emission models using deterministic approach, while limited studies are conducted on statistical approach [59]. The relationship between vehicular emission dispersion with meteorology and traffic characteristic is highly complex and non-linear. Hence there is always a scope for applying new modelling techniques to tackle such complex phenomena. In this book, recent modelling approach i.e. ANN, has been used to address the local air quality management system in urban areas, in which traffic is the main cause of urban air pollution. The work presented in this book has successfully demonstrated that ANN based vehicular pollution models are worthy of further exploration.

ANN technology is in its infancy. It is an approach that is inherently more suited for certain class of information processing operations. The modelling of exhaust emission dispersion phenomena using ANN technique, may aid in defining the capabilities of neural network. It appears that the presence of 'noise' in air quality data may limit the capability of the ANN model forecasting. This one gray area, where further work can be carried out, using suitable functions [274] in ANN based vehicular pollution modelling for proper distribution of air quality data, before actual calculations are made in hidden layer neurons. This approach may eliminate the effect of 'noise' on the air quality data and thus improve the accuracy of forecast.

A fuzzy approach may also be used in developing ANN based vehicular pollution models for estimating the number of violations of air quality standards. Thus, ANN along with the fuzzy logic theory may be used as an effective means for exploring complex interrelationships between traffic characteristics, meteorological variables and pollutant concentrations in urban areas [49, 275].

Substantial progress has been made in the application of statistical models-stochastic and regression techniques. But a very few studies have been made on hybrid modelling approach. A hybrid approach is combination of deterministic and statistical distribution

techniques used to fit the distribution of air pollutant concentrations [93, 276]. Hence, hybrid modelling studies may be carried out to study the dispersion characteristics at traffic intersections and busy arterial roads.

A Formulation of Delhi Finite Line Source Model (DFLSM)

A.1 General

The commonly used method of modelling air pollutant dispersion is represented by a differential equation, which expresses the rate of change of pollutant concentration in terms of average wind speed and turbulent diffusion. Mathematically this process is derived from the mass conservation principle [131]. The basic diffusion equation used in air quality modelling is given by:

$$\frac{\partial C}{\partial t} = -\left(u\frac{\partial C}{\partial x} + v\frac{\partial C}{\partial y} + w\frac{\partial C}{\partial z} \right) + \frac{\partial}{\partial x}K_H\frac{\partial C}{\partial x} + \frac{\partial}{\partial y}K_H\frac{\partial C}{\partial y} + \frac{\partial}{\partial z}K_z\frac{\partial C}{\partial z} + Q + R. \quad \text{(A.1)}$$

where C = pollutant concentration; t = time, x, y, z = position of the receptor relative to the source; u, v, w = wind speed coordinate in x, y and z direction; K_x, K_y, K_z = coefficients of turbulent diffusion in x, y and z direction; Q = source strength; R = sink (changes caused by chemical reaction)

A.2 Formulation of Gaussian Plume Model

The diffusion equation A.1 can be solved by two approaches. The *first,* and more complex type of solution is by numerical integration, having defined boundary conditions. The *second* approach is via simplifying assumption that the wind and turbulence functions are independent of time and position. Then, an analytical solution is possible, in which the pollutant concentration is expressed as a Gaussian distribution. Using analytical approach, the first formulation for the steady-state concentration of the downwind from a continuous point source was presented by Sutton [277], and further

M. Khare and S.M. Shiva Nagendra: *Formulation of Delhi Finite Line Source Model (DFLSM)*, Artificial Neural Networks in Vehicular Pollution Modelling (SCI) **41,** 163–173 (2007)
www.springerlink.com

developed by Pasquill [278] and Gifford [279]. The formulation of the Gaussian plume model for the continuous point source is given by:

$$C(x,y,z;H) = \frac{Q}{2\pi\sigma_y\sigma_z\bar{u}} \cdot \exp\left[-\frac{1}{2}\left(\frac{y}{\sigma_y}\right)^2\right] \times \left[\exp\left\{-\frac{1}{2}\left(\frac{z-H}{\sigma_z}\right)^2\right\} + \exp\left\{-\frac{1}{2}\left(\frac{z+H}{\sigma_z}\right)^2\right\}\right] \quad \text{(A.2)}$$

where C = pollutant concentration (mass/volume); Q = emission rate from the point source (mass/time); z = receptor height above ground (m); $\bar{u}$ = mean horizontal wind speed (m/s); H = effective stack height (m) = the sum of the physical stack height (h) and the plume rise (Δh); σ_y and σ_z = horizontal and vertical dispersion coefficients (m) at a distance x from the source; x and y = downwind and lateral distances from the source to the receptor point (m).

In the above equation, the last right-hand side term accounts for reflection of the plume at the ground by assuming an image source at distance 'H' beneath the ground surface. Figure A.1 shows the Gaussian plume model concepts considered in the above equation.

Assumptions in Gaussian plume model:

(i) Steady-state conditions, which imply that the rate of emission from the point source is constant.
(ii) Homogeneous flow, which implies that the wind speed is constant both in time and with height (wind direction shear is not considered).
(iii) Pollutant is conservative and no gravity fallout.
(iv) Perfect reflection of the plume at the underlying surface, i.e. no ground absorption.
(v) The turbulent diffusion in the x-direction is neglected relative to advection in the transport direction (x), which implies that the model should be applied for average wind speeds of more than 1 m/s ($\bar{u} > 1$ m/s).
(vi) The coordinate system is directed with its x-axis into the direction of the flow, and the v (lateral) and w (vertical) components of the time averaged wind vector are set to zero.

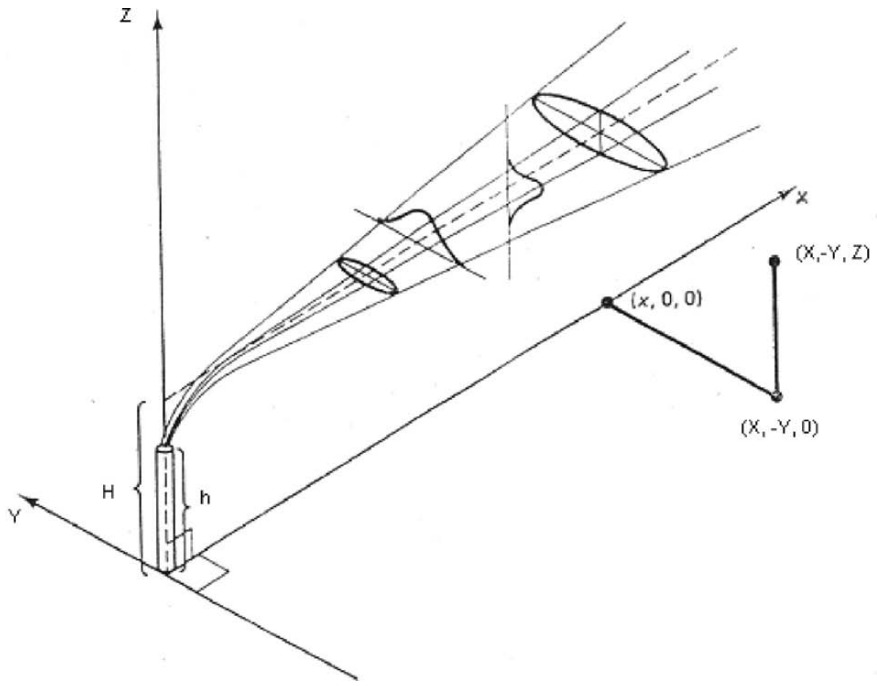

Fig. A.1. Cross section of a Gaussian plume profile in the horizontal and vertical directions.

(vii) The terrain underlying the plume is flat.
(viii) All variables are ensemble averaged, which implies long-term averaging with stationary conditions.

Many limitations arise due to the assumptions made in the formation of Gaussian plume models. For instance, the steady-state assumption implies that the Gaussian plume equation can be applied only for shorter distances (of the order of 10 km) and shorter travel time (of the order of 2 hours). In spite of their disadvantages, the Gaussian plume models have wide applications because of the following reasons:

(i) Much experience has been gained since first model formulation (in particular in the field of dispersion coefficients estimation).
(ii) The model is easy to understand and use, and is efficient in computer running time.
(iii) The model is appealing conceptually.

The basic Gaussian dispersion model applies to a single point source, such as a smoke stack, but it can be modified to account for line sources (such as emissions from motor vehicles along a highway), or area sources (one can model these as a large number of point sources).

A.3 General Finite Line Source Model

Line sources are typically encountered during the atmospheric diffusion modelling of vehicular pollution and may be treated as assemblages of finite line sources. But, because an explicit solution to the general finite line source (GFLS) problem is not possible, it has to be approximated as a series of point sources [163]. Thus, a line source may be considered to be a superposition of a series of point sources. Figure 4.1 in chapter 4 illustrates the coordinate system and the source/receptor relation used in the derivation GFLS model. Let us consider a point source of strength (emission rate) Q_p, placed at the origin of the coordinate axis. The concentration at the receptor R (x_1, y_1, z) due to this upwind point source can be represented by:

$$C = Q_p \phi(x_1, y_1, z) \tag{A.3}$$

where, ϕ (x_1, y_1, z) is some form of diffusion equation relating concentration to downwind and crosswind distances [163]. Replacing Q_p in equation A.3 with an infinitesimal part $Q_L dy_1'$ of a uniform line source of strength (emission rate) Q_L per unit length such that dC is that portion of the concentration originating from $Q_L dy_1'$:

$$dC' = Q_L \phi\left(x_1, y_1, z\right) dy' \tag{A.4}$$

Now, assume a hypothetical line source along y_1-direction so that the wind is perpendicular to it. The concentration at the receptor R (x_1, y_1, z) due to this hypothetical line source can be calculated by integrating equation A.4. It is expressed as:

$$C'(x_1, y_1, z) = \int Q_L \phi(x_1, y_1, z) dy_1' \tag{A.5}$$

Since the deterministic model is based on the Gaussian plume model, which assumes the concentration distribution perpendicular to the plume axis to be Gaussian, the function ϕ in the above equation can be replaced by the generalized plume formula for an elevated point source (equation A.2):

$$\phi(x_1, y_1, z; H) = \frac{1}{2\pi\sigma_y'\sigma_z'\bar{u}} \cdot \exp\left[-\frac{1}{2}\left(\frac{y_1}{\sigma_y}\right)^2\right] \times \left[\exp\left\{-\frac{1}{2}\left(\frac{z-H}{\sigma_z'}\right)^2\right\} + \exp\left\{-\frac{1}{2}\left(\frac{z+H}{\sigma_z'}\right)^2\right\}\right] \tag{A.6}$$

where z = receptor height above ground level; H = height of line source; $\bar{u}$ = the mean ambient wind speed at source height; σ_y', σ_z' = vertical and horizontal dispersion coefficients respectively and are functions of distance x_1 and stability class. The prime ($'$) symbol indicates the parameters in the wind coordinate system.

Now, the concentration C' at R due to this hypothetical line source for perpendicular wind direction, after proper substitution of ϕ, is given by [90]:

$$C'(x_1, y_1, z; H) = \frac{Q_L}{2\pi\sigma_y'\sigma_z'\bar{u}} \cdot \left[\exp\left\{-\frac{1}{2}\left(\frac{z-H}{\sigma_z'}\right)^2\right\} + \exp\left\{-\frac{1}{2}\left(\frac{z+H}{\sigma_z'}\right)^2\right\}\right] \times \int_{-L/2}^{L/2} \exp\left[-\frac{1}{2}\left(\frac{y_1' - y_1}{\sigma_y'}\right)^2\right] dy_1'. \tag{A.7}$$

The above equation is in the wind coordinate system and the parameters which are generally not known in this coordinate system have to be transformed into forms such that they are functions of line source coordinates. The relationship between the wind coordinate system is given by:

$$x_1 = xSin\theta - yCos\theta \tag{A.8a}$$

$$y_1 = xCos\theta + ySin\theta. \tag{A.8b}$$

Since the line source is along the y-axis,

$$dy_1' = \mathrm{Sin}\,\theta\, dy' \tag{A.8c}$$

Q_L is the emission rate per unit length in the wind coordinate system; hence in the line source coordinate system it would be $Q_L/\mathrm{Sin}\theta$ due to transformation of the length unit. So the apparent source strength Q_L is amplified by the factor $1/\mathrm{Sin}\theta$ because of obliquity of the source.

Substituting the values of y_1, y_1', x_1 and dy_1' together with the source strength correction in equation A.7, the following equation is obtained:

$$C(x_1, y_1, z; H) = \frac{Q_L}{2\pi\sigma_y'\sigma_z'\bar{u}\,\mathrm{Sin}\,\theta} \cdot \left[\exp\left\{ -\frac{1}{2}\left(\frac{z-H}{\sigma_z} \right)^2 \right\} + \exp\left\{ -\frac{1}{2}\left(\frac{z+H}{\sigma_z} \right)^2 \right\} \right] \times \int_{-L/2}^{L/2} \exp\left[\left(\frac{(y_1'\mathrm{Sin}\,\theta - x\mathrm{Cos}\,\theta - y\mathrm{Sin}\,\theta)^2}{2\sigma_y^2} \right) \right] \mathrm{Sin}\,\theta\, dy_1'. \tag{A.9}$$

Here, σ_y and σ_z are functions of downwind distance (given by $x/\mathrm{Sin}\theta$) and stability class. From the definition and properties of the *error function (one sided normal cumulative distribution function),*

$$\int_{f_1}^{f_2} \exp(-t^2)\, dt = \frac{\sqrt{\pi}}{2}\left[\mathrm{erf}(f_2) + \mathrm{erf}(-f_1) \right]. \tag{A.10}$$

Hence equation A.9 becomes:

$$C(x_1, y_1, z; H) = \frac{Q_L}{2\sqrt{2}\,\pi\,\sigma'_y\,\sigma'_z\,\bar{u}\,\mathrm{Sin}\,\theta} \times \left[\exp\left\{-\frac{1}{2}\left(\frac{z-H}{\sigma_z}\right)^2\right\} + \exp\left\{-\frac{1}{2}\left(\frac{z+H}{\sigma_z}\right)^2\right\}\right] \times \left[\mathrm{erf}\left\{\frac{\mathrm{Sin}\,\theta\left(L/2 - y\right) - x\mathrm{Cos}\,\theta}{\sqrt{2}\,\sigma_y}\right\} + \mathrm{erf}\left\{\frac{\mathrm{Sin}\,\theta\left(L/2 + y\right) + x\mathrm{Cos}\,\theta}{\sqrt{2}\,\sigma_y}\right\}\right]. \quad \text{(A.11)}$$

The source height and $\bar{u}\mathrm{Sin}\theta$ in the above equation are replaced by h_o (= H + H_p) and effective wind speed $\bar{u}_e (= \bar{u}\mathrm{Sin}\theta + u_o)$ respectively, where H_p is the plume rise and u_o is the wind correction due to vehicle wake as described below. The arguments of the error function should be positive, hence the final form of the GFLS model is as follows:

$$C(x_1, y_1, z; h_o) = \frac{Q_L}{2\sqrt{2}\,\pi\sigma_z\,\bar{u}_e} \times \left[\exp\left\{-\frac{1}{2}\left(\frac{z-h_0}{\sigma_z}\right)^2\right\} + \exp\left\{-\frac{1}{2}\left(\frac{z+h_0}{\sigma_z}\right)^2\right\}\right] \times \left[\mathrm{erf}\left\{\left|\frac{\mathrm{Sin}\,\theta\left(L/2 - y\right) - x\mathrm{Cos}\,\theta}{\sqrt{2}\,\sigma_y}\right|\right\} + \mathrm{erf}\left\{\left|\frac{\mathrm{Sin}\,\theta\left(L/2 + y\right) + x\mathrm{Cos}\,\theta}{\sqrt{2}\,\sigma_y}\right|\right\}\right]. \quad \text{(A.12)}$$

Khare and Sharma [172] modified the GFLS equation, and found that after removing error function, the model performance improved considerably for Delhi traffic conditions. The DFLS model is expressed as follows:

$$C \frac{Q_L}{2\sqrt{2}\,\pi\sigma_z\,\bar{u}_e} \times \left[\exp\left\{-\frac{1}{2}\left(\frac{z-h_0}{\sigma_z}\right)^2\right\} + \exp\left\{-\frac{1}{2}\left(\frac{z+h_0}{\sigma_z}\right)^2\right\}\right] \quad \text{(A.13)}$$

The above model avoids the point source assumption, but satisfies the finite line source approach of GM model [121]. Further, the above equation specifies one dispersion parameter as a function of wind-road orientation angle and distance from the source.

A.4 DFLS Model Inputs

A.4.1 Source Strength (Q_L)

Source strength depends on the volume of traffic using the road, its composition and the operating mode of vehicles. Emission factor listed in Table 5.4 of chapter 5 have been used to estimate source strength of CO for various types of vehicle. These emission factors are developed for Indian motor vehicle driving cycles by Indian Oil Corporation, Dehradun [265].

A.4.2 Wind Speed

In Gaussian equation the pollutant concentration is inversely proportional to wind speed. The effective wind speed ($\bar{u}_e$) is assumed to be the sum of the ambient wind component ($\bar{u}$) and wind speed correction (u_o). The 'u_o' accounts for lateral dispersion caused due to traffic wake and also concentration divergence when wind speed approaches to zero (calm wind condition) or direction becomes parallel to the roadway [92]. Ideally, $\bar{u}$ is the mean wind speed at source height. However, some parameters [92] which are being used in the DFLS model formulation are based on wind speed measurements at 4.5 m height above the ground. In case of vehicles, it is difficult to measure wind speed such a small source height (≈ 0.3 m). Therefore, wind speeds at 4.5 m have been used. In general, wind speed and directions are measured at 10 m height. Hence, Power law relationship between wind speed and height has been used to get the wind speed values at 4.5 m height. The wind speed correction is dependent on the atmospheric stability conditions and is assumed to be constant for a given stability condition, which is described by Richardson number [92]. Table A.1 shows the values of the parameters used in the DFLSM. The values of u_o are all less than 1 m/s, as is expected from the fact that only a crosswind speed ≥ 1 m/s could significantly deflect the wake generated from the traffic [108].

Table A.1 Parameters used in the deterministic mathematical model (DFLSM).

Parameter	a	b	C	β	γ	α	u_1	u_o
Stable (R_i > 0.07)	1.49	0.15	0.77	5.82	3.57	20.7	0.18	0.23
Neutral (0.07 /R_i > -0.1)	1.14	0.10	0.97	3.46	3.50	11.1	0.27	0.38
Unstable ($R_i \leq$ - 0.1)	1.14	0.03	1.33	-	-	-	-	0.63

Source: [92]

A.4.3 Vertical Dispersion Coefficient

The vertical dispersion coefficient (σ_z) is directly depends on the down wind distance from the source and atmospheric stability. The σ_z of the GM model [92] has been modified by changing the down-wind distance (x) from the line source coordinate system to a wind coordinate system by incorporating an angle-dependent factor f (θ) [91]. Equation A.14 provides the estimation σ_z.

$$\sigma_Z = \left[a + b\frac{x}{\mathrm{Sin}\theta} \right]^c \tag{A.14}$$

Where a, b and c are parameters determined by non-linear least square method [92] and are dependent on the atmospheric stability conditions. However, the term 1/Sinθ in equation A.14 has a singularity at θ = 0. Therefore, if 1/Sinθ is compared with f (θ) of the GM model, then the following expression should be used in equation A.14 instead of Sinθ, for different stability conditions [91].

For unstable and neutral conditions,

$$\mathrm{Sin}\theta \rightarrow 0.2242 + 0.7758\,\mathrm{Sin}\theta \tag{A.15a}$$

For stable conditions

$$\mathrm{Sin}\theta \rightarrow 0.1466 + 0.8534\,\mathrm{Sin}\theta \tag{A.15b}$$

A.4.4 Source Height

The effective source height (h_o) is considered as sum of the height of the line source (H) and plume rise (H_p), which can be estimated as follows. However, when the cross-road wind speed is >1m/s, the effect of plume rise is negligible [108].

Consider a plume emitted from a line source into a neutral environment with finite crosswind. Then, following the approach of Slawson and Csanady [280], the conservation of mass, momentum and buoyancy can be expressed as:

$$u' \frac{dR}{dx} = \alpha W, \tag{A.16}$$

$$u' \frac{d}{dx}(RW) = Rg\delta, \tag{A.17}$$

$$u' \frac{d}{dx}(Rg\delta) = -SRW = 0, \tag{A.18}$$

where u' = cross line wind speed; W = upward motion of the plume with width R; αW = entrainment velocity of ambient air into the plume; $\delta = (\rho_o - \rho)/\rho_o$, ρ and ρ_o = densities of the plume and the ambient air respectively; g = gravitational acceleration and $S = -\frac{g}{\rho_o} \cdot \frac{\partial \rho}{\partial z} \approx \frac{g}{T_o} \frac{\partial T}{\partial z}$, which is zero under neutral conditions. Assuming u' to be a constant, the buoyancy flux $F_l = Rgu'\delta$ is then constant; with $\frac{dz}{dx} = \frac{W}{u'}$, it gives

$$z = \left(\frac{F_l}{\alpha u'^3}\right)^{1/2} x \tag{A.19}$$

where z is the height of the plume, which is a linear function of distance, in contrast to the $x^{2/3}$ behaviour of the plume rise from stack. From equation A.19, it is evident that the plume centre height becomes undefined as $u' \to 0$. However, as the traffic wake pushes the pollutant outward, an effective advection, characterized by u_l, is expected near the road even at zero ambient cross-road wind, so that $u'(= u_a + u_l)$ does not approach zero [92]. The plume under stable conditions will reach a maximum height. Using dimensional analysis, the plume height for calm conditions would be

$z_{max} = \alpha_1 F_1^{1/3} S^{-1/2}$ whereas in the windy case $z_{max} = \alpha_2 \left(F_1 / u'S \right)^{1/2}$, where $\alpha 1$ and $\alpha 2$ are constants [92]. However, in the present work the regions are located close to the downwind from the road ($\leq$ 100m), which generally tend to approach neutral stability [92], the maximum height for the purposes of present study would not be relevant. The values of α and u_1 are listed in Table A.1, the factor F_1 is determined by the heat emission rate. It can be observed from Table A.1 the values of u_1 are comparable to u_o. In other words, u' can be replaced by u.

A.4.5 Stability Class

Stability of the atmosphere directly affects the dispersion parameter in the Gaussian models, which in turn decides the ground level concentration. A mathematical representation of stability [92], based on the numerical values of Richardson's number, has been employed in the DFLSM. This method consists of three categories of stability to represent microscale atmospheric conditions, namely- stable, unstable and neutral. However, it may be pointed out here that the stability class for computing various input parameters in the DFLSM has been assumed to be *neutral*, because near roadways, stability usually tends to approach neutrality [101, 108, 120].

B Stuttgart Neural Network Simulator Software

B.1 General

Stuttgart Neural Network Simulator (SNNS) software package is developed by institute for parallel and distributed high performance systems, university of Stuttgart, Germany. This software runs under UNIX operating system. The main features of SNNS software consist of extensive recognition of the pattern loading i.e., up to five pattern files can be loaded and dynamically switched between them without reloading again, easy to train, test and visualize the neural network model. The SNNS software consists of three main components namely a simulator kernel, graphical user interface (GUI), and a compiler. The Simulator kernel operates on the internal network data structures of the neural networks and performs all the operations on them. While, the GUI, gives the graphical representation of the neural networks and controls the kernel during the simulation run. In addition, the GUI can be used to create and modify the neural network in different ways. Lastly, a compiler is used to generate large neural networks, from a high-level network description language. The SNNS software (Version 3.1), used in the development of ANN based VEE models consists of high quality learning algorithms, efficient in training, testing and visualization of neural network model. Hence, it became popular software in the scientific community. Further, this software works on number of machines i.e. Sun, DEC, IBM, HP, SGI and operating systems of SunOS, Unix, AIX, Ultrix, Linax etc.

B.2 Simulator Kernel

The SNNS software kernel is designed to accommodate many types of neural network models. The main feature of the kernel is the

M. Khare and S.M. Shiva Nagendra: *Stuttgart Neural Network Simulator Software*, Artificial Neural Networks in Vehicular Pollution Modelling (SCI) **41,** 175–184 (2007)
www.springerlink.com

complete encapsulation of all the internal data structures and the efficient memory management. Each unit (neuron) in the network model is user definable i.e., units may be introduced, removed, or their activation values changed, similarly connections among the units may be inserted, deleted or redirected.

B.2.1 Simulator Kernel Layers

The simulator kernel is internally structured into three layers. Each layer represents a higher level of abstraction.
Layer 1: The innermost layer also called as 'memory management layer' which offers allocation and de-allocation of data structures in large blocks of contiguous memory, thus enhancing the standard UNIX memory management.
Layer 2: The next layer consists of all functions to operate on, and modify the networks including propagation and learning functions.
Layer 3: The top most layer is also called 'graphical user interface layer' consists of the function that provides an interface between kernel and the X-GUI. The same layer also consists of the input/output (I/O) file interface to the network compiler.

B.2.2 Internal Data Structures

The kernel requires numerous data structures to manage and display the network. It displays both static (units, links) and dynamic (connection weights) components of the neural network model. The allocation of data structures is carried in large blocks of several hundreds of single structure components. The units and all their components are stored in the form of unit array. When the array is filed up by requests from the user interface, the memory management automatically requests a new bigger array from the operating system. The pointers to the structure components are reallocated, and the old empty array is returned to the operating system.

B.2.3 Types of Units

There are three types of units based on their function in the neural network model. The units which are connected to inputs of the neural network model are called input units and the units whose outputs

represent the output of the neural network model are called output units. The units connecting the input and output units of the model are called hidden units. Activation functions and output functions are built in SNNS software for the process of information within units. It consists of several activation functions and four output functions. Table B.1 and B.2 lists the selected activation functions and output functions built in SNNS software respectively. However, additional activation functions and output functions can be built easily by writing 'C' codes and linked with simulator kernel.

Table B.1 List of selected activation functions built in the SNNS software.

	Function	Formula
1	Identity	$a_j(t) = net_j(t) + \theta$
2	Logistic	$a_j(t) = 1/\{1+e^{-(net_j(t) + \theta)}\}$
3	StepFunc	$a_j(t) = 1$ if $net_j(t) > 0$ $a_j(t) = 0$ if $net_j(t) < 0$
4	TanH	$a_j(t) = \tanh(net_j(t) + \theta)$
5	TanH_Xdiv2	$a_j(t) = \tanh\{(net_j(t))/2\}$

Table B.2 List of output functions built in the SNNS software.

Sl. No	Function	Formula
1	Identity	$o_j(t) = a_j(t)$
2	Clip_0_1	$o_j(t) = o$; if $a_j(t)$ [0 $o_j(t) = a_j(t)$; if $a_j(t) < 1$ $o_j(t) = 1$; if $a_j(t)$ ⟨ 1
3	Clip_1_1	$o_j(t) = -1$; if $a_j(t)$ [-1 $o_j(t) = a_j(t)$; if $-1 < a_j(t) < 1$ $o_j(t) = 1$; if $a_j(t)$ ⟨ 1
4	Threshold_0.5	$o_j(t) = o$; if $a_j(t)$ [0.5 $o_j(t) = a_j(t)$; if $a_j(t) > 0.5$

Five update modes are implemented in SNNS software to compute the new activation values of the units. These are explained as follows:

(i) ***synchronous***: units change their activation all together after each step. The kernel first computes the new activation of all units from their activation functions in some arbitrary order. After all units have their new activation value assigned, the new output of the units is computed.
(ii) ***random permutation***: the units compute their new activation and output function sequentially. The order is defined randomly but each unit is selected exactly once in every step.
(iii) ***random***: the order is defined by random number generator, i.e., single unit is chosen at random and its new output is computed and propagated before any other unit is updated. In this case some unit may be updated several times, some not at all.
(iv) ***serial***: the order is defined by ascending internal unit number, units are updated according to their internal cell number.
(v) ***topological order***: the kernel first sorts the units according to their topological position and performs activity from input to output.

B.2.4 Training a Feed-Forward Neural Network Model

Training a feed forward neural network with supervised learning consists of the following procedure: an input pattern is presented to the network. The input is then propagated forward in the net until activation reaches the output layer. This is called forward propagation phase. Then, the output of the output layer is compared with the actual output value. The errors i.e. the differences between the output of the output layer and actual output are used to compute the necessary changes of the link weights. This process is called backward propagation. The above training procedure is adopted in back propagation algorithm. In the back propagation learning algorithm weights are updated using delta rule.

B.3 Graphical User Interface

GUI displays the dynamics of the neural network model simulation. The GUI of SNNS consists of the following windows, which can be positioned and controlled Independently.

(i) A manager panel with info panel, the menu bottom GUI which opens other windows, a message line, and a status information line.
(ii) Graphical display of the neural network model in two dimensions.
(iii) File browser for loading and saving network and pattern files.
(iv) A remote panel for simulation operations.
(v) A help window to display help text.
(vi) A 3D view panel to control the three dimensional network visualization component.
(vii) A Hinton diagram display window for weight matrix.
(viii) An error graph display window, to explain the network error during training
(ix) Bignet panel to generate big regular feed-forward nets, time delay, ART1, ART2 and ARTMAP networks.
(x) Cascade panel for control of the learning phase of cascade correlation learning.
(xi) Inversion display, to control the network analyzing tool.

In addition to the above windows a confirmer and shell windows are also associated with GUI: the former displays important information to the user for conforming destructive operation like change of activation function, loading of new patterns, new network model etc. While later, indicates the success or failure of the loading or saving of a file.

B.3.1 Graphical Network Editor

The graphical interface is used to generate new neural network and modify the existing neural network. Some commands also exist to change the display style of the network. Therefore, the user has a powerful set of operations like insertion, deletion, copying, moving of units. These operations may be applied to individual units or to selections of units and may effect links as well, like copy all selected units with their input links or delete all links into the selected units. These operations allow a quick and convenient use of the graphical interface of the simulator to generate the networks than to use the network compiler. The interactive graphical network editing

facilities are especially useful for networks with simple or repetitive but not completely regular topology.

B.4 Neural Network Models Supported by SNNS Software

SNNS supports wide variety of neural network models, which includes Associate Resonance Theory (ART1); Associate Resonance Theory (ART2); Associate Resonance Theory Mapping (ARTMAP); Back-propagation for batch training (BackpropBatch); Back-propagation with momentum term (BackpropMomentum); Backpercolation; Batch-Back-propagation for recurrent networks (BBPTT); Back-propagation for recurrent networks (BPTT); Cascade correlation meta algorithm (CC); Counterpropagation; LVQ algorithm with dynamic unit allocation (Dynamic-LAQ); Hebbian learning rule (Hebbian); Back-propagation for Jordan-Elman networks (JE_BP); BackpropMomentum for Jordan-Elman networks (JE_BP_Momentum); Quickprop for Jordan_Elman networks (JE_Quickprop); Rprop for Jordan_Elman networks (JE_Rprop); Kohonen self Organizing Maps (Kohonen); Quickprop; Quickprop for recurrent networks (QPTT); Radial Basis Functions (RadialBasisLearning); Cascade Correlation for recurrent networks (RCC); Rumelhart-McCelland's delta rule (RM_delta); Resilient Propagation learning (Rprop); Vinilla Back-propagation (Std_Backpropagation); Back-propagation for Time Delay Neural Networks (TimeDelayBackprop).

The back-propagation learning method proposed by Rumelhart and McClelland [84] involves the presentation of a set of pairs of input and output patterns. It first uses the input vector to produce its own output vector and then compares it with the desired output, or target vector. If there is no difference, no learning takes place. Otherwise the weights are changed to reduce the difference.

B.5 Generalized Delta Rule

To derive a generalized delta rule for multilayer neural network, a set of non-linear (similinear) activation function has been considered. A non-linear activation function is one in which the output of a neuron is non-decreasing and differentiable of the net total output. The net output value of pattern 'p' on neuron 'j' can be computed as:

$$Net_{pj} = \sum_i W_{ji}\, O_{pi} \tag{B.1}$$

where p = input patterns; $O_i = i_i$, if neuron is an input neuron; O_{pi} = i^{th} element of the actual output pattern produced by the presentation of the input pattern p; W_{ij} = weight from the i^{th} to j^{th} neurons. Thus, a non-linear activation function is one in which

$$O_{pj} = f_j\,(Net_{pj}) \tag{B.2}$$

where 'f' is differentiable and non-decreasing.

To get the correct generalization of the delta rule, set

$$\Delta_p W_{ji} \alpha - \frac{\partial E_p}{\partial W_{ji}} \tag{B.3}$$

$$where \quad E_p = \sum_j (T_{pj} - O_{pj})^2 \tag{B.4}$$

T_{pj} = target input for 'j^{th}' component of the output pattern for 'p' pattern . Using chain rule, the equation B.3 can be represented by product of two part: *first* part reflecting the change in error as a function of the change in net input to the neuron and *second* part representing the effect of changing a particular weight on the net input. Thus, it can be defined as:

$$\frac{\partial E_p}{\partial W_{ji}} = \frac{\partial E_p}{\partial Net_{pj}} \frac{\partial Net_{pj}}{\partial W_{ji}} \tag{B.5}$$

From equation B.1, the second function is represented as

$$\frac{\partial Net_{pj}}{\partial W_{ji}} = \frac{\partial}{\partial W_{ji}} \sum_k W_{jk}\ O_{pk} = O_{pi} \tag{B.6}$$

$$\delta_{pj} = \frac{\partial E_p}{\partial Net_{pj}} \tag{B.7}$$

Let us define, Equation B.5 thus has the equivalent from

$$-\frac{\partial E_p}{\partial W_{ji}} = \delta_{pj}\ O_{pi} \tag{B.8}$$

To implement gradient descent in sum square error 'E' ($=\Sigma\ E_p$), equation B.9 has been used to estimate the change in network weights.

$$\Delta_p\ W_{ji} = \eta\ \delta_{pj}\ O_{pi} \tag{B.9}$$

To compute $\delta_{pj} = -\frac{\partial E_p}{\partial Net_{pj}}$, by applying chain rule, this partial derivative becomes product of two factors. One factor reflecting the change in error as a function of the output of the neuron and one reflecting the change in the output as a function of changes in the input. Thus, let us compute the second factor. By equation B.2

$$\delta_{pj} = -\frac{\partial E_p}{\partial Net_{pj}} = -\frac{\partial E_p}{\partial O_{pj}}\ \frac{\partial O_{pj}}{\partial Net_{pj}} \tag{B.10}$$

$$\frac{\partial O_{pj}}{\partial Net_{pj}} = f_j^{'}(Net_{pj}) \tag{B.11}$$

which is simply the derivative of the squashing function f_j for the j^{th} neuron, evaluate at the net input Net_{pj} to that neuron. To compute the first factor, consider two cases. First, assume that neuron u_j is an output neuron of the network. In this case, it follows from the definition of E_p that substituting for the two factors in equation B.10. Hence it becomes, Equation D.13 is valid for any output neuron u_j. If u_j is not an output neuron, by the chain rule,

$$\frac{\partial E_p}{\partial O_{pj}} = -(T_{pj} - O_{pj}) \tag{B.12}$$

$$\delta_{pj} = (T_{pj} - O_{pj}) \quad f_j^{'}(Net_{pj}) \tag{B.13}$$

$$\sum_k \frac{\partial E_p}{\partial Net_{pk}} \frac{\partial Net_{pk}}{\partial O_{pj}} = \sum_k \frac{\partial E_p}{\partial Net_{pk}} \frac{\partial}{\partial O_{pj}} \sum_i W_{ki} O_{pi}$$

$$= \sum_k \frac{\partial E_p}{\partial Net_{pk}} W_{kj} = -\sum_k \delta_{pk} W_{kj} \tag{B.14}$$

For this case, substituting for the two factors in equation D.10 yields

$$\delta_{pj} = f_j^{'}(Net_{pj}) \quad \sum_k \delta_{pk} W_{kj} \tag{B.15}$$

Wherever u_j is not an output neuron. Equations D.13 and D.15 give a recursive procedure for computing the 'δ' for all the neurons in the network, which are then used to compute the weight changes in the network according to equation D.9. This procedure constitutes

the generalized delta rule for a feed-forward network of non-linear neurons. The above results can be summarized in three equations.

Equation 1: the weights on each line should be changed by an amount proportional to the product of an error signal, 'δ', available to the neuron receiving input along that line and the output of the neuron sending activation along that line ($\Delta_p W_{ji} = \eta \delta_{pj} O_{pi}$).

Equation 2: determines the error signal at output neurons and is given by $\delta_{pj} = (T_{pj} - O_{pj}) f_j'(Net_{pj})$, where $f_j'(\mathrm{Net_{pj}})$ is the derivative of the non-linear activation function, which maps the total input to the neuron to an output value.

Equation 3: determines the error signal in hidden neurons for which there is no specified target is determined recursively in terms of the error signals of the neuron to which it directly connects and the weights of those connections. That is $\delta_{pj} = f_j'(Net_{pk}) \sum_k \delta_{pk} W_{kj}$ where the neuron is not an output neuron.

Thus, the application of the generalized delta rule, involves two phases: during the first phase the input is presented and propagated forward through the network to compute the output value O_{pj} for each neuron. This input is then compared with the targets resulting in an error signal δ_{pj} for each neuron. The second phase involves a backward pass through the network (analogous to the initial forward pass) during which the error signal is passed to each neuron in the network and the appropriate weight changes are made. This second backward pass allows the recursive computation of 'δ' as indicated above. The first step is to compute 'δ' for each of the output neurons. This is simply the difference between the actual and desired output values. It is followed by computation of weight changes for all connections that feed into the final layer. Then δ's for all neurons in the penultimate layer are computed. This propagates the error back one layer, and the same process can be repeated for every layer.

C Development of Univariate Stochastic Vehicular Pollution Models

C.1 General

Air pollution concentrations are strongly auto-correlated. In the absence of sufficient knowledge about the structure of the causal factors, one may start by trying to determine the current value of 'Q' by using its own past behavior [53, 59]. No theoretical assumptions are required, and the character of the effect of the previous terms can be determined empirically from the available historical data. The only condition that needs to be imposed is that the series should be sufficiently long (at least 50 and preferably 100 successive observations should be used) to allow reliable empirical identification of the character [51].

C.2 Time Series Analysis

A time series is a collection of observations generated sequentially through time at a particular location [273]. The special features of a time series are that the data are ordered with respect to time, and that successive observations are usually expected to be dependent. Indeed, it is this dependence from one time period to another, which is exploited in making reliable forecasts.

Time series analysis may be broadly divided into purely statistical method applicable to non-repeatable experiments [52] and more or less complex structural models [281]. The Box-Jenkins approach is thoroughly applied to the analysis of a variety of time series from the social and economic sciences. The application to physical

M. Khare and S.M. Shiva Nagendra: *Development of Univariate Stochastic Vehicular Pollution Models*, Artificial Neural Networks in Vehicular Pollution Modelling (SCI) **41,** 185–209 (2007)
www.springerlink.com

sciences and air pollution series are also described in the literature [53, 54, 56, 281, 282, 283, 284].

C.3 Box-Jenkins Approach

The Box–Jenkins approach for the time series analysis possesses many appealing features. It allows the air quality management board, which has data on past years pollutant concentration to forecast future concentration without having to search for other time series data such as emissions, meteorology, etc. However, the Box-Jenkins approach allows the use of several time series to explain the behavior of another series. The Box-Jenkins approach consists of extracting the predictable movements from the observed historical data. The time series is decomposed into several components, called filters. The Box-Jenkins approach primarily makes use of three linear filters: the autoregressive, the integration and the moving average filter. These filters can be considered as special type of sieves, in which time series data are sifted through a series of progressively finer sieves. As the data pass through each sieve, some characteristic components of the series are filtered out. This process terminates when no additional information is available to be filtered out.

The schematic representation of ARIMA filters is shown in Figure C.1. The integration filter processes the observed data (z_t) and produces a filtered series (w_t). The autoregressive filter produces an intermediate series (e_t) and finally the moving average filter generates random noise (a_t). The objective of applying these filters is to end up with random noise, which is unpredictable.

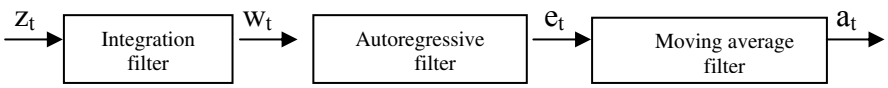

Fig. C.1. Schematic representation of ARIMA model (filters).

The nature of the different sieves and the grid sizes of the sieves are all the information required to describe the behavior of the time series. Indeed, finding the number and nature of the filters is equivalent to finding the structure, identifying the form, and constructing the model for the series. The Box-Jenkins method provides a unified approach for identifying which filters are the most appropriate for the series being analysed; for estimating the parameters describing the filters, i e. for estimating the grid size of the sieves, and for diagnosing the accuracy and reliability of the models are estimated, and finally, for forecasting.

Basically, the Box-Jenkins approach uses the concepts of autoregression and moving-average processes, where the dependent variable under study is lag-regressed on to itself and thus, giving rise to the so called autoregressive moving average (ARMA) and autoregressive integrated moving average (ARIMA) and seasonal ARIMA models [285]. These models are applicable to stationary series, where there is no systematic change in the mean values and the variance is constant over time [286, 287]. The choice of an appropriate Box-Jenkins model is not straight-forward, but require a rather elaborate procedure for identification and validation [53, 286].

C.3.1 Autoregressive Models

A time series is said to be governed by a first-order autoregressive process if the current value of the time series, z_t, can be expressed as a linear function of the previous value of the series and a random shock, a_t. Let z_{t-1} denotes the previous value of the series z_t, then autoregressive processes can be written as

$$z_t = \phi_1 \, z_{t-1} + a_t \tag{C.1}$$

where ϕ_1 is the autoregressive parameter which describes the effect of a unit change in z_{t-1} on z_t and which needs to estimated. The random shock a_t, also known as error or white noise series, is assumed to be normally and independently distributed with mean zero, constant variance σ_a^2, and independent of z_{t-1}. The term 'a_t' can also be defined as Gaussian white noise, because of normality assumption.

The equation C.1 is called as autoregressive process of order 1, AR(1).

Most air pollution time series are characterized by non-stationarity. To remove trends or the non-stationarity in the time series z_t (defined as a sequence of N observations, equidistant in time, such as z_1, z_2, z_N), the difference operators (also called the integration operators), '∇' and '∇_s', are defined as

$$\nabla z_t = z_t - z_{t-1} \qquad and \qquad \nabla_s z_t = z_t - z_{t-s} \tag{C.2}$$

where 's' denotes the period or the span, i.e. the length of the seasonal cycle. The operators may be applied 'd' and 'D' times respectively ('d' and 'D' being the order of regular and seasonal differencing respectively). To remove serial correlations in the series, two operators- autoregressive and moving average can be applied. They are expressed as polynomials of the backward shift operators, B and B^s, which are defined as

$$Bz_t = z_{t-1} \qquad and \qquad B^s z_t = z_{t-s}. \tag{C.3}$$

A p^{th} order autoregressive model AR (p) is written as:

$$z_t = \phi_1 \, z_{t-1} + \phi_2 \, z_{t-2} + - - - - - - - - - - \phi_p z_{t-p} + a_t \tag{C.4}$$

The regular and the seasonal AR operators $\phi_p(B)$ and $\Phi_P(B^s)$, are respectively polynomials of the order p in B and P in B^s, such that

$$\phi_p(B) = 1 - \phi_1 B - \phi_2 B^2 - ... - \phi_p B^p \tag{C.5.1}$$

$$and \qquad \Phi_P(B^s) = 1 - \Phi_1 B^s - \Phi_2 B^{2s} - ... - \Phi_P B^{Ps}. \tag{C.5.2}$$

C.3.2 Moving Average Models

The first order moving average model can be expressed as the current value of the series z_t and as a linear function of the current and previous errors or shocks, a_t and a_{t-1}. Mathematically, a first order moving average model MA (1) can be expressed as

$$z_t = a_t - \theta_1 \, a_{t-1} \tag{C.6}$$

where θ_1 is the moving average parameter. As with an autoregressive process, the random shock a_t, in a moving average process is assumed to be normally and independently distributed with its mean zero, and having constant variance σ_a^2. In moving average model, it is very unrealistic to think that an event that has occurred many years ago has more influence on today's situations than an event that is occurred recently. Therefore, θ_1 must restrict to satisfy $|\theta_1| < 1$. This condition is called the invertability condition of an MA (1) model [51]. The above MA (1) process in equation (C.6) can easily be extended to include additional lagged residual terms. The q^{th} order MA process, MA (q) for instance, can be expressed as:

$$z_t = a_t - \theta_1 \, a_{t-1} - \theta_2 \, a_{t-2} - \quad -.----\theta_q \, a_{t-q} \tag{C.7}$$

The regular and seasonal moving average operators are similarly defined as:

$$\theta_q(B) = 1 - \theta_1 B - \theta_2 B^2 - \ldots - \theta_q B^q \tag{C.8.1}$$

and $$\Theta_Q(B^s) = 1 - \Theta_1 B^s - \Theta_2 B^{2s} - \ldots - \Theta_Q B^{Qs} \tag{C.8.2}$$

The moving average operators express the current values of the data as a finite sum of the current and past values of the shock or random noise, a_t.

C.3.3 Mixed Autoregressive and Moving Average Models

To achieve greater flexibility of the actual time series, it is sometime advantageous to include both autoregressive and moving average terms in the model. This leads to the mixed autoregressive – moving average model (ARMA model). The general ARMA (p, q) model is given as:

$$z_t = \phi_1 z_{t-1} + \phi_2 z_{t-2} + - \quad - \phi_p z_{t-p} + a_t \quad - - \theta_1 a_{t-1} - \theta_2 a_{t-2} - - - - \theta_q a_{t-q} \qquad \text{(C.9)}$$

C.3.4 Autoregressive Integrated Moving Average Models

ARIMA models are also called as non-stationary models. Many series actually exhibit non-stationary behavior and in particular, do not vary about a fixed mean. The first difference of the series $z_t - z_{t-1}$, constitutes a stationary series. The general autoregressive integrated moving average (ARIMA) model of the order (p, d, q) is expressed as:

$$z_t = \phi_1 w_{t-1} + \phi_2 w_{t-2} + - \quad - \phi_p w_{t-p} + a_t \quad - - \theta_1 a_{t-1} - \theta_2 a_{t-2} - - - - \theta_q a_{t-q} \qquad \text{(C.10)}$$

where, $w_t = z_t - z_{t-1}$

C.4 The Box-Jenkins Univariate Modelling Approach

The application of a general class of forecasting methods involves two basic steps. The first step is to analyze the historical data series and the second, is the selection of the forecast model that fits the data [288]. These two steps are incorporated in ARIMA models and are used extensively in time series analysis. Box-Jenkins models are applicable to stationary series, where there is no systematic change in the mean values and the variance is constant over time [286]. The presence of any trends in time series data result in positive autocorrelation, i.e. the autocorrelation of stationary data drop to zero after second or third time lag, while for a non-stationary series it is significantly different from zero even for several time lags. Therefore, Box-Jenkins approach assumes stationary time series [289]. The choice of an appropriate Box-Jenkins model is not straightforward, but requires a rather elaborate procedure for identification and

validation [53, 286]. More details on B-J modeling technique can be found in Box and Jenkins [50, 51] and Khare and Sharma [59].

A univariate time series model is one, which uses only current and past data on one variable. The general class of univariate B-J seasonal models, denoted by ARIMA $_{(p, d, q)\times(P, D, Q)s}$ can be expressed as [51]:

$$\phi_p(B)\Phi_P\left(B^s\right)\nabla_s^D\nabla^d z_t = \theta_q(B)\,\Theta_Q\left(B^s\right)a_t + c. \tag{C.11}$$

Where ϕ and Φ = regular and seasonal autoregressive parameters, B = backward shift operators, ∇ = difference operators, d and D = order of regular and seasonal differencing, s = period/span, z_t = observed data series, θ and = regular and seasonal moving average parameters, a_t = random noise, p, P, q and Q represent the order of the model and c = constant.

A time series model which makes explicit use of other variables to describe the behavior of the desired series is called a multiple time series model or multivariate time series model [51, 59]. The multivariate time series model, expressing the dynamic relationship among different variables, is called a transfer function model. A transfer function model is related to the standard regression model, in that, both have a dependent variable and one or more explanatory variables [273].

The univariate modelling procedure involves mainly three steps in the proper construction of time series model. These include model identification, parameter estimation and model evaluation (diagnostic checking). More details can be found in Khare and Sharma [59], Box et al. [50], Vandaele [273], Chatfield [286], Kendall and Ord [287] and Hipel and Mcleod [290].

C.5 Development of 1-hr Average Univariate CO Models

Figure C.2 shows the 1-hour CO time series at AQCR1 (x_1-series). A visual inspection of the figures reveals that, when the local average of the concentration is relatively high (during peak hour traffic and inversion conditions), the hourly variability is also high. On the

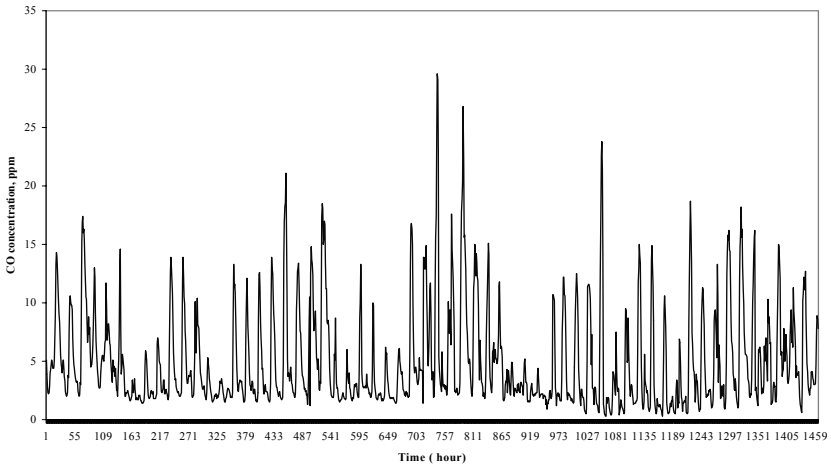

Fig. C.2. Plot of X_1 series.

other hand, whenever the local average of the concentration is also low (during trickle traffic flow), the hourly variability is also low. Therefore, variance non-stationarity seems to be present in the series. Variance non-stationarity in the time series is a situation, which corresponds to heteroscedasticity in the regression terminology [59]. However, in order for an ARIMA model to be fitted in a time series, the series must be stationary in variance [289]. Unfortunately, there is no adequate formal test to check for variance non-stationarity [291]. One practical way, to test for variance non-stationarity, in cases, where the standard deviation or the variance seems to be proportional to the local mean of the series, divide the series into interval of equal 'length', and find the mean and the corresponding standard deviation or variance of each segment. If the local mean is found to be proportional to the local standard deviation, the variance stabilizing transformation is logarithmic one. If the local mean is found to be proportional to the local variance, the variance stabilizing transformation is the square root transformation [292]. This practice was followed for x_1-series by splitting it into fifty segments, each having 24 observations. The local mean was regressed against the local standard deviation, as well as against the local variances. Both cases show statistically significant coefficients, but the case using the local standard deviation is having a much better fit. Hence,

the log-transformation is used to stabilize the variance. The log-transformed x_1-series of the AQCR1 is denoted by log x_1.

The four standard stages of the model building strategy, namely identification, estimation, diagnosis and metadiagnosis, are followed.

The plots of autocorrelation (ACF) and partial autocorrelation (PACF) functions for the log x_1 series are shown in Figures C.3(a) and (b) respectively for AQCR1. The characteristics of these plots indicate that the series is non-stationary and needs to be differenced. The plots of ACF and PACF of the differenced series are shown in Figures C.4(a) and (b) respectively. In both the ACF and PACF plots, there are significant correlations at several lags, but a specific model is not immediately distinguishable. Many tentative models are tested, and several of them are adequate. Metadiagnosis showed that the best model is an ARIMA $(1,1,1)x(0,1,1)_{24}$ for AQCR1.

The next step is that of parameter estimation which, is done by using the modified Marquardt [293] non-linear optimization iterative scheme. Table C.1 gives the final estimates of the parameters with corresponding standard deviation and 't' ratio, which is indicative of the statistical significance of the model parameters ($|\text{t-ratio}| \geq 2.0$). Figures C.5(a) and (b) show the plots of the ACF and PACF of the residuals of the univariate model for log x_1 series. There are no significant correlations in the residual ACF and PACF. The plots of the residuals are shown in Figure C.6. Portmanteau or modified Box-Pierce i.e., Q-statistic is performed at 12, 24 and 36 lags. Both the tests indicate that the residuals can be considered as white noise. Further, stationarity, invertability tests and the statistical significance of the model parameters are examined and it indicated that all the model requirements are satisfied. Finally, metadiagnosis shows that the best model is an ARIMA $(1,1,1) \times (0,1,1)_{24}$ model with the parameter as shown in Table C.1 for AQCR1.

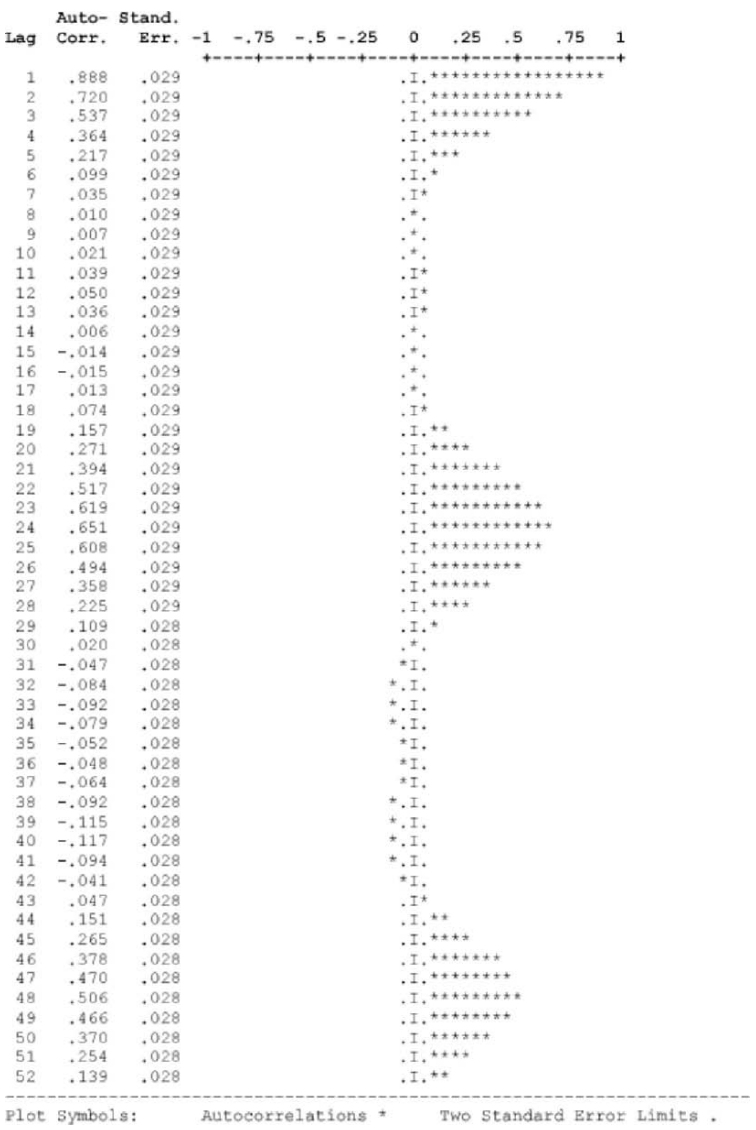

Lag	Auto-Corr.	Stand. Err.	-1 -.75 -.5 -.25 0 .25 .5 .75 1
1	.888	.029	.I.******************
2	.720	.029	.I.*************
3	.537	.029	.I.**********
4	.364	.029	.I.******
5	.217	.029	.I.***
6	.099	.029	.I.*
7	.035	.029	.I*
8	.010	.029	.*.
9	.007	.029	.*.
10	.021	.029	.*.
11	.039	.029	.I*
12	.050	.029	.I*
13	.036	.029	.I*
14	.006	.029	.*.
15	-.014	.029	.*.
16	-.015	.029	.*.
17	.013	.029	.*.
18	.074	.029	.I*
19	.157	.029	.I.**
20	.271	.029	.I.****
21	.394	.029	.I.*******
22	.517	.029	.I.*********
23	.619	.029	.I.***********
24	.651	.029	.I.************
25	.608	.029	.I.***********
26	.494	.029	.I.*********
27	.358	.029	.I.******
28	.225	.029	.I.****
29	.109	.028	.I.*
30	.020	.028	.*.
31	-.047	.028	*I.
32	-.084	.028	*.I.
33	-.092	.028	*.I.
34	-.079	.028	*.I.
35	-.052	.028	*I.
36	-.048	.028	*I.
37	-.064	.028	*I.
38	-.092	.028	*.I.
39	-.115	.028	*.I.
40	-.117	.028	*.I.
41	-.094	.028	*.I.
42	-.041	.028	*I.
43	.047	.028	.I*
44	.151	.028	.I.**
45	.265	.028	.I.****
46	.378	.028	.I.*******
47	.470	.028	.I.********
48	.506	.028	.I.*********
49	.466	.028	.I.********
50	.370	.028	.I.******
51	.254	.028	.I.****
52	.139	.028	.I.**

Plot Symbols: Autocorrelations * Two Standard Error Limits .

Fig. C.3a. Plot of the ACF of log x1 series. The vertical dot lines represent the 95 % confidence intervals (0.058).

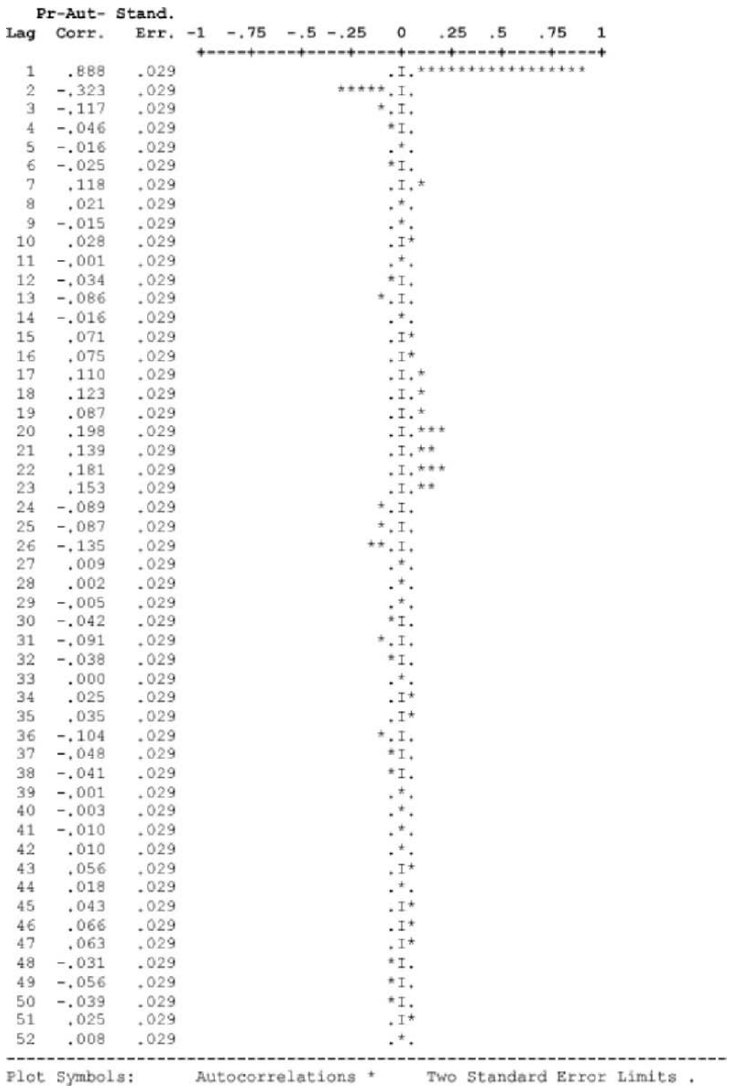

```
   Pr-Aut- Stand.
Lag  Corr.   Err. -1  -.75  -.5 -.25   0   .25  .5   .75   1
                  +----+----+----+----+----+----+----+----+
  1   .888   .029                     .I.****************
  2  -.323   .029                *****.I.
  3  -.117   .029                    *.I.
  4  -.046   .029                     *I.
  5  -.016   .029                     .*.
  6  -.025   .029                     *I.
  7   .118   .029                     .I.*
  8   .021   .029                     .*.
  9  -.015   .029                     .*.
 10   .028   .029                     .I*
 11  -.001   .029                     .*.
 12  -.034   .029                     *I.
 13  -.086   .029                    *.I.
 14  -.016   .029                     .*.
 15   .071   .029                     .I*
 16   .075   .029                     .I*
 17   .110   .029                     .I.*
 18   .123   .029                     .I.*
 19   .087   .029                     .I.*
 20   .198   .029                     .I.***
 21   .139   .029                     .I.**
 22   .181   .029                     .I.***
 23   .153   .029                     .I.**
 24  -.089   .029                    *.I.
 25  -.087   .029                    *.I.
 26  -.135   .029                   **.I.
 27   .009   .029                     .*.
 28   .002   .029                     .*.
 29  -.005   .029                     .*.
 30  -.042   .029                     *I.
 31  -.091   .029                    *.I.
 32  -.038   .029                     *I.
 33   .000   .029                     .*.
 34   .025   .029                     .I*
 35   .035   .029                     .I*
 36  -.104   .029                    *.I.
 37  -.048   .029                     *I.
 38  -.041   .029                     *I.
 39  -.001   .029                     .*.
 40  -.003   .029                     .*.
 41  -.010   .029                     .*.
 42   .010   .029                     .*.
 43   .056   .029                     .I*
 44   .018   .029                     .*.
 45   .043   .029                     .I*
 46   .066   .029                     .I*
 47   .063   .029                     .I*
 48  -.031   .029                     *I.
 49  -.056   .029                     *I.
 50  -.039   .029                     *I.
 51   .025   .029                     .I*
 52   .008   .029                     .*.
------------------------------------------------------------------------
Plot Symbols:      Autocorrelations *     Two Standard Error Limits .
```

Fig. C.3b. Plot of the PACF of log x1 series. The vertical dot lines represent the 95 % confidence intervals (0.058).

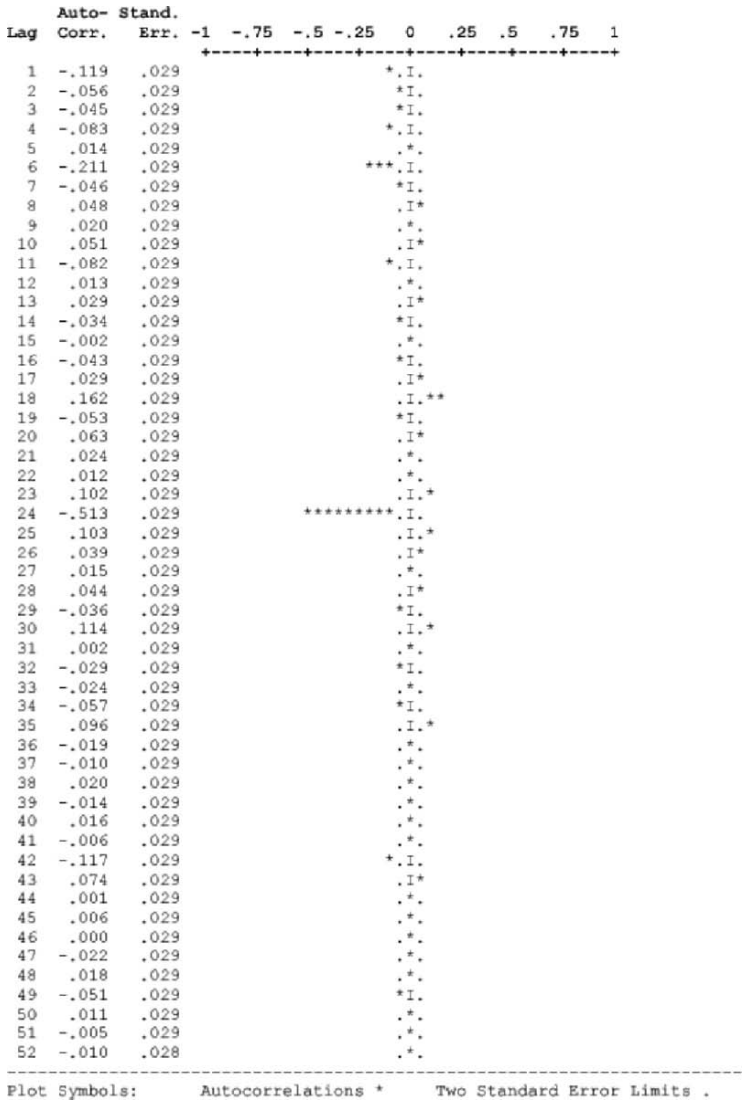

Lag	Auto-Corr.	Stand. Err.	-1 -.75 -.5 -.25 0 .25 .5 .75 1
1	-.119	.029	*.I.
2	-.056	.029	*I.
3	-.045	.029	*I.
4	-.083	.029	*.I.
5	.014	.029	.*.
6	-.211	.029	***.I.
7	-.046	.029	*I.
8	.048	.029	.I*
9	.020	.029	.*.
10	.051	.029	.I*
11	-.082	.029	*.I.
12	.013	.029	.*.
13	.029	.029	.I*
14	-.034	.029	*I.
15	-.002	.029	.*.
16	-.043	.029	*I.
17	.029	.029	.I*
18	.162	.029	.I.**
19	-.053	.029	*I.
20	.063	.029	.I*
21	.024	.029	.*.
22	.012	.029	.*.
23	.102	.029	.I.*
24	-.513	.029	*********.I.
25	.103	.029	.I.*
26	.039	.029	.I*
27	.015	.029	.*.
28	.044	.029	.I*
29	-.036	.029	*I.
30	.114	.029	.I.*
31	.002	.029	.*.
32	-.029	.029	*I.
33	-.024	.029	.*.
34	-.057	.029	*I.
35	.096	.029	.I.*
36	-.019	.029	.*.
37	-.010	.029	.*.
38	.020	.029	.*.
39	-.014	.029	.*.
40	.016	.029	.*.
41	-.006	.029	.*.
42	-.117	.029	*.I.
43	.074	.029	.I*
44	.001	.029	.*.
45	.006	.029	.*.
46	.000	.029	.*.
47	-.022	.029	.*.
48	.018	.029	.*.
49	-.051	.029	*I.
50	.011	.029	.*.
51	-.005	.029	.*.
52	-.010	.028	.*.

Plot Symbols: Autocorrelations * Two Standard Error Limits .

Fig. C.4a. Plot of the ACF of the differenced log x1 series. The vertical dot lines represent the 95 % confidence intervals (0.058).

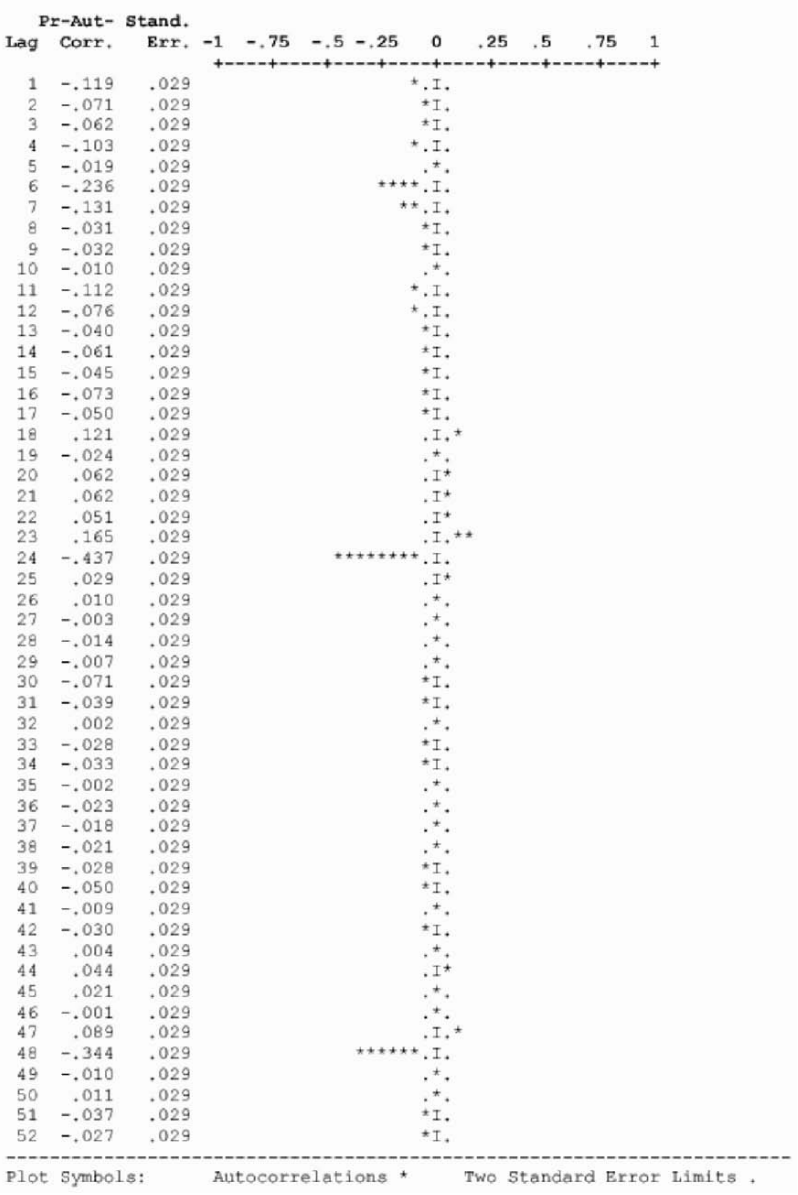

Lag	Pr-Aut-Corr.	Stand. Err.	-1 -.75 -.5 -.25 0 .25 .5 .75 1
1	-.119	.029	*.I.
2	-.071	.029	*I.
3	-.062	.029	*I.
4	-.103	.029	*.I.
5	-.019	.029	.*.
6	-.236	.029	****.I.
7	-.131	.029	**.I.
8	-.031	.029	*I.
9	-.032	.029	*I.
10	-.010	.029	.*.
11	-.112	.029	*.I.
12	-.076	.029	*.I.
13	-.040	.029	*I.
14	-.061	.029	*I.
15	-.045	.029	*I.
16	-.073	.029	*I.
17	-.050	.029	*I.
18	.121	.029	.I.*
19	-.024	.029	.*.
20	.062	.029	.I*
21	.062	.029	.I*
22	.051	.029	.I*
23	.165	.029	.I.**
24	-.437	.029	********.I.
25	.029	.029	.I*
26	.010	.029	.*.
27	-.003	.029	.*.
28	-.014	.029	.*.
29	-.007	.029	.*.
30	-.071	.029	*I.
31	-.039	.029	*I.
32	.002	.029	.*.
33	-.028	.029	*I.
34	-.033	.029	*I.
35	-.002	.029	.*.
36	-.023	.029	.*.
37	-.018	.029	.*.
38	-.021	.029	.*.
39	-.028	.029	*I.
40	-.050	.029	*I.
41	-.009	.029	.*.
42	-.030	.029	*I.
43	.004	.029	.*.
44	.044	.029	.I*
45	.021	.029	.*.
46	-.001	.029	.*.
47	.089	.029	.I.*
48	-.344	.029	******.I.
49	-.010	.029	.*.
50	.011	.029	.*.
51	-.037	.029	*I.
52	-.027	.029	*I.

Plot Symbols: Autocorrelations * Two Standard Error Limits .

Fig. C.4b. Plot of the PACF of the differenced log x1 series. The vertical dot lines represent the 95 % confidence intervals (0.058).

Table C.1 Final estimates of parameters for the log x_1 series ARIMA model at AQCR1.

Model	Parameter	Estimate	Standard deviation	t-ratio
ARIMA $(1,1,1) \times (0,1,1)_{24}$	ϕ_1	0.8153	0.0219	37.21
	θ_1	0.8742	0.0119	73.46
	Θ_1	0.9234	0.0177	52.17

Thus the final form of the model for AQCR1 is given in equation C.12.

$$(1-\phi_1 B)\ \nabla\nabla^{24} x_{1t} = (1-\theta_1 B)\left(1-\Theta B^{24}\right) a_t \qquad \text{(C.12a)}$$

$$x_{1t} = \frac{(1-\theta_1 B)\left(1-\Theta B^{24}\right) a_t}{(1-\phi_1 B)\ \nabla\nabla^{24}} \qquad \text{(C.12b)}$$

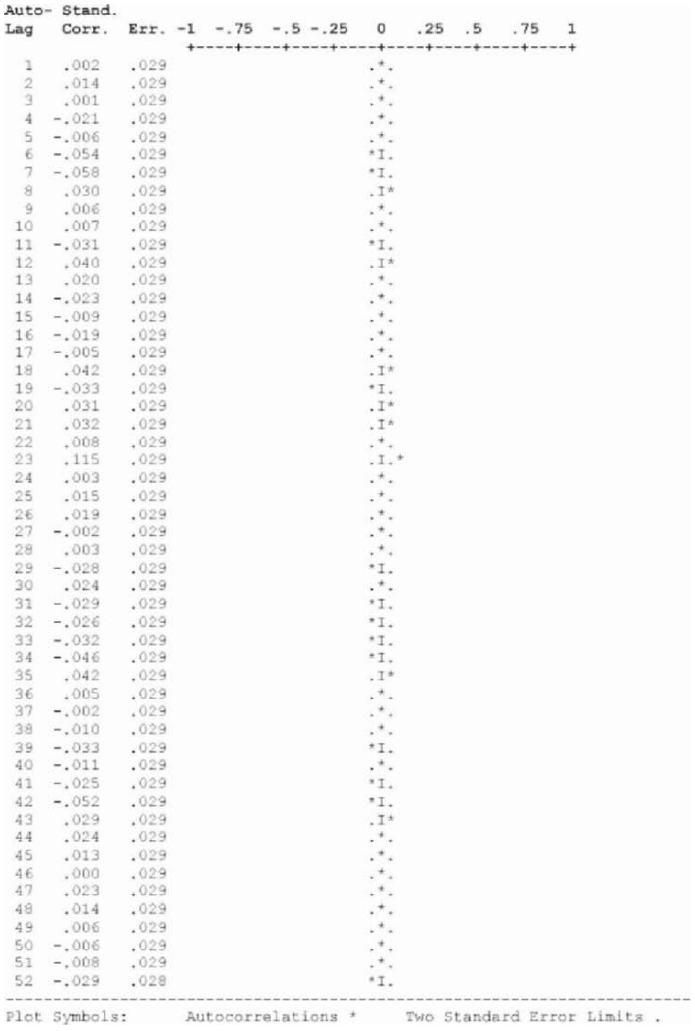

Auto- Lag	Stand. Corr.	Err.	-1 -.75 -.5 -.25 0 .25 .5 .75 1
1	.002	.029	.*.
2	.014	.029	.*.
3	.001	.029	.*.
4	-.021	.029	.*.
5	-.006	.029	.*.
6	-.054	.029	*I.
7	-.058	.029	*I.
8	.030	.029	.I*
9	.006	.029	.*.
10	.007	.029	.*.
11	-.031	.029	*I.
12	.040	.029	.I*
13	.020	.029	.*.
14	-.023	.029	.*.
15	-.009	.029	.*.
16	-.019	.029	.*.
17	-.005	.029	.*.
18	.042	.029	.I*
19	-.033	.029	*I.
20	.031	.029	.I*
21	.032	.029	.I*
22	.008	.029	.*.
23	.115	.029	.I.*
24	.003	.029	.*.
25	.015	.029	.*.
26	.019	.029	.*.
27	-.002	.029	.*.
28	.003	.029	.*.
29	-.028	.029	*I.
30	.024	.029	.*.
31	-.029	.029	*I.
32	-.026	.029	*I.
33	-.032	.029	*I.
34	-.046	.029	*I.
35	.042	.029	.I*
36	.005	.029	.*.
37	-.002	.029	.*.
38	-.010	.029	.*.
39	-.033	.029	*I.
40	-.011	.029	.*.
41	-.025	.029	*I.
42	-.052	.029	*I.
43	.029	.029	.I*
44	.024	.029	.*.
45	.013	.029	.*.
46	.000	.029	.*.
47	.023	.029	.*.
48	.014	.029	.*.
49	.006	.029	.*.
50	-.006	.029	.*.
51	-.008	.029	.*.
52	-.029	.028	*I.

Plot Symbols: Autocorrelations * Two Standard Error Limits .

Fig. C.5a. Plot of the ACF of the residuals of the univariate model for the log x1 series at AQCR1. The vertical dot lines represent the 95 % confidence intervals (0.058).

Lag	Pr-Aut-Corr.	Stand. Err.	-1 -.75 -.5 -.25 0 .25 .5 .75 1
1	.002	.029	.*.
2	.009	.029	.*.
3	.000	.029	.*.
4	-.021	.029	.*.
5	-.003	.029	.*.
6	-.054	.029	*I.
7	-.037	.029	*I.
8	.041	.029	.I*
9	.002	.029	.*.
10	-.001	.029	.*.
11	-.034	.029	*I.
12	.023	.029	.*.
13	.003	.029	.*.
14	-.017	.029	.*.
15	-.003	.029	.*.
16	-.017	.029	.*.
17	-.013	.029	.*.
18	.050	.029	.I*
19	-.031	.029	*I.
20	.027	.029	.I*
21	.020	.029	.*.
22	-.001	.029	.*.
23	.113	.029	.I.*
24	.002	.029	.*.
25	.013	.029	.*.
26	.018	.029	.*.
27	.014	.029	.*.
28	.004	.029	.*.
29	.015	.029	.*.
30	.036	.029	.I*
31	-.003	.029	.*.
32	-.010	.029	.*.
33	-.040	.029	*I.
34	-.034	.029	*I.
35	.044	.029	.I*
36	.009	.029	.*.
37	-.006	.029	.*.
38	-.030	.029	*I.
39	-.038	.029	*I.
40	-.027	.029	*I.
41	-.020	.029	.*.
42	-.039	.029	*I.
43	.005	.029	.*.
44	.009	.029	.*.
45	-.019	.029	.*.
46	-.028	.029	*I.
47	.014	.029	.*.
48	-.046	.029	*I.
49	.006	.029	.*.
50	-.014	.029	.*.
51	-.005	.029	.*.
52	-.028	.029	*I.

Plot Symbols: Autocorrelations * Two Standard Error Limits .

Fig. C.5b. Plot of the PACF of the residuals of the univariate model for the log x1 series at AQCR1. The vertical dot lines represent the 95 % confidence intervals (0.058).

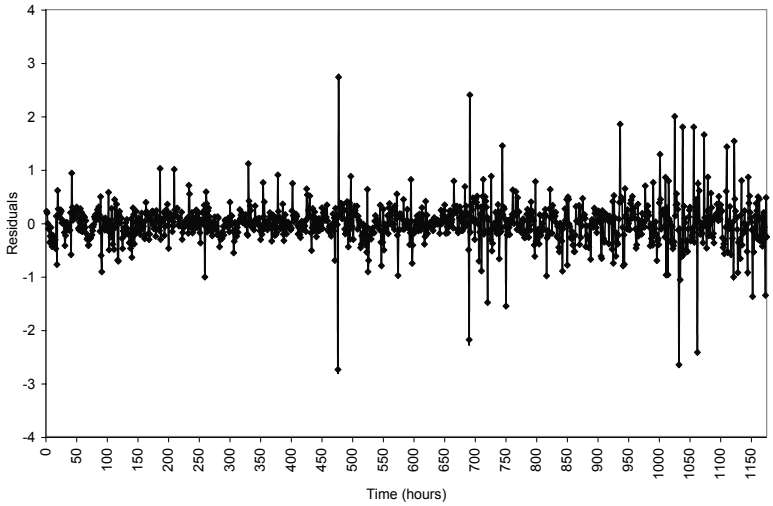

Fig. C.6. Plot of the residuals from the univariate model for log x1 series at AQCR1.

The plot of x_2 series for AQCR2 is shown in Figure C.7. Logarithmic transformation is done to stabilize the variance.

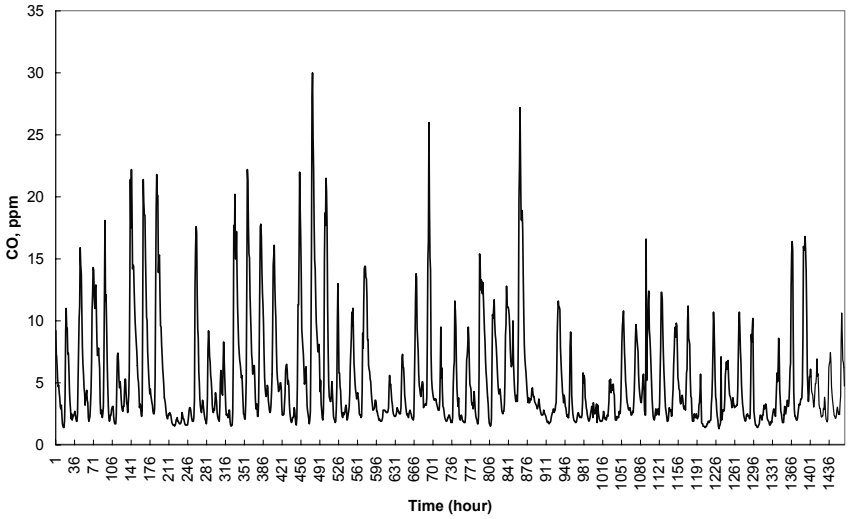

Fig. C.7. Plot of x2 series.

The plots of ACF and PACF for the x_2 series are shown in Figures C.8 (a) and (b) respectively that are indicative of the presence of variance non-stationary in the series and hence differencing is needed. Figures C.9 (a) and (b) show the ACF and PACF of differenced series respectively. The characteristics of the plots suggest an ARIMA $(1,1,0)x(0,1,1)_{24}$ model. The model parameters are estimated similar to x_1 series ARIMA model as described in previous section. Table C.2 shows the final estimates of the model parameters with standard deviation and t-ratio. Figures C.10 (a) and (b) show the plots of ACF and PACF of the residual series. The plot of the residuals from the model is shown in Figure C.11. The plots along with the portmanteau test indicate the residuals as 'white noise' series. The model is further checked for invertability and stationarity and found to satisfy all model fit requirements. Finally, the metadiagnosis also shows that ARIMA $(1,1,0)x(0,1,1)_{24}$ with model parameter shown in Table C.2 is the best suited model for the x_2 series. Thus the final form of the model for AQCR2 is given in equation 8.13.

$$(1-\phi_1 B)\ \nabla\nabla^{24} x_{2t} = \left(1-\Theta B^{24}\right) a_t \tag{18.13a}$$

$$x_{2t} = \frac{\left(1-\Theta B^{24}\right) a_t}{(1-\phi_1 B)\ \nabla\nabla^{24}} \tag{18.13b}$$

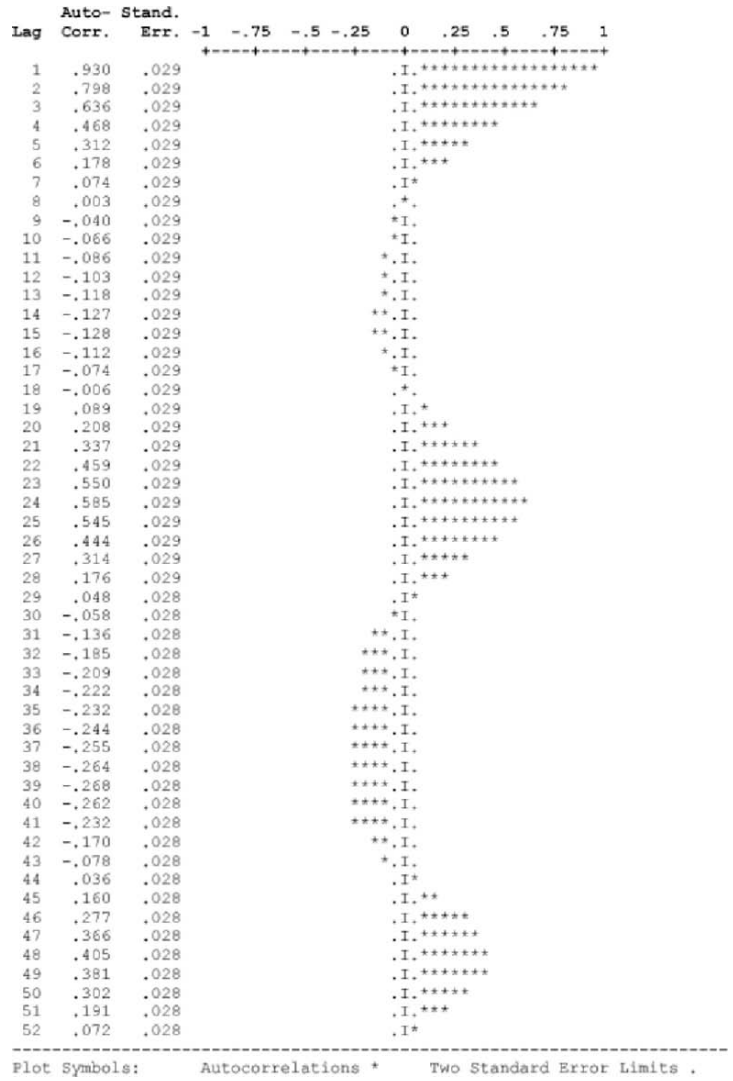

Lag	Auto-Corr.	Stand. Err.	-1 -.75 -.5 -.25 0 .25 .5 .75 1
1	.930	.029	.I.******************
2	.798	.029	.I.****************
3	.636	.029	.I.************
4	.468	.029	.I.********
5	.312	.029	.I.*****
6	.178	.029	.I.***
7	.074	.029	.I*
8	.003	.029	.*.
9	-.040	.029	*I.
10	-.066	.029	*I.
11	-.086	.029	*.I.
12	-.103	.029	*.I.
13	-.118	.029	*.I.
14	-.127	.029	**.I.
15	-.128	.029	**.I.
16	-.112	.029	*.I.
17	-.074	.029	*I.
18	-.006	.029	.*.
19	.089	.029	.I.*
20	.208	.029	.I.***
21	.337	.029	.I.******
22	.459	.029	.I.********
23	.550	.029	.I.**********
24	.585	.029	.I.***********
25	.545	.029	.I.**********
26	.444	.029	.I.********
27	.314	.029	.I.*****
28	.176	.029	.I.***
29	.048	.028	.I*
30	-.058	.028	*I.
31	-.136	.028	**.I.
32	-.185	.028	***.I.
33	-.209	.028	***.I.
34	-.222	.028	***.I.
35	-.232	.028	****.I.
36	-.244	.028	****.I.
37	-.255	.028	****.I.
38	-.264	.028	****.I.
39	-.268	.028	****.I.
40	-.262	.028	****.I.
41	-.232	.028	****.I.
42	-.170	.028	**.I.
43	-.078	.028	*.I.
44	.036	.028	.I*
45	.160	.028	.I.**
46	.277	.028	.I.*****
47	.366	.028	.I.******
48	.405	.028	.I.*******
49	.381	.028	.I.*******
50	.302	.028	.I.*****
51	.191	.028	.I.***
52	.072	.028	.I*

Plot Symbols: Autocorrelations * Two Standard Error Limits .

Fig. C.8a. Plot of ACF of the log x2 series. The vertical dot lines represent the 95 % confidence intervals (0.058).

Lag	Pr-Aut-Corr.	Stand. Err.	-1 -.75 -.5 -.25 0 .25 .5 .75 1
1	.930	.029	.I.******************
2	-.498	.029	*********.I.
3	-.130	.029	**.I.
4	-.022	.029	.*.
5	-.021	.029	.*.
6	.004	.029	.*.
7	.026	.029	.I*
8	.032	.029	.I*
9	-.014	.029	.*.
10	-.045	.029	*I.
11	-.082	.029	*.I.
12	-.012	.029	.*.
13	.001	.029	.*.
14	.019	.029	.*.
15	.025	.029	.*.
16	.091	.029	.I.*
17	.104	.029	.I.*
18	.147	.029	.I.**
19	.134	.029	.I.**
20	.178	.029	.I.***
21	.118	.029	.I.*
22	.068	.029	.I*
23	-.024	.029	.*.
24	-.172	.029	**.I.
25	-.283	.029	*****.I.
26	-.119	.029	*.I.
27	.004	.029	.*.
28	.008	.029	.*.
29	.007	.029	.*.
30	.024	.029	.*.
31	-.004	.029	.*.
32	-.005	.029	.*.
33	-.008	.029	.*.
34	-.029	.029	*I.
35	-.034	.029	*I.
36	-.008	.029	.*.
37	.009	.029	.*.
38	-.018	.029	.*.
39	-.051	.029	*I.
40	-.029	.029	*I.
41	.056	.029	.I*
42	.057	.029	.I*
43	.034	.029	.I*
44	.013	.029	.*.
45	.031	.029	.I*
46	.022	.029	.*.
47	-.006	.029	.*.
48	-.055	.029	*I.
49	-.055	.029	*I.
50	-.071	.029	*I.
51	-.005	.029	.*.
52	.009	.029	.*.

Plot Symbols: Autocorrelations * Two Standard Error Limits .

Fig. C.8b. Plot of PACF of the log x2 series. The vertical dot lines represent the 95 % confidence intervals (0.058).

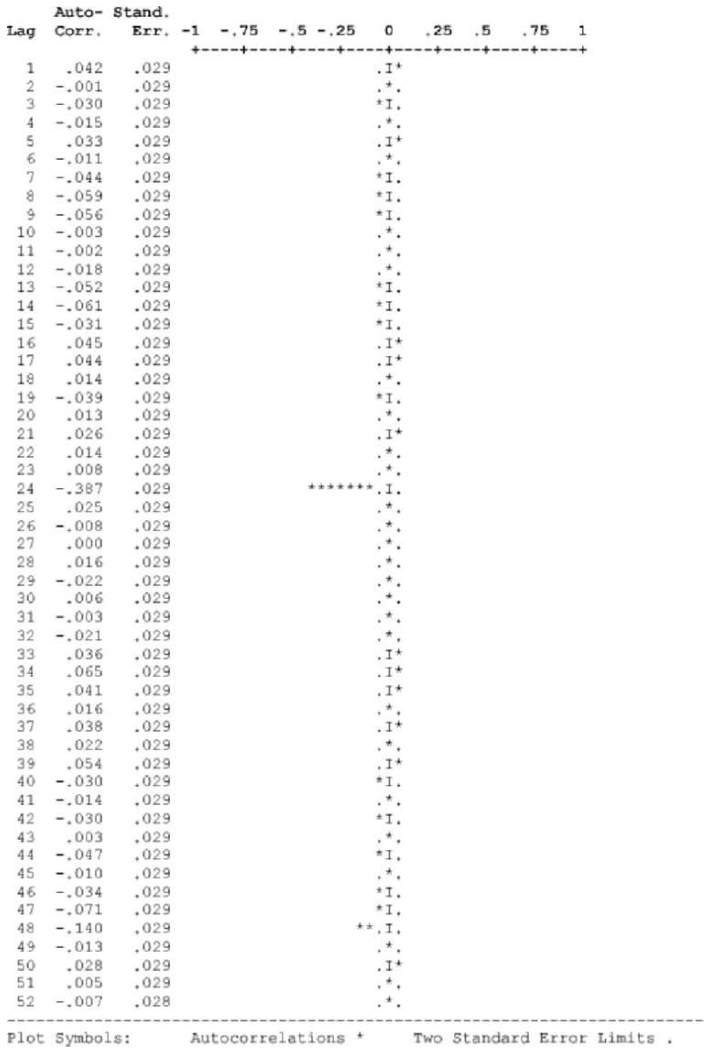

Lag	Auto-Corr.	Stand. Err.	-1 -.75 -.5 -.25 0 .25 .5 .75 1
1	.042	.029	.I*
2	-.001	.029	.*.
3	-.030	.029	*I.
4	-.015	.029	.*.
5	.033	.029	.I*
6	-.011	.029	.*.
7	-.044	.029	*I.
8	-.059	.029	*I.
9	-.056	.029	*I.
10	-.003	.029	.*.
11	-.002	.029	.*.
12	-.018	.029	.*.
13	-.052	.029	*I.
14	-.061	.029	*I.
15	-.031	.029	*I.
16	.045	.029	.I*
17	.044	.029	.I*
18	.014	.029	.*.
19	-.039	.029	*I.
20	.013	.029	.*.
21	.026	.029	.I*
22	.014	.029	.*.
23	.008	.029	.*.
24	-.387	.029	*******.I.
25	.025	.029	.*.
26	-.008	.029	.*.
27	.000	.029	.*.
28	.016	.029	.*.
29	-.022	.029	.*.
30	.006	.029	.*.
31	-.003	.029	.*.
32	-.021	.029	.*.
33	.036	.029	.I*
34	.065	.029	.I*
35	.041	.029	.I*
36	.016	.029	.*.
37	.038	.029	.I*
38	.022	.029	.*.
39	.054	.029	.I*
40	-.030	.029	*I.
41	-.014	.029	.*.
42	-.030	.029	*I.
43	.003	.029	.*.
44	-.047	.029	*I.
45	-.010	.029	.*.
46	-.034	.029	*I.
47	-.071	.029	*I.
48	-.140	.029	**.I.
49	-.013	.029	.*.
50	.028	.029	.I*
51	.005	.029	.*.
52	-.007	.028	.*.

Plot Symbols: Autocorrelations * Two Standard Error Limits .

Fig. C.9a. Plot of ACF of the differenced log x2 series. The vertical dot lines represent the 95 % confidence intervals (0.058).

```
   Pr-Aut- Stand.
Lag  Corr.   Err. -1  -.75  -.5 -.25   0   .25  .5   .75  1
                  +----+----+----+----+----+----+----+----+
  1   .042   .029                     .I*
  2  -.002   .029                     .*.
  3  -.030   .029                     *I.
  4  -.012   .029                     .*.
  5   .034   .029                     .I*
  6  -.015   .029                     .*.
  7  -.043   .029                     *I.
  8  -.054   .029                     *I.
  9  -.051   .029                     *I.
 10  -.003   .029                     .*.
 11  -.005   .029                     .*.
 12  -.020   .029                     .*.
 13  -.051   .029                     *I.
 14  -.059   .029                     *I.
 15  -.034   .029                     *I.
 16   .037   .029                     .I*
 17   .031   .029                     .I*
 18   .006   .029                     .*.
 19  -.040   .029                     *I.
 20   .012   .029                     .*.
 21   .011   .029                     .*.
 22  -.005   .029                     .*.
 23   .001   .029                     .*.
 24  -.390   .029             *******.I.
 25   .065   .029                     .I*
 26  -.019   .029                     .*.
 27  -.030   .029                     *I.
 28   .002   .029                     .*.
 29  -.006   .029                     .*.
 30   .001   .029                     .*.
 31  -.028   .029                     *I.
 32  -.063   .029                     *I.
 33  -.007   .029                     .*.
 34   .066   .029                     .I*
 35   .030   .029                     .I*
 36  -.001   .029                     .*.
 37   .005   .029                     .*.
 38  -.028   .029                     *I.
 39   .027   .029                     .I*
 40  -.013   .029                     .*.
 41   .009   .029                     .*.
 42  -.020   .029                     .*.
 43  -.012   .029                     .*.
 44  -.041   .029                     *I.
 45   .006   .029                     .*.
 46  -.035   .029                     *I.
 47  -.064   .029                     *I.
 48  -.333   .029              ******.I.
 49   .064   .029                     .I*
 50   .008   .029                     .*.
 51  -.041   .029                     *I.
 52  -.012   .029                     .*.
-------------------------------------------------------------------------
Plot Symbols:      Autocorrelations *     Two Standard Error Limits .
```

Fig. C.9b. Plot of PACF of the differenced log x2 series. The vertical dot lines represent the 95 % confidence intervals (0.058).

Lag	Auto-Corr.	Stand. Err.	-1 -.75 -.5 -.25 0 .25 .5 .75 1
1	.005	.029	.*.
2	.000	.029	.*.
3	-.019	.029	.*.
4	-.009	.029	.*.
5	.003	.029	.*.
6	-.020	.029	.*.
7	-.043	.029	*I.
8	-.049	.029	*I.
9	-.053	.029	*I.
10	-.010	.029	.*.
11	-.001	.029	.*.
12	-.017	.029	.*.
13	-.050	.029	*I.
14	-.052	.029	*I.
15	-.052	.029	*I.
16	-.012	.029	.*.
17	-.017	.029	.*.
18	-.020	.029	.*.
19	-.049	.029	*I.
20	-.001	.029	.*.
21	.010	.029	.*.
22	.009	.029	.*.
23	.025	.029	.*.
24	.082	.029	.I.*
25	.048	.029	.I*
26	.004	.029	.*.
27	.005	.029	.*.
28	.009	.029	.*.
29	-.009	.029	.*.
30	-.007	.029	.*.
31	-.028	.029	*I.
32	-.024	.029	.*.
33	-.005	.029	.*.
34	.033	.029	.I*
35	.046	.029	.I*
36	-.004	.029	.*.
37	-.018	.029	.*.
38	.002	.029	.*.
39	.020	.029	.*.
40	-.038	.029	*I.
41	-.055	.029	*I.
42	-.046	.029	*I.
43	-.015	.029	.*.
44	-.010	.029	.*.
45	-.002	.029	.*.
46	-.011	.029	.*.
47	-.038	.029	*I.
48	-.054	.029	*I.
49	.037	.029	.I*
50	.023	.029	.*.
51	.023	.029	.*.
52	-.002	.028	.*.

Plot Symbols: Autocorrelations * Two Standard Error Limits .

Fig. C.10a. Plot of the ACF of the residuals of the univariate model for the log x2 series at AQCR2. The vertical dot lines represent the 95 % confidence intervals (0.058).

Lag	Pr-Aut-Corr.	Stand. Err.	-1 -.75 -.5 -.25 0 .25 .5 .75 1
1	.005	.029	.*.
2	.000	.029	.*.
3	-.019	.029	.*.
4	-.009	.029	.*.
5	.003	.029	.*.
6	-.020	.029	.*.
7	-.043	.029	*I.
8	-.049	.029	*I.
9	-.053	.029	*I.
10	-.014	.029	.*.
11	-.006	.029	.*.
12	-.022	.029	.*.
13	-.056	.029	*I.
14	-.051	.029	*I.
15	-.058	.029	*I.
16	-.033	.029	*I.
17	-.037	.029	*I.
18	-.036	.029	*I.
19	-.044	.029	*I.
20	-.023	.029	.*.
21	-.019	.029	.*.
22	-.025	.029	.*.
23	-.005	.029	.*.
24	.060	.029	.I*
25	.052	.029	.I*
26	-.015	.029	.*.
27	-.014	.029	.*.
28	-.007	.029	.*.
29	-.021	.029	.*.
30	-.014	.029	.*.
31	-.026	.029	*I.
32	-.020	.029	.*.
33	.000	.029	.*.
34	.032	.029	.I*
35	.044	.029	.I*
36	-.003	.029	.*.
37	-.012	.029	.*.
38	.011	.029	.*.
39	.029	.029	.I*
40	-.034	.029	*I.
41	-.051	.029	*I.
42	-.035	.029	*I.
43	-.002	.029	.*.
44	-.008	.029	.*.
45	-.013	.029	.*.
46	-.019	.029	.*.
47	-.047	.029	*I.
48	-.051	.029	*I.
49	.004	.029	.*.
50	-.004	.029	.*.
51	.002	.029	.*.
52	-.012	.029	.*.

Plot Symbols: Autocorrelations * Two Standard Error Limits .

Fig. C.10b. Plot of the PACF of the residuals of the univariate model for the log x2 series at AQCR2. The vertical dot lines represent the 95 % confidence intervals (0.058).

Table C.2 Final estimates of parameters for the log x_2 series ARIMA model at AQCR2.

Model	Parameter	Estimate	Standard Deviation	t-ratio
ARIMA $(1,1,0) \times (0,1,1)_{24}$	ϕ_1	0.0952	0.0287	3.32
	Θ_1	0.9223	0.0161	57.29

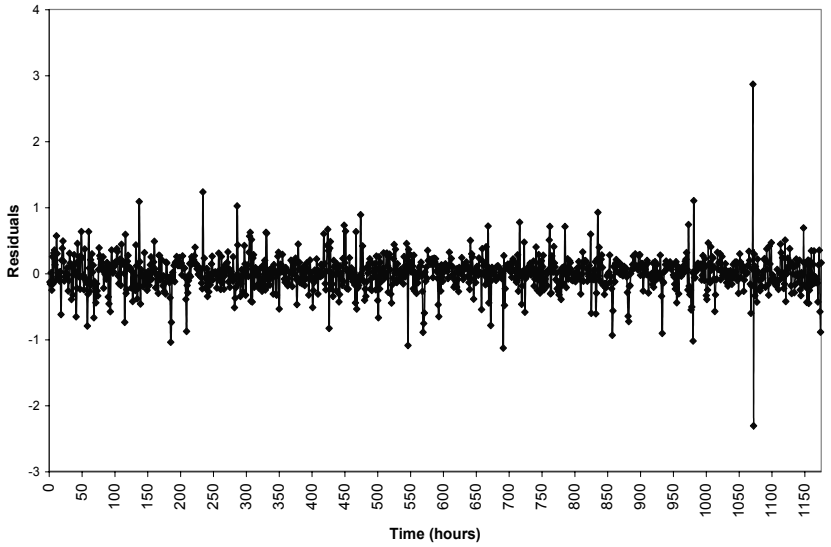

Fig. C.11. Plot of the residuals from the univariate model for log x2 series at AQCR2.

D Neuron Definitions and Synaptic Weights

Table D.1a Neuron definitions in the $ANNCO_{1hrA1}$ model.

Neuron number	Type of layer	Type of activation function	Bias
1	Input	Identity	-0.00479
2	Input	Identity	-0.00303
3	Input	Identity	-0.00356
4	Input	Identity	-0.00154
5	Input	Identity	0.00454
6	Input	Identity	-0.00871
7	Input	Identity	-0.00324
8	Input	Identity	0.00905
9	Input	Identity	0.00254
10	Input	Identity	-0.00236
11	Input	Identity	0.00703
12	Input	Identity	0.00245
13	Input	Identity	-0.00289
14	Input	Identity	0.00949
15	Input	Identity	-0.00683
16	Input	Identity	0.00846
17	Input	Identity	-0.00485
18	Hidden	Hyperbolic tangent	5.16323
19	Hidden	Hyperbolic tangent	1.57388
20	Hidden	Hyperbolic tangent	-0.65549
21	Output	Identity	7.17080

M. Khare and S.M. Shiva Nagendra: *Neuron Definitions and Synaptic Weights*, Artificial Neural Networks in Vehicular Pollution Modelling (SCI) **41,** 211–226 (2007)
www.springerlink.com

Table D.1b Synaptic weights in the $ANNCO_{1hrA1}$ model.

Source neuron (input layer)	Target neuron (hidden layer)			Source neuron (hidden layer)	Target neuron (output layer)
	18	19	20		21
1	0.15831	0.05203	0.04304	18	-0.66107
2	-0.20881	0.50732	0.46755	19	-0.13831
3	2.03689	0.27709	0.30407	20	0.16490
4	-0.44868	-0.03613	0.31942		
5	-0.36148	-0.37584	-0.12156		
6	0.12254	0.11583	0.03800		
7	-0.31756	-0.00713	0.11151		
8	0.17358	0.18449	-0.24788		
9	-0.10592	-0.31096	0.19853		
10	-0.53684	1.19278	-0.05143		
11	1.31096	-0.06436	-0.73124		
12	0.06918	-0.04417	-0.14063		
13	1.29911	0.50580	0.57351		
14	-1.79287	-0.82108	0.30317		
15	-0.17827	-0.07727	0.17400		
16	0.47920	-0.02236	-0.23817		
17	0.00107	-0.09338	0.01079		

Table D.2a Neuron definitions in the $ANNCO_{1hrB1}$ model.

Neuron number	Type of layer	Type of activation function	Bias
1	Input	Identity	0.00224
2	Input	Identity	-0.00055
3	Input	Identity	0.00467
4	Input	Identity	0.00198
5	Input	Identity	-0.00742
6	Input	Identity	0.00908
7	Input	Identity	0.00411
8	Input	Identity	0.00212
9	Input	Identity	-0.00120
10	Input	Identity	0.00378
11	Hidden	Hyperbolic tangent	0.03244
12	Hidden	Hyperbolic tangent	1.47907
13	Hidden	Hyperbolic tangent	0.34292
14	Output	Identity	-2.47934

Table D.2b Synaptic weights in the $ANNCO_{1hrB1}$ model.

Source neuron (input layer)	Target neuron (hidden layer)			Source neuron (hidden layer)	Target neuron (output layer)
	11	12	13		14
1	-0.01774	0.14153	-0.15023	11	-0.21935
2	-0.05482	-0.16932	0.02848	12	-0.79906
3	0.11320	0.29358	-0.32724	13	-0.43119
4	0.01782	-0.36714	0.10535		
5	-0.08293	0.09618	-0.01608		
6	-0.07914	-0.47127	0.00909		
7	-0.05418	0.14221	-0.00727		
8	-0.02731	-0.09402	-0.00190		
9	-0.05173	-0.23392	0.25471		
10	0.15743	0.27373	0.02501		

Table D.3a Neuron definitions in the $ANNCO_{1hrC1}$ model.

Neuron number	Type of layer	Type of activation function	Bias
1	Input	Identity	0.00207
2	Input	Identity	-0.00681
3	Input	Identity	0.00293
4	Input	Identity	0.00107
5	Input	Identity	0.00363
6	Hidden	Hyperbolic tangent	-0.55178
7	Hidden	Hyperbolic tangent	0.57984
8	Hidden	Hyperbolic tangent	0.23081
9	Output	Identity	-3.54114

Table D.3b Synaptic weights in the $ANNCO_{1hrC1}$ model.

Source neuron (input layer)	Target neuron (hidden layer)			Source neuron (hidden layer)	Target neuron (output layer)
	6	7	8		9
1	-0.04632	0.04027	0.05952	6	0.57363
2	-0.15528	0.15235	0.11554	7	-0.59587
3	0.26183	-0.25365	-0.13650	8	-0.25235
4	0.00527	-0.01375	0.02413		
5	-0.01015	0.00001	0.01595		

Table D.4a Neuron definitions in the $ANNCO_{1hrA2}$ model.

Neuron number	Type of layer	Type of activation function	Bias
1	Input	Identity	0.00207
2	Input	Identity	-0.00681
3	Input	Identity	0.00293
4	Input	Identity	0.00107
5	Input	Identity	0.00363
6	Input	Identity	-0.00773
7	Input	Identity	0.00969
8	Input	Identity	-0.00168
9	Input	Identity	0.00681
10	Input	Identity	0.00233
11	Input	Identity	-0.00382
12	Input	Identity	0.00882
13	Input	Identity	-0.00800
14	Input	Identity	0.00673
15	Input	Identity	0.00682
16	Input	Identity	-0.00066
17	Input	Identity	-0.00208
18	Hidden	Hyperbolic tangent	0.01595
19	Hidden	Hyperbolic tangent	-1.43897
20	Hidden	Hyperbolic tangent	-0.69772
21	Output	Identity	-3.15814

Table D.4b Synaptic weights in the $ANNCO_{1hrA2}$ model.

Source neuron (input layer)	Target neuron (hidden layer)			Source neuron (hidden layer)	Target neuron (output layer)
	18	19	20		21
1	-0.03260	-0.13160	0.02995	18	-0.32498
2	0.00824	0.27776	0.06891	19	0.65493
3	0.17969	-0.18366	0.20985	20	0.53567
4	0.06751	0.35674	-0.02567		
5	0.09542	0.26904	-0.08919		
6	0.07503	0.00914	0.09532		
7	-0.15863	0.39317	-0.10930		
8	-0.10637	-0.34269	-0.09502		
9	0.07167	0.11000	0.03102		
10	0.13389	0.37090	0.00517		
11	0.42102	0.04736	0.24808		
12	0.01278	-0.22312	0.11783		
13	0.03832	-0.24103	0.12948		
14	0.02573	0.40172	-0.05087		
15	-0.00325	-0.05251	0.06503		
16	-0.01568	0.22416	-0.06853		
17	0.00225	-0.01431	-0.08702		

Table D.5a Neuron definitions in the $ANNCO_{1hrB2}$ model.

Neuron number	Type of layer	Type of activation function	Bias
1	Input	Identity	0.00207
2	Input	Identity	-0.00681
3	Input	Identity	0.00293
4	Input	Identity	0.00107
5	Input	Identity	0.00363
6	Input	Identity	-0.00773
7	Input	Identity	0.00969
8	Input	Identity	-0.00168
9	Input	Identity	0.00681
10	Input	Identity	0.00233
11	Hidden	Hyperbolic tangent	-2.67685
12	Hidden	Hyperbolic tangent	-0.34942
13	Hidden	Hyperbolic tangent	-0.35607
14	Output	Identity	-3.15804

Table D.5b Synaptic weights in the $ANNCO_{1hrB2}$ model.

Source neuron (input layer)	Target neuron (hidden layer)			Source neuron (hidden layer)	Target neuron (output layer)
	11	12	13		14
1	-0.15323	0.06651	0.08363	11	0.93085
2	0.28744	0.19849	0.18802	12	-0.32623
3	-0.72705	0.04614	0.15720	13	0.39866
4	0.66764	0.17169	-0.05248		
5	-0.25799	-0.15025	-0.02138		
6	0.66636	-0.44127	-0.11173		
7	-0.27302	-0.23599	-0.22747		
8	0.10265	0.06280	0.01320		
9	0.56523	0.29254	0.04819		
10	-0.14312	0.60350	0.10465		

Table D.6a Neuron definitions in the $ANNCO_{1hrC2}$ model.

Neuron number	Type of layer	Type of activation function	Bias
1	Input	Identity	0.00207
2	Input	Identity	-0.00681
3	Input	Identity	0.00293
4	Input	Identity	0.00107
5	Input	Identity	0.00363
6	Hidden	Hyperbolic tangent	-0.58816
7	Hidden	Hyperbolic tangent	0.62155
8	Hidden	Hyperbolic tangent	0.27332
9	Output	Identity	-3.85196

Table D.6b Synaptic weights in the $ANNCO_{1hrC2}$ model.

Source neuron (input layer)	Target neuron (hidden layer)			Source neuron (hidden layer)	Target neuron (output layer)
	6	7	8		9
1	-0.05455	0.05361	0.04694	6	0.64310
2	-0.07357	0.07634	0.05015	7	-0.67971
3	0.13012	-0.12329	-0.06072	8	-0.29229
4	-0.06677	0.06494	0.04487		
5	0.01323	-0.02190	-0.00536		

Table D.7a Neuron definitions in the $ANNCO_{8hrA1}$ model.

Neuron number	Type of layer	Type of activation function	Bias
1	Input	Identity	-0.00479
2	Input	Identity	-0.00303
3	Input	Identity	-0.00356
4	Input	Identity	-0.00154
5	Input	Identity	0.00454
6	Input	Identity	-0.00871
7	Input	Identity	-0.00324
8	Input	Identity	0.00905
9	Input	Identity	0.00254
10	Input	Identity	-0.00236
11	Input	Identity	0.00703
12	Input	Identity	0.00245
13	Input	Identity	-0.00289
14	Input	Identity	0.00949
15	Input	Identity	-0.00683
16	Input	Identity	0.00846
17	Input	Identity	-0.00485
18	Hidden	Hyperbolic tangent	0.32292
19	Hidden	Hyperbolic tangent	0.07896
20	Hidden	Hyperbolic tangent	-1.26795
21	Output	Identity	-2.96655

Table D.7b Synaptic weights in the $ANNCO_{8hrA1}$ model.

Source neuron (input layer)	Target neuron (hidden layer)			Source neuron (hidden layer)	Target neuron (output layer)
	18	19	20		21
1	-0.03206	-0.16334	-0.34902	18	-0.34490
2	0.04502	-0.02707	-0.02607	19	-0.31507
3	-0.04209	0.03513	-0.19817	20	0.75589
4	-0.02162	-0.01756	0.09332		
5	0.09361	0.11624	0.30234		
6	-0.00510	0.00985	0.03920		
7	-0.07060	-0.06456	0.02332		
8	0.05212	-0.00340	-0.46738		
9	-0.17315	-0.00742	0.02507		
10	0.08170	0.13098	0.35014		
11	0.05623	0.13528	-0.34223		
12	-0.02074	0.08877	-0.16345		
13	-0.13436	-0.01130	0.24120		
14	-0.17517	-0.02903	0.29279		
15	-0.07348	0.00843	0.01256		
16	0.01964	0.12857	-0.02143		
17	-0.02427	0.05819	-0.05249		

Table D.8a Neuron definitions in the $ANNCO_{8hrB1}$ model.

Neuron number	Type of layer	Type of activation function	Bias
1	Input	Identity	-0.00063
2	Input	Identity	0.00081
3	Input	Identity	-0.00305
4	Input	Identity	0.00346
5	Input	Identity	-0.00893
6	Input	Identity	0.00264
7	Input	Identity	-0.00888
8	Input	Identity	0.00985
9	Input	Identity	-0.00033
10	Input	Identity	0.00454
11	Hidden	Hyperbolic tangent	1.52583
12	Hidden	Hyperbolic tangent	0.05478
13	Hidden	Hyperbolic tangent	0.22974
14	Output	Identity	-3.29806

Table D.8b Synaptic weights in the $ANNCO_{8hrB1}$ model.

Source neuron (input layer)	Target neuron (hidden layer)			Source neuron (hidden layer)	Target neuron (output layer)
	11	12	13		14
1	0.45041	0.02932	-0.17292	11	-0.75173
2	0.22309	0.04661	-0.01427	12	0.28041
3	0.21480	0.09240	-0.25122	13	-0.40808
4	-0.30680	0.03168	-0.03839		
5	0.12879	0.19608	0.15285		
6	-0.16781	0.06855	-0.18150		
7	0.56053	0.01906	0.01692		
8	-0.03569	-0.01469	-0.15558		
9	-0.30539	-0.16920	-0.00359		
10	0.45518	-0.08346	0.14706		

Table D.9a Neuron definitions in the $ANNCO_{8hrC1}$ model.

Neuron number	Type of layer	Type of activation function	Bias
1	Input	Identity	0.00207
2	Input	Identity	-0.00681
3	Input	Identity	0.00293
4	Input	Identity	0.00107
5	Input	Identity	0.00363
6	Hidden	Hyperbolic tangent	-0.48606
7	Hidden	Hyperbolic tangent	0.58846
8	Hidden	Hyperbolic tangent	0.21210
9	Output	Identity	-4.28758

Table D.9b Synaptic weights in the $ANNCO_{8hrC1}$ model.

Source neuron (input layer)	Target neuron (hidden layer)			Source neuron (hidden layer)	Target neuron (output layer)
	6	7	8		9
1	0.02431	-0.03069	0.00036	6	0.52157
2	0.04889	-0.05287	-0.02197	7	-0.64152
3	0.05659	-0.05042	-0.02053	8	-0.21839
4	-0.08264	0.09904	0.03421		
5	-0.00233	-0.00470	0.00321		

Table D.10a Neuron definitions in the $ANNCO_{8hrA2}$ model.

Neuron number	Type of layer	Type of activation function	Bias
1	Input	Identity	0.00072
2	Input	Identity	-0.00030
3	Input	Identity	0.00137
4	Input	Identity	-0.00263
5	Input	Identity	-0.00156
6	Input	Identity	0.00691
7	Input	Identity	-0.00453
8	Input	Identity	0.00878
9	Input	Identity	-0.00656
10	Input	Identity	0.00752
11	Input	Identity	0.00529
12	Input	Identity	-0.00187
13	Input	Identity	0.00204
14	Input	Identity	0.00199
15	Input	Identity	-0.00843
16	Input	Identity	-0.00321
17	Input	Identity	-0.00836
18	Hidden	Hyperbolic tangent	-0.66856
19	Hidden	Hyperbolic tangent	2.03216
20	Hidden	Hyperbolic tangent	-1.09419
21	Output	Identity	-2.90043

Table D.10b Synaptic weights in the $ANNCO_{8hrA2}$ model.

Source neuron (input layer)	Target neuron (hidden layer)			Source neuron (hidden layer)	Target neuron (output layer)
	18	19	20		21
1	0.10672	0.17250	0.20633	18	-0.52193
2	0.01499	0.13936	0.17162	19	-0.84740
3	-0.18388	0.44172	-0.25054	20	0.54208
4	0.42903	-0.66201	0.06561		
5	0.51733	-0.24082	0.45047		
6	0.04907	0.11880	0.13219		
7	0.42363	-0.31777	0.46070		
8	-0.54130	0.54347	-0.39106		
9	-0.20366	0.00167	-0.24871		
10	0.52868	-0.31951	0.37335		
11	-0.33818	0.95094	-0.32504		
12	-0.38312	0.60226	-0.30789		
13	0.14529	-0.07154	-0.06568		
14	0.41914	0.11192	-0.22404		
15	0.16883	0.03726	0.05905		
16	-0.38679	-0.64223	0.25067		
17	-0.06770	-0.24371	0.11601		

Table D.11a Neuron definitions in the $ANNCO_{8hrB2}$ model.

Neuron number	Type of layer	Type of activation function	Bias
1	Input	Identity	0.00207
2	Input	Identity	-0.00681
3	Input	Identity	0.00293
4	Input	Identity	0.00107
5	Input	Identity	0.00363
6	Input	Identity	-0.00773
7	Input	Identity	0.00969
8	Input	Identity	-0.00168
9	Input	Identity	0.00681
10	Input	Identity	0.00233
11	Hidden	Hyperbolic tangent	-0.61484
12	Hidden	Hyperbolic tangent	-0.89660
13	Hidden	Hyperbolic tangent	-3.81334
14	Output	Identity	-3.94131

Table D.11b Synaptic weights in the $ANNCO_{8hrB2}$ model.

Source neuron (input layer)	Target neuron (hidden layer)			Source neuron (hidden layer)	Target neuron (output layer)
	11	12	13		14
1	-0.12059	-0.20294	-0.19016	11	0.56664
2	0.32070	0.51047	-0.33367	12	-0.35583
3	-0.57415	-1.30319	-0.48777	13	0.74532
4	-0.66135	-1.00062	1.42335		
5	-0.21568	-0.48801	-0.46632		
6	-0.19135	-0.47738	0.98116		
7	-0.71347	-1.07823	-0.40611		
8	-0.18358	-0.41027	0.06304		
9	0.07355	0.23614	0.28070		
10	-0.19139	-0.12850	-2.15348		

Table D.12a Neuron definitions in the $ANNCO_{8hrC2}$ model.

Neuron number	Type of layer	Type of activation function	Bias
1	Input	Identity	0.00207
2	Input	Identity	-0.00681
3	Input	Identity	0.00293
4	Input	Identity	0.00107
5	Input	Identity	0.00363
6	Hidden	Hyperbolic tangent	-0.49001
7	Hidden	Hyperbolic tangent	0.58313
8	Hidden	Hyperbolic tangent	0.24294
9	Output	Identity	-4.45871

Table D.12b Synaptic weights in the $ANNCO_{8hrC2}$ model.

Source neuron (input layer)	Target neuron (hidden layer)			Source neuron (hidden layer)	Target neuron (output layer)
	6	7	8		9
1	-0.09674	0.11997	0.07888	6	0.56117
2	0.11389	-0.10406	-0.05356	7	-0.67313
3	0.10226	-0.08343	-0.03945	8	-0.27223
4	-0.12291	0.15597	0.07680		
5	0.04080	-0.03249	-0.01088		

Table D.13a Neuron definitions in the $ANNNO2_{24hrA1}$ model.

Neuron number	Type of layer	Type of activation function	Bias
1	Input	Identity	0.00207
2	Input	Identity	-0.00681
3	Input	Identity	0.00293
4	Input	Identity	0.00107
5	Input	Identity	0.00363
6	Input	Identity	-0.00773
7	Input	Identity	0.00969
8	Input	Identity	-0.00168
9	Input	Identity	0.00681
10	Input	Identity	0.00233
11	Input	Identity	-0.00382
12	Input	Identity	0.00882
13	Input	Identity	-0.00800
14	Input	Identity	0.00673
15	Input	Identity	0.00682
16	Input	Identity	-0.00066
17	Input	Identity	-0.00208
18	Hidden	Hyperbolic tangent	0.11470
19	Hidden	Hyperbolic tangent	2.17832
20	Hidden	Hyperbolic tangent	0.01681
21	Hidden	Hyperbolic tangent	-0.18061
22	Hidden	Hyperbolic tangent	-0.06514
23	Output	Identity	0.15778

Table D.13b Synaptic weights in the $ANNNO2_{24hrA1}$ model.

Source neuron (input layer)	Target neuron (hidden layer)					Source neuron (hidden layer)	Target neuron (output layer)
	18	19	20	21	22		23
1	-0.18333	0.68854	-0.03368	0.11240	0.10391	18	-0.10966
2	0.01002	-0.10544	-0.00898	-0.01293	-0.04050	19	-0.58753
3	0.06642	-0.21211	0.01648	-0.03722	-0.06831	20	-0.02741
4	-0.60928	-1.10906	-0.11386	0.73764	0.75628	21	0.13031
5	-0.00340	0.13715	-0.01276	0.01954	-0.03160	22	0.19014
6	-0.02219	0.60689	-0.01489	0.04220	0.03360		
7	-0.46502	-0.99465	-0.11094	0.56391	0.55755		
8	-0.04292	0.22445	0.00911	0.05889	0.06853		
9	-0.16015	-0.07926	-0.04362	0.17833	0.16667		
10	0.00368	-1.00307	0.00144	-0.01680	-0.10380		
11	0.09786	0.03782	0.02517	-0.14377	-0.17454		
12	0.06275	0.23737	0.01382	-0.06170	-0.07470		
13	0.07802	0.23726	0.01304	-0.07630	-0.12314		
14	0.06378	0.24496	0.01987	-0.07692	-0.08953		
15	0.11013	0.23543	0.01530	-0.12443	-0.17070		
16	-0.27111	-0.36556	-0.06173	0.30558	0.29727		
17	-0.04966	0.00639	-0.00919	0.05432	0.02034		

Table D.14a Neuron definitions in the $ANNNO2_{24hrB1}$ model.

Neuron number	Type of layer	Type of activation function	Bias
1	Input	Identity	0.00207
2	Input	Identity	-0.00681
3	Input	Identity	0.00293
4	Input	Identity	0.00107
5	Input	Identity	0.00363
6	Input	Identity	-0.00773
7	Input	Identity	0.00969
8	Input	Identity	-0.00168
9	Input	Identity	0.00681
10	Input	Identity	0.00233
11	Hidden	Hyperbolic tangent	0.01092
12	Hidden	Hyperbolic tangent	-1.91146
13	Hidden	Hyperbolic tangent	0.15323
14	Hidden	Hyperbolic tangent	-0.30229
15	Hidden	Hyperbolic tangent	0.42171
16	Output	Identity	-1.82050

Table D.14b Synaptic weights in the $ANNNO2_{24hrB1}$ model.

Source neuron (input layer)	Target neuron (hidden layer)					Source neuron (hidden layer)	Target neuron (output layer)
	11	12	13	14	15		16
1	0.14167	-0.47136	0.24713	-0.27942	-0.16135	11	0.06699
2	-0.08574	0.44454	-0.13353	0.17586	-0.05701	12	0.78181
3	0.03561	-0.12653	0.01221	-0.1331	-0.06097	13	0.13590
4	0.26624	1.25685	0.38315	-0.50416	-0.55670	14	-0.25773
5	0.08786	-0.31635	0.07474	-0.07969	-0.06197	15	-0.10905
6	0.13049	0.68387	0.26536	-0.34284	-0.51240		
7	0.05987	-0.12385	0.15054	-0.22968	-0.13381		
8	0.11348	0.20933	0.08932	-0.01308	-0.30992		
9	-0.04084	0.62479	-0.05313	0.17960	0.29290		
10	-0.06206	-0.03433	-0.17276	0.21364	0.02206		

Table D.15a Neuron definitions in the $ANNNO2_{24hrC1}$ model.

Neuron number	Type of layer	Type of activation function	Bias
1	Input	Identity	0.00207
2	Input	Identity	-0.00681
3	Input	Identity	0.00293
4	Input	Identity	0.00107
5	Input	Identity	-0.21548
6	Hidden	Hyperbolic tangent	-0.21548
7	Hidden	Hyperbolic tangent	0.27119
8	Hidden	Hyperbolic tangent	-0.25492
9	Hidden	Hyperbolic tangent	0.51335
10	Hidden	Hyperbolic tangent	0.19821
11	Output	Identity	-3.84471

Table D.15b Synaptic weights in the $ANNNO2_{24hrC1}$ model.

Source neuron (input layer)	Target neuron (hidden layer)					Source neuron (hidden layer)	Target neuron (output layer)
	6	7	8	9	10		11
1	0.00006	0.00264	-0.00523	0.02012	0.00998	6	0.21688
2	-0.00904	0.01453	-0.00490	0.00551	0.00652	7	-0.27478
3	-0.00200	0.01643	-0.00471	0.00736	0.00273	8	0.25750
4	-0.00087	0.00193	-0.00691	-0.00071	0.00807	9	-0.53613
5	-0.01263	0.00763	-0.00495	0.01011	-0.00121	10	-0.19916

Table D.16a Neuron definitions in the $ANNNO2_{24hrA2}$ model.

Neuron number	Type of layer	Type of activation function	Bias
1	Input	Identity	0.00207
2	Input	Identity	-0.00681
3	Input	Identity	0.00293
4	Input	Identity	0.00107
5	Input	Identity	0.00363
6	Input	Identity	-0.00773
7	Input	Identity	0.00969
8	Input	Identity	-0.00168
9	Input	Identity	0.00681
10	Input	Identity	0.00233
11	Input	Identity	-0.00382
12	Input	Identity	0.00882
13	Input	Identity	-0.00800
14	Input	Identity	0.00673
15	Input	Identity	0.00682
16	Input	Identity	-0.00066
17	Input	Identity	-0.00208
18	Hidden	Hyperbolic tangent	0.19937
19	Hidden	Hyperbolic tangent	0.36413
20	Hidden	Hyperbolic tangent	-0.10121
21	Hidden	Hyperbolic tangent	-0.45489
22	Hidden	Hyperbolic tangent	-0.03185
23	Output	Identity	-3.28973

Table D.16b Synaptic weights in the $ANNNO2_{24hrA2}$ model.

Source neuron (input layer)	Target neuron (hidden layer)					Source neuron (hidden layer)	Target neuron (output layer)
	18	19	20	21	22		23
1	0.03940	0.11796	0.00129	-0.16105	-0.00888	18	-0.33798
2	-0.07219	-0.06373	0.03949	0.04069	0.00653	19	-0.54008
3	0.05985	0.04826	-0.02434	-0.00981	-0.00657	20	0.15799
4	0.04805	0.03139	-0.02070	-0.01707	-0.01302	21	0.62502
5	-0.05202	-0.11549	0.01942	0.13442	-0.00014	22	0.04407
6	0.03362	-0.02864	-0.01423	0.04811	-0.00457		
7	0.04093	0.03260	-0.02648	-0.00485	0.00276		
8	0.17819	0.31542	-0.07745	-0.38437	-0.02221		
9	-0.04000	-0.01920	0.02001	-0.01932	0.00988		
10	0.04240	-0.04038	-0.02647	0.11991	-0.01693		
11	0.03624	0.06632	-0.02934	-0.09118	-0.00726		
12	0.04312	-0.00970	-0.01705	0.07555	0.00517		
13	0.03521	-0.00875	-0.02203	0.09182	-0.01222		
14	0.03453	-0.01010	-0.01379	0.07281	0.00456		
15	0.02640	-0.00515	-0.02407	0.07823	-0.01106		
16	0.07716	0.05389	-0.03794	0.00149	-0.00420		
17	0.04158	0.02805	-0.02426	0.04956	-0.00321		

Table D.17a Neuron definitions in the $ANNNO2_{24hrB2}$ model.

Neuron number	Type of layer	Type of activation function	Bias
1	Input	Identity	0.00207
2	Input	Identity	-0.00681
3	Input	Identity	0.00293
4	Input	Identity	0.00107
5	Input	Identity	0.00363
6	Input	Identity	-0.00773
7	Input	Identity	0.00969
8	Input	Identity	-0.00168
9	Input	Identity	0.00681
10	Input	Identity	0.00233
11	Hidden	Hyperbolic tangent	-0.14257
12	Hidden	Hyperbolic tangent	-0.33990
13	Hidden	Hyperbolic tangent	-0.14014
14	Hidden	Hyperbolic tangent	0.23251
15	Hidden	Hyperbolic tangent	0.39997
16	Output	Identity	-3.43884

Table D.17b Synaptic weights in the $ANNNO2_{24hrB2}$ model.

Source neuron (input layer)	Target neuron (hidden layer)					Source neuron (hidden layer)	Target neuron (output layer)
	11	12	13	14	15		16
1	-0.01003	-0.15576	-0.01261	0.06394	0.19695	11	0.24899
2	0.04852	0.07505	0.04749	-0.07299	-0.07166	12	0.49849
3	-0.04557	-0.04054	-0.04894	0.06278	0.03415	13	0.24637
4	-0.01694	-0.03352	-0.02640	0.03615	0.01860	14	-0.39467
5	-0.04451	0.04754	-0.04737	0.02357	-0.08728	15	-0.54996
6	-0.05042	-0.00098	-0.04138	0.03453	-0.03233		
7	-0.14760	-0.30786	-0.15057	0.23100	0.34351		
8	0.01164	-0.00518	0.01127	-0.00860	0.01676		
9	-0.07452	0.07465	-0.07036	0.05756	-0.15315		
10	-0.01185	-0.07522	-0.01452	0.03091	0.08509		

Table D.18a Neuron definitions in the $ANNNO2_{24hrC2}$ model.

Neuron number	Type of layer	Type of activation function	Bias
1	Input	Identity	-0.00008
2	Input	Identity	0.00866
3	Input	Identity	0.00214
4	Input	Identity	0.00041
5	Input	Identity	0.00564
6	Hidden	Hyperbolic tangent	0.33959
7	Hidden	Hyperbolic tangent	0.03696
8	Hidden	Hyperbolic tangent	-0.36337
9	Hidden	Hyperbolic tangent	0.39934
10	Hidden	Hyperbolic tangent	-0.55711
11	Output	Identity	-4.50506

Table D.18b Synaptic weights in the $ANNNO2_{24hrC2}$ model.

Source neuron (Input layer)	Target neuron (hidden layer)					Source neuron (hidden layer)	Target neuron (output layer)
	6	7	8	9	10		11
1	-0.01202	-0.00540	0.00100	-0.01935	0.00597	6	-0.34511
2	0.00304	0.01004	-0.01107	-0.01128	0.00640	7	-0.03588
3	0.00746	0.00191	-0.00885	-0.01262	-0.00878	8	0.36996
4	0.00115	0.00685	-0.00690	-0.01727	0.00723	9	-0.40968
5	0.02916	-0.00466	-0.03625	0.02660	-0.03689	10	0.58362

References

1. Mayer, H., 1999. Air pollution in cities. Atmospheric Environment, 33 (24), 4029-4037.
2. Sharma, P. and Khare, M., 2001. Modelling of vehicular exhaust- a review. Transportation Research, D6, 179-198.
3. Mage, D., Ozolins, G., Peterson, P., Webster, A., Orthofer, R., Vandeweerd, V. and Gwynne, M., 1996. Urban air pollution in megacities of the world. Atmospheric Environment, 30 (5), 681-686.
4. Kretzschmar, J.G., 1995. Energy related air pollution problems in the worlds ten largest megacities. In: Power, H., Moussiopoulos, N. and Berbbia, C.A. (Eds.), Air Pollution-III, Vol. 2, Computational Mechanics Inc., Southampton, Boston, pp. 3-12.
5. WHO/UNEP., 1992. Urban air pollution in megacities of the world. World Health Organization, United Nations Environment Programme, Blackwell, Oxford.
6. Hall, J.V., 1996. Assessing health effects of air pollution. Atmospheric Environment, 30 (5), 743-746.
7. Wark, K. and Warner, C.F., 1976. Air pollution: its origin and control. Harper and Row Publishers Inc., New York, USA.
8. Stern, A.C., Boubel, R.W., Turner, D.R. and Fox, D.L., 1984. Fundamentals of air pollution. Academic Press Inc., New York.
9. Rao, C.S., 1991. Environmental pollution control engineering. Wiley Eastern Limited, New Delhi, India.
10. OECD/IEA., 1991. Greenhouse gas emissions. Organization for Economic Cooperation and Development/International Energy Agency, OECD Press, Paris.
11. Faiz, A., Weaver, C.S. and Walsh, M., 1996. Air pollution from motor vehicles: standards and technologies for controlling emissions. World Bank and United Nations Environment Programme, Washington, DC.
12. Houghton, J., 1994. Transport and the environment. Eighteenth report of the Royal Commission on Environmental Pollution, Cm 2674, the stationery office, London. ISBN 0-10-137522-0.
13. Joumard, R., 1995. Transport and air pollution-some conclusions. Science of the Total Environment, 169 (1-3), 1-5.
14. Colvile, R.N., Hutchinson, E.J., Mindell, J.S., Warren, R.F., 2001. The transport sector as a source of air pollution. Atmospheric Environment, 35, 1537-1565.
15. Ragland, K.W., 1973. Multiple box model for dispersion of air pollutants from area source. Atmospheric Environment, 7, 1017-1032.
16. Stearn, A.C., 1968. Air pollution. Vol. 1., Academic Press, New York.
17. Nagendra, S.M.S. and Khare, M., 2002. Line source emission modelling- review. Atmospheric Environment, 36 (13), 2083-2098.
18. Gardner, M.W. and Dorling, S.R., 1998. Artificial neural networks: the multilayer perceptron – a review of applications in atmospheric sciences. Atmospheric Environment, 32 (14/15), 2627-2636.
19. Fenger, J., 1999. Urban air quality. Atmospheric Environment, 33 (29), 4877-4900.

20. TERI., 1993. Impact of road transportation on energy and environment- an analysis of metropolitan cities of India. Tata Energy Research Institute, Report Submitted to Ministry of Urban Development, Government of India, New Delhi, India.
21. Rejinders, L., 1992. Pollution problem, relative contribution from the road traffic. IATSS Research, 15 (2), 28-32.
22. Shiller, J.W., 1990. Environmental issues and future of the transport activity. In: Proceedings of the OPEC Seminar on the Environment, April 13-15, Vienna.
23. CPCB., 1999. Auto emissions. Parivesh newsletter, 6 (1), Central Pollution Control Board, Ministry of Environment and Forests, Government of India, India.
24. Onursal, B. and Gautam, S.P., 1997. Vehicular air pollution: experiences from seven Latin American urban centers. World Bank Technical Paper No. 373, World Bank, Washington, DC.
25. Keoleian, G.A., Kar, K., Manion, M.M. and Bulkely, J.W., 1997. Industrial ecology of the automobile: a life cycle perspective. Society of Automobile Engineers Inc., Warrendale, USA.
26. Watkins, L.H., 1991. Air pollution from road vehicles. TRRL , London, HMSO.
27. Masterson, W.L.E., Slowinski, E. and Stanitski, C.L., 1985. Chemical Principles, CBS College Publishing, New York.
28. Horowitz, J.L., 1982. Air quality analysis for urban transportation planning. MIT Press, Cambridge, Massachusetts.
29. AQIRP., 1991. Exhaust emissions of toxic air pollutants using reformulated gasoline. Air Quality Improvement Research Programme, Technical Bulletian 5, Coordinating Research Council Inc., Atlanta, Georgia.
30. Wijetilleke, L. and Karunaratne, S.A.R., 1995. Air quality management consideration for developing countries. Technical Paper 278, World Bank, Washington, DC.
31. Walsh, M.P., 1995. Global trends in motor vehicle pollution control: challenges and opportunities in 1995. In proceedings of 3rd International Conference on the Automotive Industry and the Environment, March 9-10, Geneva.
32. GEMS., 1988. Assessment of urban air quality. Global Environment Monitoring System, United Nations Environment Programme and World Health Organization, Geneva.
33. MARC., 1991. Health implications of averaging times shown. Monitoring and Assessment Research Centre, University of London, Kings College, London, UK.
34. Romieu, I., 1992. Epidemiologic studies of the health effects of air pollution due to motor vehicles. In: Mage, D.E. and Zail, O. (Eds.), Motor Vehicle Air Pollution: Public Health Impact and Control Measures, World Health Organization and Department of Public Health, Geneva.
35. Schwartz, J. and Zeger, S., 1990. Passive smoking, air pollution and acute respiratory symptoms in a daily study of student nurses. American Review of Respiratory Disease, 141 (62), pp. 7.
36. WHO., 1987. Sulfur dioxide and particulate matter. In: Air Quality Guidelines for Europe. World Health Organisation, Regional Publications, European Series 23, Copenhagen.
37. ALA., 1997. Gambling with health II. Who loses under new health standards for particulate matter. American Lung Association, Washington, DC.
38. Brunekreef, B., 1986. Childhood exposure to environmental lead. MARC Report No. 34, Monitoring and Assessment Research Center, King's College, University of London, London.
39. Longhurst, J.W.S., Lindley, S.J., Watson, A.F.R. and Conlan, D.E., 1996. The introduction of local air quality management in the United Kingdom: a review and theoretical framework. Atmospheric Environment, 30 (23), 3975-3985.

40. Elsom, D., 1997. Atmospheric pollution: a global perspective. Backwell, Oxford.
41. Longhurst, J.W.S. and Elsom, D.M., 1997. A theoretical perspective on air quality management in the United Kingdom. In: Baldasano, J.M., Brebbia, C.A., Power, H., Zannetti, P. (Eds.), Air pollution-II, Vol. 2., Computational Mechanics Inc., Southampton, Boston, pp. 525-532.
42. Laxen, D., 1993. An introduction to local air quality management. A supplement to clean air, 23, 12pp.
43. Griffin, R.D., 1994. Principles of air quality management. CRC Press, Florida.
44. UN., 1987. Effects and control of transboundary air pollution. United Nations Report prepared within the framework of the conservation on long range transboundary air pollution, New York.
45. Cohn, L.F. and McVoy, G.R., 1982. Environmental analysis of transportation system. Wiley-Interscience, New York.
46. Juda, K., 1989. Air pollution modelling. In: Cheremisinoff, P.N. (Eds.), Encyclopedia of Environmental Control Technology, Vol. 2: Air Pollution Control, Gulf Publishing Company, Houston, Texas, USA, pp. 83-134.
47. Zannetti, P., 1989. Simulating short-term, short-range air quality dispersion phenomena. In: Cheremisinoff, P.N., (Eds.), Encyclopedia of Environmental Control Technology, Vol. 2: Air Pollution Control, Gulf Publishing Company, Houston, Texas, USA, pp. 159-195.
48. Cats, G.J. and Holtslag, A.A.M., 1980. Prediction of air pollution frequency distribution- part 1. Lognormal distribution. Atmospheric Environment, 14 (2), 255-258.
49. Raimondi, F.M., Rando, F., Vitale, M.C. and Calcara, A.M.V., 1997. Short-term fuzzy DAP predictor for air pollution due to vehicular traffic. In: Jose, R.S. and Brebbia, C.A. (Eds.), Measurements and Modelling in Environmental Pollution, Computational Mechanics Inc., Southampton, Boston, pp. 189-200.
50. Box, G.E.P., Jenkins, G.M. and Reiusel, G.C., 1994. Time series analysis forecasting and control. 3rd Edition, Prentice Hall, Englewood Cliffs, New Jersey.
51. Box, G.E.P. and Jenkins, G.M., 1976. Time series analysis forecasting and control. 2nd Edition, Holdenday, San Francisco.
52. Box, G.E.P. and Jenkins, G.M., 1970. Time series analysis forecasting and control. Holdenday, San Francisco.
53. Milionis, A.E. and Davis, T.D., 1994. Regression and stochastic models for air pollution-I: review comments and suggestions. Atmospheric Environment, 28 (17), 2801- 2810.
54. Milionis, A.E. and Davis, T.D., 1994. Regression and stochastic models for air pollution-II: application to stochastic models to examine the links between ground level smoke concentrations and temperature inversion. Atmospheric Environment, 28 (17), 2811-2822.
55. Merz, P.H., Painter, H.J. and Payson, P.R., 1972. Aerometric data analysis –time series analysis and forecast and an atmospheric smog diagram. Atmospheric Environment, 6 (5), 319-342.
56. Chock, D.P., Terrel, T.R. and Levitt, S.B., 1975. Time series analysis of riverside California air quality data. Atmospheric Environment, 9 (11), 978-989.
57. Horowitz, J. and Barakat, S., 1979. Statistical analysis of the maximum concentration of an air pollutant effects of autocorrelation and non stationarity. Atmospheric Environment, 13 (6), 811-818.
58. Murray, L.C. and Farber, R.J., 1982. Time series analysis of an historical visibility data base. Atmospheric Environment, 16 (10), 2299-2308.
59. Khare, M. and Sharma, P., 2002. Modelling urban vehicle emissions. WIT press, Southampton, UK.

60. McCollister, G.W. and Wilson, K.R., 1975. Linear stochastic model for forecasting daily maxima and hourly concentrations of air pollutants. Atmospheric Environment, 9 (4), 417-423.
61. Kao, J.J. and Huang, S.S., 2000. Forecast using neural network versus Box-Jenkins methodology for ambient air quality monitoring data. Journal of Air and Waste Management Association, 50, 219-226.
62. Nagendra, S.M.S. and Khare, M., 2002. Artificial neural network based line source emission modelling- a review. In: Bondyopadhyay, J.N. and Kumar, N.D. (Eds.), Proceedings of International Conference on Advances in Civil Engineering: Water Resources and Environmental Engineering, Vol. 1, Allied Publishing Limited, New Delhi, India, pp. 663-670.
63. Rao, V. and Rao, H., 1998. C++ Neural network and fuzzy logic. 2nd Edition, BPB Publications, New Delhi, India.
64. Karunanithi, N., Whitely, D. and Malaiya, Y.K., 1992. Using neural networks in reliability prediction. IEEE Software, 53-59.
65. Bose, N.K. and Liang, P., 1998. Neural network fundamentals with graphs, algorithms and applications. Tata McGraw Hill Publishing Company Limited, New Delhi, India.
66. Zurada, J.M., 1997. Introduction to artificial neural systems. West Publishing Company, Mumbai, India.
67. Boznar, M., Lesjak, M. and Malker, P., 1993. A neural network based method for short- term predictions of ambient SO_2 concentrations in highly polluted industrial areas of complex terrain. Atmospheric Environment, 27B (2), 221-230.
68. Simpson, P.K., 1989. Foundations of neural networks. In: Sinencio, E.S. and Lau, C., (Eds), Artificial Neural Networks-Paradigms, Application and Hardware Implementations, IEEE Press, New York. pp. 3-24.
69. Wasserman, P.D., 1989. Neural computing, theory and practice. Van Nostrand Reinhold, New York.
70. French, M. and Recknagel, F.C., 1994. Modelling of algal blooms in fresh water using artificial neural network. In: Zannetti, P. (Eds.), Computer Techniques in Environmental Studies-V, Vol. 2, Computational Mechanics Inc., Southampton, Boston, pp. 87-94.
71. Rumelhart, D.E. and McClelland, J.L., 1995. Parallel distributed processing: explorations in the microstructure of cognitions. Vol. 1, 11th Edition, MIT Press, Cambridge, England.
72. French, M.N., Krajewski, W.F. and Cuyleendall, R.R., 1992. Rainfall forecasting in space and time using a neural network. Journal of Hydrology, 137 (1), 1-31.
73. McCulloch, W.S. and Pitts, W., 1943. A logical calculus of the ideas immanent in nervous activity. Bulletin of Mathematical Biophysics, 5, 115-133.
74. Fu, C. and Poch, M., 1995. System identification and real-time pattern recognition by neural networks for an activated sludge process. Environmental International, 21 (1), 57-69.
75. Mammone, R.J., 1994. Artificial neural networks for speech and vision. Chapman and Hall Neural Computing Series, London.
76. Hebb, D., 1949. The organization behavior. Wiley, New York.
77. Rosenblatt, F., 1958. The perceptron: a probabilistic model for information storage and organization in the brain. Psychological Review, 65, 386-408.
78. Minsky, M. and Papert, S., 1969. Perceptrons. MIT Press, Cambridge, MA.
79. Werbos, P.J., 1974. Beyond regression: new tools for prediction and analysis in the behavioral sciences. Master Thesis, Harvard University.
80. Parker, D.B., 1982. Learning–logic. Invention report S81-64, file 1, Office of Technology Licensing, Stanford University.

81. Rumelhart, D.E., Hinton, G.E. and Williams, R.J., 1986. Learning internal representations by error propagation. In: Rumelhart, D.E. and McClelland, J.L. (Eds.), Parallel distributed processing, 8th Edition, MIT Press, Cambridge, England, pp. 45-76.
82. Comrie, A.C., 1997. Comparing neural networks and regression model for ozone forecasting. Journal of Air and Waste Management Association, 47, 653-663.
83. Gardner, M.W. and Dorling, S.R., 1999. Neural network modelling and prediction of hourly NO_x and NO_2 concentrations in urban air in London. Atmospheric Environment, 33 (5), 709-719.
84. Rumelhart, D.E. and McClelland, J.L., 1986. Parallel distributed processing: explorations in the microstructure of cognitions. Vol. 1, 8th Edition, MIT Press, Cambridge, England.
85. Battii, R., 1992. First and second order methods for learning between steepest descent and Newton's method. Neural Computation, 4, 141-166.
86. Hayken, S., 2001. Neural networks –a comprehensive foundation. 2nd Edition, Pearson Education Inc, New Delhi, India.
87. Hornik, K., Stinchcombe, M. and White, H., 1989. Multilayer feed-forward networks are universal approximators. Neural Networks, 2, 359-366.
88. Beaton, J.L., Ranzieri, A.J., Shirley, E.C. and Skog, J.B., 1972. Mathematical approach to estimating highway impact on air quality. Federal Highway Administration Report No. FHWARD-72-36, Washington, DC.
89. Zannetti, P., 1990. Air pollution modelling-theories, computational methods and available software. Computational Mechanics Publications. Southampton, Boston.
90. Csanady, G.T., 1972. Crosswind shear effects on atmospheric diffusion. Atmospheric Environment, 6 (3), 221-232.
91. Luhar, A.K. and Patil, R.S., 1989. A general finite line source model for vehicular pollution prediction. Atmospheric Environment, 23 (3), 555-562.
92. Chock, D.P., 1978. A simple line source model for dispersion near roadways. Atmospheric Environment, 12 (4), 823- 829.
93. Jakeman, A.J., Simpson, R.W. and Taylor, J.A., 1988. Modelling distributions of air pollutant concentrations–III. The hybrid deterministic statistical distribution approach. Atmospheric Environment, 22 (1), 163-174.
94. Moseholm, L., Silva, J. and Larson, T.C., 1996. Forecasting carbon monoxide concentration near a sheltered intersections using video traffic surveillance and neural networks. Transportation Research D1, 15-28.
95. Sutton, O.G., 1932. A theory of eddy diffusion in the atmosphere. In: Proceedings of Royal Society, London, A 135 (826), pp. 143.
96. Waller, R.E., Commins, B.T and Lawther, P.J., 1965. Air pollution in a city street. Britsh Journal Industrial Medicine, 22, 128-138.
97. Chen, T.C and March, F., 1971. Effect of highway configurations on environmental problems dynamics of highway associated air pollution. In: Englund, H.M. and Berry, T. (Eds.), 2nd International Clean Air Congress, Academic Press, New York, pp. 35-40.
98. Dilley, J.F. and Yen, K.T., 1971. Effect of mesoscale type wind on the pollutant distribution from a line source. Atmospheric Environment, 5 (10), 843-851.
99. Peters, L.K. and Klinzing, G.E., 1971. The effect of variable diffusion coefficients and velocity on the dispersion of pollutants. Atmospheric Environment, 5 (7), 497-504.
100. Lamb, R.G. and Neiburger, M., 1971. An interim version of a generalized urban air pollution model. Atmospheric Environment, 5 (4), 239-264.
101. Calder, K.L., 1973. On estimating air pollution concentrations from a highway in an oblique wind. Atmospheric Environment, 7 (9), 863-868.

102. Dabberdt, W.F., Ludwing, F.L. and Jr. Jhonson, W.B., 1973. Validation and application of an urban diffusion model for vehicular pollutants. Atmospheric Environment, 7 (7), 603-618.
103. Sharma, V. and Myrup, O.L., 1975. Diffusion from a line source in an urban atmosphere. Atmospheric Environment, 9, 907-922.
104. Stukel, J.J., Soloman, R.L. and Hudson, J.L., 1975. A model for the dispersion of particulate or gaseous pollutants from a network of streets and highways. Atmospheric Environment, 9 (11), 990-999.
105. Nicholson, S.E., 1975. A pollution model for street- level air. Atmospheric Environment, 9 (1), 19-31.
106. Fay, T.A. and King, D. Eng., 1975. Wake induced dispersion of automobile exhaust pollutants. Journal of Air Pollution Control Association, 1 (1), 44-75.
107. Cadle, S.H., Chock, D.P., Heuss, J.M., and Monson, P.R., 1976. Result of the General Motors sulfate dispersion experiments. General Motors Research Publication, GMR-2107, General Motor Corporation, Warren, USA.
108. Chock, D.P., 1977. General Motors sulphate dispersion experiment: an overview of the wind temperature and concentration fields. Atmospheric Environment, 11 (6), 553-559.
109. Egan, B.A., Epstein, B.A., Keefe, M., League, J. and Lavery, T.C., 1973. Development of procedure to simulate motor vehicle pollution levels. Environment Research and Technology, Inc., Report No. ERT-P-343F, Lexington, MA.
110. Zimmerman, J.P. and Thompson, R.S., 1975. Users guide for HIWAY. A Highway Air Pollution Model, EPA- 650/4-74-008.
111. Chock, D.P., 1977. General Motors sulphate dispersion experiment: assessment of the EPA HIWAY model. Journal of Air Pollution Control Association, 27, 39-45.
112. Noll, K.E., Miller, T.L. and Calggett, M., 1978. A comparison of three highway line source dispersion models. Atmospheric Environment, 12 (6/7), 1323 -1329.
113. Ward, C.E., Rangier, A.J. and Shirley, E.C., 1977. CALINE 2 - An improved microscale model for the dispersion of air pollutants from a line source. Federal Highway Administration Report, FHWA-RD-77-74, Washington, DC.
114. Benson, P.E., 1979. CALINE 3: A versatile dispersion model for predicting air pollutant levels near highway and arterial roads. Final Report, FHWA/CA/ TL. -79/23, California Department of Transportation, Sacramento, CA.
115. Benson, P.E., 1989. CALINE 4: A dispersion model for predicting air pollutant concentrations near roadway. Final Report, FHWA/CA/TL. -84/15. California Department of Transportation, Sacramento, CA.
116. Middleton, D.R., Butler, J.D. and Colwill, D.M., 1979. Gaussian plume dispersion model applicability to a complex motorway interchange. Atmospheric Environment, 13 (7), 1039-1049.
117. Colwill, D.M., Middleton, D.R. and Bulter, J.D., 1979. A Gaussian plume dispersion model applicable to a complex motorway interchange. TRRL Supplementary Report 505, Crowthorne, Berkshire.
118. DeTar, D.F., 1979. A new model for estimating concentrations of substances emitted from a line sources. Journal of the Air Pollution Control Association, 29 (2), 138-141.
119. Green, N.J., Bullin, J.A and Polasek, J.C., 1979. Dispersion of carbon monoxide from roadways at low wind speeds. Journal of Air Pollution Control Association, 29 (10), 1057-1061.
120. Rao, S.T., Sedefian, L. and Czapski, U.H., 1979. Characteristics of turbulence and dispersion of pollutants near major roadways. Journal of Applied Meteorology, 18, 283-293.

121. Rao, S.T., Sistal, G., Keenan, M.T. and Wilson, J.S., 1980. An evaluation of some commonly used highway dispersion models. Journal of Air Pollution Control Association, 30 (3), 239-246.
122. Carpenter, W.A. and Clemena, G.G., 1975. Analysis and comparative evaluation of AIRPOL-4. Virginia Highway and Transportation Research Council Report, VHTRC75-R55, Charlottesville, VA.
123. Danard, M.B., 1972. Numerical modelling of carbon monoxide concentration near a Highway. Journal of Applied Meteorology, 11, 947-957.
124. Krisch, J.W. and Mason, B.F., 1975. Mathematical models for air pollution studies involving the Oregon I205 Highway Project. Systems Science and Software Report, SSSR-76-2744, LaJolla, CA.
125. Pitter, R.L., 1976. Users manual ROADS, PSMG, VISI. Oregon Graduate Center, Beaverton, Oregon.
126. Peterson, W.B., 1980. Users guide for highway air pollution model. EPA- 60018- 80 – 018.
127. Rao, S.T. and Keenan, M.T., 1980. Suggestion for improvement of EPA-HIWAY model. Journal of Air Pollution Control Association, 30 (3), 247-256.
128. Chang, T.Y., Norbeck, J.M. and Weinstock, B., 1980. Urban center CO air quality projections. Journal of Air Pollution Control Association, 30 (9), 1022-1025.
129. Sedefian, L., Rao, T. and Czapski, U., 1981. Effects of traffic generated turbulence on near field dispersion. Atmospheric Environment, 15 (4), 527-536.
130. Munshi, U. and Patil, R.S., 1981. Application of ATDL type models to Bombay. Journal of Air Pollution Control Association, 31, 998-1001.
131. Hickman, A.J. and Colwill, D.M., 1982. The estimation of air pollution concentration from road traffic. TRRL Laboratory Report No. 1052, Crowthorne, Berkshire.
132. Rodden, J.B., Green, N.J., Messina, A.D. and Bullian, J.A., 1982. Comparison of roadway pollutant dispersion models using the Texas data. Journal of Air Pollution Control Association, 32 (12), 1226-1228.
133. Bullian, J.A., Polasek, J.C. and Green, N.J., 1980. Analytical and experimental assessment of highway impact on air quality: data analysis and model evaluation. Texas Transportation Institute Research Report No. 218-5F, Chemical Engineering Department, Texas, A&M University, College Station, TX.
134. Eskridge, R.E. and Rao, S.T., 1983. Measurement and prediction of traffic induced and velocity fields near roadways. Journal of Climate and Applied Meteorology, 22, 1431-1443.
135. Nelli, J.P. Messina, A.D. Bullin, J.A., 1983. Analysis and modelling of air quality at street intersections. Journal of Air Pollution Control Association, 33, 760-764.
136. Segal, H., 1983. Microcomputer graphics in atmospheric dispersion modelling. Journal of Air Pollution Control Association, 33 (6), 247-256.
137. Hickman, A.J. and Waterfield, V.H., 1984. A users guide to the computer programs for predicting air pollution from road traffic. TRRL Supplementary Report No. 806, Crowthorne, Berkshire.
138. Cohn, L.F. and Gaddipati, S.R., 1984. An interactive graphics method for use in highway air quality analysis. Journal of Air Pollution Control Association, 34 (11), 1137-1139.
139. Padmanabhamurthy, B. and Gupta, R.P., 1984. Meteorological potential for urban air pollution in India. Mausam, 35 (2), 233-242.
140. Beiruti, A.A.R. and Al-Omishy, H.K., 1985. Traffic atmospheric diffusion model. Atmospheric Environment, 19 (9), 1519-1524.
141. Cooper, D.C., 1987. Indirect source impact analysis carbon monoxide modelling. Journal of Air Pollution Control Association, 37 (11), 1308-1313.

142. Hlavinka, M.W. Korpics, J.J. and Bullin, J.A., 1987. TEXIN-2: a versatile model for predicting carbon monoxide concentrations near intersections. Journal of Air Pollution Control Association, 37 (7), 819-822.
143. Kunler, M., Kraft, J., Koch, W. and Windt, H., 1988. Dispersion of car emissions in the vicinity of a highway. In: Grefen, K and Lobel, J. (Eds.), Environmental Meteorology, Kulwer Academic Publishers, London.
144. Hoydysh, W. Orentlicher, M. and Dabberdt, W., 1987. Air movement and vehicular pollution in urban street canyons. In: Sterrett, F.S., (Eds.), Environmental Sciences Vol. 2, The New York Academy of Sciences, New York.
145. Khalil, M.A.K. and Rasmussen, R.A., 1988. Carbon monoxide in an urban environment: application a receptor model for source apportionment. Journal Air Pollution Control Association, 38 (7), 901-906.
146. Gronskei, K.E., 1988. The influence of car speed on dispersion of exhaust gases. Atmospheric Environment, 22 (2), 273-281.
147. Sculley, R.D., 1989. Vehicle emissions rate analysis for carbon monoxide hot spot modelling. Journal of Air Pollution Control Association, 31 (10), 911-924.
148. Cooper, D.C., 1989. Persistence factor for mobile sources (roadway) carbon monoxide modelling. Journal of the Air and Waste Management Association, 39 (5), 714-720.
149. Singh, M.P., Goyal, P., Basu, S., Agarwal, P., Nigam, S., Kumari, M. and Panwar, T.S., 1990. Predicted and measured concentrations of traffic carbon monoxide over Delhi. Atmospheric Environment, 24A (4), 801-810.
150. Kono, H. and Ito, S., 1990. A micro scale dispersion model for motor vehicle exhaust gas in urban areas- OMG volume source model. Atmospheric Environment, 24B (2), 243-252.
151. Kono, H. and Ito, S., 1990. A comparison of concentration estimates by the OMG volume- source dispersion model with three line source dispersion models. Atmospheric Environment, 24B (2), 253-260.
152. Zanaidi, M.A., Singh, M.P. and Karim, M., 1991. Traffic CO dispersion pattern in Kuwait. Atmospheric Environment, 25A (5/6), 909-914.
153. Miles, G.H., Jakeman, A.J. and Bai, J., 1991. A method for predicting the frequency distribution of air pollution from vehicle traffic, basic meteorology, and historical concentrations to assist urban planning. Journal of Environmental International, 17, 575-580.
154. Nieuwstadt, F.T.M., 1992. A large-eddy simulation of a line source in a convective atmospheric boundary layer-I, dispersion characteristics. Atmospheric Environment, 26A (3), 485-495.
155. Nieuwstadt, F.T.M., 1992. A large-eddy simulation of a line source in a convective atmospheric boundary layer-II, dynamics of a buoyant line source. Atmospheric Environment, 26A (3), 497-503.
156. Benson, P.E., 1992. A review of the development and application of the CALINE-3 and CALINE-4 Models. Atmospheric Environment, 26B (3), 379-390.
157. Alexopolos, A., Assimacopoulos, D. and Mitsoulis, E., 1993. Model for traffic emissions estimation. Atmospheric Environment, 27B (4), 435-446.
158. Qin, Y. and Kot, S.C., 1993. Dispersion of vehicular emission in street canyons, Guangzhou, city, south China (PRC). Atmospheric Environment, 27B (3), 283-291.
159. Burden, N.C., Whitwell, I. and Longhurst, J.W.S., 1994. Testing the tools of an air quality management: a comparison of predictions of nitrogen dioxide concentrations by CALINE-4 and DMRB models with monitored levels at the M4/M5 interchange in Bristol, UK. In: Power, H., Tirabassi, T. and Brebbia, C.A. (Eds.), Air Pollution V, Computational Mechanics Inc., Southampton, Boston, pp. 335-344.

160. Akeredoiu, F.A., Oluwole, A.F., Betika, E.A. and Ogunsola, O.J., 1994. Modelling of carbon monoxide concentration from motor vehicles travelling near roadway intersections in Lugos, Nigeria. In: Baldanano, J.M., Brebbia, C.A., Power, H. and Zannetti, P. (Eds.), Air Pollution II: Pollution Control and Monitoring, Vol. 2, Computational Mechanics Inc., Southampton, Boston, pp. 149-157.
161. Chan, L.Y., Hung, W.T. and Qin, Y., 1995. Assessment of vehicular emission dispersion models applied in street canyons in Guangzhou, PRC. Journal of Environmental International, 21 (1), 39-46.
162. Derwent, R.G. Middleton, D.R., Field, R.A., Goldstone, M.E., Lester, J.N. and Perry, R., 1995. Analysis and interpretation of air quality data from an urban roadside location in central London over the period from July 1991 to July 1992. Atmospheric Environment, 29(8), 923-946.
163. Esplin, G.L., 1995. Approximate explicit solution to the general line source problem. Atmospheric Environment, 29 (12), 1459-1463.
164. Clifford, M.J., Clarke, R. and Riffat, S.B., 1995. Local aspects of vehicular pollution. Atmospheric Environment, 31 (2), 271-276.
165. Dabberdt, W., Hoydysh, W., Schorling, M., Yang, F. and Holynskyi, O., 1995. Dispersion modelling at urban intersections. The Science of the Total Environment, 169 (1-3), 93-102.
166. Yu, L.E., Hildemann, L.M. and Ott, W.R., 1996. A mathematical, model for predicting trends in carbon monoxide emissions and exposure on urban arterial highways. Journal of Air and Waste Management Association, 46, 430-440.
167. Chock, D.P., and Winkler, S.L., 1997. Air quality prediction using a fixed layer depth vertical structure in the urban airshed model. Environmental Science and Technology, 31 (2), 359-370.
168. Gualteri, G. and Tartaglia, M., 1998. Predicting urban traffic air pollution: a gis fame work. Transportation Research, D5, 337-347.
169. Karim, M.M. and Matsui, H., 1998. A mathematical model of wind flow, vehicle wake and pollution concentration in urban road microenvironments- part I: model description. Transportation Research D3, 81-92.
170. Karim, M.M., Matsui, H., and Guensler, R., 1998. A mathematical model of wind flow, vehicle wake and pollution concentration in urban road microenvironments-part II: model results. Transportation Research D3, 171-191.
171. Karim, M.M., 1999. Traffic pollution inventories and modelling in metropolitan Dhaka, Bangladesh. Transportation Research, D4, 291-312.
172. Khare, M. and Sharma, P., 1999. Performance evaluation of general finite line source model for Delhi traffic conditions. Transportation Research D4, 65-70.
173. Sivacoumar, R. and Thanasekaran, K., 1999. Line source models for vehicular pollution prediction near roadways and model evaluation through statistical analysis. Environmental Pollution, 104, 389-395.
174. Goyal, P. and Ramakrishna, T.V.B.P.S., 1999. A line source model for Delhi. Transportation Research D4, 241-249.
175. Buckland, A.T. and Middleton, D.R., 1999. Nomograms for calculating pollution with in street canyons. Atmospheric Environment, 33 (7), 1017-1036.
176. Hao, J., He, D., Wu, Y., Fu, L. and He, K., 2000. A study of the emission and concentration distribution of vehicular pollutants in the urban area of Beijing. Atmospheric Environment, 34(3), 453-465.
177. Kousa, A., Kukkonen, J., Karppinen, A., Aarnio, P. and Koskenfalo, T., 2001. Statistical and diagnostic evaluation of a new-generation urban dispersion modelling system against an extensive data set in the Helsinki area. Atmospheric Environment, 35(27), 4617-4628.

178. Sivacoumar, R. and Thanasekaran, K., 2001. Comparison and performance evaluation of models used for vehicular pollution prediction. Journal of Environmental Engineering, ASCE, 127 (6), 524-530.
179. Kiihlwein, J., Wiekert, B., Trukenmuller, A., Theloke, J. and Friedrich, R., 2002. Emission modelling in high spatial and temporal resolution and calculation of pollutant concentrations for comparisons with measured concentrations. Atmospheric Environment, 36 (1) Supplement, 7-18.
180. Jorquera, H., 2002. Air quality at Santiago, Chile: a box modelling approach-I carbon monoxide, nitrogen oxides and sulfur dioxide. Atmospheric Environment, 36 (2), 315-330.
181. Dufort, E.C. and Frankel, S.P., 1953. Stability condition in the numerical treatment of parabolic differential equation. Mathematical Tables National Research Council, Washington, 7, 135pp.
182. Ragland, K.W., Pierce, J.J., 1975. Boundary layer model for air pollutant accumulations due to highway traffic. Journal of Air Pollution Control Association, 25, 48-51.
183. Eskridge, R.E., Binkowski, F.S., Hunt, J.C.R., Clark, T.L. and Demerjain, K.C., 1979. Highway modelling-II: advection and diffusion of SF_6 tracer gas. Journal of Applied Meteorology, 18 (4), 401-412.
184. Eskridge, R.E. and Hunt, J.C.R., 1979. Highway modelling-I: prediction of velocity and turbulence fields in the wake of vehicles. Journal of Applied Meteorology, 18 (4), 387-400.
185. Chock, D.P., 1982. General Motors sulfate dispersion experiment: an analysis of the wind field near the road. In: Modelling of Dispersion of Transport Pollution, Symposium Proceedings Series No. 22, Institute of Mathematics and its Applications, UK. pp. 1-37.
186. Eskridge, P.E. and Thompson, R.S., 1982. Experimental and theoretical study of the wake of a block-shaped vehicle in a shear-free boundary flow. Atmospheric Environment, 16 (12), 2821-2836.
187. Maddukuri, C.S., 1982. A numerical model of diffusion of carbon monoxide near highways. Journal of Air Pollution Control Association, 32 (8), 834-836.
188. Eskridge, R.E. and Rao, S.T., 1986. Turbulent diffusion behind vehicle: experimentally determined mixing parameters. Atmospheric Environment, 20 (5), 851-860.
189. Thompson, R.S. and Eskridge, R.E., 1987. Turbulent diffusion behind vehicles: experimentally determined influence of vertex pair in vehicle wake. Atmospheric Environment, 21 (10), 2091-2097.
190. RIVM., 1991. National environmental survey 2:1990-2010. Publication of the National Institute of Public Health and Environmental Protection (RIVM), Bilthorn, Netherlands.
191. Van den Hout, K.D., Baars, H.P. and Duijn, N.J., 1989. Effects of buildings and street on air pollution by road traffic. In: Basser, L.J. and Mulder, W.C. (Eds.), Proceedings of the 8th World Clean Air Congress, Vol. 4, Elsevier, Amsterdam., Hague, Netherlands.
192. Eerens, H.C., Sliggers, C.J. and Hout, K.D.V., 1993. The car model, the Dutch method to determine city street air quality. Atmospheric Environment, 27B (4), 389-399.
193. Heida, H., Jang, A.L. and Huygen, C., 1989. Model calculation of street air concentrations for carbon monoxide. In: Brasser, L.J. and Mulder, W.C. (Eds.), Vol. 3, Elsevier, Amsterdam, Hague, Netherlands, pp. 233-238.
194. Harkonen, T., Valkonen, E., Kukkonen, J., Rantakrans, E., Jalkanen, L. and Lahtinen, K., 1995. An operational dispersion model for predicting pollution from a road. International Journal of Environmental and Pollution, 4-6, 602-610.

195. Harkonen, J., Walden, J. and Kukkonen, J., 1996a. Comparison of model predictions and measurements near a major road in an urban area. In: Kretzchgman, J. and Cosemans, G., (Eds.), Proceedings of 4th Workshop on Harmonisation with in Atmospheric Dispersion Modelling for Regulatory Purposes, Vol. 2, Ostende, Belgium, Installing Voor Technologish Onderzock, Mol. Belgium, pp. 453-460.
196. Harkonen, T., Valkonen, E., Kukkonen, J., Rantakrans, E., Lahtinen, K., Karppinen, A. and Jalkanen, L., 1996b. A model for the dispersion of pollution from a road network. Vol. 23, Finnish Meteorological Institute, Publication on Air Quality, Helsinki, p. 34.
197. NILU., 1996. ROADAIR 3.11 users manual. Norwegian Institute for Air Research, Kjeller, Norway.
198. Karppinen, A., Kukkonen, J., Konttinen, M., Rantakrans, E., Valkonen, E., Harkonen, J., Koskentalo, T. and Elolahde, T., 1997. Comparison of dispersion model predictions and the results from an urban air quality measurement network. In: Power, H. Tirabassis, T and Brebbia, C.A. (Eds.), Air Pollution-V, Computational Mechanics Inc., Southampton, Boston. pp. 405-411.
199. Karppinen, A., Kukkonen, J., Konttinen, M., Harkonen, J., Valkonen, E., Rantakrans, E., Koskentalo, T. and Elolahde, T., 1998. The emission dispersion and chemical transformation of traffic –originated nitrogen oxides at the Helsink metropolitan area. International Journal of Vehicle Design, 20 (1-4), 131-136.
200. Maurizi, A. and Tampieri, F., 1999. Velocity probability density functions in Lagrangian dispersion models for in homogeneous turbulence. Atmospheric Environment, 33 (2), 281-289.
201. Koeltzsch, K., 1999. On the relationship between the Lagrangian and Eulerian time scale. Atmospheric Environment, 33 (1), 117-128.
202. Huang, H., Akutsu, Y., Arai, M. and Tamura, M., 2000. A two dimensional air quality model in an urban street canyon: evaluation and sensitivity analysis. Atmospheric Environment, 34 (5), 689-698.
203. Karppinen, A., Kukkonen, J., Elolahde, T., Kunttinen, M., Kuskentalo, T. and Rantukrans, E., 2000. A modelling system for predicting urban air pollution: model prediction and applications in the Helsinki metropolitan area. Atmospheric Environment, 34 (22), 3723-3733.
204. Karppinen, A., Kukkonen, J., Ecolahde, T., Konttinen, M. and Koskentalo, T., 2000. A modelling system for predicting urban air pollution: comparison of model predictions with the data of an urban measurement network in Helsinki. Atmospheric Environment, 34 (22), 3735-3743.
205. Chang, C.T., Tsai, C.J., Lee, C.T., Chang, S.Y., Cheng, M.T. and Chein, H.M., 2001. Differences in PM_{10} concentrations measured by β-gauge monitor and hi-volume sampler. Atmospheric Environment, 35 (33), 5741-5748.
206. Rao, K.S., Gunter, R.L., White, J.R., and Hosker, R.P., 2002. Turbulence and dispersion modelling near highways. Atmospheric Environment, 36(27), 4337-4346.
207. McGuire, T and Noll, K.E., 1971. Relationship between concentrations of atmospheric pollutants and average time. Atmospheric Environment, 5 (5), 291-298.
208. Tiao, G.C., Box, G.E.P. and Harmming, W.I., 1975. Analysis of Los Angeles photochemical smog data: a statistical overview. Atmospheric Environment, 25, 260pp.
209. Aron, R.H. and Aron, I.M., 1978. Statistical forecasting models: carbon monoxide concentrations in the Los Angles basin. Journal of Air Pollution Control Association, 28 (7), 681-684.
210. Hirtzel, C.S. and Quon, J.E., 1979. Statistical dependence of hourly carbon monoxide measurements. Journal of Air Pollution Control Association, 29 (2), 161-163.

211. Ledolter, J. and Tiao, G.C., 1979. Statistical models for ambient air pollution, with spatial reference to the Los Angles catalyst study (LSCS) data. Environmental Science and Technology, 13 (10), 1233-1240.
212. Chang, T.Y., Norbeck, J.M. and Weinstock, B., 1980b. NO_2 air quality precursor relationship: an ambient air quality evaluation in the Los Angles basin. Journal of Air Pollution Control Association, 30 (2), 157-162.
213. Lincoln, D.R. and Rubin, E.S., 1980. Contribution of mobile sources to ambient particulate concentrations in a Downtown urban area. Journal of Air Pollution Control Association, 30 (7), 777-780.
214. Zamurs, J. and Piracci, R.J., 1982. Modelling of carbon monoxide hot spots. Journal of Air Pollution Control Association, 32 (9), 947-954.
215. Mikkelsen, T., Troen, I. and Larsen, S.E., 1982. On the finite line source problem in diffusion theory. Atmospheric Environment, 16 (11), 2591-2594.
216. Jakeman, A.J., Bai, J. and Miles, G.H., 1991. Prediction of seasonal extremes of 1-hour average urban CO concentrations. Atmospheric Environment, 25B (2), 219-229.
217. Bardeschi, A., Colucci, A., Granelle, V., Gangnetti, M., Tamponi, M. and Tebaldi, G., 1991. Analysis of the impact on air quality of motor vehicle traffic in the Milan urban area. Atmospheric Environment, 25B, 415-428.
218. Hsu, K.J., 1992. Time- series analysis of the interdependence among air pollutants. Atmospheric Environment, 26B (4), 491-503.
219. Hernandez, E., Martin, F. and Valero, F., 1991. State – space modeling for atmospheric pollution. Journal of Applied Meteorology, 30 (6), 793-811.
220. Manteiga, W.G., Sanchez, J.M.P., Cao, R. and Jurado, I.G., 1993. Time series analysis for ambient concentrations. Atmospheric Environment, 27A (2), 153-158.
221. Trier, A. and Firinguetti, L., 1994. A time series investigation of visibility in an urban atmosphere-I. Atmospheric Environment, 28 (5), 991-996.
222. Liu, J.J., Chan, C.C. and Jeng, F.T., 1994. Predicting personal exposure levels to carbon monoxide (CO) in Taipei, based on actual CO measurements in microenvironments and a Monte Carlo simulation method. Atmospheric Environment, 28 (14), 2361-2368.
223. Zhang, Y., Bishop, G.A. and Stedman, D.H., 1994. Automobile emissions are statistically 'γ' distributed. Environmental Science and Technology, 28 (7), 1370-1374.
224. Glen, W.G., Zelenka, M.P. and Graham, R.C., 1996. Relating meteorological variables and trend in motor vehicle emissions to monthly urban carbon monoxide concentrations. Atmospheric Environment, 30 (25), 4225-4232.
225. Cernuschi, S., Giugliano, M., Lonati, G. and Marzolo, F., 1998. Development and application of statistical models for CO concentration and duration events in the Milan urban area. The Science of the Total Environment, 220 (2-3), 147-156.
226. Comrie, A.C. and Diem, J.E., 1999. Climatology and forecast modelling of ambient carbon monoxide in Phoenix, Arizona. Atmospheric Environment, 33 (30), 5023-5036.
227. Maffeis, G., 1999. Prediction of carbon monoxide acute air pollution episodes. Model formulation and first application in Lombardy. Atmospheric Environment, 33 (23), 3859-3872.
228. Sharma, P., Khare, M. and Chakrabarti, S.P., 1999. Application of extreme value theory for predicting violations of air quality standards for an urban road intersection. Transportation Research D4, 201-216.
229. Sharma, P. and Khare, M., 1999. Application of intervention analysis for assessing the effectiveness of CO pollution control legislation in India. Transportation Research D4, 427-432.

230. Sharma, P. and Khare, M., 2000. Real-time prediction of extreme ambient carbon monoxide concentrations due to vehicular emissions using univariate linear stochastic models. Transportation Research D5, 59-69.
231. Sharma, P. and Khare, M., 2001. Short-time, real – time prediction of extreme ambient carbon monoxide concentrations due to vehicular exhaust emissions using transfer function noise models. Transportation Research D6, 141-146.
232. Olcese, L.E., Palanear, G.P. and Toselli, B.M., 2001. An inexpensive method to estimate CO and NO_x emissions from mobile sources. Atmospheric Environment, 35 (35), 6213-6218.
233. Stedman, J.R., Goodwin, J.W.L., King, K. Murrells, T.P., and Bush, T.J., 2001. An empirical model for predicting urban roadside nitrogen dioxide concentration in the UK. Atmospheric Environment, 35(8), 1451-1463.
234. Schalkoff, R., 1992. Pattern recognition: statistical, structural and neural approaches. Wiley, New York.
235. Rage, M.A., and Tock, R.W., 1996. A simple neural network for estimating emission rates of hydrogen sulphide and ammonia from single point source. Journal of Air and Waste Management Association, 46, 953-962.
236. Nagendra, S.M.S. and Khare, M., 1999. Artificial neural network technique in short-term air pollution modelling. In: Proceedings of National Seminar on Wind Engineering, Department of Aerospace Engineering, Indian Institute of Technology, Kharagpur, December 2-3, pp. 96-110.
237. Dorzdowicz, B., Benz, S.J., Sonta, A.S.M., and Scenna, N.J., 1997. A neural network based model for the analysis of carbon monoxide concentration in the urban area of Rosario. In: Power, H. Tirabassis, T. and Brebbia, C.A. (Eds.), Air Pollution V, Computational Mechanics Inc., Southampton, Boston, pp. 677-685.
238. Shi, J.P. and Harrison, R.M., 1997. Regression modelling of hourly NO_x and NO_2 concentration in urban air in London. Atmospheric Environment, 31 (24), 4081-4094.
239. Perez, P. and Trier, A., 2001. Prediction of NO and NO_2 concentrations near a street with heavy traffic in Santiago, Chile. Atmospheric Environment, 35 (10), 1783-1789.
240. Viotti, P., Liuti, G. and Genova, P.D., 2002. Atmospheric urban pollution: applications of an artificial neural network (ANN) to the city of Perugia. Ecological Modelling, 148 (1), 27-46.
241. Kukkonen, J., Partanen, L., Karppinen, A., Ruuskanen, J., Junninen, H., Kolehmainen, M., Niska, H., Dorling, S., Chatterton, T., Foxall, R. and Cawley, G., 2003. Extensive evaluation of neural network models for the prediction of NO_2 and PM10 concentrations, compared with a deterministic modelling system and measurements in central Helsinki. Atmospheric Environment, 37(),4539-4550.
242. Nagendra, S. M.S. and Mukesh Khare., 2004 Artificial Neural Network based Line Source Models for Vehicular Exhaust Emission Predictions of an Urban Roadway. Journal of Transportation Research Part D: Transport and Environment, 9 (3), 199-208.
243. Benarie, M.M., 1982. Air pollution modelling operations and their limits. In: Fronza, G. and Melli, P. (Eds.), Mathematical models for planning and controlling air quality, Pergamon press, New York, pp. 109-115.
244. Finzi, G. and Tebaldi, G., 1982. A mathematical model for air pollution forecast and alarm in an urban area. Atmospheric Environment, 16 (9), 2055-2059.
245. Kretzschmar, J.G., de Baere, G. and Vandervee, J., 1976. Validation of the emission frequency distribution model in the region of Antwerpen, Belgium. In: Proceedings Seventh International Technical Meetings on Air Pollution Modelling and its Application, Airlie House (Virginia), NATO/CCMS Publication N 51, pp. 235-270.

246. Nieuwstadt, F.T.M., 1980. Prediction of air pollution frequency distribution – III, the Gaussian plume model. Atmospheric Environment, 14 (2), 259-265.
247. North, M., Harnandez, E. and Garcia, R., 1984. Frequency analysis of high CO concentrations in Madrid by stochastic process modelling. Atmospheric Environment, 18 (10), 2049-2054.
248. Benarie, M.M., 1980. Urban air pollution modelling. The MIT press, London.
249. Juda, K., 1986. Modelling of the air pollution in the Cracow area. Atmospheric Environment, 20 (12), 2449-2458.
250. EPA., 1992. Users guide for the industrial source complex dispersion models. US Environmental Protection Agency, Office of Air Quality Planning and Standards, Washington, DC.
251. Rao, S.T., Chen, M., Keenan, M., Sistla, G., Peddada, R., Wotzak, G. and Kolak, N., 1978. Dispersion of pollutants near highways: experimental design and data acquetion procedures. EPA–600-4-78-037. NTIS. PB-284-866, US Environmental Protection Agency, Research Triangle Park, NC.
252. Rao, S.T., Sistla, G., Eskridge, R.E. and Peterson, W.B., 1986. Turbulent diffusion behind vehicles: evaluation of roadway models. Atmospheric Environment, 20, 1095-1103.
253. Georgopoulos, P.G. and Seinfeld, J.H., 1982. Statistical distribution of air pollutant concentrations. Environmental Science and Technology, 16, 401-416A.
254. Kapoor, S.G. and Terry, W.R., 1985. A comparison of two automatic systems for building rector time-series models in air pollution research. In: Anderson, D.D. (Eds.), Time Series Analysis: Theory and Practice, Vol. 7, Elsevier Science Publishers, Cincinnati, OH, pp. 200-211.
255. Gardner, M.W. and Dorling, S.R., 2000. Statistical surface ozone models: an improved methodology to account for non-linear behaviour. Atmospheric Environment, 34 (1), 21-34.
256. Gardner, M.W. and Dorling, S.R., 1996. Neural network modelling of the influence of local meteorology on surface ozone concentrations. In: Proceedings of International Conference on GeoComputation, University of Leeds, UK, pp. 359-370.
257. Perez, P., Trier, A. and Reyes, J., 2000. Prediction of $PM_{2.5}$ concentrations several hours in advance using neural network in Santiago, Chile. Atmospheric Environment, 34 (8), 1189-1196.
258. Alsugair, A.M. and Al-Qudrah, A.A., 1998. Artificial neural network approach for pavement maintenance. Journal of Computing in Civil Engineering, ASCE, 2 (4), 249-255.
259. Sarle, W., 1997. Neural network frequently asked questions- ftp://ftp.sas.com/pub/neural/ FAQ.html.
260. Swingler., 1996. Applying neural networks: a practical guide. Academic Press, London.
261. Berry, T., and Linoff, J., 1997. Data mining techniques. John Wiley and Sons, New York.
262. Lee, Y., Oh., S. and Kim, M., 1991. The effect of initial weights on premature saturation in back-propagation learning. In: International Conference on Neural Networks, Vol. 1, Seattle, pp. 765-770.
263. Willmott, C.J., 1982. Some comments on the evaluation of model performance. Bullitain of American Meteorological Society, 63, 1309-1313.
264. CPCB., 1999. Status of air quality in national capital region. Central Pollution Control Board, New Delhi, India.
265. Pundir, P.P., Jain, A.K. and Gogia, D.K., 1994. Vehicle emissions and control perspectives in India. Indian Institute of Petroleum, Dehradun, India.

266. Schnelle, K.B. and Dey, P.R., 2000. Atmospheric dispersion modelling compliance guide. McGraw Hill Inc., New York.
267. Kolehmainen, M., Martikainen, H. and Runskanen, J., 2001. Neural networks and periodic components used in air quality forecasting. Atmospheric Environment, 35 (5), 815-825.
268. Willmott, C.J., 1981. On the validation of models. Physical Geography, 2, 184-194.
269. MaRae, G.J. and Seinfeld, J.H., 1983. Development of a second generation mathematical model for urban air pollution –II. Evaluation of model performance. Atmospheric Environment, 17(3), 501-522.
270. Khare, M., 1989. Dispersion of coke oven emissions. Ph. D. Thesis, Department of Civil Engineering, University of Newcastle upon Tyne, UK.
271. Fox, D.G., 1981. Judging air quality model performance. Bulltain of American Meteorological Society, 62, 599-609.
272. Willmott, C.J., Ackleson, S.G., Davis, R.E., Feddema, J.J., Klink, K.M., Legates, D.R., O'Donnel, J. and Powe, C.M., 1985. Statistics for the evaluation and comparison of models. Journal of Geophysics Research, 90, 8995-9005.
273. Vandaele, W., 1983. Applied time series and Box-Jenkins model. Academic Press Inc., New York.
274. Goddard, N., Lynne, K.T., Mintz, T. and Bukys, L., 1989. The Rochester connechonist simulator. Technical Report No. 233., University of Rochester, New York.
275. Tao, Y. and Xinmiao, Y., 1998. Fuzzy comprehensive assessment, fuzzy clustering analysis and its application for urban traffic environment quality evaluation. Transportation Research D3, 51-57.
276. Gokhale, S. and Khare, M., 2004. A review of deterministic, stochastic and hybrid vehicular exhaust emission models. International Journal of Transport and Management, 2, 59-74.
277. Sutton, O.G., 1947. The problem of diffusion in the lower atmosphere. Quaternary Journal of Royal Meteorological Society, 73, pp. 257.
278. Pasquill, F., 1961. The estimation of the dispersion of wind borne material. Meteorological Magazine, 90, 33-49.
279. Gifford, F.A., 1961. Use of routine meteorological observations for estimating atmospheric diffusion. Nuclear Safety, 2, 47p.
280. Slawson, P.R. and Csanady, G.T., 1967. On the mean path of bent-over chimney plumes. Journal of Fluid Mechanics, 28, 311-322.
281. Schlink, U., Herbarth, O. and Tetzlaff, G., 1997. A component time-series model for SO_2 data: forecasting, interpretation and modification. Atmospheric Environment, 31 (9), 1285-1295.
282. Simpson, R.W. and Layton, A.P., 1983. Forecasting peak ozone levels. Atmospheric Environment, 17 (9), 1649-1654.
283. Robeson, S.M. and Steyn, D.G., 1990. Evaluation and comparison of statistical forecast models for daily maximum ozone concentrations. Atmospheric Environment, 24B, 303-312.
284. Crabtree, B.F., Ray, S.C., Schmidt, P.M., O'Connor, P.J. and Schmidt, D.D., 1990. The individual over time- time series applications in health care research. Journal of Clinical Epidemiology, 43 (3), 241-260.
285. Salcedo, R.L.R., Alvim Ferraz, M.C.M., Alves, C.A., and Martins, F.G., 1999. Time series analysis of air pollution data. Atmospheric Environment, 33 (15), 2361-2372.
286. Chatfield, C., 1996. The analysis of time series an introduction. 5th Edition, Chapman & Hall, London.
287. Kendall, S.M. and Ord, J.K., 1990. Time series. 3rd Edition, Edward Arnold Press, Paris.

288. Makridakis, S., Wheelwright, S.C. and McGee, V.E., 1983. Forecasting: methods and applications. 2nd Edition, John Wiley & Sons, New York.
289. McCleary, R. and Hay, R.A., 1980. Applied time series analysis for the social sciences. Sage, Beverly Hills.
290. Hipel, K.W. and Mcleod, A.I., 1994. Time series modelling of water resources and environmental systems. Elsevier Science, Amsterdam, Netherlands.
291. Granger, C.W.J. and Newbold, P., 1976. Forecasting transformed series. Journal of Royal Statistical Society, B, 189-203.
292. Milis, T.C., 1991. Time series techniques for economists. Cambridge University Press, Cambridge.
293. Marquardt, D.W., 1963. An analysis for least squares estimation of non-linear parameters. Journal of the Society for Industrial and Applied Mathematics, 11, 431-441.